Technische Universität München

Fakultät für Chemie

Lehrstuhl für Pharmazeutische Radiochemie

Novel Structural Concepts for the Development of complex-based Radiopharmaceuticals and Ligand Systems

Alexander Josef Wurzer

Vollständiger Abdruck der von der Fakultät für Chemie der Technischen Universität München zur Erlangung des akademischen Grades eines

Doktors der Naturwissenschaften (Dr. rer. nat.)

genehmigten Dissertation.

Vorsitzender: Prof. Dr. Dr. h.c. Horst Kessler

Prüfer der Dissertation:

1. Prof. Dr. Hans-Jürgen Wester
2. Prof. Dr. Matthias Eiber

Die Dissertation wurde am 23.10.2019 bei der Technischen Universität München eingereicht und durch die Fakultät für Chemie am 27.11.2019 angenommen.

Table of Contents

Abstract

The reason for the current dominance of ^{68}Ga-labeled tracers for PET imaging of e.g. PSMA expression in prostate cancer (PCa) needs to be critically assessed. A major advantage of these radiopharmaceuticals is the lack or apparent lack of suitable alternatives, offering, in particular, efficient and reliable ^{18}F-labeling technologies with proven clinical relevance.

Aim of this work was the development of ^{18}F-labeled PSMA inhibitors that can be labeled by isotopic exchange (IE) at a Silicon Fluoride Acceptor (SiFA) moiety. An unsolved problem of this labeling technology is the pronounced lipophilicity of conjugates bearing SiFA moieties, impairing the pharmacokinetics of corresponding radiopharmaceuticals. In order to overcome this limitation, a novel, so-called radiohybrid (rh) concept was developed that is based on the use of a hydrophilic metal-chelate in close proximity to SiFA. The rh-concept offers the unique possibility to label one identical radiopharmaceutical either with ^{18}F or a radiometal, resulting in [^{18}F][M]rhPSMA (M=metal) and the chemically identical [^{19}F][*M]rhPSMA (*M=radiometal).

Several rhPSMA inhibitors were synthesized by solid-phase peptide synthesis. Human serum albumin (HSA) binding was measured by affinity high-performance liquid chromatography, while the lipophilicity of each tracer was determined by the shake-flask method in octanol and PBS buffer. *In vitro* experiments (IC_{50}, internalization) were carried out on LNCaP cells. *In vivo* studies (biodistribution, µPET, metabolite analyses) were conducted on LNCaP tumor-bearing male CB-17 SCID mice.

On the laboratory scale, ^{18}F-labeling of rhPSMAs by IE was completed in < 20 min (radiochemical yields: 58 ± 10%, radiochemical purity: > 97%) with molar activities of 11-60 GBq/µmol. Based on the manual procedure, a fully automated GMP-compliant procedure was set up, yielding [^{18}F][^{nat}Ga]rhPSMA-7/7.3 in radiochemical yields of approximately 50 ± 10% and molar activities of 100-300 GBq/µmol in 15.75 min. Moreover, ^{18}F-incorporation in similar yields was also achieved by means of an aqueous labeling approach using ^{18}O-enriched target water (≤ 0.5 mL).

Abstract

The diagnostic tracers (i.e. [^{18}F][^{nat}Ga]rhPSMA, [^{19}F][^{68}Ga]rhPSMA) rhPSMA-7 to -10, demonstrated similar or even higher affinities to and internalization by LNCaP cells, when compared to reference ligands [^{18}F]PSMA-1007 and [^{18}F]DCFPyL. Moreover, all tracers showed medium-to-low lipophilicity and high HSA binding. Biodistribution studies in LNCaP tumor-bearing mice revealed a high tumor uptake and favorable excretion kinetics. In first proof-of-concept studies in patients suffering from metastasized prostate cancer, [^{18}F][^{nat}Ga]rhPSMA-7 and the enantiomeric pure derivative [^{18}F][^{nat}Ga]rhPSMA-7.3 showed the typical uptake pattern of PSMA-targeted ligands with high uptake in tumor lesions, low background accumulation as well as low retention in the bladder and ureters in PET scans. Noteworthy no elevated uptake in undiseased bone was determined.

Regarding the theranostic ligands (i.e. [^{18}F][^{nat}Lu]rhPSMA, [^{19}F][^{177}Lu]rhPSMA), the lead compounds rhPSMSA-7, -7.3 and -10 showed similar or higher PSMA affinities and internalization rates, compared to the state-of-the-art ^{177}Lu-labeled tracers PSMA I&T and PSMA-617. These rhPSMA ligands revealed a favorable biodistribution distinguished by a high tumor uptake and fast excretion from non-target tissues in LNCaP tumor-bearing mice. In a first proof-of-concept study in a PCa patient, [^{177}Lu][^{19}F]rhPSMA-7.3 displayed a 1.5-fold higher tumor-to-kidney ratio, compared to [^{177}Lu]PSMA I&T.

In conclusion, rhPSMA ligands represent the first series of radiopharmaceuticals developed under the radiohybrid concept. The unparalleled simplicity of radiosynthesis of [^{18}F]rhPSMA tracers by IE and the possibility to produce identical ^{68}Ga-labeled counterparts are unique features of this approach. The diagnostic tracers [^{18}F][^{nat}Ga]rhPSMA-7/7.3 have been evaluated in more than 2000 patients and are currently under clinical development. Extension of the concept to theranostic tracers is currently under development, while the first candidate, [^{177}Lu][^{19}F]rhPSMA-7.3, was already clinically assessed in a small cohort of patients.

Zusammenfassung

Der Grund für die derzeitige Dominanz von ^{68}Ga-markierten Tracern für die PET Bildgebung von z.B. der PSMA-Expression bei Prostatakrebs muss kritisch bewertet werden. Ein Hauptvorteil dieser Radiopharmaka ist der Mangel bzw. der scheinbare Mangel geeigneter Alternativen, im speziellen effizienter und verlässlicher ^{18}F-Markierungsstrategien mit klinisch bewiesener Relevanz.

Das Ziel dieser Arbeit war die Entwicklung von ^{18}F-markierten PSMA-Inhibitoren, die durch Isotopenaustausch (IA) an einer Silicium-Fluorid-Akzeptor (SiFA) Gruppe radioaktiv markiert werden können. Ein ungelöstes Problem dieser Markierungstechnologie ist die ausgeprägte Lipophilie der SiFA Gruppe, welche die Pharmakokinetik entsprechender Radiopharmaka beeinträchtigt. Um diese Einschränkung zu überwinden, wurde in dieser Arbeit das sogenannte radiohybride (rh) Konzept entwickelt. Hierbei wird ein hydrophiler Metallkomplex in kurzer Distanz zu der SiFA Einheit eingeführt. Das rh-Konzept bietet dabei die einzigartige Möglichkeit eine einzige Verbindung entweder mit ^{18}F oder einem Radiometall markieren zu können. Dabei ist die [^{18}F][M]rhPSMA Verbindung (M=Metall) chemisch identisch zu der entsprechenden [^{19}F][*M]rhPSMA Verbindung (*M=Radiometall).

Eine Reihe verschiedener rhPSMA Inhibitoren wurden durch Festphasen-Peptidsynthese hergestellt. Die Bindung zu Humanalbumin wurde mittels Affinitäts-Hochleistungsflüssigkeitschromatographie ermittelt. Die Lipophilie der jeweiligen Tracer wurde durch die Schüttelmethode in Octanol und PBS-Puffer bestimmt. *In vitro* Experimente (IC_{50} und Internalisierung) wurden an LNCaP Zellen durchgeführt. Für *in vivo* Studien (Biodistribution, µPET, Metabolitenanalyse) wurden LNCaP tumortragende, männliche CB-17 SCID Mäuse verwendet.

Im Labormaßstab konnte die ^{18}F-Markierung der rhPSMA Liganden durch IA in < 20 min (radiochemische Ausbeute: 58 ± 10%, radiochemische Reinheit: > 97%) mit molaren Aktivitäten von 11-60 GBq/µmol durchgeführt werden. Basierend auf der manuellen Prozedur wurde eine vollautomatisierte GMP-konforme Synthese entwickelt, welche [^{18}F][^{nat}Ga]rhPSMA-7/7.3 in radiochemischen Ausbeuten von ca. 50 ± 10% und molaren Aktivitäten von 100-300 GBq/µmol in 15.75 min lieferte. Des Weiteren wurde eine ähnliche

Zusammenfassung

^{18}F-Inkorporation mittels einer wässrigen Markierungsstrategie in ^{18}O-angereichertem Wasser (≤ 0.5 mL) erzielt.

Die diagnostischen Tracer (d.h. [^{18}F][^{nat}Ga]rhPSMA, [^{19}F][^{68}Ga]rhPSMA) rhPSMA-7 bis -10 zeigten ähnliche oder sogar bessere Affinitäten und Internalisierungsraten an LNCaP Zellen im Vergleich zu den Referenzverbindungen [^{18}F]PSMA-1007 und [^{18}F]DCFPyL. Außerdem wiesen alle Tracer eine geringe bis mittlere Lipophilie und eine hohe Bindung zu Humanalbumin auf. Die Biodistributionsstudien an LNCaP tumortragenden Mäusen offenbarten hohe Tumoraufnahmen und eine vorteilhafte Exkretionskinetik. In ersten Proof of Concept Studien in Patienten mit metastasierendem Prostatakrebs zeigte [^{18}F][^{nat}Ga]rhPSMA-7 und das enantiomerenreine Derivat [^{18}F][^{nat}Ga]rhPSMA-7.3 das typische Aufnahmeprofil von PSMA-gerichteten Liganden in den durchgeführten PET Aufnahmen. Beide Liganden wiesen eine hohe Aufnahme in Tumorläsionen, eine geringe Hintergrundakkumulation und eine geringe Aufnahme in der Blase, sowie den Harnleitern auf. Des Weiteren wurde keine erhöhte Aufnahme in nicht-erkrankten Knochen festgestellt.

Hinsichtlich der theranostischen Liganden (d.h. [^{18}F][^{nat}Lu]rhPSMA, [^{19}F][^{177}Lu]rhPSMA) zeigten die Leitverbindungen rhPSMA-7, -7.3 und -10 ähnliche oder bessere PSMA Affinitäten und Internalisierungsraten, im Vergleich zu den State of the Art ^{177}Lu-markierten Verbindungen PSMA I&T und PSMA-617. Diese rhPSMA Liganden offenbarten zudem eine vorteilhafte Biodistribution in LNCaP tumortragenden Mäusen, welche sich durch eine hohe Tumoraufnahme und eine schnelle Exkretion von Hintergrundgeweben ausgezeichnete. In einer ersten Proof of Concept Studie in einem Patienten mit Prostatakrebs zeigte [^{177}Lu][^{19}F]rhPSMA-7.3 ein 1.5-fach besseres Tumor-zu-Nieren Verhältnis, verglichen mit [^{177}Lu]PSMA I&T.

Zusammengefasst repräsentieren die rhPSMA Liganden eine erste Serie von Radiopharmaka, die unter dem radiohybriden Konzept entwickelt wurden. Die beispiellose Einfachheit der Radiosynthese der [^{18}F]rhPSMA Tracer durch IA und die Möglichkeit die identische ^{68}Ga-markierte Verbindung herzustellen, sind einzigartige Merkmale dieses Ansatzes. Die diagnostischen Tracer [^{18}F][^{nat}Ga]rhPSMA-7/7.3 wurden in mehr als 2000 Patienten evaluiert und sind in klinischer Entwicklung. Derzeit wird die Erweiterung des Konzepts auf theranostische Tracer durchgeführt. Der erste Kandidat [^{177}Lu][^{19}F]rhPSMA-7.3 wurde im Zuge dessen bereits in einer kleinen Kohorte von Patienten evaluiert.

I. Introduction

1. Prostate Cancer

In 2018 prostate cancer (PCa) was again the most common non-cutaneous malignancy among males in Europe, accountable for over 13.000 deaths every year in Germany[1, 2]. As survival rates decrease with disease progression, early diagnosis is a key factor for a positive therapy outcome[3]. Currently, an elevated level of the prostate specific antigen (PSA) in the blood is used as a first hint for PCa, usually followed by digital rectal examination (DRE). Final confirmation depends on sonography-guided needle biopsy and subsequent histopathological verification[4]. In the late 1980s, the broad use of PSA as a serum marker for PCa led to a dramatic increase in PCA-diagnosis, especially of early stage disease[5]. An initial screening study in 1986 led to the first US Food and Drug Administration (FDA) approval of PSA testing for early detection of PCa and specified 4.0 ng/mL as the normal PSA range limit[6]. Noteworthy biopsy-detected PCa, including high-grade disease is not rare among men with PSA levels of 4.0 ng/mL or less[7]. Furthermore, elevated PSA values may also result from other non-malignant conditions, such as prostatitis or benign prostatic hyperplasia[8-10]. Due to complications associated with over-diagnosis and over-treatment, systematic population-based PSA screening is one of the most controversially discussed topics in urology and is currently not recommended in the guidelines of the European Association of Urology[4].

One of the most important and reliable prognostic predictors in PCa is the Gleason score (GS), developed between 1966 and 1974 by Donald Gleason and colleagues[11]. It is an architectural grading system, judging the histological morphology of glandular tissue from biopsy samples on a scale of 1 (well-differentiated) to 5 (poorly-differentiated). Addition of the Gleason grade of the most extensive (primary) pattern and the most common (secondary) pattern results in final Gleason scores, ranging from 2 to 10 [12, 13]. Increasing Gleason grade is generally associated with high disease aggressiveness and poor prognosis[14].

Besides the Gleason score and the PSA level, the TNM (Tumor, Node, Metastasis) classification is used in order to accurately stage the disease. It basically describes the extent of the main tumor (T), infiltration in nearby lymph nodes (N) and the presence of regional and distant metastases (M)[15]. Pooling of this information helps clinicians to assign patients to certain risk

groups, in order to give treatment recommendations and predict prognosis. For patients with primary diagnosis of intermediate to high-risk PCa, as well as for patients with recurrent disease, computed tomography (CT), magnetic resonance imaging (MRI) and bone scintigraphy are the recommended modalities for detecting tumors, staging and/or evaluating treatment response[4, 16, 17].

Functional imaging modalities, like positron emission tomography (PET) or single-photon emission computed tomography (SPECT), have a rapidly evolving role in the diagnosis of PCa, particularly in the staging of extraprostatic disease, in the restaging after biochemical relapse and in response assessment. In this context, PET probes targeting the prostate-specific membrane antigen (PSMA) have gained increasing importance for the clinical management of patients suffering from PCa. The gaining acceptance for PSMA-targeted PET probes was also reflected by a recently published consensus on molecular imaging of PCa at the European Association of Nuclear Medicine Focus 1 meeting[18, 19].

2. Prostate-specific membrane antigen

The prostate-specific membrane antigen (PSMA) is a type II transmembrane protein composed of a large extracellular portion (707 amino acids), a single transmembrane portion (24 amino acids) and a short NH_2-terminal cytoplasmic tail (19 amino acids)[20]. It is expressed as a non-covalently linked homodimer, which serves as a glutamate-preferring carboxypeptidase (therefore also referred to as GCPII, EC 3.4.17.21) and possesses both folate hydrolase and NAALADase activity (Figure 1)[21-23]. For enzymatic activity, dimerization is required, despite the structural independence of the active site in each monomer[24, 25].

As a NAALADase, PSMA effects the conversion of *N*-acetyl-aspartyl-glutamate (NAAG) to NAA and free glutamate in the central and peripheral nervous system, in order to terminate the neurotransmitter activity of NAAG and for glutamate provisioning[26, 27]. In this context, several neurological disorders like Alzheimer, schizophrenia or multiple sclerosis were shown to display dysregulated PSMA levels[28-30]. In the small intestine, enzymatic hydrolase activity of PSMA is crucial for folate absorption in humans. PSMA mediates the cleavage of glutamate moieties from poly-γ-glutamated folate, resulting in multiple releases of glutamate and mono-glutamylated folate, which can be transported through the intestinal wall into the blood stream[31, 32].

Apart from the nervous and digestive system, physiological PSMA expression was found in the proximal tubules of the kidney, and in a lower density in salivary glands and in the prostate epithelium[21, 33]. Recent studies indicated a much broader PSMA expression in a variety of other human tissues including heart, liver, lung and bladder, however expression levels appear to be substantially lower as in the aforementioned sites and its physiological function remains unclear[34, 35].

Compared to healthy prostate tissue, PSMA expression is upregulated markedly in the majority of prostatic malignancies[36]. Previous studies demonstrated that the number of PSMA-positive cells correlates with disease aggressiveness and stage, with highest levels found in hormone-refractory and metastatic (castration-resistant) PCa[37, 38]. These unique characteristics render the PSMA expression level as a potential independent biomarker for the prognosis of PCa[39, 40].

So far, the precise enzymatic function of PSMA in PCa has not been completely solved. Several studies indicate that overexpression of PSMA might be crucial for cancer progression. Yao

et al. reported that PSMA-overexpression and inherently increased hydrolytic activity leads to higher folate levels, which promote cell growth[23, 41]. Additionally, it was shown that PSMA is part of an intertwined cascade of cell-surface peptidases, regulating endothelial cell invasion and upregulation might facilitate prostate carcinogenesis[33, 42].

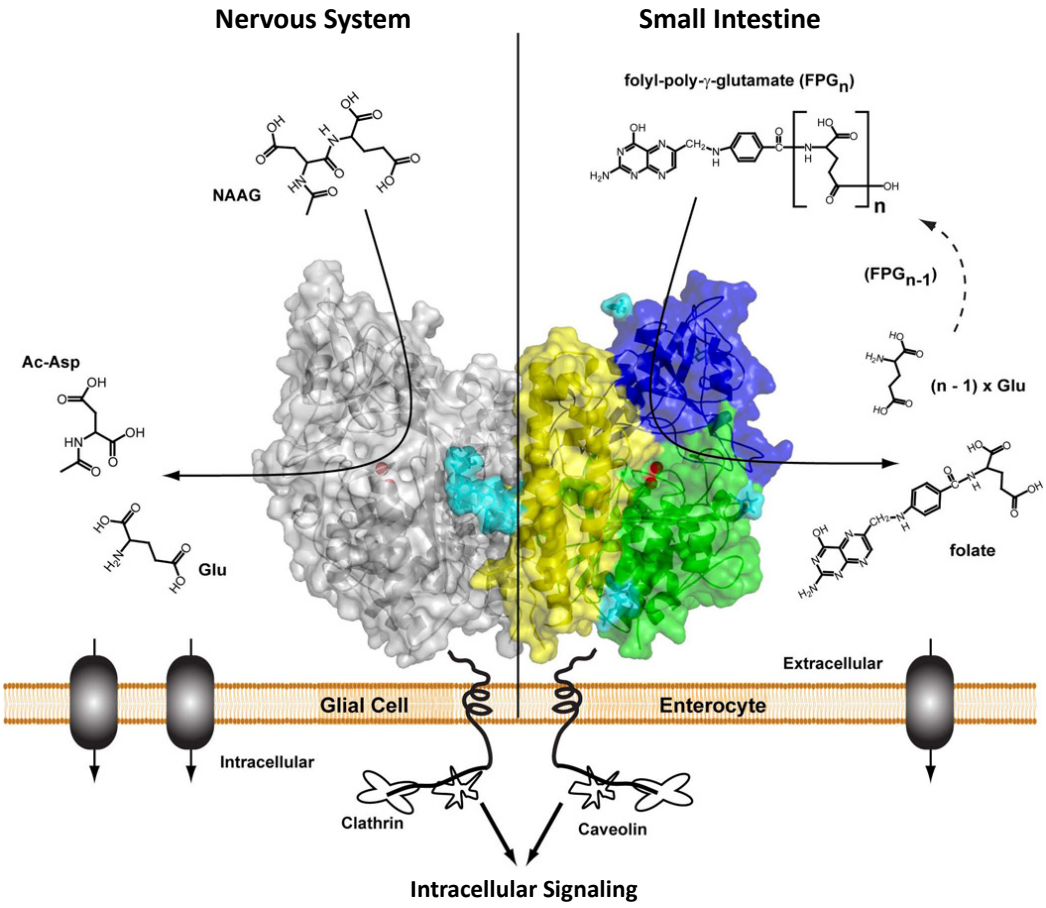

Figure 1: Crystal structure of the human PSMA homodimer. The right monomer shows the individual domains of the extracellular part: the protease domain; amino acids 57-116 and 352-590 (green), the apical domain; amino acids 117-351 (blue), and the *C*-terminal domain; amino acids 591-750 (yellow). The second monomer (left) is colored gray. *N*-linked sugar moieties are colored cyan, and the active-site Zn^{2+} ions are shown as red spheres. Left panel: NAAG catabolism in the mammalian nervous system. Right panel: Folate hydrolase at the plasma membrane of enterocytes (taken from Barinka *et al.*[28]).

This thesis is supported by the fact that PSMA is upregulated in the neovasculature of a variety of other solid tumors (including gliomas, colon, breast and renal cancer), implying a substantial role in tumor angiogenesis[43-45]. This characteristic involvement of PSMA in a variety of oncological diseases, especially in PCa, promoted the development of PSMA-targeted agents in recent years.

3. Design of PSMA-addressing ligands

Regarding the molecular structure of PSMA, the extracellular, transmembrane and cytosolic compartment of each monomer display distinctive functions in the recognition and transport of substrate molecules through the cell membrane.

PSMA undergoes constitutive receptor-mediated endocytosis *via* clathrin-coated pits, which is significantly enhanced if monoclonal antibodies are directed against it[46]. It was shown that interaction of the cytosolic domain of PSMA with clathrin and the clathrin adaptor protein-2 (AP-2) regulates the endocytic machinery[47]. Additionally, association of the intracellular tail with the actin-crosslinking protein filamin A modulates the internalization process and enzyme activity[48].

The extracellular portion of PSMA, generally responsible for substrate recognition, can be divided in three sub-domains: i) a domain with protease activity, ii) a helical domain, located at the dimer interface and iii) an apical domain, which altogether form the binding cavity[28, 49]. The whole extracellular part is highly *N*-glycosylated, which is inevitable for the correct folding, subsequent secretion and enzyme activity[50-52].

At the interface of the three extracellular sub-domains, the binuclear zinc site is located. The two zinc atoms are coordinated by the side chains of glutamic acid (Glu425), two aspartic acids (Asp387/453) and two histidines (His337/553). A water molecule asymmetrically bridges the zinc ions and is further coordinated by a glutamate residue (Glu424). As a result of these interactions, the water molecule displays a nucleophilic character, which is essential for hydrolysis of a bound substrate[25, 49, 53]. The active site divides the binding cavity into the non-pharmacophore S1 site and the glutamate-sensing S1' site (Figure 2 A).

The latter is formed by an array of amino acids (Phe209, Arg210, Asn257, Glu424, Glu425, Gly427, Leu428, Gly518, Lys699, and Tyr700), which secure specificity to glutamate and glutamate-like moieties *via* an ingenious network of polar hydrogen bondings and ionic interactions. The overall site measures approximately 8 × 8 × 8 Å – noteworthy, a flexible loop, which forms the glutamate sensor (Tyr692-Ser704) can substantially increase the pocket by more than 4 Å[25, 54, 55].

Contrary to the pharmacophore compartment, the S1 site appears to be less restrictive and can accommodate diverse structural modifications. Its molecular geometry can be described with a funnel, narrowing from the entrance lid (approx. Ø 20 Å) towards the binuclear active

site (approx. Ø 8 Å)[25]. Most importantly, the S1 site harbors a strongly positively charged region, which is composed by an apposition of arginine side chains (Arg463, Arg534 and Arg536). The "arginine patch" provides an explanation for the preference of molecules comprising aromatic character (cation-π interactions) or negatively charged moieties in this region (Figure 2 C)[53, 56-58].

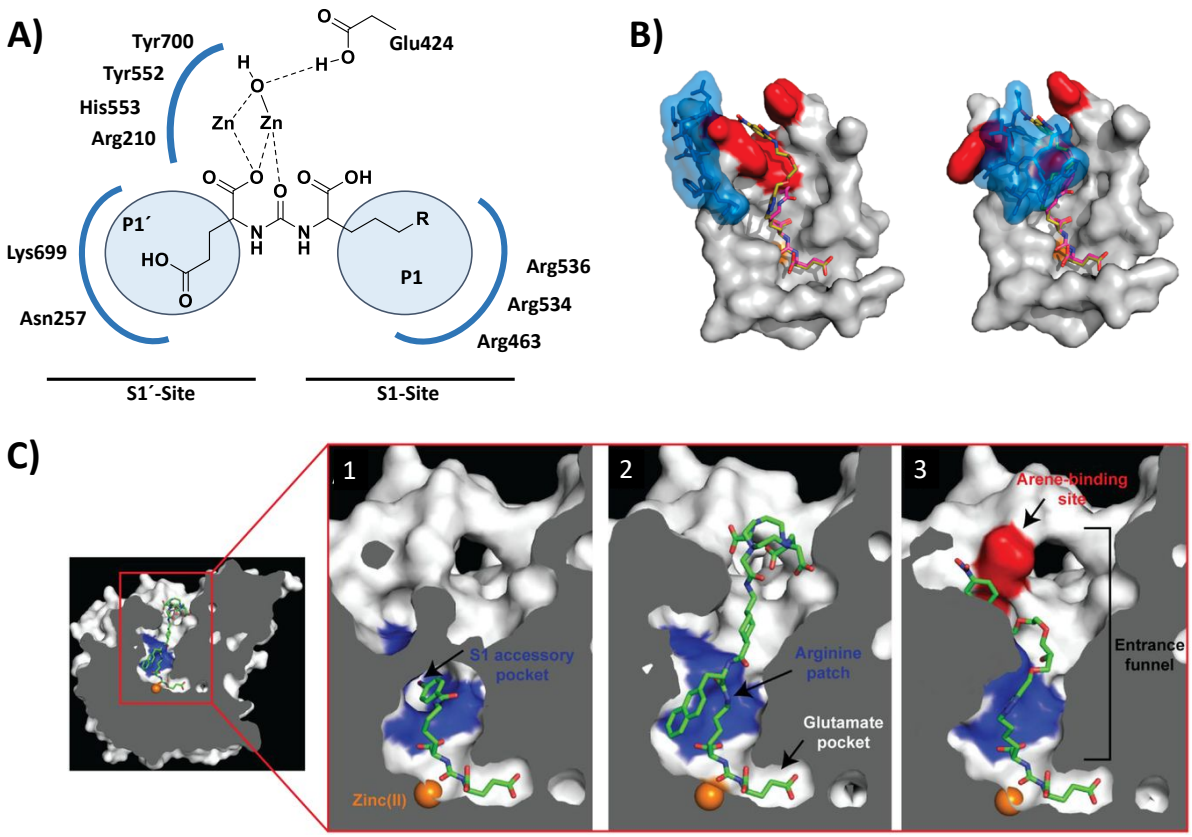

Figure 2: **A**) Suggested binding mode and interactions of urea-based inhibitors at the active site of PSMA. The modification sites P1 and P1' of the inhibitor are highlighted in blue[59]. **B**) Binding of the urea-based inhibitor Arm-P2 to PSMA for an opened (left) and closed (right) configuration of the entrance lid (blue). The arene-binding site is colored in red[60]. **C**) Cross-section of PSMA showing internal inhibitor-binding cavity. Within the entrance funnel, the S1 accessory pocket (blue), arginine patch (blue) and arene-binding site (red) are highlighted. Corresponding interactions are shown for the PSMA inhibitors DCIBzl (1), PSMA-617 (2) and ARM-P4 (3)[61]. Figures were taken from Zhang *et al.*[60] and Kopka *et al.*[61].

One of the first potent PSMA inhibitors was 2-(phosphonomethyl)pentanedioic acid (2-PMPA), discovered in 1996, by Jackson *et al.* – a small molecule glutamate-derived hydroxyphosphinyl derivative[62]. Crystal structure analysis of 2-PMPA in complex with PSMA revealed that its phosphonate group strongly interacts with the binuclear zinc site in the binding pocket. The pentanedioic acid moiety, mimicking natural glutamate-containing substrates, was introduced to bind at the glutamate recognition region of PSMA[63].

Based on these findings and following research efforts, a variety of other potent PSMA inhibitors were designed, which commonly feature a glutamate-derived moiety, addressing the pharmacophore S1' site, connected to a zinc-chelating group, which is then further functionalized[64]. Prominent families of moieties, binding to the binuclear zinc site of PSMA, are thiol-, phosphorous- or urea-based molecules[64-67]. Due to efficient synthetic access and high achievable affinities, urea-containing binding motifs, like Glu-urea-Lys (EuK), Glu-urea-Cys (EuC) or Glu-urea-Glu (EuE), were developed and investigated in detail for diverse pharmaceutical applications, concerning PSMA[58, 64, 68, 69]. It was found that *L*-configuration of the amino acids composing the inhibitor motif is inevitable for potent binding at the active site[64, 70].

Apart from the active site area, the binding cavity contains two further well-studied regions, which are generally exploited for the design of high-affinity PSMA ligands, especially for the optimization of distal moieties within a molecule: the arene-binding site and the S1 accessory hydrophobic pocket. The former is located close to the entrance lid and is covered by a flexible loop (Trp541-Gly548), which exists in an open and a closed conformation, depending on the PSMA-bound substrate. In the open state, corresponding ligands can interact with the arene-binding site (composed of Arg463, Arg511, Trp541), mostly *via* π-stacking of aromatic moieties, and thus increase affinity (Figure 2 B and C)[60, 61, 71, 72]. In close vicinity to the "arginine patch", the S1 accessory hydrophobic pocket with dimensions of approximately 7 × 8.5 × 9 Å is located. It can be accessed after simultaneous repositioning of the side chains of Arg463 and Arg546 and provides additional space for lipophilic groups, which thus might further optimize binding affinities (Figure 2 C)[73-75].

4. Imaging of PSMA

Morphological imaging modalities, like multiparametric magnetic resonance imaging (mpMRI) or CT are widely employed for the diagnosis and staging of PCa. However, the majority of metastatic lymph nodes in PCa (approximately 80%) are smaller than 8 mm and thus cannot be detected *via* morphological imaging modalities[76, 77]. In this context, molecular imaging techniques, such as PET, proved to be superior, especially in the staging of extraprostatic disease, in the restaging after biochemical relapse and in response assessment.

At the recent EANM Focus 1 meeting on imaging of PCa, CT and diphosphonate bone scanning were rarely recommended for most patients. On the other side mpMRI and especially prostate cancer-targeted PET were frequently advocated[19].

Radiolabeled ligands for PET can target various aspects of tumor biology *in vivo* such as an enhanced glucose metabolism or an unregulated cell proliferation *via* [^{18}F]fluorodeoxyglucose (FDG) or e.g. choline-based tracers, respectively[78, 79]. Despite promising initial results in PCa patients, it was found that many metabolic PET agents, including ^{18}F-FDG, ^{11}C-acetate, ^{11}C-choline or ^{18}F-choline, still displayed insufficient overall detection rates[80-84]. Among these, choline-based tracers were most intensively evaluated, particularly for the diagnosis of metastatic lymph nodes but revealed only a moderate pooled sensitivity of 49%, as determined in a meta-analysis conducted in 2013[85].

In contrast, PSMA-addressing PET probes show outstanding potential to further increase detection rates and considerably improve the clinical management of patients suffering from PCa. Currently, the most widely employed and investigated PSMA-targeted ligands for PET applications are either labeled with [^{68}Ga]gallium or [^{18}F]fluorine.

4.1 ^{68}Ga-labeled PSMA-targeted ligands

The radiometal ^{68}Ga ($t_{½}$ = 68 min), possesses suitable decay characteristics ($E_{\beta+,\,mean}$ = 0.83 MeV, 90%) for PET imaging and is readily available from commercially distributed ^{68}Ge/^{68}Ga radionuclide generators. However, the overall activity, obtained from a single batch production from conventional generators (typically with a max. activity of 1.8 GBq) is sufficient for only 3-4 patients under optimal conditions (≈ 1.5 GBq product activity)[86]. To meet the needs of large PET centers, several productions per day or multiple generators are required, which significantly increases costs. Moreover, in combination with the rather short half-life, in house productions are favorable, and delivery to remote clinics is challenging[87]. Nevertheless, ^{68}Ga-labeled ligands are currently the most commonly used class of PSMA-addressing compounds for PCa imaging[88].

PSMA-11

In 2012, Eder *et al.* introduced [^{68}Ga]PSMA-11 (PSMA-HBED-CC), which is routinely used in many clinics for PET imaging of PCa[89, 90]. Herein, the urea-based binding motif EuK is connected through a spacer to the open chained HBED-CC (*N,N*'-bis[2-hydroxy-5-(carboxyethyl)benzyl] ethylenediamine-*N,N*'-diacetic acid) chelator, which allows chelation of gallium with fast kinetics, even at ambient temperatures and results in complexes of high stability[91]. Due to its favorable sensitivity and specificity, [^{68}Ga]PSMA-11 proved in several studies its eligibility for the diagnosis of PCa, especially for the detection of lymph node and bone metastases[92, 93]. Compared to ^{11}C-choline as well as to ^{18}F-fluorocholine, [^{68}Ga]PSMA-11 showed significantly higher tumor uptake and better detection rates, especially at low PSA levels[94, 95].

PSMA I&T

Encouraged by the immense impact of PSMA-11, Wirtz *et al.* introduced the theranostic ligand PSMA I&T (for Imaging & Therapy) in 2015[96]. This molecule features a EuK binding motif, conjugated to a highly optimized peptidic spacer, designed for improved PSMA affinities and internalization rates. Due to the implemented cyclen-based DOTA-GA (2-(4,7,10-tris(carboxymethyl)-1,4,7,10-tetraazacyclododecan-1-yl)pentanedioic acid) chelator, PSMA I&T offers the possibility to be labeled with a variety of other trivalent radiometal cations, additional to ^{68}Ga, such as ^{177}Lu, ^{90}Y or ^{213}Bi, enabling its further use for

endoradiotherapeutic treatment of PCa[96]. Moreover, in a first proof-of-concept study, ^{111}In-complexed PSMA I&T was successfully used for preoperative SPECT/CT imaging and subsequent radioguided removal of tumor lesions[97].

PSMA-617

A different theranostic compound initially tested for ^{68}Ga-based PET imaging of PCa is PSMA-617. The ligand is equipped with a PSMA-addressing EuK moiety, connected *via* a short peptidic sequence to a DOTA (1,4,7,10-tetraazacyclododecane-1,4,7,10-tetraacetic acid) chelator, which allows complexation with a wide range of radiometals for diagnostic and therapeutic purposes, similar to PSMA I&T. A unique characteristic of [^{68}Ga]PSMA-617 is its fast renal excretion in rodents, which was however not completely transferable to human applications[98].

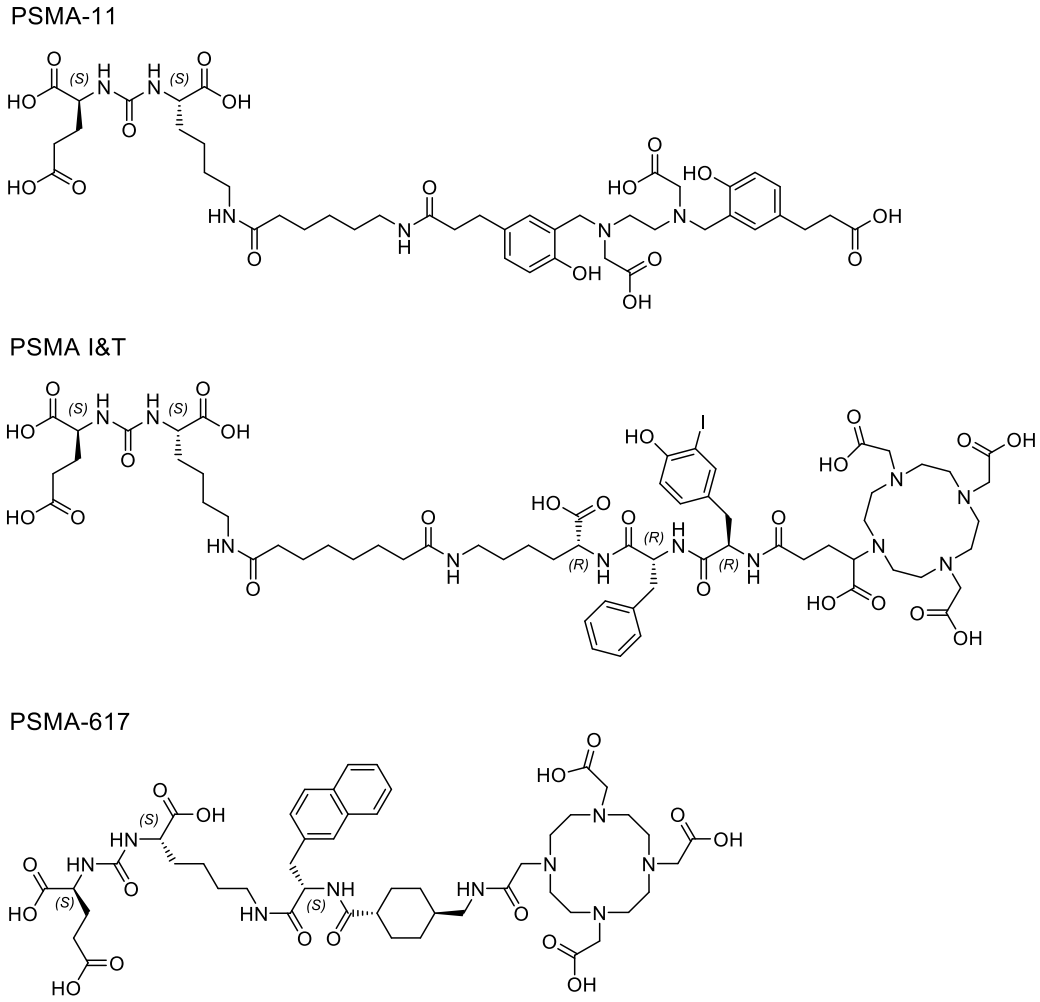

Figure 3: PSMA-targeted ligands: PSMA-11, PSMA I&T and PSMA-617 which are used for ^{68}Ga-labeling and PET imaging of PCa.

4.2. ^{18}F-labeled PSMA-targeted ligands

Recently, several groups have focused on the development of novel PSMA-targeted ligands which can be labeled with ^{18}F ($E_{\beta+,\,mean}$ = 0.25 MeV, 97%). Due to its longer half-life ($t_{½}$ = 109.8 min) and its lower positron energy, ^{18}F-labeled ligands offer advantages in terms of routine handling and image quality, compared to their ^{68}Ga-labeled counterparts[99]. Additionally, the possibility of a large-scale production in a cyclotron, routinely with starting activities of 100 GBq and more, could increase the patient throughput per clinical production and therefore reduce costs. In combination with the sufficiently long half-life, a centralized production and following delivery to distant satellite centers become feasible, which provides especially smaller clinics access to PET radiopharmaceuticals[87].

[^{18}F]DCFBC

One of the first ^{18}F-labeled PSMA-addressing ligands was [^{18}F]DCFBC, introduced in 2008 by Mease *et al.*[100]. The low-molecular-weight compound features an urea-bridged Glu-urea-Cys binding moiety (EuC), connected to the radiolabeled [^{18}F]fluorobenzyl group. This first-generation ligand demonstrated the ability to detect high-grade primary PCa and metastatic lesions[101]. However, a major drawback of [^{18}F]DCFBC is its slow clearance kinetic and concomitant high blood pool activities, which can potentially interfere with the detection of lymph node metastases, that are adjacent to large blood vessels, especially in the retroperitoneum and pelvis[102, 103].

[^{18}F]DCFPyL

In the following years, the same group developed the successor molecule [^{18}F]DCFPyL[104]. The core of this second-generation agent is made up of the EuK moiety, which is further functionalized with a ^{18}F-labeled nicotinic acid derivative. Due to its increased PSMA-affinity and rapid plasma clearance, [^{18}F]DCFPyL demonstrated higher tumor uptakes, compared to [^{18}F]DCFBC, resulting in optimized tumor-to-background ratios and especially in lower liver accumulation[105]. Despite considerable activity accumulation in the urinary system and fast appearance in the bladder, [^{18}F]DCFPyL demonstrated superiority in the detection of metastatic lesions, compared to the golden standard [^{68}Ga]PSMA-11 in a small preliminary study and is currently further evaluated in clinical trials[106].

[^{18}F]PSMA-1007

With the intention to transfer the favorable biodistribution behavior of [^{177}Lu]PSMA-617 to a ^{18}F-labeled PSMA tracer, the structural analogue [^{18}F]PSMA-1007 was developed. Herein, a peptide backbone that is structurally based on PSMA-617, is conjugated *via* two glutamic acids to 6-[^{18}F]fluoronicotinic acid[107]. First patient studies revealed a slow tracer kinetic, resulting in favorable tumor-to-background ratios at late imaging time points (i.e. 2-3 h post injection)[108]. [^{18}F]PSMA-1007 is mainly excreted *via* the hepatobiliary system, which potentially limits the sensitivity of the tracer in detecting liver metastases[109]. However, tracer-associated accumulation in the urinary bladder over time is very low, leading to improved contrast of adjacent PCa lesions[110].

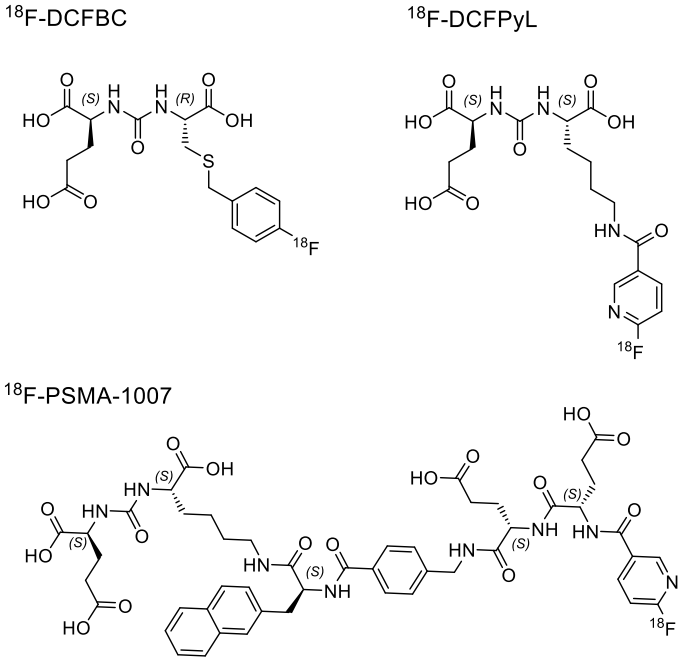

Figure 4: ^{18}F-labeled PSMA-targeted ligands, [^{18}F]DCFBC, [^{18}F]DCFPyL and [^{18}F]PSMA-1007 which are used for PET imaging of PCa.

5. Endoradiotherapy of PCa

In approximately 10-20% of patients suffering from prostate cancer, metastatic castration-resistant prostate cancer (mCRPC) develops within 5 years of follow-up[111]. It broadly defines disease progression, despite surgical or medical castration and is considered as the lethal form of the disease[112]. After failure of initial curative treatment attempts (i.e. radical prostatectomy and external radiation therapy), conventional therapeutic approaches for progressed disease include chemotherapy, androgen-ablation and radionuclide therapy with $^{223}RaCl_3$ (Xofigo). Despite the continuous advances in the treatment of PCa, prognosis for patients suffering from mCRPC is still poor[16, 113].

As a consequence of the urgent need for improved treatment protocols, especially for patients with late-stage disease, the receptor-targeted radioligand therapy (RLT) was introduced. Herein, PSMA-addressing ligands are labeled with therapeutic α- or β^--emitting nuclides, in order to deliver a cytotoxic level of radiation directly to the target tissue and to ideally minimize damage to healthy tissues[114].

Initial studies at Johns Hopkins in 2002, with [^{123}I]MIP-1095 for SPECT, paved the way for the first-ever endoradiotherapy of mCRPC with a small-molecule compound, using the ^{131}I-labeled structural analogue[115]. Based on the patient-individual dose estimation, applying the ^{124}I-labeled compound in PET, RLT was conducted on 28 patients under a compassionate-use protocol with one cycle of [^{131}I]MIP-1095. A good therapy response, defined by a PSA decline of > 50%, was observed in 61% of patients and modest to complete reduction of bone-pain was achieved in 85%[116].

Based on the extensive research efforts in the following years, ^{177}Lu-labeled PSMA I&T and PSMA-617 were developed by our group and the German Cancer Research Center, respectively, and are currently the most often used compounds for endoradiotherapy of PCa. Comparison of the biodistribution profiles of both ligands in mice, revealed an almost identical *in vivo* behavior with similar uptake in all organs, except of the kidneys, in which a significantly lower accumulation was observed for [^{177}Lu]PSMA-617[96, 98]. The extremely fast renal excretion in rodents was however not observed in humans, as demonstrated in a comparative study with [^{177}Lu]PSMA I&T, carried out in Bad Berka[117]. The results point towards a nearly identical pharmacokinetic of both tracers and clinical efficacy is assumed to be similar with no clear advantage of one compound[117]. During therapy, no severe acute or long-term side effects

were observed, besides xerestomia[118, 119]. Due to the favorable safety and high efficacy, RLT with ^{177}Lu-labeled PSMA-addressing ligands is considered to be superior to other third-line therapies in mCRPC patients, as determined in a German multicenter study[120].

6. Silicon Fluoride Acceptors in radiopharmacy

The introduction of [^{18}F]fluorine into molecules can be achieved by nucleophilic or electrophilic reactions, starting from [^{18}F]fluoride or [^{18}F]fluorine gas (and subsequently generated electrophilic species thereof), respectively. In the majority of the developed and routinely applied synthetic pathways, ^{18}F-incorporation is achieved *via* carbon-fluorine bond formation, most commonly in order to avoid large structural modifications that might impair biological properties, especially in small-molecule compounds. Since direct C-F bond creating reactions typically require alkaline conditions and dipolar aprotic solvents, they are not applicable to larger molecules, such as peptides or proteins. In these cases, a common approach is to use prosthetic groups that are ^{18}F-labeled and conjugated to the biologically active compound afterwards[121-123].

Generally, an ideal ^{18}F-labeling reaction should proceed fast, under mild reaction conditions (e.g. low temperature, no aggressive/toxic additives) and without the need for a time-consuming HPLC-based purification step yielding the product in high radiochemical yields and molar activities. Further, with respect to clinical infrastructure, simple and robust approaches that can be accomplished without major technical skills and minimal technical equipment are highly desired. Most of the conventional labeling approaches do not fulfill all of these requirements and much research effort has been devoted into the optimization and development of novel ^{18}F-labeling techniques[121-123]. In this context the isotopic exchange (IE) of stable (natural) ^{19}F-fluoride by the PET isotope ^{18}F-fluoride, was introduced as a promising new concept for radiopharmaceutical applications.

6.1 Historical development

As early as 1984, Kilbourn and co-workers described the successful synthesis of the neuroleptics [^{18}F]Spiroperidol and [^{18}F]Haloperidol by means of isotopic exchange[124]. This and most of following works were IE reactions based at C-F bonds. However, due to the necessity of harsh reaction conditions, high precursor amounts and time-consuming purification steps, the ^{18}F-labeled products were obtained in low radiochemical yields and low molar activities, unsuitable for *in vivo* applications[124-126]. From a historical point of view, the insufficient molar activity is considered as the major reason why IE reactions based on C-F bonds have never

found widespread application in the synthesis of PET radiopharmaceuticals[127]. In order to circumvent this limitation, the ^{18}F-labeling approach by means of IE was further examined on the boron-fluoride and silicon-fluoride bond.

In the case of boron-fluorides, the first examples in radiochemistry were described in the early 1960s and solely based on [^{18}F]tetrafluoroborates, which were synthesized by IE starting from metal ^{18}F-fluorides[128, 129]. Ligands bearing B-^{18}F bonds did however not find widespread application in radiopharmacy until 2005, when Perrin and co-workers re-discovered the concept and introduced arylfluoroborates as valuable functional building blocks in the synthesis of PET probes[130]. From there on, the labeling approach was steadily optimized and applied in several ligand systems, for imaging of e.g. somatostatin type-2 receptors[131], gastrin-releasing peptide receptors[132], integrins[133] or lately PSMA[134].

Due to similar chemical characteristics, the history of radioligands based on the Si-^{18}F bond is closely related to the aforementioned development of boron-fluoride radiochemistry. Starting in 1958, the first IE reactions were examined on SiF_4 and alkyfluorosilanes using different metal ^{18}F-fluorides[135-137]. The first *in vivo* application of a Si-^{18}F compound, [^{18}F]fluorotrimethylsilane, was described in 1985 by Rosenthal and co-workers. However [^{18}F]fluorotrimethylsilane was found to be instantly hydrolyzed, resulting in the release of free [^{18}F]fluoride. Already back then, the authors postulated the necessity of bulky substituents around the silicon in order to decrease the hydrolysis rate of silicon-fluorides[138]. In addition, Walsh *et al.* reiterated to shield the Si-F bond to increase hydrolytic stability during the examination of alkoxysilanes as potential ^{18}F-labeling precursors[139]. In 2006, the working group of Schirrmacher proved that sterically demanding substituents around the silicon (e.g. phenyls or branched alkyls) could preserve the Si-^{18}F bond and prevent fast hydrolysis in aqueous media[140]. These results were supported by the findings of Blower and co-workers working on ^{18}F-fluorination of alkoxysilanes in nucleophilic substitutions[141]. A systematic evaluation of different silicon fluoride acceptor (SiFA) building blocks confirmed the strong correlation between the hydrolytic half-life of the Si-F bond and the steric nature of the substituents at the silicon[142]. Based on the aforementioned studies, fluoro-di-*tert*-butylphenylsilane and *para*-substituted analogues thereof were further investigated. *In vivo*

studies in mice with [^{18}F]SiFA-TATE, an octreotate-based somatostatin receptor agonist, revealed no elevated activity accumulation in bone and thus high hydrolytic stability of the Si-^{18}F bond. However, due to the bulky and highly lipophilic SiFA, the activity was predominantly accumulating in the liver and gastrointestinal system[143]. More recent examples and further optimization of the SiFA-methodology are summarized in chapter "6.3 State of the Art of SiFA-bearing ligands".

6.2 Labeling chemistry

6.2.1 General aspects

Silicon and fluorine display by nature a strong affinity to each other, which is also expressed by the high bond energy of 565 kJ/mol, compared to 485 kJ/mol of C-F bonds[144]. The strong difference in electronegativity of silicon and fluorine results in a high polarization of the Si-F bond and explains the kinetic instability of simple organofluorosilanes, which is mandatory for IE with [^{18}F]fluoride or reactions with other silophiles[145, 146]. Moreover, the vacant low energy d-orbitals of tetravalent silicon allow the formation of hypervalent (5- or 6-coordinated) intermediates in reactions with Lewis bases[147, 148]. Due to the greater covalent radius of silicon, compared to carbon, organosilanes tend to be more prone for nucleophilic substitutions at the silicon atom, as their carbon-centered analogues[146]. These unique characteristics of organofluorosilanes build the foundation for the development of the ^{18}F-labeling methodology based on silicon fluoride acceptors.

6.2.2 Mechanism and energetic analysis

In order to shed light upon the underlying mechanism and energy profile, the IE reaction was examined in detail for different exemplary SiFA groups by means of density functional theory (DFT) calculations and kinetic experiments. The IE of fluoride at the tetravalent silicon atom was proposed to proceed *via* the formation of a pentacoordinate trigonal bipyramidal siliconate anion in analogy to the known mechanisms for nucleophilic substitutions at silicon (Figure 5)[148-150].

DFT calculations of the enthalpy and Gibbs free energy revealed that the energy barrier during the isoenergetic replacement of ^{19}F-fluoride by ^{18}F-fluoride is very low and the equilibrium is reached very rapidly, which is favorable for efficient and fast fluoride exchange at

organofluorosilanes. Moreover, due to the small concentration of $^{19}F^-$ and the ^{18}F-labeled SiFA, a reaction of both is unlikely which makes the IE reaction virtually irreversible[149].

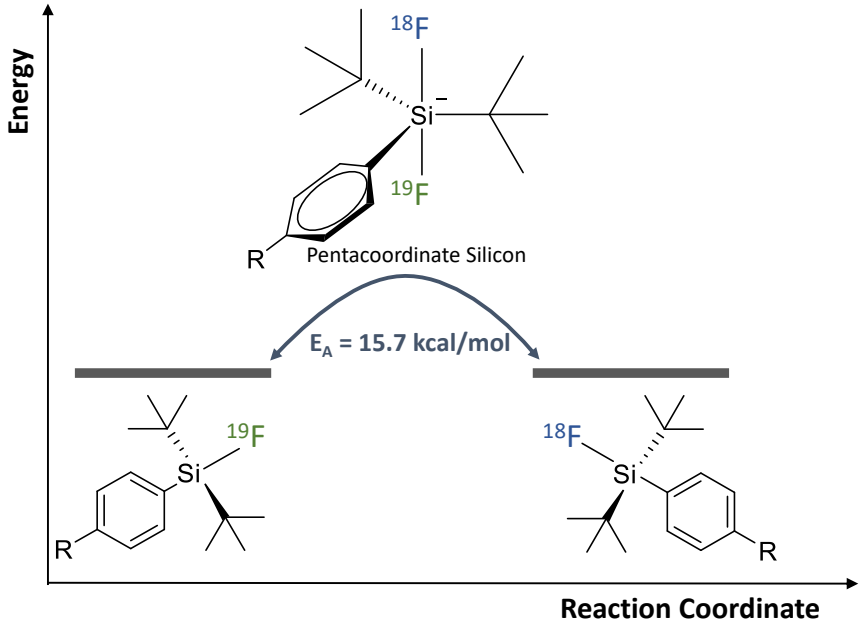

Figure 5: Energy diagram of the isoenergetic ^{19}F-^{18}F isotopic exchange at a di-*tert*-butylfluoro(phenyl)silane derivative. Proposed mechanism *via* formation of the trigonal bipyramidal siliconate anion intermediate. The activation energy (E_A) was determined for ^{18}F-labeling of $SiFAN^+Br^-$ [151].

Further kinetic studies were conducted in order to verify the obtained theoretical calculations by experimentally determining the Arrhenius preexponential factor (*A*) and activation energy (E_a) for the ^{19}F-^{18}F isotopic exchange at an exemplary model compound ($SiFAN^+Br^-$; *N*-(4-(di-*tert*-butylfluorosilyl)benzyl)-2-hydroxy-*N*,*N*-dimethylethylammonium bromide)[151]. The Arrhenius preexponential factor represents the frequency of collisions between reactant molecules and was found to be four orders of magnitudes larger than measured for ^{18}F-fluorination of ethyleneglycol-di-*p*-tosylate, which represents a commonly applied prosthetic group for labeling of precursor molecules in radiochemistry ($A_{SiFA} = 7.6 \times 10^{13}\ M^{-1}s^{-1}$ versus $A_{Tosylate} = 2.9 \times 10^{9}\ M^{-1}s^{-1}$)[151, 152]. The activation energy for the IE reaction at the SiFA group was measured to be 15.7 kcal/mol, which is slightly lower than for the ^{18}F-labeling of ethyleneglycol-di-*p*-tosylate (E_a = 17.1 kcal/mol)[151]. In combination, both kinetic parameters serve as an explanation for the experimentally observed high rates of fluoride exchange at silicon fluoride acceptors in a short time interval at low temperatures.

6.2.3 ^{18}F-labeling of Silicon Fluoride Acceptors

In fluoro-di-*tert*-butylphenylsilane, which is one of the most commonly applied silicon fluoride acceptor, the Si-F bond is shielded by two *tert*-butyl groups and a phenyl ring. In order to ensure facile conjugation to a biological active ligand, different functional groups were introduced at the *para*-position, like e.g. a carboxylic acid (SiFA-benzoic acid; SiFA-BA)[153] or an aldehyde (SiFA-aldehyde; SiFA-A)[140, 149].

In ^{18}F-labeling reactions of SiFA-BA and derivatives, radiochemical ^{18}F-incorporation of > 80% were observed resulting in a final RCY of approximately 50 ± 10% after purification. Moreover, the IE proceeded fast (5 min) and at ambient temperature. The typically applied amount of the precursor was low (25-150 nmol) which resulted in non-optimized molar activities of up to 60 GBq/µmol. Due to the mild reaction conditions, no side products were detected and thus allowed for a simple and fast cartridge-based purification of the tracers (Figure 6)[143, 154-156].

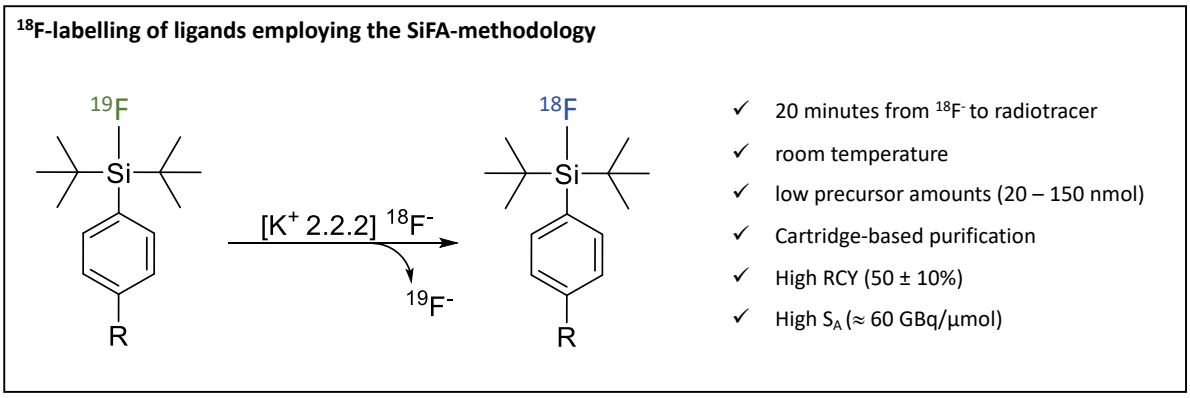

Figure 6: Isotopic exchange reaction at the SiFA moiety, employing the *Munich Method* for drying of [^{18}F]fluoride and elution with [$K^+ \subset$ 2.2.2]OH^- [157]. The shown characteristics were reported for labeling of SiFA-bearing octreotate derivatives[127, 143, 155, 156].

The reaction is preferably performed in dry, aprotic media due to strong hydrogen bonding of [^{18}F]fluoride in aqueous solution, which reduces its nucleophilic properties[140, 158]. The rather time-consuming drying step, e.g. azeotropically under reduced pressure with acetonitrile can be avoided due to the compatibility of the SiFA-labeling approach with the so-called *Munich Method*[156, 157]. In this drying process [^{18}F]fluoride is trapped on a strong anion exchange cartridge which is then purged with air and acetonitrile. Afterwards "dried" [^{18}F]fluoride can be eluted by a suitable salt, which is most commonly the complex formed by Kryptofix 222 (4,7,13,16,21,24-Hexaoxa-1,10-diazabicyclo[8.8.8]hexacosane) and potassium hydroxide[157].

In combination with the *Munich Method*, the ^{18}F-labeling of a peptide, bearing a SiFA group can be typically performed in less than 20 minutes in a manual procedure[127]. Noteworthy, Schirrmacher and others demonstrated that the IE reaction at the SiFA moiety even proceeds in aqueous solutions upon heating after longer reaction times[140, 159].

6.3 State of the art of SiFA-bearing ligands

Hitherto, the SiFA-methodology has been applied in various ligands for imaging of e.g. $\alpha_v\beta_3$ integrins[154], gastrin-releasing peptide receptors[154], transferrin receptors[160] and somatostatin receptors[140] – with a strong focus on the latter. In initial preclinical *in vivo* studies of SiFA-functionalized octreotate derivatives, most of the injected activity was found in the liver and gastro-intestinal system, which was proposed to be a consequence of the strong lipophilic nature of fluoro-di-*tert*-butylphenylsilane resulting in excretion mostly *via* the hepatobiliary pathway (Figure 7)[143]. With the aim to increase hydrophilicity of following generations of SiFA-containing peptides, incorporation of hydrophilic modifiers such as carboxylic acids, carbohydrates or polyethylene glycol, and combinations thereof were tested [143, 154, 155, 161]. Moreover, a positive charge in the form of a tertiary ammonium salt was introduced in the SiFA building block[151]. Applying these strategies, the lipophilicity of initial SiFA-octreotates (octanol-water partition coefficient; log $P_{O/W}$ = 2.2) could be significantly increased (third-generation SiFA-ocreotates; log $P_{O/W}$ = −1.2), which resulted in a markedly improved *in vivo* performance in preclinical experiments (Figure 7)[143].

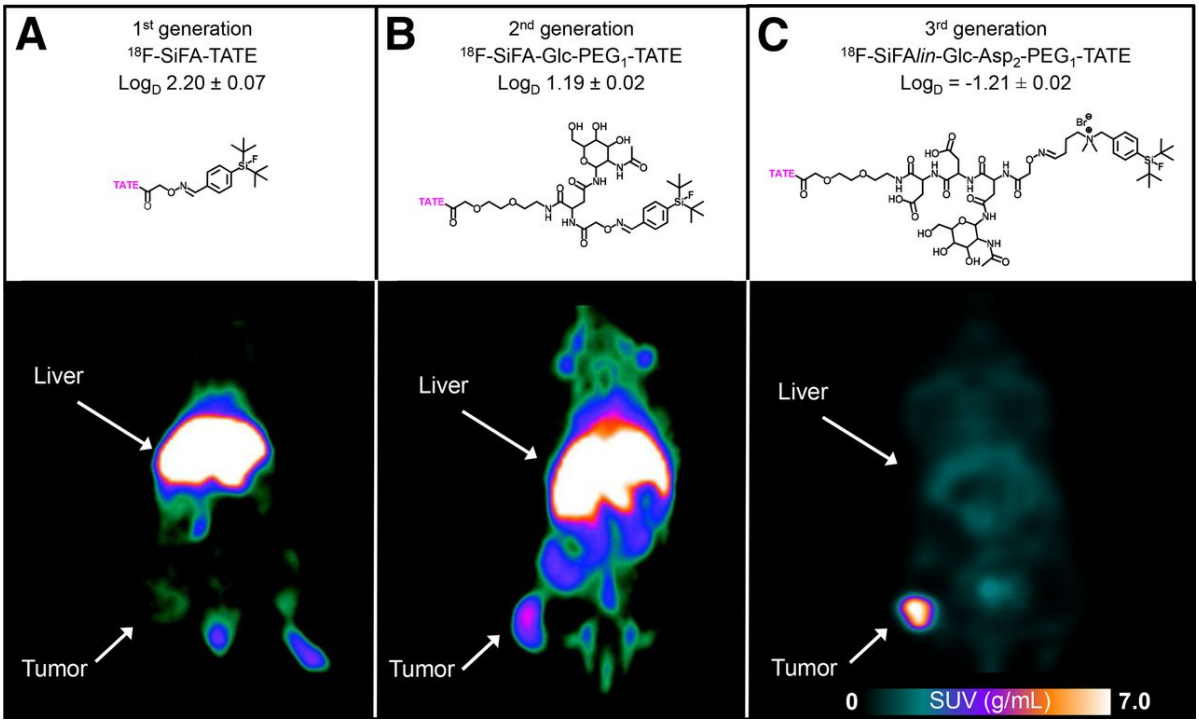

Figure 7: Illustration of the development process of SiFA-bearing somatostatin analogs. Small-animal PET images (coronal slices, 50-90 min p.i.) were evaluated in AR42J tumor-bearing rodents: **A**) ^{18}F-SiFA-TATE, **B**) ^{18}F-SiFA-Glc-PEG$_1$-TATE, **C**) ^{18}F-SiFAlin-Glc-Asp$_2$-PEG$_1$-TATE. SUV: standardized uptake value. Figures were taken from Niedermoser *et al.*[143].

Hitherto, the highest hydrophilicity for a SiFA-tagged compound was reported for an RGD (arginine-glycine-aspartic acid) peptide, targeting $\alpha_v\beta_3$ integrins (log $P_{O/W}$ = −2.0), which is however still significantly lower compared to well investigated ^{68}Ga- or ^{18}F-labeled agents (e.g. [^{68}Ga]avebetrin; log $P_{O/W}$ = −3.9 or [^{18}F]Galacto-RGD; log $P_{O/W}$ = −3.2)[154, 162, 163].

The strong lipophilic character of SiFA conjugates can serve as an explanation for the often-observed high off-target accumulation in preclinical studies, resulting in lower tumor-to-background values, compared to reference ligands[143, 154, 155, 161]. As a consequence, none of the SiFA-bearing ligands described so far showed the potential for a translation to first proof-of-concept studies in humans. Thus, a confirmation of whether [^{18}F]SiFA can provide sufficiently hydrolytic stability in humans and does not result in detectable ^{18}F-fluoride uptake in bone is still missing.

7. Objectives

The favorable expression characteristics of PSMA in PCa allowed for the development of highly optimized PSMA-targeted radiopharmaceuticals for diagnostic and therapeutic applications, and their rapid bench-to-bedside translation. For PET imaging an emerging demand arose especially for ^{18}F-labeled ligands due to possibility of large-scale productions and favorable nuclide properties. However, a major disadvantage of this class of PET tracers lies in commonly elaborate and time-consuming radiolabeling procedures, resulting in low radiochemical yields and molar activities. In order to circumvent these limitations, new unorthodox strategies like e.g. the ^{18}F-^{19}F isotopic exchange reaction at silicon fluoride acceptors (SiFAs) have been developed and enabled ^{18}F-labeling in high yields in simple and fast procedures. The main drawback is the necessity of bulky groups at the SiFA moiety to ensure sufficient stability of the Si-F bond, which however increased lipophilicity and resulted in unfavorable biodistribution profiles of SiFA conjugates, preventing their clinical translation.

For that reason, the primary objective of this work was to develop a universally applicable methodology to increase the hydrophilicity of SiFA-bearing ligands. Therefore, a hydrophilic chelator should be implemented in close proximity to the SiFA group in order to outbalance its lipophilic nature. The key feature of this approach is the possibility of complexation of (radio)metals, resulting in radiohybrid (rh) ligands, in which either covalently bond fluorine or the chelated metal is present as radioactive isotope. Therefore, both the ^{18}F-labeled cold metal complex (e.g. [^{18}F][^{nat}Ga]rhPSMA) and the radiometallated ligand (e.g. [^{19}F][^{68}Ga]rhPSMA) display the identical chemical structure and thus identical targeting capacities, *in vivo* distribution and pharmacokinetics.

The concept should be initially validated for PSMA-addressing ligands with gallium, as complexed metal cation. With respect to clinical infrastructure, equipment and specific requirements either the ^{18}F-labeled [^{nat}Ga]rhPSMA or the respective ^{68}Ga-labeled [^{19}F]rhPSMA ligand can be applied for PET imaging of PCa. Due to the chemical identity, the experiences obtained with one ligand can be transferred to the other twin (Figure 8 A).

A further objective of this work was the development of the theranostic radiohybrid concept. Complexation by lutetium allows for application of the [^{177}Lu][^{19}F]rhPSMA compound for peptide radioligand therapy of PCa. Likewise, the ^{18}F-labeled [^{nat}Lu]rhPSMA can be employed for PET-based diagnosis, dosimetry and follow-up imaging. Theranostic radiohybrids could

therefore further advance personalized medicine by providing one probe, which would truly bridge PET-based imaging and therapy (Figure 8 B).

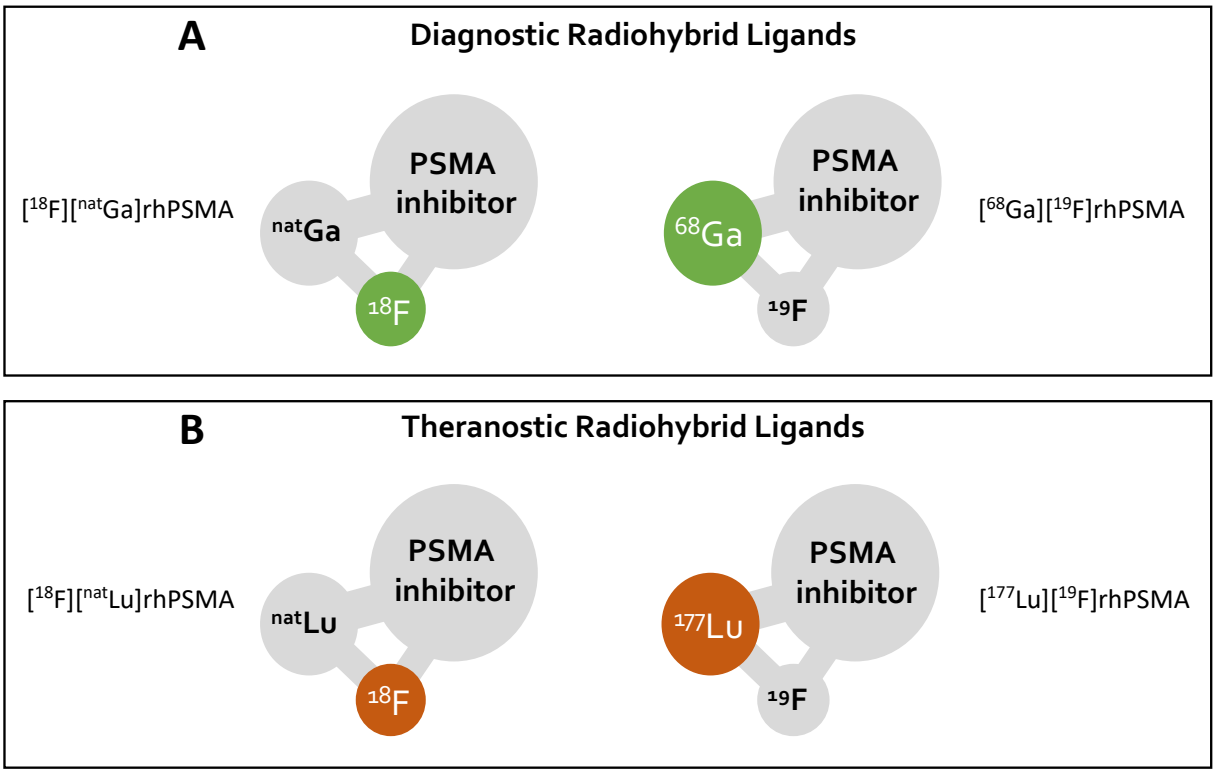

Figure 8: The radiohybrid concept exemplified on PSMA inhibitors: a molecular species that offers two binding sites for radionuclides, a Silicon Fluoride Acceptor (SiFA) for [^{18}F]fluorine and a chelate for radiometallation. One of these binding sites is "labeled" with a radioisotope, the other one is silent, thus "labeled" with a nonradioactive isotope. These pair of compounds, either pure imaging pairs (**A**) or theranostic pairs (**B**) represent chemically identical species (monozygotic chemical twins) and thus exhibit identical *in vivo* characteristics (affinity, lipophilicity, pharmacokinetics, etc.). Note: ^{68}Ga in (**A**) and ^{177}Lu in (**B**) are examples that can be substituted by other (radio)metals.

Regarding ^{18}F-labeling chemistry, the procedure described in literature for [^{18}F]fluorination of SiFA-bearing compounds should be optimized in this work for rhPSMA ligands. In order to provide clinics access to ^{18}F-labeled rhPSMA ligands, an automated process for GMP-compliant radiosynthesis should be developed. Thereafter, it should be investigated, whether an efficient and fast [^{18}F]fluorination of SiFA ligands can also be established in an aqueous solution, thus further simplifying the automated production process.

II. Material and Methods

1. General information

The protected amino acid analogs were purchased from Bachem (Bubendorf, Switzerland), Carbolution Chemicals (St. Ingbert, Germany) or Iris Biotech (Marktredwitz, Germany). The 2-Chlorotrityl chloride resin (2-CTC) resin was obtained from Sigma-Aldrich (Steinheim, Germany). Chematech (Dijon, France) delivered the chelators NOTA, DOTA, DOTA-GA and derivatives thereof. All necessary solvents and other organic reagents were purchased from either Alfa Aesar (Karlsruhe, Germany), Sigma-Aldrich (Steinheim, Germany), Fluorochem (Hadfield, United Kingdom) or VWR (Darmstadt, Germany). Solid-phase peptide synthesis was carried out by manual operation using a syringe shaker (Intelli-Mixer, Neolab, Heidelberg, Germany). Analytical and preparative high-performance liquid chromatography (HPLC) was performed using Shimadzu gradient systems (Shimadzu, Neufahrn, Germany), each equipped with a SPD-20A UV/Vis detector (220 nm, 254 nm). A Nucleosil 100 C18 (125 × 4.6 mm, 5 µm particle size) column (CS Chromatographie Service, Langerwehe, Germany) was used for analytical measurements at a flow rate of 1 mL/min. Specific gradients, the corresponding retention times (t_R) and the capacity factors (K') are cited in the text. Preparative HPLC purification was done with a Multospher 100 RP-18 (250 × 10 mm, 5 µm particle size) column (CS Chromatographie Service) at a constant flow rate of 5 mL/min. Analytical and preparative radio-RP-HPLC was performed using a Nucleosil 100 C18 (125 × 4.0 mm, 5 µm particle size) column (CS Chromatographie Service). Eluents for all HPLC operations were water (solvent A) and acetonitrile (solvent B), both containing 0.1% trifluoroacetic acid. Electrospray ionization-mass spectra for characterization of the substances were acquired on an Expression^L CMS mass spectrometer (Advion, Harlow, United Kingdom). Radioactivity was detected through connection of the outlet of the UV-photometer to a HERM LB 500 NaI detector (Berthold Technologies, Bad Wildbad, Germany). NMR spectra were recorded on Bruker (Billerica, United States) AVHD-300 or AVHD-400 spectrometers at 300 K. pH values were measured with a SevenEasy pH-meter (Mettler Toledo, Gießen, Germany). Activity quantification was performed using a 2480 WIZARD^2 automatic gamma counter (PerkinElmer, Waltham, United States). Radio-thin layer chromatography (TLC) was carried out with a Scan-RAM detector (LabLogic Systems, Sheffield, United Kingdom).

2. Solid-phase peptide synthesis

2-CTC resin loading (General Procedure 1 (GP1))

Loading of the 2-Chlorotrityl chloride resin (2-CTC) resin with a Fmoc-protected amino acid (AA) was carried out by stirring a solution of the 2-CTC resin (1.60 mmol/g) and Fmoc-AA-OH (1.5 eq.) in anhydrous DCM with DIPEA (3.8 eq.) at rt for 2 h. Remaining tritylchloride was capped by the addition of methanol (2 mL/g resin) for 15 min. Subsequently the resin was filtered and washed with DCM (2 × 5 mL/g resin), DMF (2 × 5 mL/g resin), methanol (5 mL/g resin) and dried *in vacuo*. Final loading *l* of Fmoc-AA-OH was determined by the following equation:

$$l\ \left[\frac{mmol}{g}\right] = \frac{(m_2 - m_1)\times 1000}{(M_W - M_{HCl})\ m_2}$$

m_2 = mass of loaded resin [g]
m_1 = mass of unloaded resin [g]
M_W = molecular weight of AA [g/mol]
M_{HCl} = molecular weight of HCl [g/mol]

On-resin amide bond formation (GP2)

For conjugation of a building block to the resin-bound peptide, a mixture of TBTU with HOBt or HOAt was used for pre-activation of the carboxylic acid with DIPEA or 2,4,6-trimethylpyridine as a base in DMF (10 mL/g resin). After 5 min at rt, the solution was added to the swollen resin. The exact stoichiometry and reaction time for each conjugation step is given in the respective synthesis protocols. After reaction, the resin was washed with DMF (6 × 5 mL/g resin).

On-resin Fmoc-deprotection (GP3)

The resin-bound Fmoc-peptide was treated with 20% piperidine in DMF (*v*/*v*, 8 mL/g resin) for 5 min and subsequently for 15 min. Afterwards, the resin was washed thoroughly with DMF (8 × 5 mL/g resin).

On-resin Dde-deprotection (GP4)

The Dde-protected peptide was dissolved in a solution of 2% hydrazine monohydrate in DMF (*v*/*v*, 5 mL/g resin) and shaken for 20 min (GP4a). In the case of present Fmoc-groups,

Dde-deprotection was performed by adding a solution of imidazole (0.92 g/g resin), hydroxylamine hydrochloride (1.26 g/g resin) in NMP (5.0 mL/g resin) and DMF (1.0 mL/g resin) for 3 h at rt (GP4b). After deprotection the resin was washed with DMF (8 × 5 mL/g resin).

On-resin Allyl-deprotection (GP5)

The allyl-protecting group was removed by the addition of triisopropylsilane (TIPS, 50.0 eq.) and tetrakis(triphenylphosphine)palladium(0) ($Pd(PPh_3)_4$, 0.3 eq.) dissolved in DCM (8 mL/g resin). After 1.5 h at rt, the resin was washed with DCM (6 × 5 mL/g resin) and DMF (6 × 5 mL/g resin).

tBu/Boc deprotection (GP6)

Removal of *t*Bu/Boc-protecting groups was carried out by dissolving the crude product in a mixture of TFA/TIPS/water (*v*/*v*/*v*; 95/2.5/2.5) and stirring for 1-6 h at rt. Product formation was monitored by RP-HPLC analysis. The solvent was evaporated and the residue was dissolved in a mixture of *tert*-butanol and water. After lyophilisation the crude peptide was obtained.

Peptide cleavage from the resin (GP7)

Preservation of acid labile protecting groups (GP7a): The resin-bound peptide was dissolved in a mixture of DCM/TFE/AcOH (*v*/*v*/*v*; 6/3/1, 8 mL/g resin) and shaken for 30 min. The solution containing the fully protected peptide was filtered off and the resin was treated with another portion of the cleavage solution for 30 min. Both fractions were combined and acetic acid was removed under reduced pressure by successively adding toluene and water. After lyophilisation of remaining water, the crude fully protected peptide was obtained.

Deprotection of acid labile protecting groups (GP7b): The fully protected resin-bound peptide was dissolved in a mixture of TFA/TIPS/water (*v*/*v*/*v*; 95/2.5/2.5) and shaken for 30 min. The solution was filtered off and the resin was treated in the same way for another 30 min. Both filtrates were combined, stirred for additional 1-6 h at rt. Product formation was monitored by RP-HPLC. After removing TFA under a stream of nitrogen, the residue was dissolved in a mixture of *tert*-butanol and water and freeze-dried.

3. Synthesis of PSMA-binding motifs and functionalization

Glu-urea-Glu ((tBuO)EuE(OtBu)$_2$) (1)

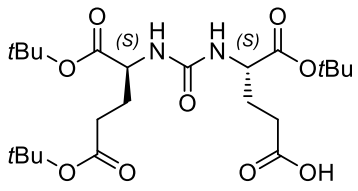

Chemical Formula: $C_{23}H_{40}N_2O_9$
Molecular Weight: 488,58

The *t*Bu-protected Glu-urea-Glu binding motif (*t*BuO)EuE(O*t*Bu)$_2$ was synthesized in analogy to a previously published procedure with some modifications[71]:

Di-*tert*-butyl (1*H*-imidazole-1-carbonyl)-*L*-glutamate (i)

A solution of DCM containing 2.00 g (7.71 mmol, 1.0 eq.) 1-di-*tert*-butyl-*L*-glutamate·HCl was cooled on ice for 30 min and afterwards treated with 2.68 mL (19.3 mmol, 2.5 eq.) TEA and 37.9 mg (0.31 mmol, 0.04 eq.) DMAP. After additional stirring for 5 min, 1.38 g (8.84 mmol, 1.1 eq.) of 1,1'-carbonyldiimidazole (CDI) dissolved in DCM were slowly added over a period of 30 min. The reaction mixture was further stirred overnight and enabled to warm to rt. The reaction was stopped using 8 mL saturated $NaHCO_3$ and subsequent washing steps with water (2 × 20 mL) and brine (2 × 20 mL). The remaining solvent was removed *in vacuo* and the crude product (*S*)-Di-*tert*-butyl 2-(1*H*-imidazole-1-carboxamido)pentanedioate (**i**) was used without further purification. RP-HPLC (10 to 90% B in 15 min): t_R = 14.5 min, K' = 5.59. Calculated monoisotopic mass ($C_{17}H_{27}N_3O_5$): 353.2; found: m/z = 376.3 $[M+Na]^+$.

5-benzyl 1-(tert-butyl) (((*S*)-1,5-di-tert-butoxy-1,5-dioxopentan-2-yl)carbamoyl)-*L*-glutamate (ii)

A solution of 2.72 g (7.71 mmol, 1.0 eq.) (*S*)-Di-*tert*-butyl-2-(1*H*-imidazole-1-carboxamido) pentanedioate (**i**) in 1,2-dichloroethane (DCE) was cooled on ice for 30 min. After the addition of 2.15 mL (15.4 mmol, 2.0 eq.) TEA and 2.54 g (7.71 mmol, 1.0 eq.) H-*L*-Glu(OBzl)-O*t*Bu·HCl, the solution was stirred overnight at 40 °C. The remaining solvent was evaporated and the crude product purified using silica gel flash-chromatography with an eluent mixture containing ethyl acetate, hexane and TEA (*v*/*v*/*v*; 49/49/2). After removal of the solvent, 5-benzyl-1-(*tert*-butyl)-(((*S*)-1,5-di-tert-butoxy-1,5-dioxopentan-2-yl)carbamoyl)-*L*-glutamate (**ii**) was obtained

as a colourless oil. RP-HPLC (10 to 90% B in 20 min): t_R = 17.4 min, K' = 6.91. Calculated monoisotopic mass ($C_{30}H_{46}N_2O_9$): 578.3; found: m/z = 411.3 [M−3*t*Bu+H]$^+$, 467.3 [M−2*t*Bu+H]$^+$, 523.3 [M−*t*Bu+H]$^+$, 601.5 [M+Na]$^+$.

(*t*BuO)EuE(O*t*Bu)$_2$ (iii)

To synthesize (*t*BuO)EuE(O*t*Bu)$_2$**,** 3.17 g (5.47 mmol, 1.0 eq.) of 5-benzyl-1-(*tert*-butyl)-(((*S*)-1,5-di-tert-butoxy-1,5-dioxopentan-2-yl)carbamoyl)-*L*-glutamate (**ii**) were dissolved in 75 mL EtOH and 0.34 g (0.57 mmol, 0.1 eq.) palladium on activated charcoal (10%) were given to this solution. The flask containing the reaction mixture was initially purged with H_2 and the solution was stirred over night at rt under light H_2-pressure (760 Torr). The crude product was purified through Celite and the solvent evaporated *in vacuo*. The product (**iii**) was obtained as a hygroscopic solid (overall: 79%). RP-HPLC (10% to 90% B in 15 min): t_R = 11.3 min, K' = 4.14. Calculated monoisotopic mass ($C_{23}H_{49}N_2O_9$): 488.3; found: m/z = 489.4 [M+H]$^+$, 516.4 [M+Na]$^+$.

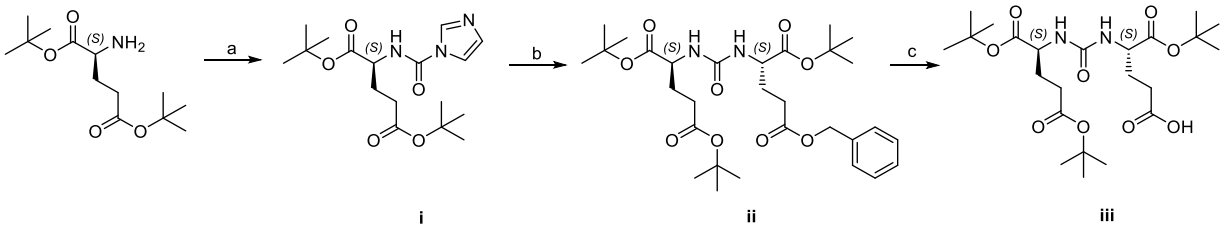

Scheme 1: Synthesis of (*t*BuO)EuE(O*t*Bu)$_2$: a) DCI, TEA, DMAP (DCM); b) H-*L*-Glu(OBzl)-O*t*Bu·HCl, TEA (DCE); c) Pd/C (10%), H_2 (EtOH).

Lys-urea-Glu ((tBuO)KuE(OtBu)$_2$) (2)

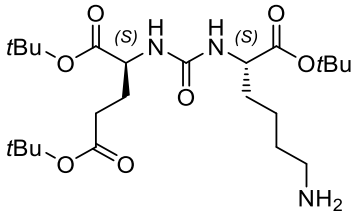

Chemical Formula: $C_{24}H_{45}N_3O_7$
Molecular Weight: 487,64

Synthesis of the *t*Bu-protected Lys-urea-Glu binding motif ((*t*BuO)KuE(O*t*Bu)$_2$*)* was carried out in analogy to (*t*BuO)EuE(O*t*Bu)$_2$ by using H-*L*-Lys(Cbz)-O*t*Bu·*HCl* instead of H-*L*-Glu(OBzl)-O*t*Bu·HCl[71]. The product was obtained as a waxy solid (overall: 89%). RP-HPLC (10 to 90% B in 15 min): t_R = 12.6 min, K' = 4.73. Calculated monoisotopic mass ($C_{24}H_{45}N_3O_7$): 487.6; found: m/z = 488.3 $[M+H]^+$, 510.3 $[M+Na]^+$.

Conjugation of (tBuO)KuE(OtBu)$_2$ (2) to the peptide (GP8)

The peptide (1.0 eq.) was dissolved in DMF (0.1 mL/mg) and HOBT (1.0 eq.), TBTU (1.0 eq.) and DIPEA (4.5 eq.) were added. After a pre-activation time of 15 min, (*t*BuO)KuE(O*t*Bu)$_2$ (1.5 eq.) was added and stirred for 12 h at rt. For cleavage of the *t*Bu-esters, TFA was added and the solution was stirred for 45 min at rt. After evaporation of the solvent, the crude product was purified by RP-HPLC.

PfpO-Sub-(tBuO)KuE(OtBu)$_2$ (3)

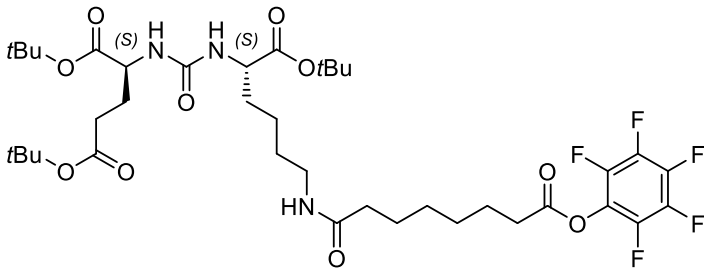

Chemical Formula: $C_{38}H_{56}F_5N_3O_{10}$
Molecular Weight: 809,87

Synthesis of the suberic acid active ester (di-pentafluorophenyl suberate, Sub(OPfP)$_2$) and conjugation to (*t*BuO)KuE(O*t*Bu)$_2$ (2) was performed as described previously[71]. Briefly, 600 mg (1.2 mmol, 1.0 eq.) of (*t*BuO)KuE(O*t*Bu)$_2$ were dissolved in THF (110 mL) and 411 µL (2.40 mmol, 2.0 eq.) DIPEA were added. The resulting solution was slowly added to a mixture

of 2.43 g (4.80 mmol, 4.0 eq.) Sub(OPfp)$_2$ in THF and stirred for 2 h at rt. After removing the solvents *in vacuo*, the crude product was purified by silica gel flash-chromatography, applying a stepwise gradient of EtOAc in hexane (*v*/*v*; 10 to 90% EtOAc). The product was obtained as a colorless oil (69%). RP-HPLC (10 to 90% B in 20 min): t_R = 15.5 min, K' = 6.05. Calculated monoisotopic mass ($C_{38}H_{56}F_5N_3O_{10}$): 809.4; found: m/z = 810.6 $[M+H]^+$, 832.4 $[M+Na]^+$.

Conjugation of the EuK-sub-moiety (3) to the peptide (GP9)

The N-terminal deprotected peptide (1.0 eq.) was added to a solution of **3** (1.2 eq.) in DMF (0.1 mL/mg peptide) and TEA (8 eq.) was added. After stirring the solution for 2 h at rt, DMF was removed *in vacuo*. For cleavage of the *t*Bu-esters, TFA was added and the solution was stirred for 45 min at rt. After evaporation of TFA, the crude product was purified by RP-HPLC.

$SnBu_3$-BA-(OtBu)KuE(OtBu)$_2$ (4)

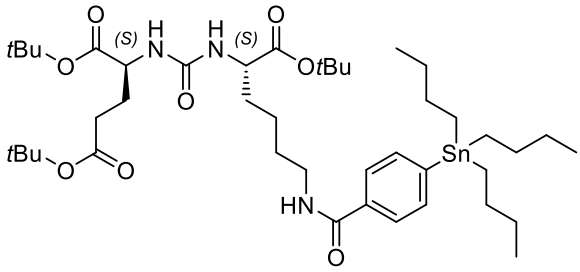

Chemical Formula: $C_{43}H_{75}N_3O_8Sn$
Molecular Weight: 880,80

Synthesis of di-*tert*-butyl (((*S*)-1-(*tert*-butoxy)-1-oxo-6-(4-(tributylstannyl)benzamido)hexan-2-yl)carbamoyl)-*L*-glutamate ($SnBu_3$-BA-(O*t*Bu)KuE(O*t*Bu)$_2$) was carried out, as described previously[71, 164]. Briefly, to a solution of 86.4 mg (0.18 mmol, 1.2 eq.) of (*t*BuO)KuE(O*t*Bu)$_2$ and 75.0 mg (0.15 mmol, 1.0 eq.) *N*-succinimidyl 4-(tri-*n*-butylstannyl)benzoate in DCM (1.5 mL), 92.6 µL (0.66 mmol, 4.5 eq.) TEA were added. After 12 h at rt, the reaction mixture was washed with water (50 mL). The organic phase was separated and all volatiles were removed *in vacuo*. The crude product was obtained as a pale-yellow oil (91%) and used without further purification. RP-HPLC (20 to 40% B in 20 min): t_R = 12.5 min, K' = 4.68. Calculated monoisotopic mass ($C_{43}H_{75}N_3O_8Sn$): 881.5; found: m/z = 882.7 $[M+H]^+$, 1764.5 $[2M+H]^+$.

3. Synthesis of chelators and functionalization

1,4,7-triazacyclononane-1,4,7-tris[methylene(2-carboxyethyl)phosphinic acid] (5, TRAP)

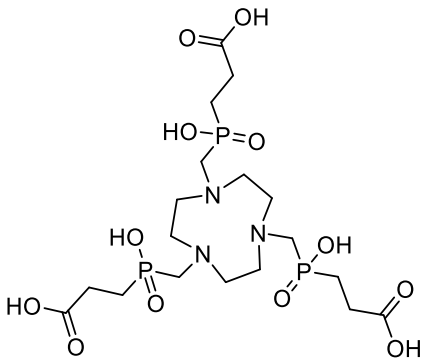

Chemical Formula: $C_{18}H_{36}N_3O_{12}P_3$
Molecular Weight: 579,42

The chelator TRAP was synthesized as described previously[165]. Briefly, a solution of 1.86 g (14.4 mmol, 1.0 eq.) 1,4,7-triazacyclononane and 9.00 g (65.2 mmol, 4.5 eq.) (2-carboxyethyl)phosphinic acid in 6 M aq. HCl (35 mL) was heated to 70 °C and 6.00 g (200 mmol, 2.3 eq.) paraformaldehyde were added in small portions during a period of 36 h. Then, all volatiles were distilled off *in vacuo* and the remaining HCl was removed by repeatedly adding small portions of water (4 × 20 mL) and evaporating to dryness. The crude product was purified by ion exchange chromatography (DOWEX 50WX2 hydrogen form, eluent: water). After removing water, TRAP·$2H_2O$ could be obtained as a colorless solid (29%). RP-HPLC (0 to 20% B in 15 min): t_R = 5 min, K' = 1.28. Calculated monoisotopic mass ($C_{18}H_{36}N_3O_{12}P_3$): 579.15; found: m/z = 580.5 [$M+H^+$].

Propargyl-TRAP (6)

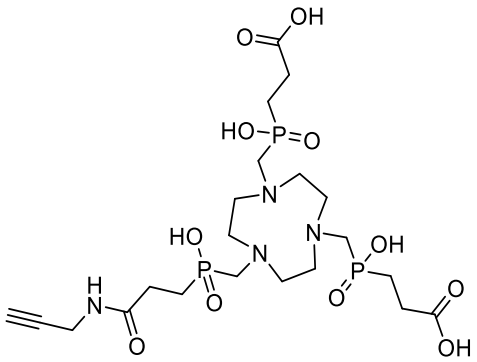

Chemical Formula: $C_{21}H_{39}N_4O_{11}P_3$
Molecular Weight: 616,48

Preparation of propargyl-TRAP was carried out as described previously[166]. In short, 110 mg (178 µmol, 1.0 eq.) TRAP·2 H_2O, 397 µL (2.28 mmol, 12.8 eq.) DIPEA, and 14.0 µL (218 µmol, 1.2 eq.) propargylamine were dissolved in DMSO (400 µL). Then 217 mg (570 µmol, 3.2 eq.) HATU were added in several portions over 10 min. After 1 h at rt, the reaction was quenched with water (600 µL) and the pH was adjusted to 3, by the addition of 1 M aq. HCl. Pre-purification was achieved by gel permeation chromatography (Sephadex G-10 medium, mobile phase: water, adjusted to pH 3 with 1 M aq. HCl). Fractions containing the product were identified by MS, pooled and concentrated *in vacuo*. Final purification was performed by preparative RP-HPLC, affording propargyl-TRAP as a colorless solid (46%). RP-HPLC (2 to 40% B in 20 min): t_R = 6.0 min, K' = 1.73. Calculated monoisotopic mass ($C_{21}H_{39}N_4O_{11}P_3$)*:* 616.5; found: m/z = 617.5 $[M+H]^+$.

^{1}H-NMR (300 MHz, D_2O, 300 K) δ = 1.96–2.08 (m, 6H, C(O)-C**H**$_2$), 2.46–2.55 (m, 2H, P^B-C**H**$_2$-C), 2.59–2.70 (m, 4H, P^A-C**H**$_2$-C), 3.36 (d, 2H, $^2J_{PH}$ = 6 Hz, P^B-C**H**$_2$-N), 3.41 (d, 4H, $^2J_{PH}$ = 6 Hz, P^A-C**H**$_2$-N), 3.47–3.48 (m, 12H, ring-C**H**$_2$), 3.95 (d, 2H, C**H**$_2$-C≡CH, $^4J_{HH}$ = 3 Hz) ppm*. ^{13}C[^{1}H]-NMR (101 MHz, D_2O, 300 K) δ = 24.61 (d, $^1J_{PP}$ = 95 Hz, P^B-**C**-C), 25.07 (d, $^1J_{PP}$ = 94 Hz, P^A-**C**-C), 26.71 (d, $^2J_{PP}$ = 4 Hz, P^B-C-**C**), 27.82 (d, $^2J_{PP}$ = 3 Hz, P^A-C-**C**), 28.89 (**C**-C≡C), 51.29 / 51.41 / 51.50 (three different ring-C), 53.66 (d, $^1J_{PP}$ = 91 Hz, N-**C**-P^A), 53.66 (d, $^1J_{PP}$ = 90 Hz, N-**C**-P^B), 71.79 (C-C≡**C**), 79.65 (C-**C**≡C), 174.46 (d, $^3J_{PP}$ = 14 Hz, N(H)-**C**=O^B), 177.24 (d, $^3J_{PP}$ = 13 Hz, **C**=O^A) ppm*. ^{31}P[^{1}H]-NMR (162 MHz, D_2O, 300 K) δ = 37.99 (P^A), 38.68(P^B) ppm. Indices ^{A} and ^{B} indicate P and O atoms belonging to the undecorated^A and decorated^B side arm, respectively.

Coupling of propargyl-TRAP (6) to the peptide (GP10)

For conjugation of azide-functionalized peptides to propargyl-TRAP *via* copper(I)-catalyzed alkyne-azide cycloaddition a previously developed procedure was applied[166]. Briefly, propargyl-TRAP (1.0 eq.) was dissolved in water (40 mM solution) and combined with a solution of the peptide (1.1 eq.) in a 1:1 (*v*/*v*) mixture of *t*BuOH and water (20-40 mM). Subsequently, a solution of sodium ascorbate (0.5 M, 50 eq.) in water was added. In order to start the reaction, an aqueous solution of $Cu(OAc)_2 \cdot H_2O$ (0.05 M, 1.2 eq.) was added, which resulted in a brown precipitate that dissolved after stirring in a clear green solution. For demetallation of TRAP, an aqueous solution of NOTA (8 mM, 12 eq.) was added and the pH was adjusted to 2.2 with 1 M aq. HCl. After either 1 h at 60 °C or 48 h at rt the mixture was directly subjected to preparative RP-HPLC purification.

Conjugation of DOTA-GA anhydride (GP11)

The *N*-terminal deprotected peptide (1.0 eq.) was dissolved together with DOTA-GA anhydride (1.5 eq.) and DIPEA (10.0 eq.) in dry DMF. After stirring the reaction mixture overnight at rt, DMF was removed *in vacuo*, yielding the crude product.

4. Synthesis of the Silicon Fluoride Acceptor

4-(Di-tert-butylfluorosilyl)benzoic acid (7, SiFA-BA)

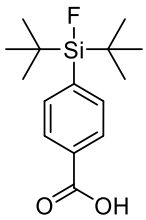

Chemical Formula: $C_{15}H_{23}FO_2Si$
Molecular Weight: 282,43

Synthesis of 4-(Di-*tert*-butylfluorosilyl)benzoic acid (SIFA-BA) was performed according to a previously published procedure with some modifications[153]. All water- and oxygen-sensitive reactions were carried out in dried reaction vessels under argon using a vacuum gas manifold:

((4-bromobenzyl)oxy)(tert-butyl)dimethylsilane (i)

To a stirred solution of 4.68 g (25.0 mmol, 1.0 eq.) 4-bromobenzylalcohol in anhydrous DMF (70 mL), 2.04 g (30.0 mmol, 1.2 eq.) imidazole and 4.52 g (30.0 mmol, 1.2 eq.) TBDMSCl were added and the resulting mixture was stirred at rt for 16 h. The mixture was then poured into ice-cold H_2O (250 mL) and extracted with Et_2O (5 × 50 mL). The combined organic fractions were washed with sat. aq. $NaHCO_3$ (2 × 100 mL) and brine (100 mL), dried, filtered and concentrated *in vacuo* to give the crude product which was purified by flash column chromatography (silica, 5% EtOAc in petrol, *v*/*v*) to give **i** as a colorless oil (95%). RP-HPLC (50 to 100% B in 15 min): t_R = 15 min, K' = 5.82. ^{1}H-NMR (400 MHz, $CDCl_3$, 300 K): δ = 0.10 (6H, s, $SiMe_2$*t*Bu), 0.95 (9H, s, $SiMe_2$*t*Bu), 4.69 (2H, s, CH_2OSi), 7.21 (2H, d), 7.46 (2H, d) ppm.

Di-tert-butyl(4-((tert-butyldimethylsilyloxy)methyl)phenyl)fluorosilane (ii)

At –78 °C under stirring, a solution of 7.29 mL (1.7 mol/L, 12.4 mmol, 2.4 eq.) *t*BuLi in pentane was added to a solution of 1.56 g (5.18 mmol, 1.0 eq.) of ((4-bromobenzyl)oxy)(*tert*-butyl)dimethylsilane (i) in dry THF (15 mL). After the reaction mixture was stirred for 30 min at –78 °C, the suspension was added dropwise over a period of 30 min to a cooled (–78 °C) solution of 1.12 g (6.23 mmol, 1.2 eq.) di-*tert*-butyldifluorosilane in dry THF (10 mL). The reaction mixture was allowed to warm to rt over a period of 12 h and then hydrolyzed with sat. aq. NaCl (100 mL). The organic layer was separated and the aqueous layer was extracted

with diethyl ether (3 × 50 mL). The combined organic layers were dried over magnesium sulfate and filtered. The filtrate was concentrated *in vacuo* to afford **ii** as a yellowish oil (95%). It was used for subsequent reactions without further purification. RP-HPLC (50 to 100% B in 20 min): t_R = 19 min, K' = 7.64.

4-(Di-tert-butylfluorosilanyl)benzyl alcohol (iii)

A catalytic amount of concentrated aq. HCl (0.5 mL) was added to a suspension of 1.88 g (4.92 mmol, 1.0 eq.) **ii** in methanol (50 mL). The reaction mixture was stirred for 18 h at rt and the solvent was removed under reduced pressure. The residue was redissolved in diethyl ether (40 mL) and the solution was washed with sat. aq. $NaHCO_3$ (80 mL). The aqueous layer was extracted with diethyl ether (3 × 50 mL). The combined organic layers were dried over magnesium sulfate and filtered. The filtrate was concentrated *in vacuo* to afford **iii** as a yellow oil (98%) that solidified. The product was used without further purification. RP-HPLC (50 to 100% B in 15 min): t_R = 8.2 min, K' = 2.73.

4-(Di-tert-butylfluorosilyl)benzaldehyde (iv)

A solution of 1.37 g (5.10 mmol, 1.0 eq.) of the alcohol **iii** in dry dichloromethane (20 mL) was added dropwise to a stirred ice-cooled suspension of 2.75 g (12.8 mmol, 2.5 eq.) pyridinium chlorochromate in dry dichloromethane (60 mL). After the reaction mixture was stirred for 30 min at 0 °C and for 2.5 h at rt, anhydrous diethyl ether (40 mL) was added and the supernatant solution was decanted from the black gum-like material. The insoluble material was washed thoroughly with diethyl ether and the combined organic phases were passed through a short pad of silica gel (10 cm per g crude product) for filtration. The solvents were removed *in vacuo* to yield aldehyde **iv** as a yellowish oil (96%). RP-HPLC (50 to 100% B in 15 min): t_R = 10.5 min, K' = 3.77.

4-(Di-tert-butylfluorosilyl)benzoic acid (v)

At room temperature, 1 M aq. $KMnO_4$ (30 mL) was added to a mixture of 1.31 g (4.92 mmol, 1.0 eq.) of the aldehyde **iv** in *tert*-butanol (30 mL), DCM (3.3 mL), and 1.25 M aq. $NaH_2PO_4 \cdot H_2O$ buffer (20 mL) at pH 4.0-4.5. After the mixture was stirred for 25 min, it was cooled to 5 °C, whereupon excess $KMnO_4$ (0.78 g, 4.92 mmol, 1.0 eq.) was added. The reaction was then quenched by the addition of sat. aq. Na_2SO_3 (50 mL). Upon addition of 2 M aq. HCl, all of the MnO_2 dissolved. The resulting solution was extracted with diethyl ether (3 × 100 mL). The combined organic layers were washed with sat. aq. $NaHCO_3$ solution (100 mL), dried over $MgSO_4$, filtered, and concentrated under reduced pressure. The obtained solid was purified by recrystallization from Et_2O/n-hexane (1:3, *v*/*v*), yielding **v** (60%) as a colorless solid. RP-HPLC (50 to 100% B in 15 min): t_R = 8.5 min, K' = 2.86. Calculated monoisotopic mass ($C_{15}H_{23}FO_2Si$): 282.4; found: m/z = 281.1 $[M-H]^-$, 235.1 $[M-COOH]^-$.

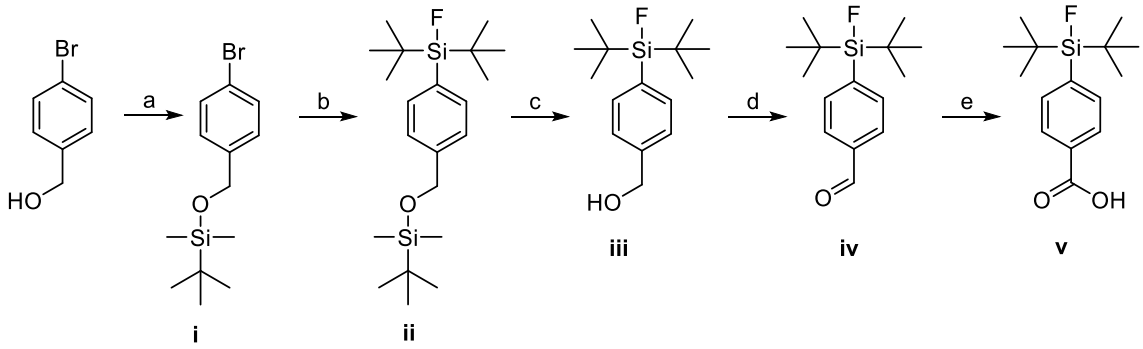

Scheme 2: Synthesis of SiFA-BA: a) TBDMSCl, imidazole (DMF); b) *t*BuLi, di-*tert*-butyldifluorosilane (THF); c) HCl (MeOH); d) pyridinium chlorochromate (DCM); e) $KMnO_4$ (DCM, *tert*-butanol, NaH_2PO_4 buffer).

5. Synthesis of rhPSMA ligands

rhPSMA-101 (8)

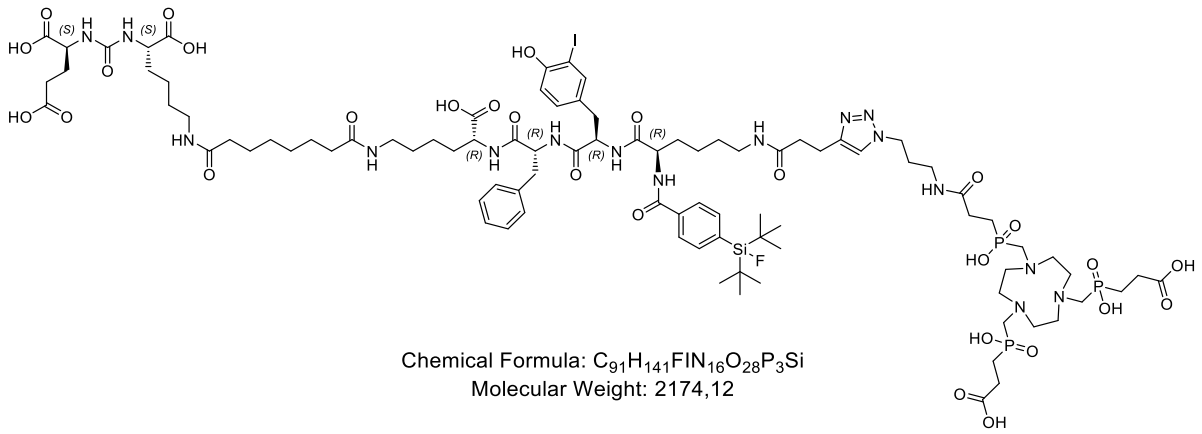

rhPSMA-101 was synthesized according to standard Fmoc-based solid-phase peptide synthesis on a 2-Chlorotrityl chloride (2-CTC) resin, applying the above-mentioned methods. Resin-bound Fmoc-*D*-Lys(Boc)-OH was Fmoc deprotected with piperidine in DMF (GP3) and Fmoc-*D*-Phe-OH (1.5 eq.) was added with HOBT (1.5 eq.), TBTU (1.5 eq.) and DIPEA (4.5 eq.) in DMF for 1.5 h (GP2). Consecutive Fmoc-cleavage steps and conjugation of Fmoc-*D*-Tyr(3-I)-OH and Fmoc-*D*-Lys(Dde)-OH were performed analogously (GP2 and 3). After functionalization of the deprotected *N*-terminal α-NH_2 with SiFA-BA (1.5 eq.), by the addition of HOBT (1.5 eq.), TBTU (1.5 eq.) and DIPEA (4.5 eq.) in DMF for 2 h (GP2), the remaining Dde group is removed with hydrazine in DMF (GP4a). Conjugation of 4-pentynoic acid (2.5 eq.) was carried out with HOBT (2.5 eq.), TBTU (2.5 eq.) and DIPEA (7.5 eq.) as activation reagents in DMF for 1.5 h (GP2). Subsequently, the peptide was cleaved from the resin under concomitant Boc deprotection with TFA (GP7b). The peptide was then reacted with the PfpO-Sub-(*t*BuO)KuE(O*t*Bu)$_2$ moiety (1.2 eq.) and TEA (8 eq.) in DMF (GP9). After final *t*Bu-cleavage with TFA (GP6) and subsequent RP-HPLC-based purification the peptide (1.0 eq.) was conjugated to propargyl-TRAP (1.0 eq.) in a copper(I)-catalyzed alkyne-azide cycloaddition (GP10). RP-HPLC purification yielded rhPSMA-101 (5%) as a colourless solid. RP-HPLC (10 to 90% B in 15 min): t_R = 11.1 min, K' = 4.05. Calculated monoisotopic mass ($C_{91}H_{141}FIN_{16}O_{28}P_3Si$): 2172.8; found: m/z = 1088.8 $[M+2H]^{2+}$.

rhPSMA-102 (9)

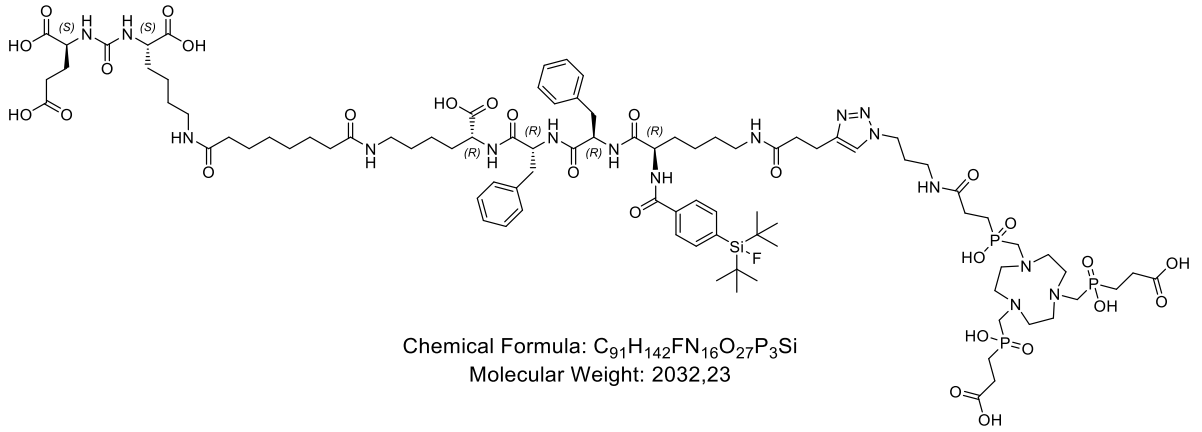

The synthesis of rhPSMA-102 was accomplished according to the procedure of **8**, substituting the *N*-terminal 3-Iodotyrosine-residue by phenylalanine; Fmoc-*D*-Phe-OH was conjugated analogously, applying HOBt (1.5 eq.), TBTU (1.5 eq.) and DIPEA (4.5 eq.) in DMF for 1.5 h (GP2). The purified product (20%) was obtained as a colorless solid. RP-HPLC (10 to 90% B in 15 min): t_R = 13.2 min, K' = 5.00. Calculated monoisotopic mass ($C_{91}H_{142}FN_{16}O_{27}P_3Si$): 2030.9; found: m/z = 1016.8 $[M+2H]^{2+}$.

rhPSMA-201 (10)

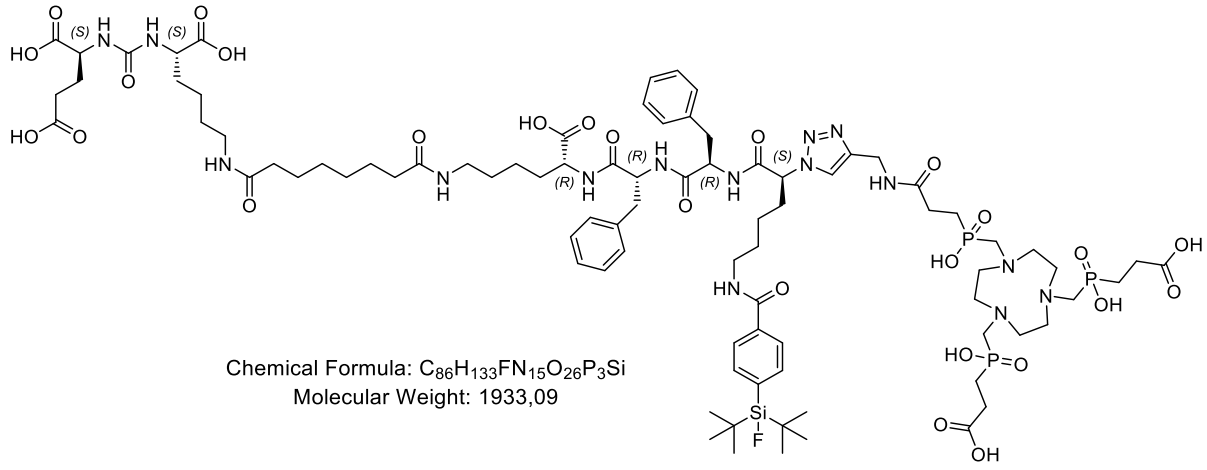

The synthesis of the protected resin-bound lys-phe-phe peptide scaffold of rhPSMA-201 was performed as described for **8**. After *N*-terminal Fmoc cleavage (GP3), the azide-functionalized lysine derivative N_3-*L*-Lys(Fmoc)-OH (2.0 eq.) was conjugated with HATU (2.0 eq.) and DIPEA (6.0 eq.) for 2 h in DMF (GP2). Following synthetic steps were carried out analogously to **8**. After RP-HPLC purification rhPSMA-201 (20%) was obtained as a colorless solid. RP-HPLC (10

to 90% B in 15 min): t_R = 10.8 min, K' = 3.91. Calculated monoisotopic mass ($C_{86}H_{133}FN_{15}O_{26}P_3Si$): 1931.9; found: m/z = 967.8 $[M+2H]^{2+}$, 645.5 $[M+3H]^{3+}$.

rhPSMA-202 *(11)*

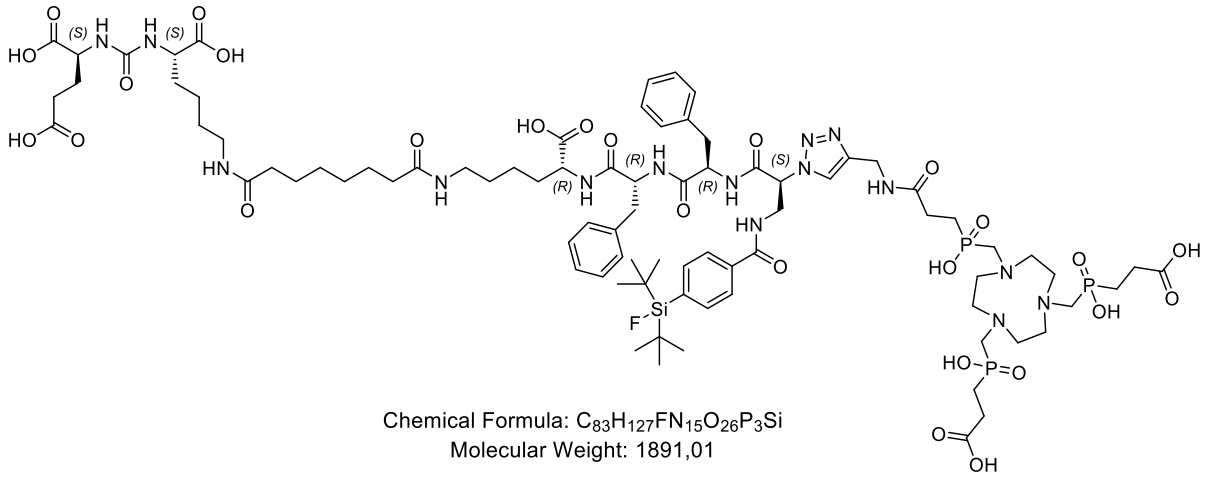

Chemical Formula: $C_{83}H_{127}FN_{15}O_{26}P_3Si$
Molecular Weight: 1891,01

The synthesis of the protected resin-bound lys-phe-phe scaffold of rhPSMA-202 was achieved in analogy to **8**. After *N*-terminal Fmoc deprotection (GP3), the azide-functionalized 2,3-diaminopropionic acid derivative N_3-*L*-Dap(Fmoc)-OH (2.0 eq.) was conjugated with HOBT (2.0 eq.), TBTU (2.0 eq.) and DIPEA (6.0 eq.) for 2 h in DMF (GP2). Subsequent synthetic steps were carried out, as described for **8**. RP-HPLC purification yielded rhPSMA-202 (12%) as colorless solid. RP-HPLC (10 to 90% B in 15 min): t_R = 10.5 min, K' = 3.77. Calculated monoisotopic mass ($C_{83}H_{127}FN_{15}O_{26}P_3Si$): 1889.8; found: m/z = 1891.6 $[M+H]^+$, 946.0 $[M+2H]^{2+}$.

rhPSMA-203 (12)

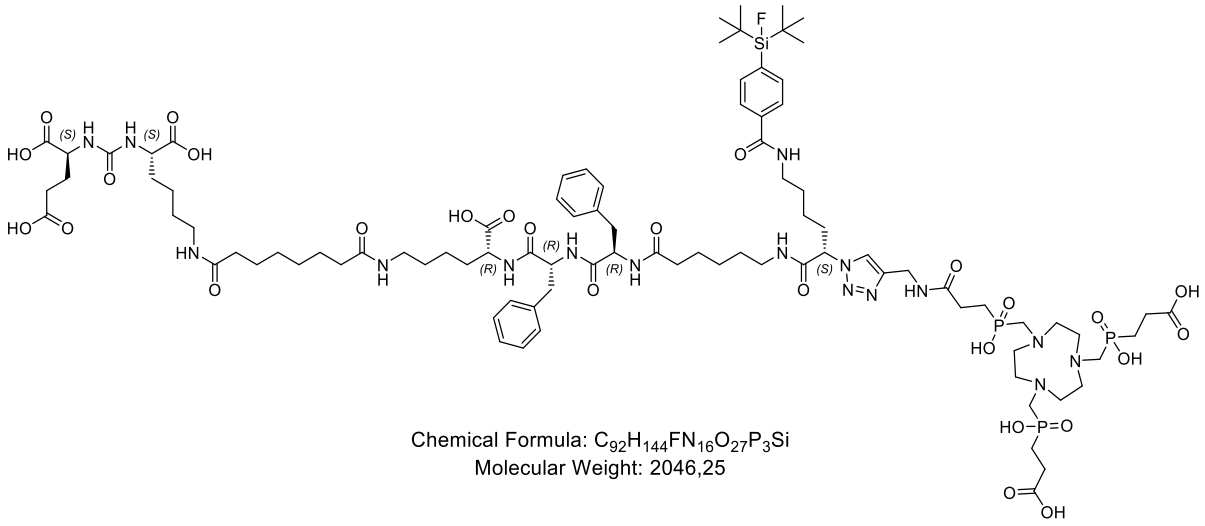

Chemical Formula: $C_{92}H_{144}FN_{16}O_{27}P_3Si$
Molecular Weight: 2046,25

The synthesis of the protected resin-bound lys-phe-phe scaffold of rhPSMA-203 was accomplished, as described for **8**. After cleavage of the remaining Fmoc group (GP3), Fmoc-6-ahx-OH (2.0 eq.) was reacted by the addition of HOBT (2.0 eq.), TBTU (2.0 eq.) and DIPEA (6.0 eq.) as coupling reagents for DMF for 2 h (GP2). Fmoc-deprotection was achieved with piperidine (GP3) and N_3-*L*-Lys(Fmoc)-OH (2.0 eq.) was conjugated with HATU (2.0 eq.) and DIPEA (6.0 eq.) for 2 h in DMF (GP2). The following steps were carried out, applying the same synthetic strategy, as described for **8**. rhPSMA-203 was obtained as a colorless solid (8%) after RP-HPLC purification. RP-HPLC (10 to 90% B in 15 min): t_R = 10.7 min, K' = 3.86. Calculated monoisotopic mass ($C_{92}H_{144}FN_{16}O_{27}P_3Si$): 2044.9; found: m/z = 1024.1 $[M+2H]^{2+}$, 683.0 $[M+3H]^{3+}$.

rhPSMA-204 (13)

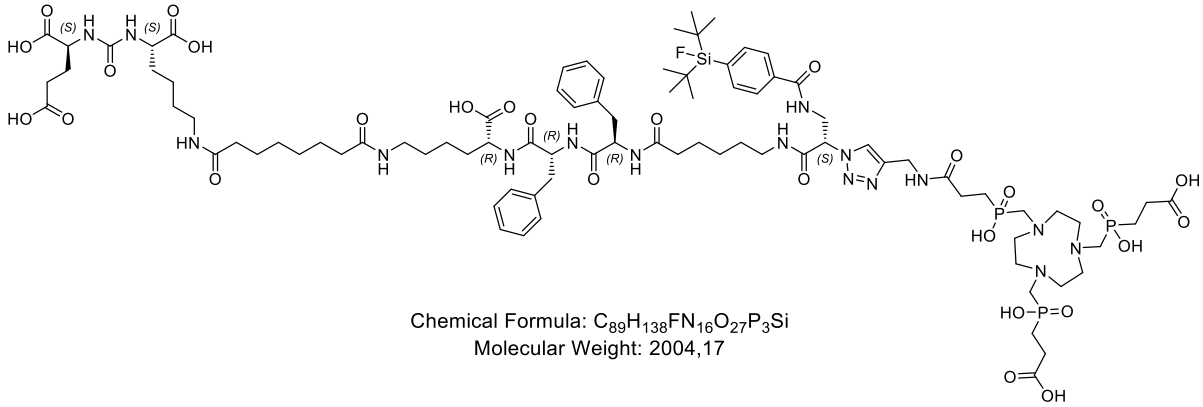

The synthesis of the protected resin-bound lys-phe-phe scaffold of rhPSMA-204 was performed as described for **8**. After *N*-terminal Fmoc cleavage (GP3), Fmoc-6-ahx-OH (2.0 eq.) was conjugated with HOBT (2.0 eq.), TBTU (2.0 eq.) and DIPEA (6.0 eq.) in DMF for 2 h (GP2). Next, the *N*-terminal Fmoc group was cleaved (GP3) and N_3-*L*-Dap(Fmoc)-OH (2.0 eq.) was conjugated with HOBT (2.0 eq.), TBTU (2.0 eq.) and DIPEA (6.0 eq.) for 2 h in DMF (GP2). Following synthetic steps were carried out in analogy to **8**. After RP-HPLC purification rhPSMA-204 (3%) was obtained as a colorless solid. RP-HPLC (10 to 90% B in 15 min): t_R = 10.3 min, K' = 3.68. Calculated monoisotopic mass ($C_{89}H_{138}FN_{16}O_{27}P_3Si$): 2002.9; found: m/z = 1002.8 $[M+2H]^{2+}$, 655.5 $[M+3H]^{3+}$.

rhPSMA-301 (14)

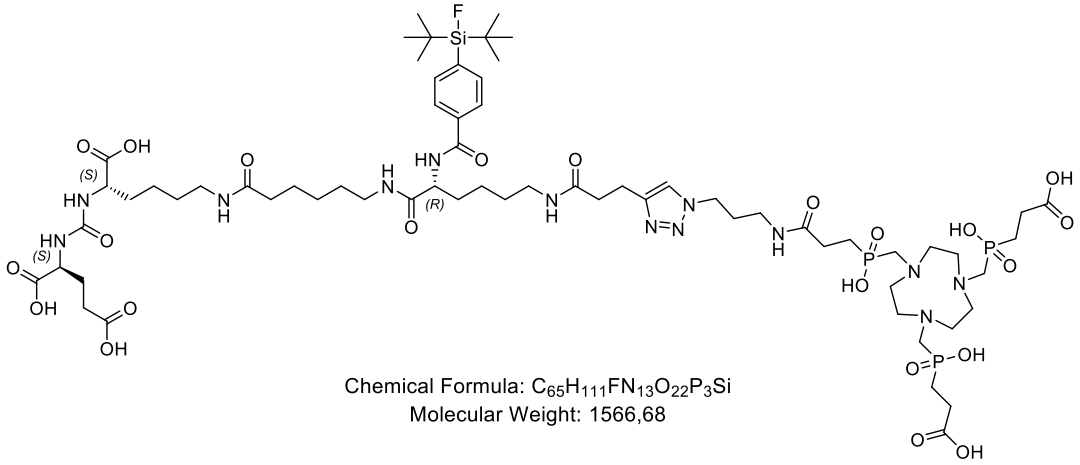

Resin-bound 6-Fmoc-ahx-OH was Fmoc deprotected with piperidine in DMF (GP3) and Dde-*D*-Lys(Fmoc)-OH (1.5 eq.) was conjugated with HOBT (1.5 eq.), TBTU (1.5 eq.) and DIPEA (4.5 eq.) in DMF for 2 h (GP2). After Fmoc-cleavage (GP3), 4-pentynoic acid (2.5 eq.) was coupled with HOBT (2.5 eq.), TBTU (2.5 eq.) and DIPEA (7.5 eq.) in DMF for 1.5 h (GP2). Dde-cleavage was accomplished with hydrazine in DMF (GP4a) and SiFA-BA (1.5 eq.) was reacted with HOBT (1.5 eq.), TBTU (1.5 eq.) and DIPEA (4.5 eq.) in DMF for 2 h (GP2). The peptide was cleaved from the resin with TFA (GP7b) and conjugated to (*t*BuO)KuE(O*t*Bu)$_2$ (1.5 eq.) with HOBT (1.5 eq.), TBTU (1.5 eq.) and DIPEA (4.5 eq.) in DMF for 12 h (GP8). Cleavage of the *t*Bu-protecting groups was achieved by the addition of TFA (GP6) and after RP-HPLC-based purification the azide-functionalized peptide was conjugated to propargyl-TRAP in a copper(I)-catalyzed click reaction (GP10). RP-HPLC purification yielded rhPSMA-301 (18%) as a colorless solid. RP-HPLC (10 to 90% B in 15 min): t_R = 9.5 min, K' = 3.32. Calculated monoisotopic mass ($C_{65}H_{111}FN_{13}O_{22}P_3Si$): 1565.7; found: m/z = 1566.3 $[M+H]^+$, 784.0 $[M+2H]^{2+}$.

rhPSMA-302 (15)

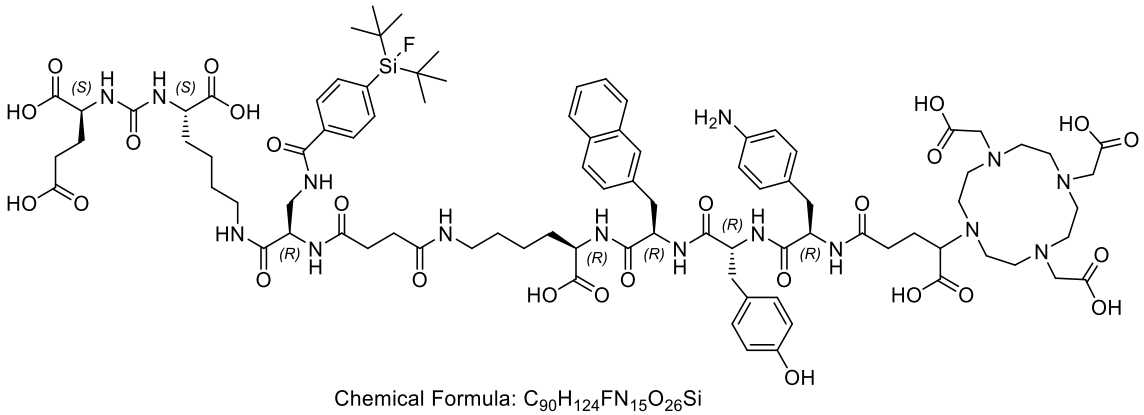

Chemical Formula: $C_{90}H_{124}FN_{15}O_{26}Si$
Molecular Weight: 1879,14

Resin-bound Fmoc-*D*-Dap(Dde)-OH was Fmoc deprotected with piperidine in DMF (GP3) and succinic anhydride (7.0 eq.) was added with DIPEA (7.0 eq.) in DMF for 2.5 h. Conjugation of Fmoc-*D*-Lys-OAll·HCl (1.5 eq.) was achieved by adding a mixture of HOBt (1.5 eq.), TBTU (1.5 eq.) and DIPEA (4.5 eq.) in DMF for 2 h (GP2). After cleavage of the Fmoc-group with piperidine (GP3), the free amine was conjugated to Fmoc-*D*-2-Nal-OH (1.5 eq.) with HOBT (1.5 eq.), TBTU (1.5 eq.) and DIPEA (4.5 eq.) in DMF for 2 h (GP2). Following Fmoc-deprotection and conjugation steps of Fmoc-*D*-Tyr(O*t*Bu)-OH (1.5 eq.) and Fmoc-*D*-Phe(4-NHBoc)-OH (1.5 eq.) were carried out analogously (GP2 and 3). Subsequent orthogonal Dde-deprotection was performed using imidazole and hydroxylamine hydrochloride dissolved in a mixture of NMP and DMF (GP4b). SIFA-BA (1.5 eq.) was reacted with the free amine of the side chain with HOBt (1.5 eq.), TBTU (1.5 eq.) and DIPEA (4.5 eq.) as activation reagents in DMF for 2 h (GP2). After Fmoc-deprotection with piperidine (GP3), DOTA-GA(*t*Bu)$_4$ was reacted with HOBT (1.5 eq.), TBTU (1.5 eq.) and DIPEA (4.5 eq.) in DMF for 2 h (GP2). After mild cleavage of the peptide from the resin (GP7a), *(tBuO)KuE(OtBu)$_2$* was conjugated (GP8). The allyl-protecting group was removed by the addition of Pd(PPh$_3$)$_4$ dissolved in DCM (GP5). Final cleavage of the *t*Bu-ester (GP6) and RP-HPLC purification yielded rhPSMA-302 as a colorless solid (14%). RP-HPLC (10 to 90% B in 15 min): t_R = 9.6 min, K' = 3.36. Calculated monoisotopic mass ($C_{90}H_{124}FN_{15}O_{26}Si$): 1877.9; found: m/z = 1879.5 $[M+H]^+$, 940.3 $[M+2H]^{2+}$.

rhPSMA-4 (16)

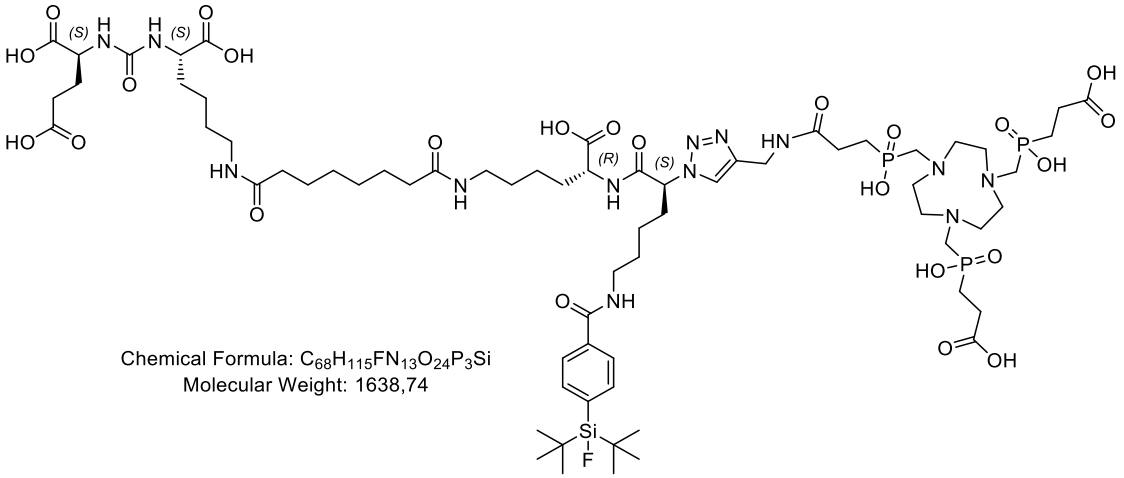

Resin-bound Fmoc-*D*-Lys(Boc)-OH was Fmoc-deprotected with piperidine in DMF (GP3) and conjugated to N_3-*L*-Lys(Fmoc)-OH (2.0 eq.) with HATU (3.0 eq.), HOAt (3.0 eq.) and DIPEA (6.0 eq.) for 2 h in DMF (GP2). After cleavage of the Fmoc-group (GP3), SIFA-BA (1.5 eq.) was added with HOBt (1.5 eq.), TBTU (1.5 eq.) and DIPEA (4.5 eq.) in DMF for 2 h (GP2). Subsequent cleavage from the resin with TFA yielded the fully deprotected peptide backbone (GP7b). For conjugation of the EuK moiety, PfpO-Sub-(*t*BuO)KuE(O*t*Bu)$_2$ (1.2 eq.) was added in a mixture of TEA (8 eq.) and DMF (GP9). Cleavage of the *t*Bu-esters was performed by adding TFA (GP6). In a final step the purified peptide (1.1 eq.) was reacted with propargyl-TRAP (1.0 eq.) in a copper(I)-catalyzed click reaction (GP10). After RP-HPLC purification rhPSMA-4 (4%) was obtained as a colourless solid. RP-HPLC (10 to 90% B in 15 min): t_R = 8.5 min, K' = 2.86. Calculated monoisotopic mass ($C_{68}H_{115}FN_{13}O_{24}P_3Si$): 1637.7; found: m/z = 1638.2 $[M+H]^+$, 820.0 $[M+2H]^{2+}$.

rhPSMA-5 (17)

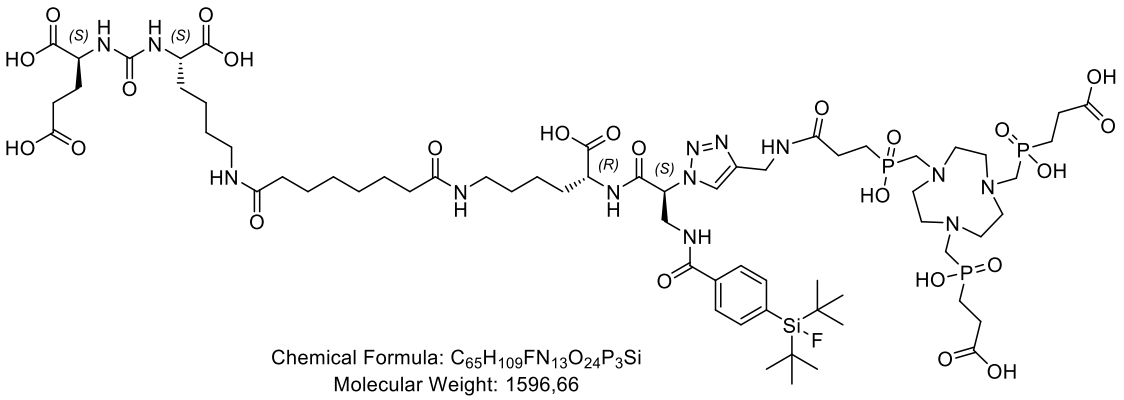

The synthesis of rhPSMA-5 was accomplished according to the procedure of **16**, substituting the *N*-terminal azidolysine-residue by an azide-functionalized diaminopropionic acid derivative; N_3-*L*-Dap(Fmoc)-OH (2.0 eq.) was conjugated with HATU (3.0 eq.), HOAt (3.0 eq.) and DIPEA (6.0 eq.) for 2 h in DMF (GP2). After RP-HPLC purification, rhPSMA-5 (4%) was obtained as a colourless solid. RP-HPLC (10 to 90% B in 15 min): t_R = 8.5 min, K' = 2.86. Calculated monoisotopic mass ($C_{65}H_{109}FN_{13}O_{24}P_3Si$): 1595.7; found: m/z = 1596.5 $[M+H]^+$, 799.1 $[M+2H]^{2+}$.

rhPSMA-6 (18)

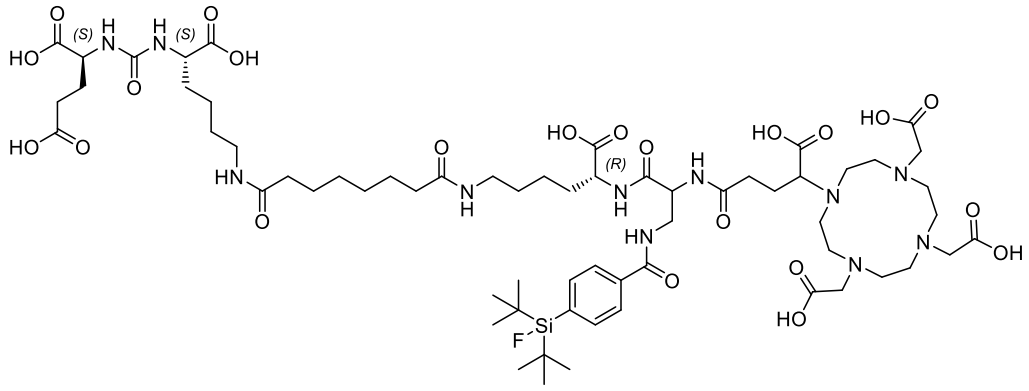

Chemical Formula: $C_{63}H_{102}FN_{11}O_{22}Si$
Molecular Weight: 1412,65

Resin-bound Fmoc-*D*-Lys(Boc) was Fmoc deprotected with 20% piperidine in DMF (GP3) and Fmoc-*D*-Dap(Dde)-OH (2.0 eq.) was conjugated applying HOBt (2.0 eq.), TBTU (2.0 eq.) and DIPEA (6.0 eq.) in DMF for 2 h (GP2). After orthogonal Dde-deprotection with imidazole and hydroxylamine hydrochloride in a mixture of NMP and DMF (GP4b), SIFA-BA (1.5 eq.) was conjugated with HOBt (1.5 eq.), TBTU (1.5 eq.) and DIPEA (4.5 eq.) in DMF for 2 h (GP2). Subsequent Fmoc-deprotection (GP3) and mild cleavage from the resin with TFE and AcOH in DCM (GP7a) yielded the *t*Bu-protected peptide backbone. Condensation of DOTA-GA anhydride (1.5 eq.) was performed by adding DIPEA (10 eq.) in DMF (GP11). After *t*Bu-deprotection in TFA (GP6), the PfpO-Sub-(*t*BuO)KuE(O*t*Bu)$_2$ moiety (1.2 eq.) was added in a mixture of TEA (8 eq.) and DMF (GP9). Final cleavage of the *t*Bu-esters in TFA (GP6) and RP-HPLC purification yielded rhPSMA-6 (70%) as a colorless solid. RP-HPLC (10 to 90% B in 15 min): t_R = 9.1 min, K' = 3.14. Calculated monoisotopic mass ($C_{63}H_{102}FN_{11}O_{22}Si$): 1411.7; found: m/z = 1412.3 $[M+H]^+$, 706.8 $[M+2H]^{2+}$.

rhPSMA-7 (19)

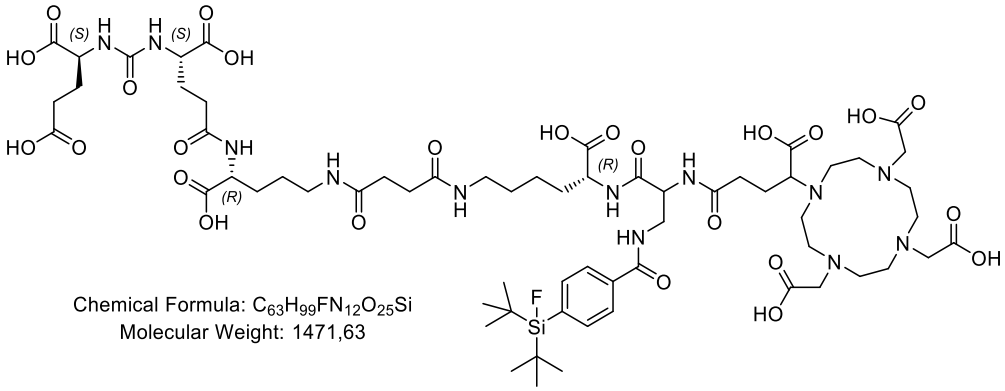

Resin-bound Fmoc-*D*-Orn(Dde)-OH was Fmoc-deprotected with piperidine in DMF (GP3) and (*t*BuO)EuE(O*t*Bu)$_2$ (2.0 eq.) was conjugated with HOBt (2.0 eq.), TBTU (2.0 eq.) and DIPEA (6.0 eq.) in DMF for 4.5 h (GP2). After cleavage of the Dde-group with 2% hydrazine in DMF (GP4a), a solution of succinic anhydride (7.0 eq.) and DIPEA (7.0 eq.) in DMF was added and reacted for 2.5 h. Conjugation of Fmoc-*D*-Lys-OAll·HCl (1.5 eq.) was achieved by adding a mixture of HOBt (1.5 eq.), TBTU (1.5 eq.) and DIPEA (4.5 eq.) in DMF for 2 h (GP2). After cleavage of the Fmoc-group with piperidine in DMF (GP3), the free amine was conjugated to Fmoc-*D*-Dap(Dde)-OH (2.0 eq.) after pre-activation of the amino acid in a mixture of HOBt (2.0 eq.), TBTU (2.0 eq.) and DIPEA (6.0 eq.) in DMF for 2 h (GP2). Following orthogonal Dde-deprotection was done using imidazole and hydroxylamine hydrochloride dissolved in a mixture of NMP and DMF (GP4b). SIFA-BA (1.5 eq.) was reacted with the free amine of the side chain with HOBt (1.5 eq.), TBTU (1.5 eq.) and DIPEA (4.5 eq.) as activation reagents in DMF for 2 h (GP2). The allyl-protecting group was removed by the addition of TIPS (50.0 eq.) and Pd(PPh$_3$)$_4$ (0.3 eq.) dissolved in DCM (GP5). After Fmoc-deprotection with piperidine (GP3), the peptide was cleaved from the resin under preservation of the acid labile protecting groups by using a mixture of TFE and AcOH in DCM (GP7a). Final condensation of DOTA-GA anhydride (1.5 eq.) was achieved with piperidine (10 eq.) in DMF (GP11). After cleavage of the *t*Bu-esters of the EuE moiety with TFA (GP6), the crude peptide was purified by RP-HPLC, yielding rhPSMA-7 (24%) as a colorless solid. RP-HPLC (10 to 70% B in 15 min): t_R = 10.4 min, K' = 3.73. Calculated monoisotopic mass ($C_{63}H_{99}FN_{12}O_{25}Si$): 1470.7; found: m/z = 1471.8 $[M+H]^+$, 736.7 $[M+2H]^{2+}$.

rhPSMA-7.1 (20)

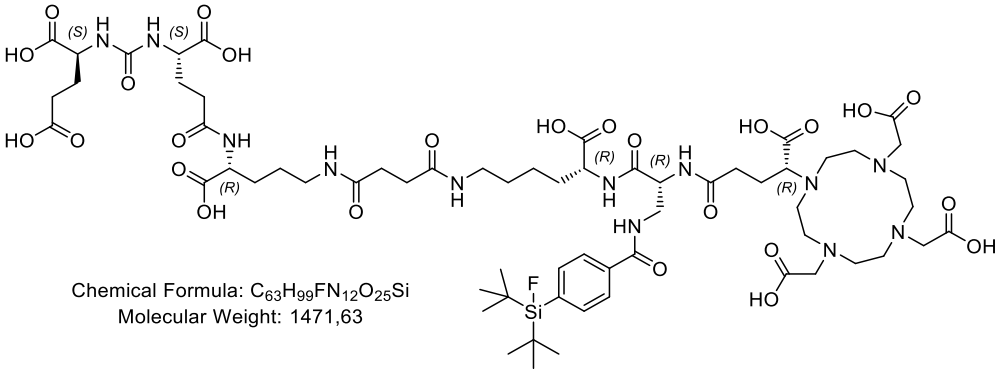

The first synthetic steps for preparation of the four different stereoisomers of rhPSMA-7 are identical and carried out together, starting from resin-bound Fmoc-*D*-Orn(Dde)-OH. After cleavage of the Fmoc group with piperidine in DMF (GP3), (*t*BuO)EuE(O*t*Bu)$_2$ (2.0 eq.) was conjugated with HOAt (2.0 eq.), TBTU (2.0 eq.) and DIPEA (6.0 eq.) in DMF for 4.5 h (GP2). After cleavage of the Dde-group with a mixture of hydrazine in DMF (GP4a), a solution of succinic anhydride (7.0 eq.) and DIPEA (7.0 eq.) in DMF was added and left to react for 2.5 h. Subsequently, the conjugated succinic acid was pre-activated, by adding a mixture of HOAt (2.0 eq.), TBTU (2.0 eq.) and DIPEA (6.0 eq.) in DMF. After 20 min, Fmoc-*D*-Lys(O*t*Bu)·HCl (2.0 eq.) dissolved in DMF was added and left to react for 2.5 h (GP2). Subsequent cleavage of the Fmoc-group was performed, by adding a mixture of piperidine in DMF (GP3). Fmoc-*D*-Dap(Dde)-OH (2.0 eq.) was pre-activated in a mixture of HOAt (2.0 eq.), TBTU (2.0 eq.) and 2,4,6-trimethylpyridine (6.7 eq.) in DMF and added to the resin-bound peptide for 2.5 h (GP2). Following orthogonal Dde-deprotection was done using imidazole and hydroxylamine hydrochloride dissolved in a mixture of NMP and DMF for 3 h (GP4b). SiFA-BA (1.5 eq.) was reacted with the free amine of the side chain with HOAt (1.5 eq.), TBTU (1.5 eq.) and DIPEA (4.5 eq.), as activation reagents in DMF for 2 h (GP2). After Fmoc-deprotection with piperidine (GP3), (*R*)-DOTA-GA(*t*Bu)$_4$ (2.0 eq.) was conjugated with HOAt (2.0 eq.), TBTU (2.0 eq.) and 2,4,6-trimethylpyridine (6.7 eq.) in DMF for 2.5 h (GP2). Cleavage from the resin with simultaneous deprotection of acid labile protecting groups was performed in TFA for 6 h (GP7b). After RP-HPLC-based purification, rhPSMA-7.1 was obtained as a colorless solid (19%). RP-HPLC (10 to 70% B in 15 min): t_R = 10.4 min, K' = 3.73. Calculated monoisotopic mass ($C_{63}H_{99}FN_{12}O_{25}Si$): 1470.7; found: m/z = 1471.9 $[M+H]^+$, 736.5 $[M+2H]^{2+}$.

rhPSMA-7.2 (21)

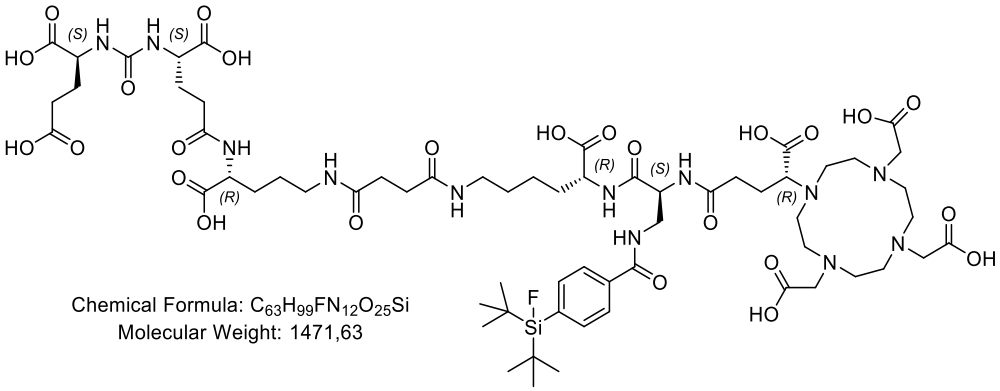

The resin-bound peptide backbone (*t*Bu$_2$)EuE(*t*Bu)-orn-suc-lys(O*t*Bu)-NH$_2$ was synthesized as described for rhPSMA-7.1. Fmoc-*L*-Dap(Dde)-OH (2.0 eq.) was conjugated with HOAt (2.0 eq.), TBTU (2.0 eq.) and 2,4,6-trimethylpyridine (6.7 eq.) in DMF and for 2.5 h (GP2). Following orthogonal Dde-deprotection, conjugation of SiFA-BA and Fmoc-cleavage was carried out as described for rhPSMA-7.1. (*R*)-DOTA-GA(*t*Bu)$_4$ (2.0 eq.) was conjugated with HOAt (2.0 eq.), TBTU (2.0 eq.) and 2,4,6-trimethylpyridine (6.7 eq.) in DMF for 2.5 h (GP2). Cleavage from the resin with simultaneous deprotection of acid labile protecting groups was performed in TFA for 6 h (GP7b). rhPSMA-7.2 was obtained as a colorless solid (25%), after RP-HPLC-based purification. RP-HPLC (10 to 70% B in 15 min): t_R = 10.3 min, K' = 3.68. Calculated monoisotopic mass ($C_{63}H_{99}FN_{12}O_{25}Si$): 1470.7; found: m/z = 1471.7 $[M+H]^+$, 736.4 $[M+2H]^{2+}$.

rhPSMA-7.3 (22)

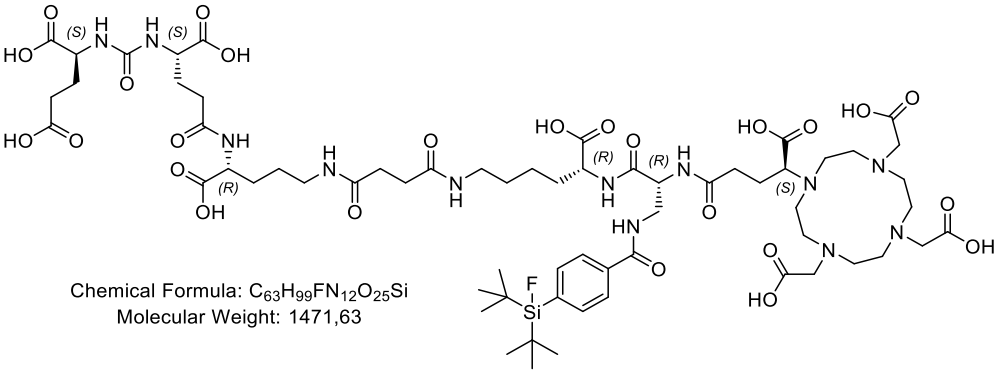

The resin-bound peptide backbone (*t*Bu$_2$)EuE(*t*Bu)-orn-suc-lys(O*t*Bu)-NH$_2$ was synthesized as described for rhPSMA-7.1. Fmoc-*D*-Dap(Dde)-OH (2.0 eq.) was pre-activated in a mixture of HOAt (2.0 eq.), TBTU (2.0 eq.) and 2,4,6-trimethylpyridine (6.7 eq.) in DMF and added to the resin for 2.5 h (GP2). Following orthogonal Dde-deprotection, conjugation of SiFA-BA and

Fmoc-cleavage was carried out as described for rhPSMA-7.1. (*S*)-DOTA-GA(*t*Bu)$_4$ (2.0 eq.) was conjugated with HOAT (2.0 eq.), TBTU (2.0 eq.) and 2,4,6-trimethylpyridine (6.7 eq.) in DMF for 2.5 h (GP2). Cleavage from the resin with simultaneous deprotection of acid labile protecting groups was performed in TFA for 6 h (GP7b). After RP-HPLC-based purification rhPSMA-7.3 was obtained as a colorless solid (35%). RP-HPLC (10 to 70% B in 15 min): t_R = 10.3 min, K' = 3.68. Calculated monoisotopic mass ($C_{63}H_{99}FN_{12}O_{25}Si$): 1470.7; found: m/z = 1471.8 $[M+H]^+$, 736.6 $[M+2H]^{2+}$.

rhPSMA-7.4 (23)

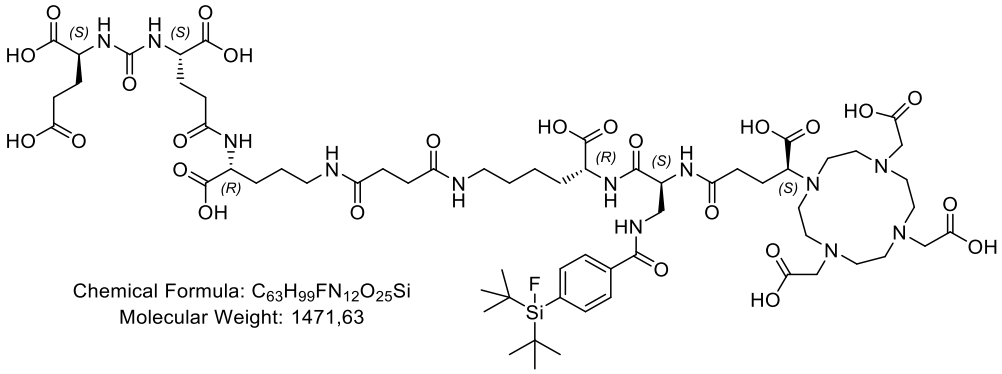

The resin-bound peptide backbone (*t*Bu$_2$)EuE(*t*Bu)-orn-suc-lys(O*t*Bu)-NH$_2$ was synthesized as described for rhPSMA-7.1. Fmoc-*L*-Dap(Dde)-OH (2.0 eq.) was conjugated with HOAt (2.0 eq.), TBTU (2.0 eq.) and 2,4,6-trimethylpyridine (6.7 eq.) in DMF for 2.5 h (GP2). Following orthogonal Dde-deprotection, conjugation of SiFA-BA and Fmoc-cleavage was carried out as described for rhPSMA-7.1. (*S*)-DOTA-GA(*t*Bu)$_4$ (2.0 eq.) was conjugated with HOAT (2.0 eq.), TBTU (2.0 eq.) and 2,4,6-trimethylpyridine (6.7 eq.) in DMF for 2.5 h (GP2). Cleavage from the resin with simultaneous deprotection of acid labile protecting groups was performed in TFA for 6 h (GP7b). rhPSMA-7.4 was obtained as a colorless solid (27%), after RP-HPLC-based purification. RP-HPLC (10 to 70% B in 15 min): t_R = 10.3 min, K' = 3.68. Calculated monoisotopic mass ($C_{63}H_{99}FN_{12}O_{25}Si$): 1470.7; found: m/z = 1471.9 $[M+H]^+$, 736.6 $[M+2H]^{2+}$.

rhPSMA-8 (24)

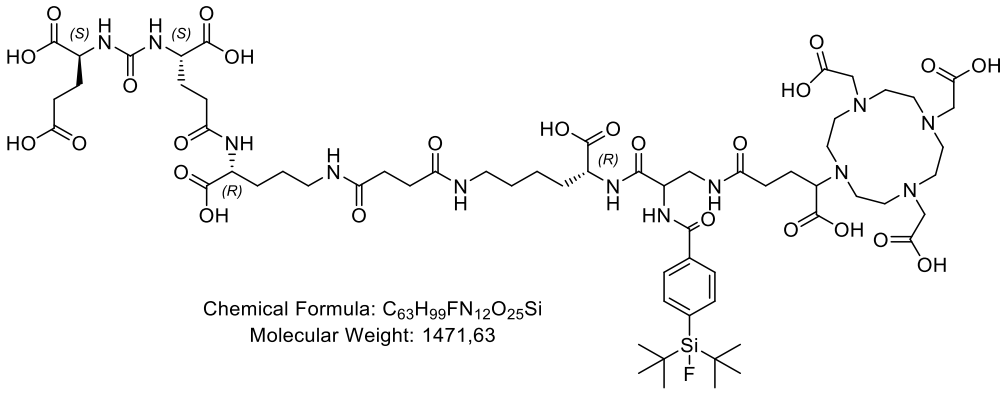

Synthesis of rhPSMA-8, was carried out as described for rhPSMA-7, with one deviation; After conjugation of Fmoc-*D*-Dap(Dde)-OH, the Fmoc-protecting group was cleaved with piperidine in DMF (GP3) and SiFA-BA was reacted with the free *N*-terminus of the peptide. After removing the allyl-protecting group with TIPS (50.0 eq.) and $Pd(PPh_3)_4$ (0.3 eq.) dissolved in DCM (GP5), the remaining Dde-group was cleaved by a solution of imidazole and hydroxylamine hydrochloride dissolved in NMP and DMF (GP4b). Following conjugation of DOTA-GA and final deprotection were carried out as described for rhPSMA-7. After RP-HPLC purification, rhPSMA-8 (11%) was obtained as a colorless solid. RP-HPLC (10 to 70% B in 15 min): t_R = 10.4 min, K' = 3.73. Calculated monoisotopic mass ($C_{63}H_{99}FN_{12}O_{25}Si$): 1470.7; found: m/z = 1471.7 $[M+H]^+$, 736.8 $[M+2H]^{2+}$.

rhPSMA-9 (25)

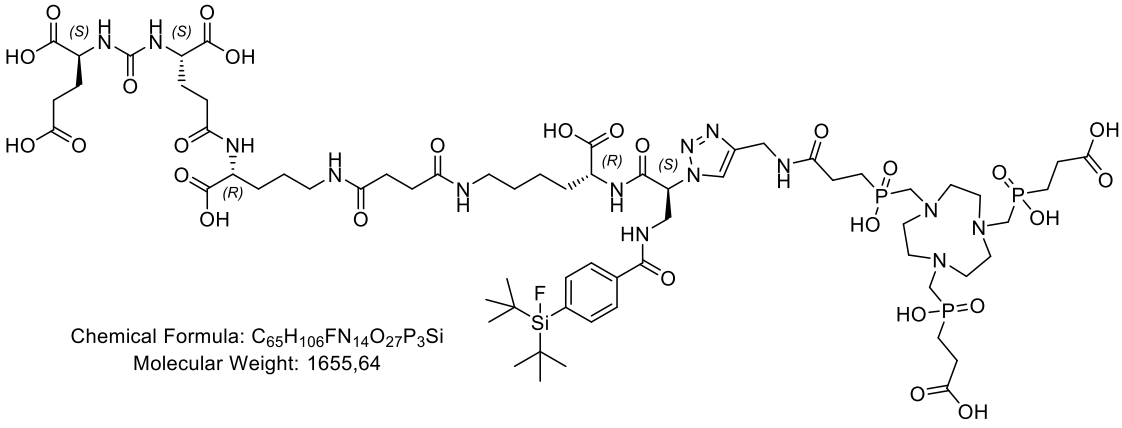

The peptide backbone of rhPSMA-9 was prepared analogously to rhPSMA-7. A difference was the use of N_3-*L*-Dap(Fmoc)-OH instead of Fmoc-*D*-Dap(Dde)-OH, which was required for the final click reaction with propargyl-TRAP. The azido-substituted amino acid N_3-*L*-Dap(Fmoc)-OH

(2.0 eq.) was conjugated with HATU (3.0 eq.), HOAt (3.0 eq.) and DIPEA (6.0 eq.) in DMF for 2 h (GP2). After Fmoc-deprotection with 20% piperidine (GP3), SiFA-BA (1.5 eq.) was reacted with HOBt (1.5 eq.), TBTU (1.5 eq.) and DIPEA (4.5 eq.) as activation reagents in DMF for 2 h (GP2). Removal of the allyl-protecting group was performed by the addition of TIPS (50.0 eq.) and $Pd(PPh_3)_4$ (0.3 eq.) dissolved in DCM (GP5). After cleavage from the resin with TFA under concurrent deprotection of all acid labile protecting groups (GP7b), the purified EuE-azido-conjugate (1.1 eq.) was reacted with propargyl-TRAP (1.0 eq.) in a copper(I)-catalyzed click reaction (GP10). RP-HPLC purification yielded rhPSMA-9 (9%) as a colourless solid. RP-HPLC (10 to 90% B in 15 min): t_R = 8.7 min, K' = 2.95. Calculated monoisotopic mass ($C_{65}H_{106}FN_{14}O_{27}P_3Si$): 1654.6; found: m/z = 1655.6 $[M+H]^+$, 828.4 $[M+2H]^{2+}$.

rhPSMA-10 (26)

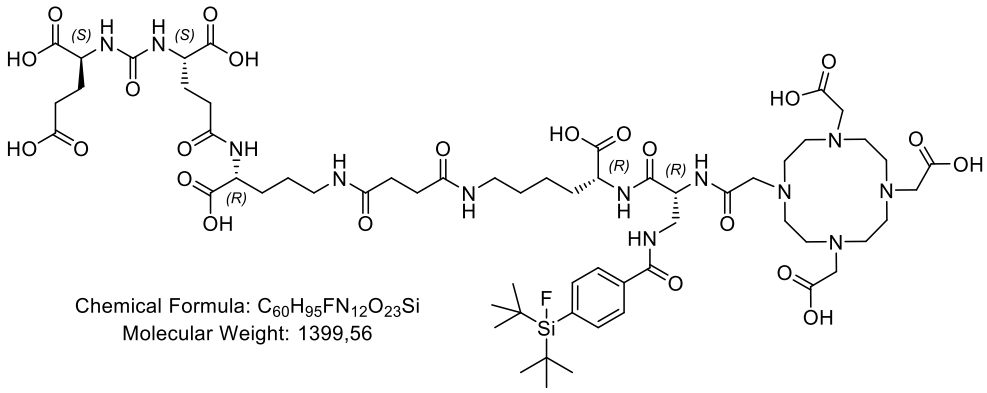

rhPSMA-10 was synthesized in analogy to rhPSMA-7.3, by using DOTA instead of DOTA-GA. The *tert*-butyl protected chelator, DOTA(tBu)$_3$ was conjugated to the free *N*-terminus with a mixture of HOAt (2.0 eq.), TBTU (2.0 eq.) and 2,4,6-trimethylpyridine (6.7 eq.) for 2 h in DMF (GP2). Cleavage from the resin and deprotection of acid labile protecting groups was performed in TFA for 6 h (GP7b). After RP-HPLC-based purification, rhPSMA-10 (18%) was obtained as a colorless solid. RP-HPLC (10 to 70% B in 15 min): t_R = 10.5 min, K' = 3.77. Calculated monoisotopic mass ($C_{60}H_{95}FN_{12}O_{23}Si$): 1398.6; found: m/z = 1399.6 $[M+H]^+$, 700.6 $[M+2H]^{2+}$.

rhPSMA-11 (27)

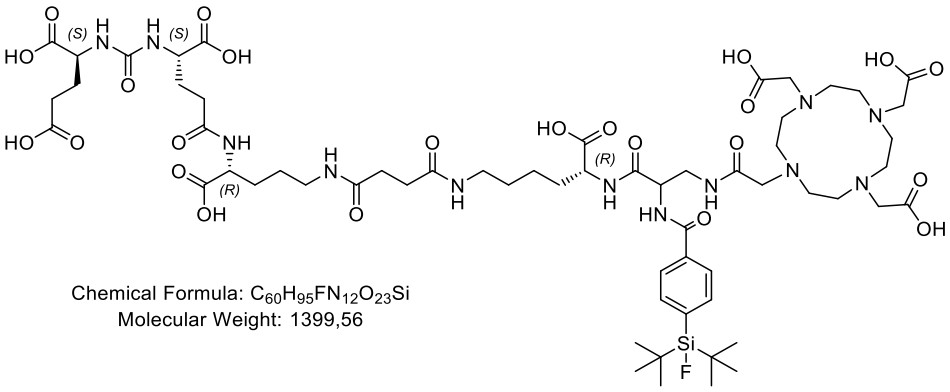

The synthesis of rhPSMA-11 was performed as described for rhPSMA-8, by using DOTA instead of DOTA-GA. The chelator, DOTA(*t*Bu)$_3$ was conjugated in a mixture of HOAt (1.5 eq.), TBTU (1.5 eq.) and DIPEA (4.5 eq.) in DMF for 4 h (GP2). Cleavage from the resin under concomitant deprotection was carried out in TFA for 6 h (GP7b). After RP-HPLC-based purification, rhPSMA-11 was obtained as a colorless solid (11%). RP-HPLC (10 to 70% B in 15 min): t_R = 9.7 min, K' = 3.41. Calculated monoisotopic mass ($C_{60}H_{95}FN_{12}O_{23}Si$): 1398.6; found: m/z = 1399.8 $[M+H]^+$, 700.7 $[M+2H]^{2+}$.

6. Synthesis of cold metal complexes

6.1 Synthesis of ^{nat}Ga-TRAP complexes

500 µL of a 2 mM stock solution of the rhPSMA precursor (1.0 eq.) in DMSO were combined with 75 µL of a 20 mM $Ga(NO_3)_3$ (1.5 eq.) solution in water (Tracepur®, Merck, Darmstadt, Germany). Complexation occurred instantaneously at rt. The reaction was monitored by RP-HPLC and mass spectrometry. If required, purification of the crude ligand was performed by RP-HPLC.

[^{nat}Ga][^{19}F]rhPSMA-101: RP-HPLC (10 to 90% B in 15 min): t_R = 11.0 min, K' = 4.0. Calculated monoisotopic mass ($C_{91}H_{138}FGaIN_{16}O_{28}P_3Si$): 2238.7; found: m/z = 1120.9 $[M+2H]^{2+}$, 747.7 $[M+3H]^{3+}$.

[^{nat}Ga][^{19}F]rhPSMA-102: RP-HPLC (10 to 90% B in 15 min): t_R = 13.3 min, K' = 5.05. Calculated monoisotopic mass ($C_{91}H_{139}FGaN_{16}O_{27}P_3Si$): 2096.8; found: m/z = 1050.1 $[M+2H]^{2+}$.

[^{nat}Ga][^{19}F]rhPSMA-201: RP-HPLC (10 to 90% B in 15 min): t_R = 10.7 min, K' = 3.86. Calculated monoisotopic mass ($C_{86}H_{130}FGaN_{15}O_{26}P_3Si$): 1997.8; found: m/z = 1000.2 $[M+2H]^{2+}$.

[^{nat}Ga][^{19}F]rhPSMA-202: RP-HPLC (10 to 90% B in 15 min): t_R = 10.4 min, K' = 3.73. Calculated monoisotopic mass ($C_{83}H_{124}FGaN_{15}O_{26}P_3Si$): 1955.7; found: m/z = 981.2 $[M+2H]^{2+}$.

[^{nat}Ga][^{19}F]rhPSMA-203: RP-HPLC (10 to 90% B in 15 min): t_R = 10.6 min, K' = 3.82. Calculated monoisotopic mass ($C_{92}H_{141}FGaN_{16}O_{27}P_3Si$): 2110.8; found: m/z = 1057.8 $[M+2H]^{2+}$.

[^{nat}Ga][^{19}F]rhPSMA-204: RP-HPLC (10 to 90% B in 15 min): t_R = 10.3 min, K' = 3.68. Calculated monoisotopic mass ($C_{89}H_{135}FGaN_{16}O_{27}P_3Si$): 2068.8; found: m/z = 1035.8 $[M+2H]^{2+}$.

[^{nat}Ga][^{19}F]rhPSMA-301: RP-HPLC (10 to 90% B in 15 min): t_R = 9.4 min, K' = 3.27. Calculated monoisotopic mass ($C_{65}H_{108}FGaN_{13}O_{22}P_3Si$): 1631.6; found: m/z = 1633.1 $[M+H]^{+}$, 817.0 $[M+2H]^{2+}$.

[^{nat}Ga][^{19}F]rhPSMA-302: RP-HPLC (10 to 90% B in 15 min): t_R = 9.7 min, K' = 3.41. Calculated monoisotopic mass ($C_{90}H_{121}FGaN_{15}O_{26}Si$): 1943.8; found: m/z = 1945.4 $[M+H]^{+}$, 973.8 $[M+2H]^{2+}$.

***[^{nat}Ga][^{19}F]rhPSMA-4*:** RP-HPLC (10 to 90% B in 15 min): t_R = 8.4 min, K' = 2.82. Calculated monoisotopic mass ($C_{68}H_{112}FGaN_{13}O_{24}P_3Si$): 1703.6; found: m/z = 1705.4 $[M+H]^{+}$, 853.3 $[M+2H]^{2+}$.

[^{nat}Ga][^{19}F]rhPSMA-5: RP-HPLC (10 to 90% B in 15 min): t_R = 9.5 min, K' = 3.32. Calculated monoisotopic mass ($C_{65}H_{106}FGaN_{13}O_{24}P_3Si$): 1661.6; found: m/z = 1663.8 $[M+H]^+$, 832.6 $[M+2H]^{2+}$.

[^{nat}Ga][^{19}F]rhPSMA-9: RP-HPLC (10 to 90% B in 15 min): t_R = 9.0 min, K' = 3.09. Calculated monoisotopic mass ($C_{65}H_{103}FGaN_{14}O_{27}P_3Si$): 1720.5; found: m/z = 1720.8 $[M+H]^+$, 861.1 $[M+2H]^{2+}$.

6.2 Synthesis of ^{nat}Ga-DOTA-GA and ^{nat}Ga-DOTA complexes

Small scale: 500 µL of a 2 mM stock solution of the rhPSMA precursor (1.0 eq.) in DMSO were combined with 150 µL of a 20 mM $Ga(NO_3)_3$ solution (3.0 eq.) in water (Tracepur®, Merck, Darmstadt, Germany). The reaction mixture was heated for 30 min at 75 °C. Outcome of the reaction was monitored by RP-HPLC and subsequent mass spectrometry. If required, the complexed compound was purified by RP-HPLC.

Large scale: For ^{nat}Ga-complexation at larger scales (> 50 mg uncomplexed compound), the ligand (1.0 eq.) was dissolved in a 1:1 mixture (*v*/*v*) of *t*BuOH in H_2O (Tracepur®, Merck, Darmstadt, Germany) and an aqueous solution of $Ga(NO_3)_3$ (5.0 eq., 0.7 M) was added. After heating the resulting mixture for 35 min at 75 °C, the peptide was purified by RP-HPLC.

[^{nat}Ga][^{19}F]rhPSMA-6: RP-HPLC (10 to 90% B in 15 min): t_R = 9.1 min, K' = 3.14. Calculated monoisotopic mass ($C_{63}H_{99}FGaN_{11}O_{22}Si$): 1477.6; found: m/z = 1479.5 $[M+H]^+$, 740.2 $[M+2H]^{2+}$.

[^{nat}Ga][^{19}F]rhPSMA-7: RP-HPLC (10 to 70% B in 15 min): t_R = 10.4 min, K' = 3.73. Calculated monoisotopic mass ($C_{63}H_{96}FGaN_{12}O_{25}Si$): 1536.6; found: m/z = 1539.4 $[M+H]^+$, 770.3 $[M+2H]^{2+}$.

[^{nat}Ga][^{19}F]rhPSMA-7.1: RP-HPLC (10 to 70% B in 15 min): t_R = 10.5 min, K' = 3.77. RP-HPLC (25 to 35% B in 40 min): t_R = 31.4 min, K' = 13.27. Calculated monoisotopic mass ($C_{63}H_{96}FGaN_{12}O_{25}Si$): 1536.6; found: m/z = 1539.4 $[M+H]^+$, 770.3 $[M+2H]^{2+}$.

[^{nat}Ga][^{19}F]rhPSMA-7.2: RP-HPLC (10 to 70% B in 15 min): t_R = 10.4 min, K' = 3.73. RP-HPLC (25 to 35% B in 40 min): t_R = 27.9 min, K' = 11.68. Calculated monoisotopic mass ($C_{63}H_{96}FGaN_{12}O_{25}Si$): 1536.6; found: m/z = 1539.2 $[M+H]^+$, 770.2 $[M+2H]^{2+}$.

[^{nat}Ga][^{19}F]rhPSMA-7.3: RP-HPLC (10 to 70% B in 15 min): t_R = 10.4 min, K' = 3.73. RP-HPLC (25 to 35% B in 40 min): t_R = 28.1 min, K' = 11.77. Calculated monoisotopic mass ($C_{63}H_{96}FGaN_{12}O_{25}Si$): 1536.6; found: m/z = 1539.0 $[M+H]^+$, 770.1 $[M+2H]^{2+}$.

[^{nat}Ga][^{19}F]rhPSMA-7.4: RP-HPLC (10 to 70% B in 15 min): t_R = 10.5 min, K' = 3.77. RP-HPLC (25 to 35% B in 40 min): t_R = 29.1 min, K' = 12.23. Calculated monoisotopic mass ($C_{63}H_{96}FGaN_{12}O_{25}Si$): 1536.6; found: m/z = 1539.1 $[M+H]^+$, 770.2 $[M+2H]^{2+}$.

[^{nat}Ga][^{19}F]rhPSMA-8: RP-HPLC (10 to 70% B in 15 min): t_R = 10.4 min, K' = 3.73. Calculated monoisotopic mass ($C_{63}H_{96}FGaN_{12}O_{25}Si$): 1536.6; found: m/z = 1539.1 $[M+H]^+$, 770.5 $[M+2H]^{2+}$.

[^{nat}Ga][^{19}F]rhPSMA-10: RP-HPLC (10 to 70% B in 15 min): 9.5 min, K' = 3.32. Calculated monoisotopic mass ($C_{60}H_{92}FGaN_{12}O_{23}Si$): 1464.5; found: m/z = 1467.3 $[M+H]^+$, 733.9 $[M+2H]^{2+}$.

6.3 Synthesis of ^{nat}Lu-DOTA-GA and ^{nat}Lu-DOTA complexes

The corresponding ^{nat}Lu-complexes were prepared from a 2 mM aqueous solution of the PSMA inhibitor (1.0 eq.) with a 20 mM solution of $LuCl_3$ (2.5 eq.) in water (Tracepur®, Merck, Darmstadt, Germany), heated to 95 °C for 30 min. Formation of the ^{nat}Lu-chelate was confirmed using RP-HPLC and MS. If required, the complexed compound was purified by RP-HPLC.

[^{nat}Lu][^{19}F]rhPSMA-7: RP-HPLC (10 to 70% B in 15 min): t_R = 9.5 min, K' = 3.32. Calculated monoisotopic mass ($C_{63}H_{96}FLuN_{12}O_{25}Si$): 1642.6; found: m/z = 1645.4 $[M+H]^+$, 823.3 $[M+2H]^{2+}$.

[^{nat}Lu][^{19}F]rhPSMA-7.3: RP-HPLC (10 to 70% B in 15 min): t_R = 9.6 min, K' = 3.36. Calculated monoisotopic mass ($C_{63}H_{96}FLuN_{12}O_{25}Si$): 1642.6; found: m/z = 1644.8 $[M+H]^+$, 823.1 $[M+2H]^{2+}$.

[^{nat}Lu][^{19}F]rhPSMA-8: RP-HPLC (10 to 70% B in 15 min): t_R = 10.0 min, K' = 3.55. Calculated monoisotopic mass ($C_{63}H_{96}FLuN_{12}O_{25}Si$): 1642.6; found: m/z = 1644.7 $[M+H]^+$, 822.6 $[M+2H]^{2+}$.

[^{nat}Lu][^{19}F]rhPSMA-10: RP-HPLC (10 to 70% B in 15 min): t_R = 9.6 min, K' = 3.36. Calculated monoisotopic mass ($C_{60}H_{92}FLuN_{12}O_{23}Si$): 1570.6; found: m/z = 1572.2 $[M+H]^+$, 786.6 $[M+2H]^{2+}$.

[^{nat}Lu][^{19}F]rhPSMA-11: RP-HPLC (10 to 70% B in 15 min): t_R = 9.9 min, K' = 3.5. Calculated monoisotopic mass ($C_{60}H_{92}FLuN_{12}O_{23}Si$): 1570.6; found: m/z = 1572.1 $[M+H]^+$, 786.7 $[M+2H]^{2+}$.

7. Radiolabeling

7.1 ^{68}Ga-labeling

^{68}Ga-labeling was carried out using an automated system (GallElut^{+} by Scintomics, Germany) as described previously[167]. Briefly, the ^{68}Ge/^{68}Ga-generator with SnO_2 matrix (iThemba LABS, Somerset West, South Africa) was eluted with 1.0 M aq. HCl, from which a fraction (1.25 mL) of approximately 80% of the activity (500-700 MBq) was transferred into a reaction vial (5 mL). Before elution the reactor was loaded with 2-5 nmol of a respective chelator conjugate in an aqueous 2.7 M HEPES solution (DOTA/DOTA-GA-conjugates: 900 µL, TRAP-conjugates: 400 µL). After elution the vial was heated for 5 min at 95 °C. Purification was done by passing the reaction mixture over a solid-phase extraction cartridge (Sep-Pak C 8 light, 145 mg, 37-55 µm, Waters, Eschborn, Germany) which was purged with water (10 mL). The purified product was eluted with 2 mL of a 1:1 (*v*/*v*) mixture of ethanol and water followed by phosphate buffered saline (1 mL). After removing most of the ethanol *in vacuo*, the purity of the radiolabeled compounds was determined by radio-RP-HPLC and radio-TLC (ITLC-SG chromatography paper, mobile phase: 0.1 M trisodium citrate and Silica gel 60 RP-18 F_{254}s, mobile phase: 3:2 mixture (v/v) of MeCN in H_2O, supplemented with 10% of 2 M NaOAc solution and 1% of TFA.

7.2 ^{18}F-labeling

For manual ^{18}F-labeling a previously published procedure with minor modifications was applied[156]. Aqueous [^{18}F]fluoride (approx. 0.6-2.0 GBq/mL) provided by the Klinikum rechts der Isar (Munich, Germany) was passed through a SAX cartridge (Sep-Pak Accell Plus QMA Carbonate Plus Light, 46 mg, 40 µm, Waters), which was preconditioned with 10 mL of water. After most of the remaining water was removed with 20 mL of air, residual water was removed by rinsing the cartridge with 10 mL of anhydrous acetonitrile (for DNA synthesis, max. 10 ppm H_2O, VWR) followed by 20 mL of air. For cartridge elution, a solution of $[K^{+}\subset 2.2.2]OH^{-}$ cryptate in 500 µL of anhydrous acetonitrile was used, which was freshly prepared by dissolution of the lyophilized cryptate prior to the elution process. The cryptate was prepared by lyophilisation of a solution of 2.2.2-cryptand (Kryptofix® 222, 91 µmol, 1.1 eq., Sigma-Aldrich) and KOH (83 µmol, 1.0 eq., 99.99% semiconductor grade, Sigma Aldrich) in 1.0 mL of water.

The eluate was then partly neutralized with 30 µL of a 1 M solution of oxalic acid (99.999%, trace metals basis, Sigma-Aldrich) in anhydrous acetonitrile. The resulting mixture (eluate and oxalic acid) or an aliquot thereof was used for fluorination of 10-150 nmol of the respective SiFA-conjugated labeling precursor (1 mM solutions in anhydrous DMSO, > 99.9%, Simga Aldrich) for 5 min at rt. For purification by means of solid phase extraction, Oasis HLB Plus Light cartridges (30 mg, 30 µm, Waters) preconditioned with 10 mL of ethanol and 10 mL of H_2O, were used. For this purpose, the labeling mixture was diluted with 9 mL PBS (pH 5, adjusted with 1 M aq. HCl) and passed through the cartridge followed by 10 mL PBS (pH 5) and 10 mL of air. The labeled product and the unlabeled precursor were eluted from the HLB cartridge with 0.3-2.0 mL of a 1:1 mixture (*v*/*v*) of EtOH in water. Radiochemical purity of the ^{18}F-labeled compound was determined by radio-RP-HPLC and radio-TLC (Silica gel 60 RP-18 F_{254}s, mobile phase: 3:2 mixture (v/v) of MeCN in H_2O, supplemented with 10% of 2 M NaOAc solution and 1% of TFA).

Based on the manual labeling procedure, an automated radiosynthesis of ^{18}F-labeled rhPSMA ligands was developed and established on a GRP 2V module (Scintomics, Fürstenfeldbruck, Germany) at the Department of Nuclear Medicine (TUM). A brief description of the automatized production of [^{18}F][^{nat}Ga]rhPSMA-7/7.3 is provided in chapter "III. 7.3 Automated ^{18}F-labeling of rhPSMA ligands".

7.3 ^{177}Lu-labeling

For ^{177}Lu-labeling a previously published procedure was applied with minor modifications[96, 168]. The labeling precursor (e.g. [^{19}F]rhPSMA-7, 1.0 nmol, 10 µL, 1 mM in DMSO) was added to 10 µL of 1.0 M aq. NH_4OAc buffer (pH 4.5). Subsequently, 20 to 110 MBq $^{177}LuCl_3$ (specific activity (S_A) > 3000 GBq/mg, 740 MBq/mL, 0.04 M HCl, ITG, Garching, Germany) were added and the mixture was filled up to 100 µL with water (Tracepur®, Merck, Darmstadt, Germany). The reaction mixture was heated for 15-30 min at 95 °C and the radiochemical purity was determined using radio-RP-HPLC and radio-TLC (Silica gel 60 RP-18 F_{254}s, 3:2 mixture (*v*/*v*) of MeCN in H_2O, supplemented with 10% of 2 M NaOAc solution and 1% of TFA).

7.4 ^{125}I-labeling

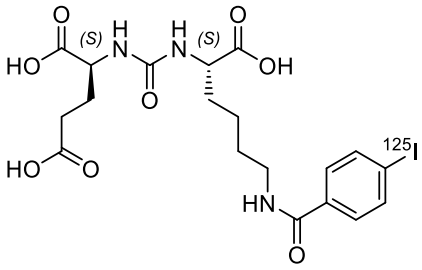

([^{125}I]I-BA)KuE
Chemical Formula: $C_{19}H_{24}{}^{125}IN_3O_8$
Molecular Weight: 547,32

[^{125}I]NaI as an alkaline solution (74 TBq/mmol, 3.1 GBq/mL, 40 mM NaOH) was purchased from Hartmann Analytic (Braunschweig, Germany). The reference ligand for *in vitro* studies (((*S*)-1-carboxy-5-(4-([^{125}I]iodo)benzamido)pentyl)carbamoyl)-*L*-glutamic acid (([^{125}I]I-BA)KuE) was prepared according to a previously published procedure[71, 169]. Briefly, approximately 0.1 mg of the stannylated precursor $SnBu_3$-BA-(O*t*Bu)KuE(O*t*Bu)$_2$ (4) was dissolved in a mixture of 20 µL peracetic acid, 5.0 µL [^{125}I]NaI (40 mM in NaOH, 15 ± 5 MBq, 74 TBq/mmol), 20 µL MeCN and 10 µL acetic acid. The reaction solution was incubated for 10 min at rt and loaded on a Sep-Pak C18 Plus Short cartridge (360 mg, 55-105 µm, Waters) which was initially preconditioned with 10 mL MeOH followed by 10 mL water. After purging with 10 mL of water, the cartridge was eluted with 2.0 mL of a 1:1 mixure (*v*/*v*) of EtOH and MeCN. The eluate was evaporated to dryness under a gentle nitrogen stream at 70 °C and treated with 500 µL TFA for 30 min. After removing TFA in a stream of nitrogen, the crude product was purified by RP-HPLC yielding ([^{125}I]I-BA)KuE (5 ± 2 MBq). RP-HPLC (20 to 40% B in 20 min): t_R = 13.0 min, K' = 7.13.

8. *In vitro* experiments

8.1 Cell culture

PSMA-positive LNCAP cells (300265; Cell Lines Service, Eppelheim, Germany) were cultivated in Dulbecco modified Eagle medium/Nutrition Mixture F-12 with Glutamax (1:1) (DMEM-F12, Biochrom, Berlin, Germany) supplemented with fetal bovine serum (10%, FBS Zellkultur, Berlin, Germany) and kept at 37 °C in a humidified CO_2 atmosphere (5%). A mixture of trypsin and EDTA (0.05%, 0.02%) in PBS (Biochrom) was used in order to harvest cells. Cells were counted with a Neubauer hemocytometer (Paul Marienfeld, Lauda-Königshofen, Germany).

8.2 Affinity determinations (IC_{50})

Quantification of the binding affinity to PSMA was measured by determination of the half-maximal inhibitory concentration (IC_{50}) of each inhibitor using ([^{125}I]I-BA)KuE as radioactive reference ligand. For this purpose, the respective ligand was diluted (serial dilution 10^{-4} to 10^{-10}) in Hank's balanced salt solution (HBSS, Biochrom). In the case of metal-complexed ligands, the crude reaction mixture containing the purified metal-complexed inhibitor and remaining metal chloride/nitrate, was diluted analogously without further purification. Cells were harvested 24 ± 2 h prior to the experiment and seeded in 24-well plates (1.5×10^5 cells in 1 mL/well). After removal of the culture medium, the cells were carefully washed with 500 µL of HBSS supplemented with 1% bovine serum albumin (BSA, Biowest, Nuaillé, France) and left 15 min on ice for equilibration in 200 µL HBSS (1% BSA). Next, 25 µL per well of solutions containing either HBSS (1% BSA, control) or the respective ligand in increasing concentration (10^{-10}-10^{-4} M in HBSS) were added with subsequent addition of 25 µL of ([^{125}I]I-BA)KuE (2.0 nM) in HBSS (1% BSA). After incubation on ice for 60 min, the experiment was terminated by removal of the medium and consecutive rinsing with 200 µL of HBSS (1% BSA). The media of both steps were combined in one fraction and represent the amount of free radioligand. Afterwards, the cells were lysed with 250 µL of 1 M aq. NaOH for at least 10 min. After a washing step (250 µL of 1 M NaOH), both fractions representing the amount of bound ligand were united. Quantification of all collected fractions was accomplished in a γ-counter. All IC_{50} determinations were carried out at least three times per ligand.

8.3 Internalization studies

For internalization studies, LNCaP cells were harvested 24 ± 2 h before the experiment and seeded in poly-*L*-lysine coated 24-well plates (1.25×10^5 cells in 1 mL/well, Greiner Bio-One, Kremsmünster, Austria). After removal of the culture medium, the cells were washed once with 500 µL DMEM-F12 (5% BSA) and left to equilibrate for at least 15 min at 37 °C in 200 µL DMEM-F12 (5% BSA). Each well was treated with either 25 µL of either DMEM-F12 (5% BSA, control) or 25 µL of a 100 µM 2-PMPA (2-(phosphonomethyl)-pentandioic acid, Tocris Bioscience, Bristol, United Kingdom) solution in PBS for blockade. Next, 25 µL of the radioactive-labeled PSMA inhibitor (5.0 nM in PBS for ^{18}F- and ^{68}Ga-rhPSMA, 10.0 nM in PBS for ^{177}Lu-rhPSMA) was added and the cells were incubated at 37 °C for 60 min. The experiment was terminated by placing the 24-well plate on ice for 3 min and removal of the medium. Each well was carefully washed with 250 µL of ice-cold HBSS. Both fractions from the first steps representing the amount of free radioligand were combined. Removal of surface-bound activity was accomplished by incubation of the cells with 250 µL of ice-cold PMPA (10 µM in PBS) solution for 5 min and rinsed again with another 250 µL of ice-cold PBS. The internalized activity was determined by incubation of the cells in 250 µL of 1 M aq. NaOH for at least 10 min. The obtained fractions were combined with those of the subsequent washing step with 250 µL of 1 M aq. NaOH. Each experiment (control and blockade) was performed in triplicate. Free, surface bound and internalized activity was quantified in a γ-counter. All internalization studies were complemented by external reference studies using ([^{125}I]I-BA)KuE (c = 0.2 nM), which were performed analogously. Data were corrected for non-specific binding and normalized to the specific-internalization observed for the radioiodinated reference compound.

8.4 Octanol-PBS partition coefficient

Approximately 1 MBq of the labeled tracer was dissolved in 1 mL of a 1:1 mixture (*v*/*v*) of PBS (pH 7.4) and *n*-octanol in a reaction vial (1.5 mL). After vigorous mixing of the suspension for 3 min at rt, the vial was centrifuged at 15000 g for 3 min (Biofuge 15, Heraus Sepatech, Osterode, Germany) and 100 µL aliquots of both layers were measured in a gamma counter. The experiment was repeated at least six times.

8.5 Determination of human serum albumin binding

Human serum albumin (HSA) binding of the PSMA-addressing ligands was determined according to a previously published procedure *via* HPLC[170]. A Chiralpak HSA column (50 x 3 mm, 5 µm, H13H-2433, Daicel, Tokyo, Japan) was used at a constant flow rate of 0.5 mL/min at rt. Mobile phase A was a freshly prepared 50 mM aq. solution of NH_4OAc (pH 6.9) and mobile phase B was isopropanol (HPLC grade, VWR). The applied gradient for all experiments was 100% A (0 to 3 min), followed by 80% A (3 to 40 min). Prior to the experiment, the column was calibrated using nine reference substances with a HSA binding in the range of 13 to 99%[170, 171]. All substances, including the examined PSMA ligands, were dissolved in a 1:1 mixture (*v*/*v*) of isopropanol and a 50 mM aq. solution of NH_4OAc (pH 6.9) with a final concentration of 0.5 mg/mL. Non-linear regression was established with the OriginPro 2016G software (Northampton, United States; Figure 9).

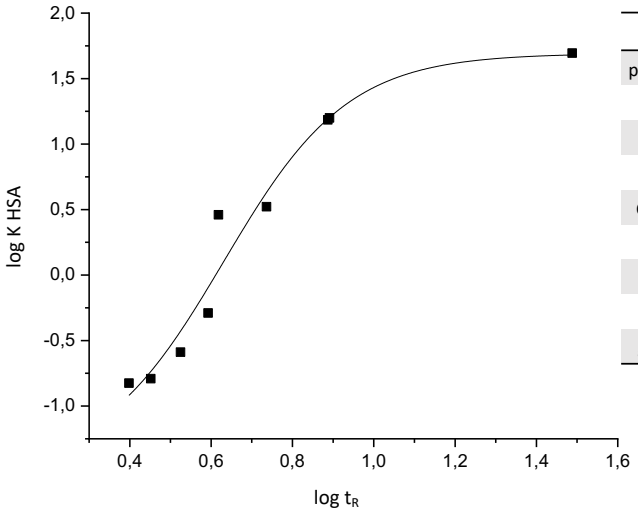

reference	t_R	K‘	log t_R	lit. HSA [%]	log K HSA
p-benzyl alcohol	2.50	0.25	0.40	13.15	-0.82
aniline	2.83	042	0.45	14.06	-0.79
phenol	3.35	0.68	0.52	20.69	-0.59
benzoic acid	3.92	0.96	0.59	34.27	-0.29
Carbamazepin	4.15	1.08	0.62	75.00	0.46
p-nitrophenol	5.45	1.73	0.74	77.65	0.52
estradiol	7.71	2.86	0.89	94.81	1.19
probenecid	7.78	2.89	0.89	95.00	1.20
glibenclamide	30.76	14.38	1.49	99.00	1.69

Figure 9: Exemplary sigmoidal plot, showing the correlation between human serum albumin (HSA) binding of selected reference substances and their retention time (t_R) on a Chiralpak HSA column (Daicel, Tokyo, Japan). The HSA binding values were obtained from literature (lit. HSA [%]) and the respective logarithmic value of the affinity constant (log K HSA) was calculated[170, 171]. log t_R: logarithmic value of experimentally determined retention time. K´: capacity factor.

9. *In vivo* experiments

All animal experiments were conducted in accordance with general animal welfare regulations in Germany (German animal protection act, as amended on 18.05.2018, Art. 141 G v. 29.3.2017 I 626, approval no. 55.2-1-54-2532-71-13) and the institutional guidelines for the care and use of animals. To establish tumor xenografts, LNCaP cells (approx. 10^7 cells) were suspended in 200 µL of a 1:1 mixture (*v*/*v*) of DMEM F-12 and Matrigel (BD Biosciences, Germany), and inoculated subcutaneously onto the right shoulder of 6-8 weeks old CB17-SCID mice (Charles River, Sulzfeld, Germany). Mice were used for experiments when tumors had grown to a diameter of 5-10 mm (3-6 weeks after inoculation).

9.1 *µPET* imaging

Imaging studies were performed at a Siemens Inveon small-animal PET system (Siemens Healthineers, Erlangen, Germany) at the Department of Nuclear Medicine (TUM). Data were reconstructed as single frames employing a three-dimensional ordered subset expectation maximum (OSEM3D) algorithm, followed by data analysis (ROI-based quantification) using the Inveon Research Workplace software. For PET studies mice were anesthetized with isoflurane and injected with 2-20 MBq (0.15-0.25 nmol) of the ^{68}Ga- or ^{18}F-labeled tracer into the tail vein. Static images were recorded 1 h p.i. with an acquisition time of 15 min.

9.2 Biodistribution studies

Approximately 2-20 MBq (0.2 nmol) of the radioactively labeled PSMA inhibitors were injected into the tail vein of LNCaP tumor-bearing male CB-17 SCID mice and sacrificed after 1 or 24 h p.i.. Selected organs were removed, weighted and measured in a γ-counter. For competition studies, 8 mg/kg of 2-PMPA in PBS was co-administered.

9.3 Metabolite studies

Analytical Set-Up

Information about the used HPLC and TLC system are provided in the general information section. The HPLC system was connected to a high-sensitivity radiation detector (Flowstar^2 LB514, Berthold Technologies, Bad Wildbad, Germany). The gradient for all HPLC operations was: 5% B isocratic 0-3 min, 25-35 % B 3-43 min, 95-95 % B 43-48 min, using a Multospher 100 RP18 (125 × 4.6 mm, 5 µm particle size) column (CS Chromatographie Service, Langerwehe, Germany). Radio-TLC analysis was performed on Silica gel coated sheets (60 RP-18 F_{254}s) with a 3:2 mixture (*v*/*v*) of MeCN in H_2O supplemented with 10% of 2 M NaOAc solution and 1% of TFA as mobile phase.

Determination of *in vivo* distribution of [^{18}F][^{nat}Ga]rhPSMA-7.1 to -7.4

In order to quantify the relative uptake of each isomer [^{18}F][^{nat}Ga]rhPSMA-7.1 to -7.4 a tumor-bearing male CB-17-SCID mouse was injected with the racemic mixture of [^{18}F][^{nat}Ga]rhPSMA-7 (180-280 MBq, A_M = 247-349 GBq/µmol, produced at the Klinikum rechts der Isar). The animal was left under anesthesia for 30 min and sacrificed. Urine, blood, liver, kidneys and tumor were collected and processed to the hereafter described procedures.

The urine sample was centrifuged for 5 min at 9000 rpm to yield a clear solution and directly subjected to radio-RP-HPLC analysis. Blood was diluted to 1 mL with H_2O and centrifuged twice at 13000 g for 5 min. The supernatant was collected and loaded on a Strata X cartridge (33 µm Polymeric Reversed Phase, 500 mg, Phenomenex, Aschaffenburg, Germany) which was preconditioned with 5 mL MeOH followed by 5 mL H_2O. After washing with 5 mL of H_2O, the cartridge was eluted with a 3:2 mixture (*v*/*v*) of MeCN in H_2O supplemented with 1% TFA. The eluate was diluted with water and analyzed by radio-RP-HPLC. Tumor, kidneys and liver were homogenised using either a Potter-Elvehjem tissue grinder (Kontes Glass, Vineland, United States) or a MM-400 ball mill (Retsch, Haan, Germany).

Extraction *via* the Potter-Elvehjem Tissue Grinder

Tumor and kidneys were separately homogenised in the tissue homogeniser with 1 mL of extraction buffer (850 µL 1 M HEPES pH 7.4, 100 µL 20 mM PMPA and 100 µL 1 M NaCl) for 30 min. The resulting homogenate was collected and centrifuged at 13000 g for 5 min. Subsequently, the supernatant was collected, centrifuged again (13000 g, 5 min) and loaded on a Strata X cartridge (33 µm Polymeric Reversed Phase 500 mg) preconditioned with 5 mL MeOH, followed by 5 mL H_2O. After washing with 5 mL H_2O, the cartridge was eluted with a 3:2 mixture (*v*/*v*) of MeCN in H_2O supplemented with 1% TFA. For radio-RP-HPLC analysis the eluates were diluted with water.

Extraxtion *via* the MM-400 Ball Mill

The organs (tumor, kidney, liver) were separately homogenised in a 2 mL tube together with 3 grinding balls (3 mm diameter) and 1 mL of extraction buffer (850 µL 1 M HEPES pH 7.4, 100 µL 20 mM PMPA and 100 µL 1 M NaCl) for 10 min at 30 Hz. The homogenate was centrifuged at 13000 g for 5 min and the supernatant was collected. Subsequently the pellet was suspended in 1 mL of extraction buffer and homogenized again with the ball mill for 10 min at 30 Hz. After centrifugation (13000 g, 5 min), both supernatants were combined and loaded on a Strata X cartridge (33 µm Polymeric Reversed Phase 500 mg) preconditioned with 5 mL MeOH followed by 5 mL H_2O. Following washing and elution steps were performed as described above for the procedure using the Potter-Elvehjem Tissue grinder.

Finally, the ratios of the individual isomers were determined from the HPLC profiles of the extracted samples and compared to the ratios of the isomers from the quality control of the racemic mixture of [^{18}F][^{nat}Ga]rhPSMA-7. For HPLC data processing, the Systat (San Jose, United States) software package PeakFit was used. PeakFit allows for automated nonlinear separation, analysis and quantification of HPLC elution profiles by deconvolution procedures that uses a Gaussian response function with a Fourier deconvolution/filtering algorithm (Figure 10).

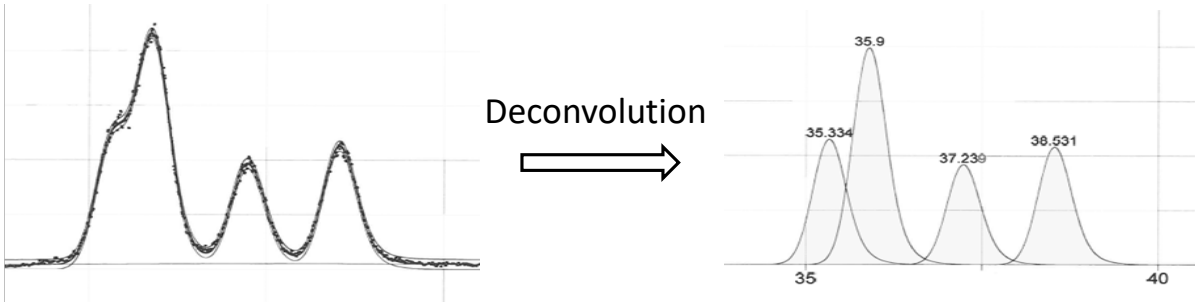

Figure 10: Deconvolution and integration of an exemplary HPLC chromatogram of the quality control of racemic [^{18}F][^{nat}Ga]rhPSMA-7, using Systat Peakfit software.

Defluorination experiments

For defluorination studies, 8-12 MBq (< 0.6 nmol) of the respective ^{18}F-labeled ligand ([^{nat}Ga]rhPSMA-7.1 to -7.4) was injected into the tail vein of female healthy CB17-SCID mice (n=4). Mice were left under anesthesia for 30 min and the urine was collected using a bladder catheter. Urine samples were pooled and centrifuged for 5 min at 9000 rpm to remove suspended solids. The supernatant was directly used for radio-RP-HPLC analysis employing the aforementioned conditions and a RP-18 end-capped column (Multospher 100 RP18, 125 × 4.6 mm, 5 µm particle size, CS Chromatographie Service, Langerwehe, Germany). For *ex vivo* experiments, each compound was incubated for certain time intervals with urine samples from female healthy CB-17-SCID mice which were subsequently analyzed by radio-RP-HPLC.

10. Human applications

Clinical evaluation in patients was conducted under compassionate use in compliance with the German Medicinal Products Act, AMG §13 2b, and in accordance with the responsible regulatory body (Government of Oberbayern) at the Klinikum rechts der Isar (Munich, Germany).

10.1 Clinical PET imaging with ^{18}F-labeled rhPSMA ligands

All subjects were examined on a Biograph mCT scanner (Siemens Medical Solutions, Erlangen, Germany) or a Biograph mMR scanner (Siemens Medical Solutions, Erlangen, Germany). All PET scans were acquired in 3D-mode with an acquisition time of 2-4 min per bed position. Emission data were corrected for randoms, dead time, scatter, and attenuation and were reconstructed iteratively by an ordered-subsets expectation maximization algorithm (four iterations, eight subsets) followed by a postreconstruction smoothing Gaussian filter (5 mm full width at one-half maximum).

Images were obtained after injection of 191-417 MBq of [^{18}F][^{nat}Ga]rhPSMA-7/7.3 at 50-220 min p.i.. Routinely, patients received an injection of 20 mg furosemide at the time of tracer application.

The mean and maximum standardized uptake values (SUV_{mean}/SUV_{max}) of parotid glands, submandibular glands, lungs, mediastinal blood pool, liver, spleen, pancreas head, duodenum, kidneys, bladder and non-diseased bone were analyzed. For calculation of the SUV, circular regions of interest were drawn around areas with focally increased uptake in transaxial slices and automatically adapted to a three-dimensional volume of interest (VOI) at a 50% isocontour. Lesions were visually considered as suggestive of relapses or metastases and were analyzed using SUV_{max} and SUV_{mean} as described above. Gluteal muscle served as background.

10.2 Human application of [^{177}Lu][^{19}F]rhPSMA-7.3

In a comparative dosimetric study, one patient with mCRPC PSMA-avid lesions on pretherapeutic PET received 1.03 GBq of [^{177}Lu]PSMA I&T, followed by 0.91 GBq of [^{177}Lu][^{19}F]rhPSMA-7.3 after 3 weeks. The uptake of both tracers was quantified in liver, kidneys and metastases by scintigraphy at multiple time points between 1 and 168 h. Each scan was obtained at a speed of 12 cm/min on a dual-headed SYMBIA T6 (Siemens Medical Solutions, Erlangen, Germany) equipped with 9.5 mm NaI(Tl) crystals and medium-energy low-penetration collimators. A 20% and a 12% energy window were placed around the 208 keV and 113 keV peak of ^{177}Lu, respectively.

III. Results and Discussion

1. First-generation rhPSMA ligands

Since its introduction in 2015, radiolabeled PSMA I&T has been a valuable tool in the clinical management of PCa patients. After the first successful application of [^{68}Ga]PSMA I&T in PET and subsequent PSMA-targeted radioligand therapy employing the ^{177}Lu-labeled compound, PSMA I&T has been further applied in various centers, both for imaging and therapy[117, 172]. Due to its excellent PSMA-targeting properties including favorable pharmacokinetics with high tumor-to-organ ratios, the general peptide scaffold of PSMA I&T was used for the design of the first-generation rhPSMA ligands in this work.

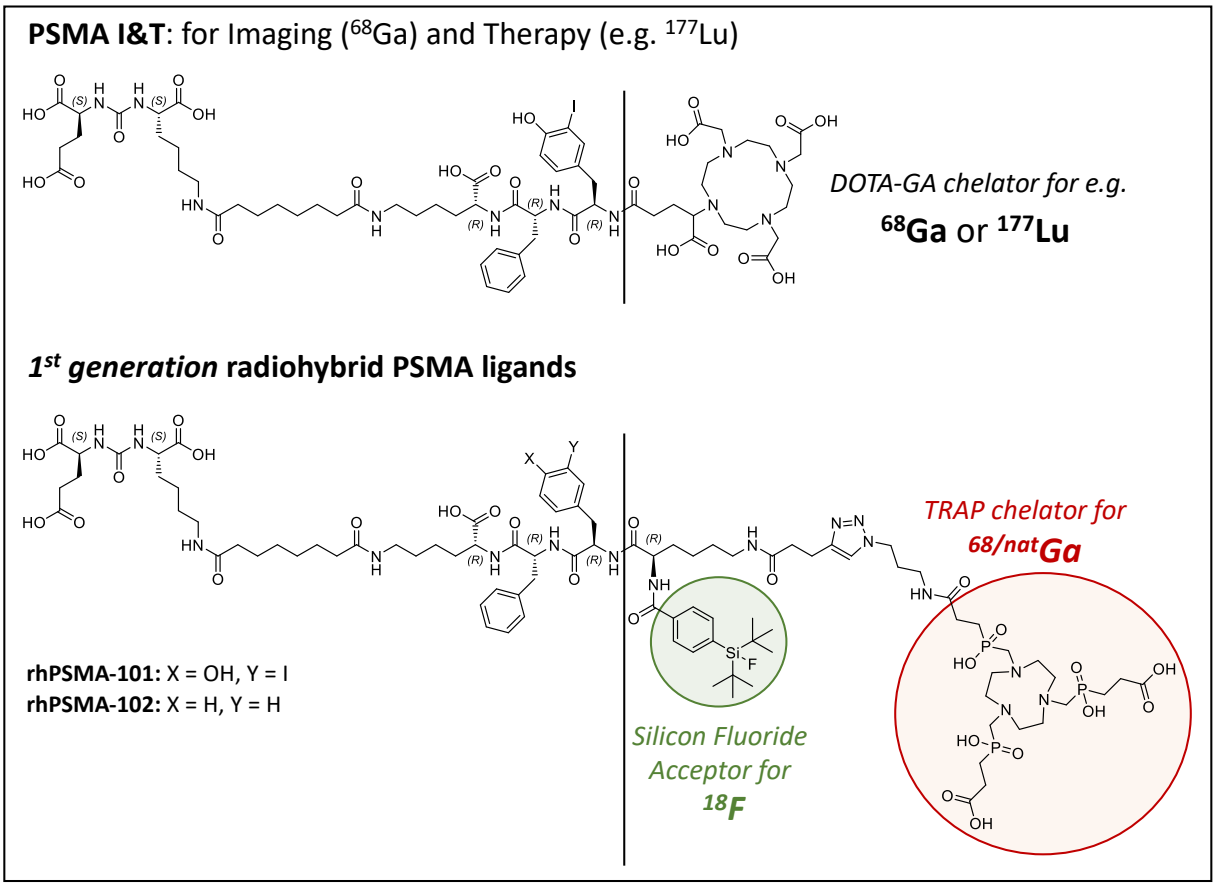

Figure 11: First-generation radiohybrid PSMA-addressing ligands (rhPSMA-101 and rhPSMA-102, depicted as uncomplexed inhibitors), derived from the parent compound PSMA I&T. Both ligands are equipped with a silicon fluoride acceptor (green) for ^{18}F-labeling and a TRAP chelator (red) for complexation of $^{68/nat}$Ga.

In rhPSMA-101, the peptide scaffold of PSMA I&T was extended by a bifunctional amino acid, in order to conjugate the SiFA group and the chelator. With the intention to avoid sterical repulsion within the sensitive binding region of PSMA, the bulky SiFA moiety was placed at a distant position to the EuK binding motif. The resulting close spatial proximity to the chelator might in turn be beneficial to compensate the high lipophilicity of SiFA. With the aim to maximize this effect, the hydrophilic phophinate-based TRAP chelator was used instead of DOTA-GA, that is utilized in PSMA I&T. Due to intramolecular hydrolysis of active esters, which would be required for amide-bond formation, it was only possible to conjugate TRAP in a copper-catalyzed alkyne-azide cycloaddition[173]. The peptide was therefore further functionalized with an azide-moiety and conjugated to propargyl-TRAP in a click reaction.
In rhPSMA-102, the linker was slightly modified by replacing the 3-iodotyrosine residue by a phenylalanine in analogy to the PSMA-TUM-1 ligand[71].
Both ligands could be prepared *via* a mixed solid-phase/solution-phase synthesis strategy. After the final copper-catalyzed click addition of TRAP and subsequent purification, rhPSMA-101 and rhPSMA-102 could be obtained in yields of 5 and 20%, respectively.

PSMA-affinity (IC_{50}, competitive binding assay on LNCaP cells), lipophilicity (log $P_{O/PBS}$, by means of the distribution in octanol and PBS pH 7.4), as well as binding to human serum albumin (HSA) of the newly developed (radio)metal chelates was determined and compared to the parent compound [$^{nat/68}$Ga]PSMA I&T (Table 1). Compared to [^{nat}Ga]PSMA I&T, both new ligands displayed 10 to 30-fold decreased affinities to PSMA. The optimized peptide linker employed in PSMA I&T aims to address the arene-binding site of PSMA which is located in the immediate vicinity of the entrance lid of the active site and can potentially increase affinities due to π-stacking of aromatic moieties. The most obvious explanation for the significantly lower affinities of [^{nat}Ga][^{19}F]rhPSMA-101 and -102 would be that either the position of the sterically demanding SiFA moiety or its combination with the dipeptide sequences phe-phe and phe-I-tyr is not well tolerated, probably due to repulsive interactions at the arene binding site.

Table 1: Affinity, lipophilicity and binding to human serum albumin of [$^{nat/68}$Ga][^{19}F]rhPSMA-101 and -102. Affinities to PSMA (IC_{50} [nM]) on LNCaP cells (1 h, 4 °C, n=3), lipophilicities as octanol/PBS (pH 7.4) partition coefficient (log $P_{O/PBS}$, n=6) and binding to human serum albumin (HSA) as percent binding (determined on a Chiralpak HSA column); mean values ± SD. Data of the reference ligand PSMA I&T were obtained from previous works of our group[96, 174].

compound [$^{nat/68}$Ga][^{19}F]	**IC_{50}** **[nM]**	**lipophilicity** **log $P_{O/PBS}$**	**HSA-binding** **[%]**
rhPSMA-101	114 ± 8	-	-
rhPSMA-102	373 ± 71	−2.7 ± 0.1	97
[$^{nat/68}$Ga]PSMA I&T	9.4 ± 2.9	−4.3 ± 0.3	52

The most encouraging result of this initial *in vitro* study was the measured low lipophilicity of [^{68}Ga][^{19}F]rhPSMA-102 with a log $P_{O/PBS}$ of −2.7 demonstrating that the pronounced lipophilic character of the SiFA-benzoic-acid (log $P_{O/PBS}$ > 4) can be compensated by means of a chelator. Despite intense efforts, the lowest lipophilicity observed for a compound tagged with a SiFA group so far was measured for an $\alpha_v\beta_3$-integrin targeted RGD (arginine-glycine-aspartic acid) peptide with a log $P_{O/PBS}$ = −2.0[154]. The higher hydrophilicity of [^{68}Ga][^{19}F]rhPSMA-102 clearly indicates that placement of the SiFA group in close proximity to a chelator could be a very promising design element to decrease the lipophilicity of SiFA-bearing ligands.

2. Second-generation rhPSMA ligands

The main goal of the following rhPSMA development process was to increase the binding affinity of the 1st generation ligands, by a) varying the distances between inhibitor, SiFA and chelator, b) using SiFA as lipophilic moiety to address the arene-binding pocket, and c) using SiFA as lipophilic moiety to address the accessory binding pocket of PSMA.

a) Varying the distances between inhibitor, SiFA and chelator

With the aim to shorten the distance of the SiFA moiety to the chelator, an azide-functionalized lysine derivative was applied which allows to omit the pentynoic acid spacer for the required copper-catalyzed click conjugation of TRAP. Additionally, with rhPSMA-202 the effect of an even shorter distance of SiFA to the peptide backbone on PSMA-affinity was examined by substituting the SiFA-conjugated lysine with a diaminopropionic acid (dap) derivative.

With respect to possible sterical repulsion of SiFA inside the arene binding pocket, an aminohexanoic acid (ahx) spacer was introduced between the lys(SiFA)/dap(SiFA) moieties and the phe-phe dipeptide sequence in rhPSMA-203 and -204 (Figure 12).

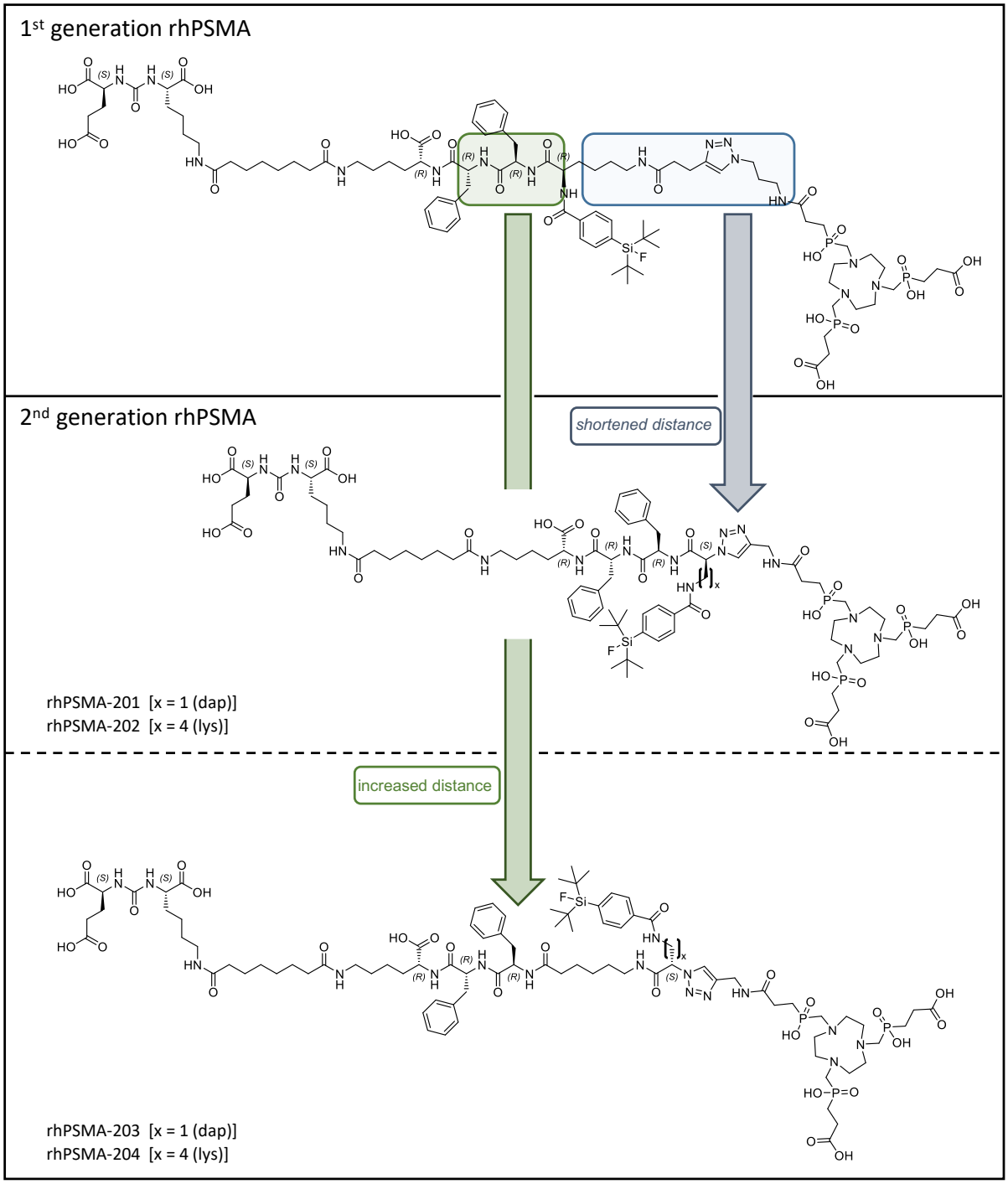

Figure 12: Second-generation radiohybrid PSMA-addressing ligands (rhPSMA-201 to -204, depicted as uncomplexed inhibitors). Novel ligands are structurally derived from rhPSMA-102, by varying the distance of the SiFA moiety to the EuK binding motif and the chelator.

The short-chained ligands rhPSMA-201/202 could be synthesized *via* a straightforward synthetic protocol, in analogy to first-generation ligands and were obtained in final yields of 20 and 12%, respectively. The ahx-spacer derivatives rhPSMA-203/204 could be prepared through a similar approach with an overall yield of 8 and 3%, respectively.

Table 2: PSMA binding affinities (IC_{50} [nM]) of [^{nat}Ga][^{19}F]rhPSMA-101 to 204 and [^{nat}Ga]PSMA I&T on LNCaP cells (1 h, 4 °C, n=3). Values are expressed as mean ± SD. Data of the reference ligand was obtained from Wirtz *et al.*[96].

compound [^{nat}Ga][^{19}F]**rhPSMA-**	**IC_{50}** **[nM]**
101	114 ± 8
102	373 ± 71
201	52 ± 4.5
202	55 ± 5.7
203	142 ± 17
204	148 ± 26
[^{nat}Ga]PSMA I&T	9.4 ± 2.9

The binding affinities of [^{nat}Ga][^{19}F]rhPSMA-201 and -202 with the shortened distance between SiFA and the chelator displayed an almost seven-fold increased affinity compared to the structural analogue [^{nat}Ga][^{19}F]rhPSMA-102. Introduction of the ahx-spacer in [^{nat}Ga][^{19}F]rhPSMA-203 and -204 resulted in an approximately two-fold higher affinity compared to [^{nat}Ga][^{19}F]rhPSMA-102 but lower affinities as measured for the aforementioned derivatives without the spacer. Varying the distance of SiFA to the peptide scaffold by replacing lys by dap did not lead to significantly different affinities in the respective pairs of ligands, [^{nat}Ga][^{19}F]rhPSMA-201/202 and [^{nat}Ga][^{19}F]rhPSMA-203/204 (Table 2).

In a large number of SiFA-containing peptides known from literature, the SiFA group was introduced at a distant position from the respective binding motif in order to avoid unfavorable effects on the pharmacophore with regard to sterical repulsion and lipophilicity[143, 154, 161]. In a recently published work from Niedermoser *et al.*, an octreotate derivative was optimized by varying the linker length between the binding motif and the attached SiFA[143]. The same applies for a variety of PSMA-addressing ligands that contain functional building blocks like fluorescent dyes or albumin binders which also display

challenging physical properties regarding solubility or molecular size comparable to SiFA. These functional units were preferably introduced *via* a spacer at a distant position from the binding motif[175-178]. Therefore, it was all the more surprising that the measured binding affinities of [^{nat}Ga][^{19}F]rhPSMA-203 and -204 were approximately three-fold lower compared to the derivatives without ahx-spacer.

Consequently, the following rhPSMA ligands were optimized without the utilization of an additional spacer between the urea-based inhibitor component and the SiFA group. With the aim to gain more insight into the tolerability of the SiFA moiety in the binding pocket of PSMA, two model compounds were synthesized and evaluated. Herein, SiFA was intended to address either the S1 accessory hydrophobic pocket or the arene-binding site of PSMA.

b) Using SiFA as lipophilic moiety to address the arene-binding

In the aforedescribed rhPSMA ligands, the SiFA group was implemented into the peptide scaffold which already contained two lipophilic amino acid residues (i.e. phe-phe or phe-3-I-tyr). These aromatic moieties were found to improve binding affinities due to favorable interactions with the arene-binding site. However, in combination with the SiFA group, the resulting array of hydrophobic and sterically demanding moieties could potentially increase repulsion inside the binding pocket of PSMA, resulting in lower binding affinities and additionally in an increased lipophilicity of the whole ligand. With this model compound, a minimalistic rhPSMA ligand was synthesized which solely contained the SiFA group in the linker region between the EuK-based inhibitor and the TRAP-chelator without further hydrophobic amino acid residues (Figure 13).

[^{nat}Ga]PSMA I&T 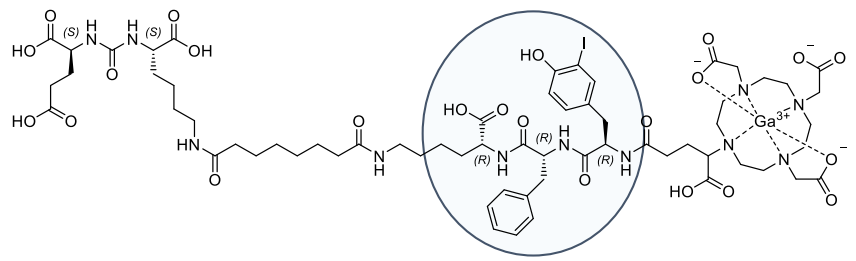	IC_{50} = 9.4 ± 2.9 nM
[^{nat}Ga][^{19}F]rhPSMA-301 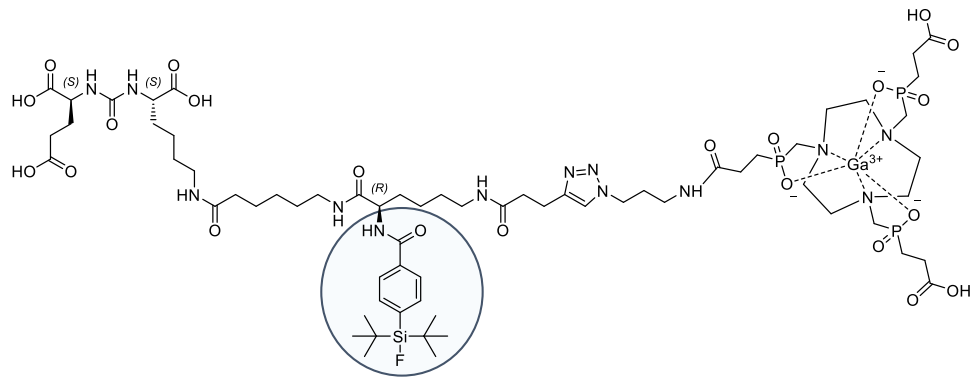	IC_{50} = 25 ± 4.6 nM

Figure 13: Targeting of the arene-binding site of PSMA with the SiFA group of [^{nat}Ga][^{19}F]rhPSMA-301 and the aromatic spacer of [^{nat}Ga]PSMA-I&T (blue circles). PSMA binding affinities (IC_{50} [nM]) of [^{nat}Ga][^{19}F]rhPSMA-301 and [^{nat}Ga]PSMA I&T on LNCaP cells (1 h, 4 °C, n=3). Values are expressed as mean ± SD. Data of the reference ligand was obtained from Wirtz *et al*.[96].

Applying an analogous synthetic strategy as for the first-generation ligands, rhPSMA-301 was obtained in an overall yield of 18% after the copper-catalyzed click addition of propargyl-TRAP and final purification. With [^{nat}Ga]rhPSMA-301 (IC_{50} = 25 ± 4.6 nM), the PSMA binding affinity could be further improved by approximately a factor of two, compared to [^{nat}Ga][^{19}F]rhPSMA-201/-202 (IC_{50} = 52-55 nM). These results support the assumption that the binding tunnel of PSMA leading to the pharmacophore is indeed able to encompass the SiFA moiety. However, a combination of SiFA with other sterically demanding building blocks in close vicinity seems to be less tolerated resulting in lower affinities. At this point it is not clear if the arene-binding site of PSMA can be addressed by the SiFA group in a similar manner like it is possible by the aromatic amino acid residues of PSMA I&T. The significantly lower binding affinity compared to [^{nat}Ga]PSMA I&T however indicate that further fine-tuning regarding the position of SiFA is required in order to achieve similar high affinity binding to PSMA at the pharmacophore and the arene-binding site.

c) Using SiFA as lipophilic moiety to address the accessory binding pocket of PSMA

The S1 accessory hydrophobic pocket is located next to the arginine patch and in close vicinity to the glutamate binding site at the active site of PSMA [64, 73, 74]. In the course of the continuous optimization process of PSMA inhibitors, addressing of this pocket by lipophilic side chains was found to improve binding affinities and internalization rates.

A prominent example for a ligand that is known to interact with this hydrophobic binding pocket is (I-BA)KuE (((*S*)-1-carboxy-5-(4-iodobenzamido)pentyl)carbamoyl)-*L*-glutamic acid; also referred to as DCIBzl), which was used in this work in its radioiodinated form as standard radioligand for *in vitro* studies[58]. In this inhibitor the iodo-phenyl residue binds into the S1 accessory pocket of PSMA contributing to its high affinity (see molecular modelling shown in Figure 2 **C**)[61, 73].

Likewise, Wirtz *et al.* developed a derivative of PSMA I&T with an iodo-phenylalanine residue in immediate proximity to the EuK binding motif in order to increase plasma protein binding[179]. Incorporation of this hydrophobic moiety resulted in similar high binding affinities of respective ligands compared to PSMA I&T[179]. Based on these results the further optimized PSMA-41 was developed by our group[174]. Consequently, a formal SiFA-BA for iodo-phenylalanine substitution in PSMA-41 was used in this pilot study to investigate, whether SiFA could also be used to enhance PSMA binding by interaction with the S1 accessory pocket (Figure 14).

The peptide scaffold of rhPSMA-302 was prepared *via* a solid-phase/solution-phase synthesis strategy. After final conjugation of the DOTA-GA-chelator, the ligand was obtained in an overall yield of 14% after RP-HPLC-based purification. The reference PSMA-41 was obtained in a yield of 23%. The PSMA binding affinity of [^{nat}Ga][^{19}F]rhPSMA-302 was however more than ten-fold lower compared to the parent compound [^{nat}Lu]PSMA-41 (Figure 14)[174].

[^{nat}Lu]PSMA-41 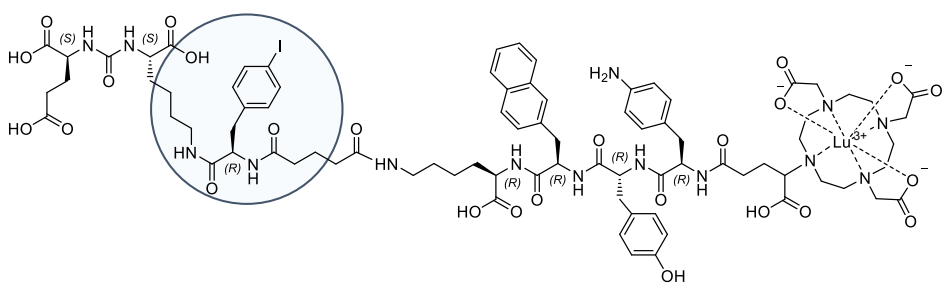	IC_{50} = 6.8 ± 3.2 nM
[^{nat}Ga][^{19}F]rhPSMA-302 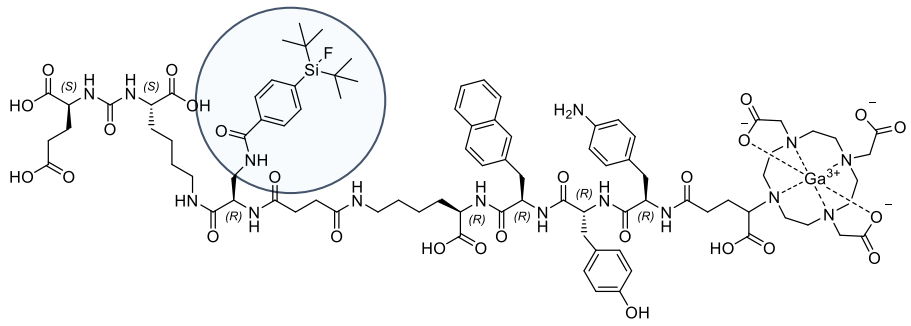	IC_{50} = 83 ± 18 nM

Figure 14: Approaches to adress the S1 accessory pocket of PSMA with the iodo-phenylalanine residue of [^{nat}Lu]PSMA-41 and the SiFA moiety of [^{nat}Ga][^{19}F]rhPSMA-302 and the iodo-phenylalanine residue of [^{nat}Lu]PSMA-41 (blue circles). PSMA binding affinities (IC_{50} [nM]) of [^{nat}Lu]PSMA-41 and [^{nat}Ga][^{19}F]rhPSMA-302 on LNCaP cells (1 h, 4 °C, n=3). Values are expressed as mean ± SD. Data of the reference ligand [^{nat}Lu]PSMA-41 was obtained from Schmidt *et al*.[174].

Noteworthy, the comparability of these results is limited due to different metal-chelates and the slightly modified length of the linker. However, as demonstrated in several studies by our group and others, the chosen metal ion (gallium or lutetium) as well as minor modifications of the linker do not significantly affect the binding affinities of otherwise identical inhibitors[71, 96, 174, 180]. Hence, it can be assumed that the lower affinity of [^{nat}Ga][^{19}F]rhPSMA-302 is rather a result of the substitution of the iodo-phenylalanine residue with the bulky SiFA group and the resulting sterical repulsion in the binding funnel of PSMA. Consequently, the structure of the SiFA moiety seems to be unsuited to interact with the S1 accessory pocket.

3. Third-generation rhPSMA ligands

3.1 EuK-based rhPSMA ligands

The results obtained with rhPSMA-301 and rhPSMA-302 already revealed some helpful insights into the structure-affinity relationship of PSMA-addressing inhibitors comprising a SiFA group. Positioning of the bulky SiFA moiety seems to be more favorable at a defined distance to the urea-based binding motif suitable to address the arene-binding site of the PSMA binding pocket. In addition, combination of SiFA with other sterically demanding and hydrophobic residues in close proximity to the SiFA moiety seem to be less tolerated.

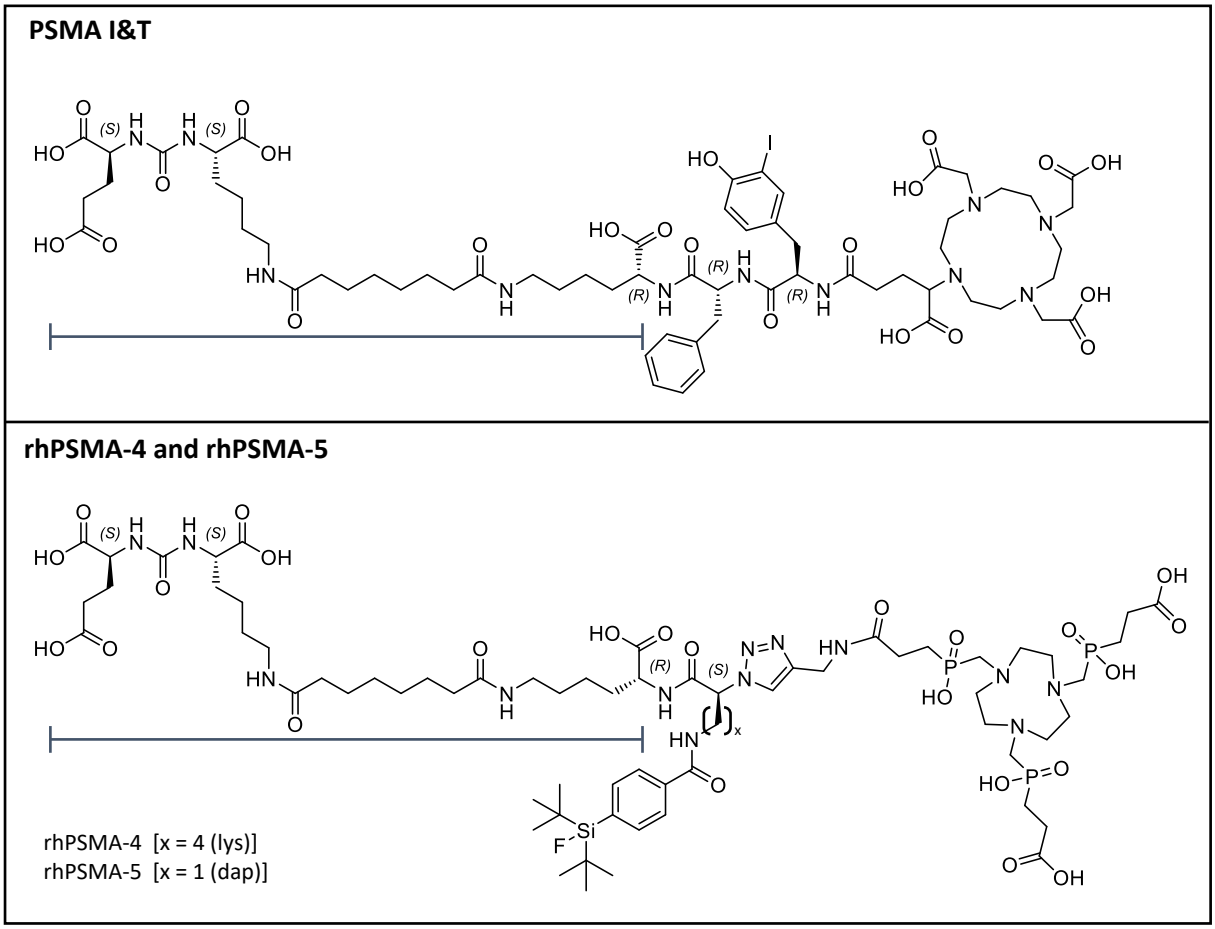

Figure 15: Structural formulas of rhPSMA-4 and -5 (depicted as uncomplexed inhibitors) displaying an identical linker design as PSMA I&T with the aim to optimize the distance of the SiFA moiety to the binding motif.

Consequently, the 3rd generation of SiFA-conjugated PSMA inhibitors tried to overcome these limitations by formal replacement of the phe-phe-sequence by SiFA. A linker moiety identical to that of PSMA I&T was therefore utilized and combined with an azido-lysine derivative which allows functionalization with the SiFA group at the side chain of lysine and conjugation of the TRAP chelator by click chemistry in close proximity (rhPSMA-4). In a second approach, the azido-lysine derivative was substituted by an azido-functionalized diaminopropionic acid derivative in order to examine the effect of a shortened distance of the SiFA group to the peptide backbone (rhPSMA-5, Figure 15).

Applying a mixed solid-phase/solution phase synthetic strategy, the ligands rhPSMA-4 and -5 could be obtained in an overall yield of 4% after purification.

Surprisingly, both 3rd generation rhPSMA ligands showed excellent affinities (Table 3). Identical to PSMA I&T, the EuK binding motif in rhPSMA-4 and -5 is connected *via* a suberic acid spacer to the side chain of a lysine which is then individually functionalized for each ligand. The resulting negative charge from the α-carboxylic acid of the lysine at this position is known from literature to be favorable for PSMA binding affinities and might serve as an explanation for the improved binding affinities compared to [^{nat}Ga][^{19}F]rhPSMA-301[71, 96, 181]. Additionally, the distance of hydrophobic residues to the binuclear zinc site seems to be crucial in order to achieve favorable interactions between SiFA and the arene-binding site. In PSMA I&T and all of its structurally related derivatives (e.g. PSMA I&S, PSMA I&F), an optimal distance was found to be 15 C-X bonds (X = C or N) between the peptidic sequence containing the hydrophobic residues and the EuK binding motif[96, 180, 182]. In contrary to rhPSMA-302 (7 C-X bonds), the novel ligands of the third series had the identical linker length as PSMA I&T. This optimized linker design might allow binding of the SiFA moiety at the arene-binding site similar to the phe-3-I-tyr array of PSMA I&T and therefore could serve as an explanation for the improved binding affinities that are comparable to ^{nat}Ga-PSMA I&T.

Table 3: PSMA binding affinities (IC_{50} [nM]) of [^{nat}Ga][^{19}F]rhPSMA-201, -202, -301, -4, -5 and [^{nat}Ga]PSMA I&T on LNCaP cells (1 h, 4 °C, n=3). Values are expressed as mean ± SD. Data of the reference ligand was obtained from Wirtz *et al.*[96].

compound [^{nat}Ga][^{19}F]rhPSMA-	**IC_{50} [nM]**
201	52 ± 4.5
202	55 ± 5.7
301	25 ± 4.6
4	11 ± 1.8
5	11 ± 2.5
[^{nat}Ga]PSMA I&T	9.4 ± 2.9

In contrast to the linker length, the slightly different length of the side chains of dap and lys and thus the distance of the SiFA moiety to the peptide scaffold seems to have no effect on the PSMA affinity, as demonstrated by the identical IC_{50}s of [^{nat}Ga][^{19}F]rhPSMA-4 and -5. This is in accordance with the similar affinities of the 2nd generation dap/lys-ligand pairs [^{nat}Ga][^{19}F]rhPSMA-201/-202 and -203/-204.

3. 2 Effect of the chelator

Due to the pronounced hydrophilic nature of the TRAP chelator with its three carboxylates and three phosphinates, TRAP was initially assumed to be the chelator of choice. However, for conjugation to the peptidic inhibitor, the building blocks (Figure 16, upper scheme) need to be functionalized with an alkyne or azide in order to be coupled in a copper-catalyzed click reaction. Alternative conjugation *via* classical peptide synthesis failed due to phosphinate mediated hydrolysis of the active ester component[173]. Besides the sophisticated synthetic route, these necessary modifications prevent a close conjugation of the chelator to SiFA which is thought to be mandatory for efficient compensation of its lipophilicity. Furthermore, TRAP is not able to form stable complexes with most of therapeutic radionuclides (including ^{177}Lu, ^{90}Y, ^{213}Bi, ^{225}Ac) thus limiting its use to diagnostic applications with ^{68}Ga[165, 183]. Consequently, the suitability of the commercially available DOTA-GA chelator, which is already employed in a variety of PSMA-addressing ligands for diagnostic and therapeutic applications, was investigated (Figure 16, rhPSMA-6)[71, 96, 179].

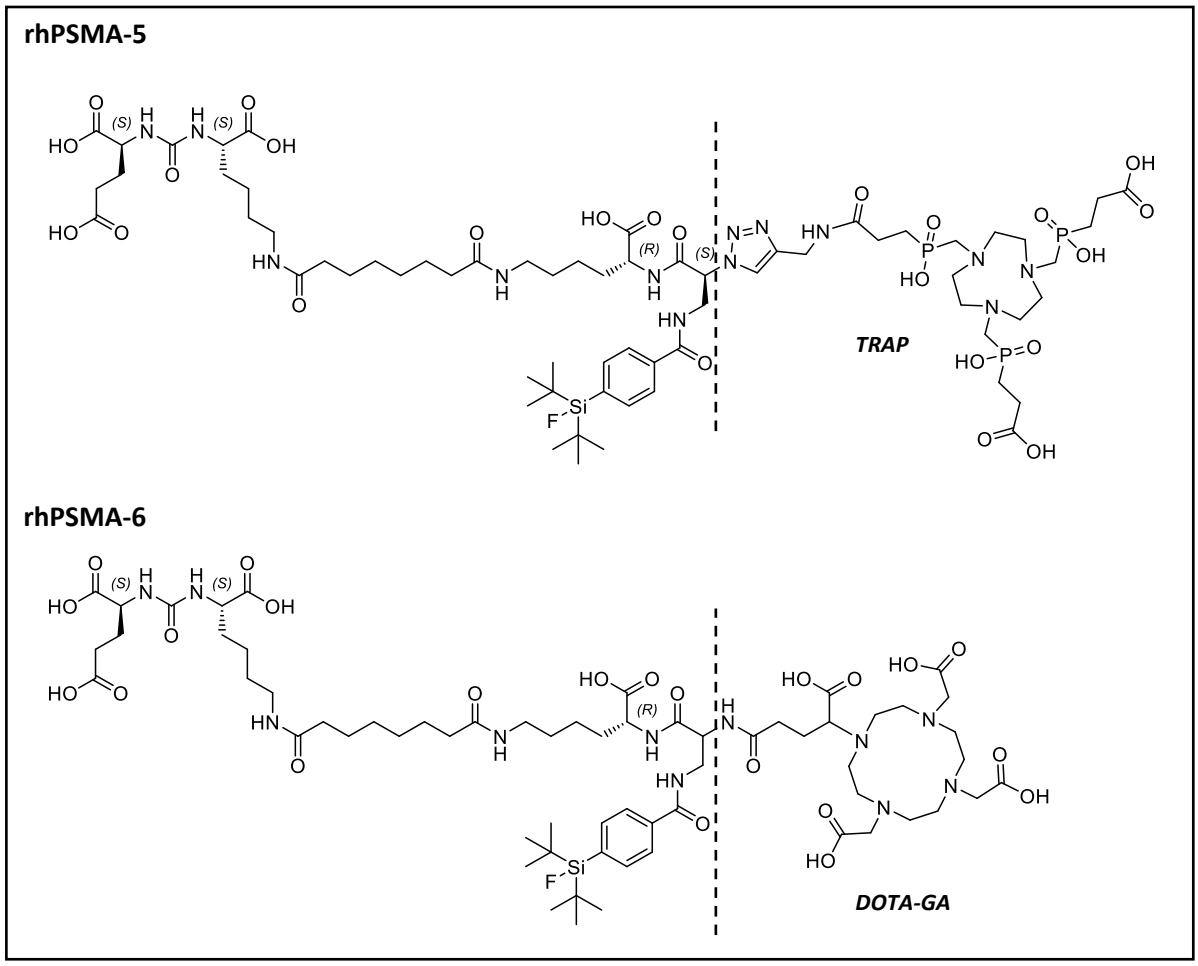

Figure 16: Structural formulas of uncomplexed TRAP-based rhPSMA-5 and the DOTA-GA-derivative rhPSMA-6.

Starting with the peptide scaffold of rhPSMA-5, the *N*-terminal azido-aminopropionic acid was replaced by diaminopropionic acid allowing simple conjugation of SiFA-BA and DOTA-GA by means of amide-bond formation. After purification, rhPSMA-6 was obtained in a final yield of 70%. Noteworthy, racemization of *D*-diaminopropionic acid occurred during the conjugation step of Fmoc-*D*-Dap(Dde)-OH, resulting in the *D*- and *L*-configured stereoisomers (see chapter 3.4 for details). The following evaluations were performed employing the racemic mixture of rhPSMA-6 (Table 4).

Table 4: Summary of investigated *in vitro* parameters of rhPSMA-5 and -6, and the reference PSMA I&T. PSMA binding affinities (IC_{50} [nM]) on LNCaP cells (1 h, 4 °C, n=3). Internalized activity in LNCaP cells (1 h, 37 °C) as a percentage of the reference ligand ([^{125}I]I-BA)KuE, n=3). Lipophilicity expressed as octanol/PBS (pH 7.4) partition coefficient (log $P_{O/PBS}$, n=6). Values are expressed as mean ± SD. Data of the reference ligand were obtained from Wirtz *et al.*[96].

compound [$^{nat/68}$Ga][^{19}F]	**IC_{50}** **[nM]**	**IC_{50} [nM]** **uncomplexed**	**Internalization** **[%]**	**lipophilicity** **log $P_{O/PBS}$**
rhPSMA-5	11 ± 2.5	8.5 ± 1.7	43 ± 3.4	−3.0 ± 0.1
rhPSMA-6	7.3 ± 0.2	6.4 ± 0.2	33 ± 2.1	−2.8 ± 0.1
[$^{nat/68}$Ga]PSMA I&T	9.4 ± 2.9	10.2 ± 3.5	59 ± 1.7	−4.3 ± 0.3

Both rhPSMA compounds displayed binding affinities similar or even better than PSMA I&T, demonstrating that the DOTA-GA chelator represents and excellent alternative to TRAP, both regarding binding affinity and lipophilicity. Most probably the closer proximity of SiFA and DOTA-GA by means of amide bond formation results in a better compensation of the lipophilic SiFA block. For *in vivo* studies both ligands were labeled with ^{68}Ga and injected into LNCaP tumor-bearing SCID mice (Figure 17). In the static PET images, both rhPSMA ligands showed favorable imaging properties 1 h p.i. with high accumulation in PSMA-expressing tissues (e.g. tumor and kidneys) and low background uptake. Regarding the *in vivo* performance of the TRAP- and DOTA-GA-conjugated tracer, no clear advantage of one compound over the other could be assessed by the initial PET imaging experiments.

With log $P_{O/PBS}$ values of −2.8 for [^{68}Ga][^{19}F]rhPSMA-6 and −3.0 for [^{68}Ga][^{19}F]rhPSMA-5, both compounds showed fast blood clearance and low accumulation in non-target tissues, only negligible uptake in the liver and preferred renal elimination.

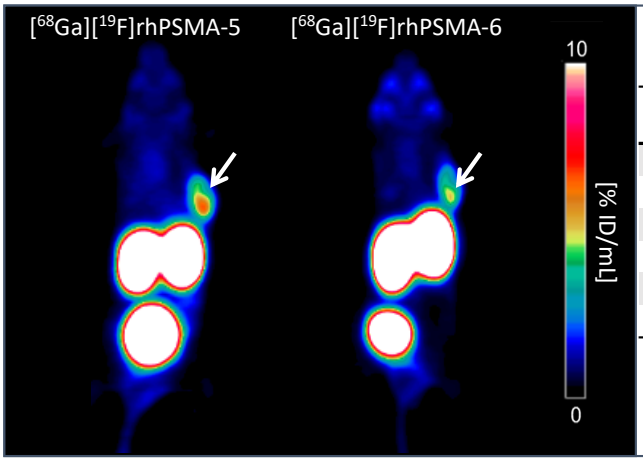

ROI-Quantification

organ	[68Ga][19F]rhPSMA-5 [% ID/mL]	[68Ga][19F]rhPSMA-6 [% ID/mL]
tumor	4. 8 ± 1.3	4.0 ± 0.2
salivary glands	1.4 ± 0.2	2.1 ± 0.3
muscle	0.58 ± 0.01	0.57 ± 0.2
kidney	35 ± 7.9	46 ± 6.1
heart	1.5 ± 0.1	1.4 ± 0.3
liver	1.4 ± 0.1	1.3 ± 0.3

Figure 17: Representative PET images (maximum intensity projection, dorsal frame) of [^{68}Ga][^{19}F]rhPSMA-5 (left) and [^{68}Ga][^{19}F]rhPSMA-6 (right) in LNCaP tumor-bearing SCID mice (1 h p.i., 15 min acquisition time) and quantification of activity uptake in selected organs (region of interest (ROI)). Values are expressed as mean ± SD (n=4). % ID/mL = percentage of the injected dose per mL. Arrows indicate tumor positions.

3.3 EuE-based rhPSMA ligands

In the vast majority of diagnostic and therapeutic PSMA ligands such as PSMA-HBED-CC, PSMA I&T, PSMA-617, the EuK (Glu-urea-Lys) binding motif is applied[89, 96, 98]. In addition, the EuE (Glu-urea-Glu) binding motif, evaluated by Kozikowski and co-workers, was found to be a valuable inhibitor motif with comparable affinity[64, 86, 184, 185]. Recently, two highly optimized EuE-based ^{18}F-labeled PSMA ligands were published and examined in preclinical studies[86]. Both ligands displayed favorable *in vitro* and *in vivo* properties with high binding affinities and internalization capacities as well as favorable imaging properties with fast background clearance and high tumor accumulation in first proof-of-concept studies in PCa patients[86].

Thus, in a next step, the EuE-based versions of rhPSMA-5 and -6, resulting in rhPSMA-7 (EuE and DOTA-GA) and rhPSMA-9 (EuE and TRAP) were synthesized and assessed. With the aim, to leave the linker length unchanged, the suberic acid spacer was replaced by ornithine conjugated to succinic acid, additionally providing an additional carboxylic group close to the inhibitor moiety. In a closely related derivative of rhPSMA-7, SiFA and the DOTA-GA chelator switched their positions at the trifunctional diaminopropionic acid, resulting in rhPSMA-8. Moreover, the DOTA-GA chelator of rhPSMA-7 was substituted by DOTA, resulting in rhPSMA-10. In order to evaluate the effect of metal complexation, the respective uncomplexed ligands were also evaluated. (Figure 18).

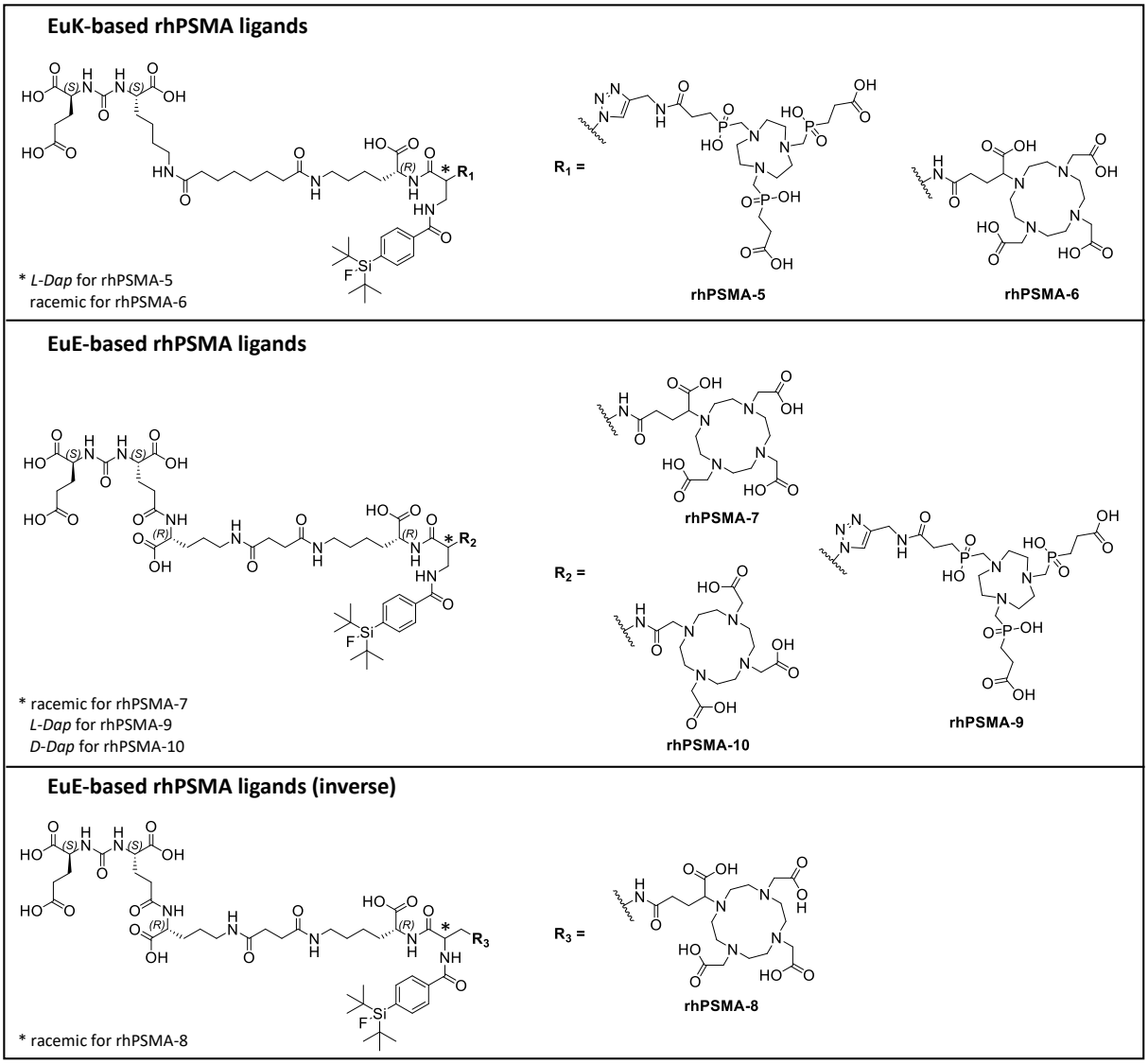

Figure 18: Radiohybrid (rh) PSMA ligands (depicted as uncomplexed inhibitors) comprising of a EuE-based binding motif, a SiFA moiety and a TRAP-, DOTA- or DOTA-GA-chelator.

The EuE-based ligands were prepared *via* straightforward solid-phase/solution-phase peptide synthesis. After purification, the ligands rhPSMA-7 to -10 were obtained in yields of 9-24%. As already observed for rhPSMA-6, racemization occurred during conjugation of diprotected diaminopropionic acid (Fmoc-*D*-Dap(Dde)-OH), resulting in the respective *D*- and *L*-configured stereoisomers of rhPSMA-7 and -8. For rhPSMA-10 an optimized synthetic procedure was employed (see chapter 3.4 for details), suppressing racemization of dap during peptide synthesis and thus only the desired *D*-Dap configured ligand was obtained.

3.3.1 *In vitro* characterization

In vitro data of the synthesized (radio)metal-chelated rhPSMA ligands were compared to the well-established fluorinated PSMA ligands DCFPyL and PSMA-1007, evaluated under the same experimental conditions[86]. Due to the chemical identity of the [^{68}Ga][^{19}F]rhPSMA with the respective [^{nat}Ga][^{18}F]rhPSMA compound only the ^{68}Ga-labeled twin was utilized in experiments that required the radioactive compound. Moreover, the uncomplexed ^{18}F-labeled rhPSMA ligands were evaluated.

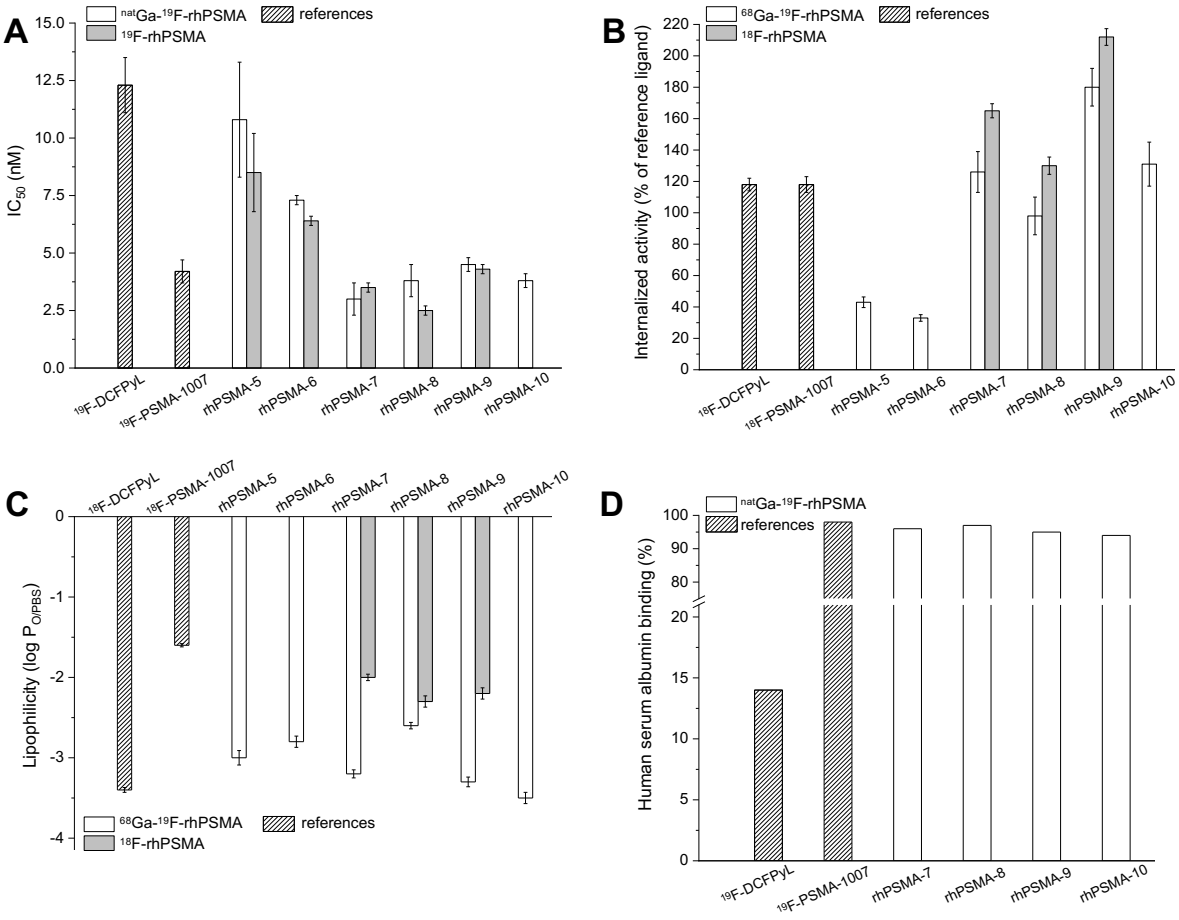

Figure 19: **A**) Binding affinities (IC_{50} [nM], 1 h, 4 °C; n=3) of [^{nat}Ga][^{19}F]rhPSMA-5 to -10 (white bars), [^{19}F]rhPSMA-5 to -10 (grey bars), [^{19}F]DCFPyL and [^{19}F]PSMA-1007; **B**) internalized activity of [^{18}F]DCFPyL, [^{18}F]PSMA-1007, [^{68}Ga][^{19}F]rhPSMA-5 to -10 (white bars) and [^{18}F]rhPSMA-5 to -10 with free chelator (grey bars), in LNCaP cells (1 h, 37 °C) as a percentage of the reference ligand ([^{125}I]I-BA)KuE; n=3); **C**) lipophilicity of [^{18}F]DCFPyL, [^{18}F]PSMA-1007, [^{68}Ga][^{19}F]rhPSMA-5 to -10 (white bars) and [^{18}F]rhPSMA-5 to -10 with free chelator (grey bars), expressed as octanol/PBS (pH 7.4) partition coefficient (log $P_{O/PBS}$; n=6); **D**) human serum albumin binding of [^{19}F]DCFPyL, [^{19}F]PSMA-1007, [^{nat}Ga][^{19}F]rhPSMA-5 to -10 (white bars), determined on a Chiralpak HSA column. Data of reference ligands DCFPyL and PSMA-1007 were taken from a previously published study[86]. Values are expressed as mean ± SD.

The EuK-based ligands rhPSMA-5 and -6 showed PSMA affinities somewhat better than that obtained for [^{19}F]DCFPyL. Significantly higher PSMA affinities were measured for the reference ligand [^{19}F]PSMA-1007 and the EuE-based inhibitors rhPSMA-7 to -10. No significantly different IC_{50}-values were found for the individual Ga-complexed and metal-free rhPSMA compounds (Figure 19 A).

Analogously, internalization was up to 6-fold higher for all EuE-based rhPSMA ligands compared to rhPSMA-5 and -6 (Figure 19 B).

The superiority of EuE-based inhibitors derivatized in the same manner as described for rhPSMA-7 to 10 has been previously reported in a detailed study on the structure-activity relationship of EuE- and EuK-based PSMA-inhibitors conducted by Babich and co-workers[186]. In a series of otherwise identical PSMA-inhibitors, Glu(Lys(R))-urea-Glu based inhibitors, comprising of a free carboxylate (of Lys) in close proximity to the inhibitor motif, showed the highest affinities. The authors speculated that the EuE motif and the free carboxylate of Lys may increase the ligand interaction with PSMA[186].

All newly developed rhPSMA inhibitors showed a low log $P_{O/PBS}$ value between −2.0 to −3.5 (Figure 19 C). Interestingly, compared to the respective uncomplexed analogues, the lipophilicity was somewhat lower for the Ga-chelated rhPSMA ligands even though their carboxylates are coordinated to the metal ion. Whether this unexpected observation is a general characteristic of rhPSMA is still under investigation. A similar low lipophilicity was determined for [^{18}F]DCFPyL (−3.4), whereas [^{18}F]PSMA-1007 was found to be of rather lipophilic nature (−1.6). Despite their low lipophilicity all of the SiFA-containing ligands exhibited strong HSA interactions (> 94%) which were in the same order of magnitude as [^{19}F]PSMA-1007 (98%) and significantly higher than [^{19}F]DCFPyL (14%) (Figure 19 D).

3.3.2 *In vivo* characterization

Taking into account the results of the *in vitro* assessment, only the EuE-based ligands [^{68}Ga][^{19}F]rhPSMA-7 to -10 were evaluated in biodistribution studies in male LNCaP tumor-bearing CB17 SCID mice at 1 h p.i. and compared to the fluorinated reference ligands [^{18}F]PSMA-1007 and [^{18}F]DCFPyL (Figure 20).

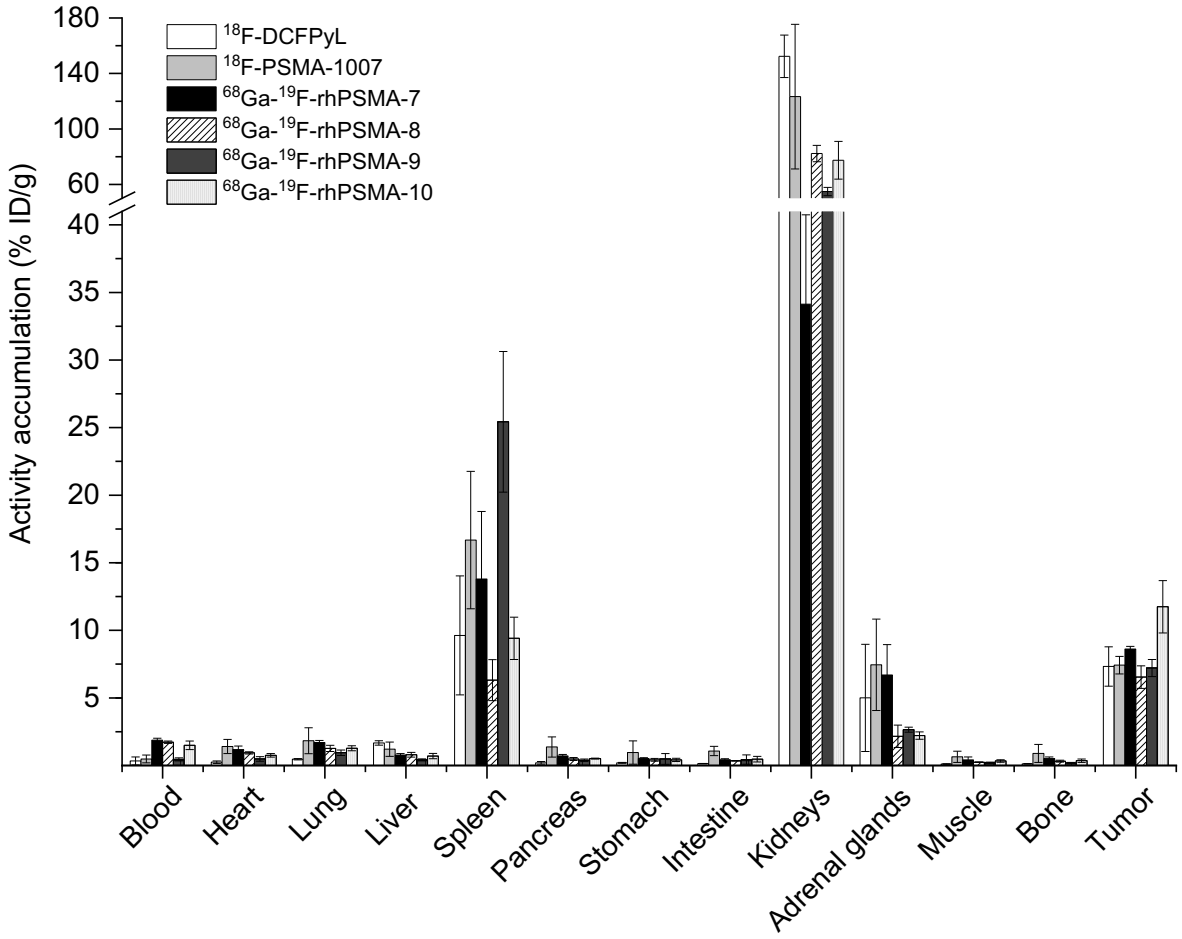

Figure 20: Biodistribution of [^{68}Ga][^{19}F]rhPSMA-7 to -10 and the reference ligands [^{18}F]DCFPyL and [^{18}F]PSMA-1007 at 1 h p.i. in LNCaP tumor-bearing SCID mice (n=3-4). Data of reference ligands were taken from a previously published study by our group[86]. Values are expressed as a percentage of injected dose per gram (% ID/g), mean ± SD.

The comparative biodistribution of the six PSMA ligands depicted in Figure 20 revealed similar pharmacokinetics of all ligands with high uptake in PSMA-expressing tissues, e.g. LNCaP tumor, kidneys, but also in spleen and adrenal gland. The tumor uptake at 1 h p.i. was similar for [^{18}F]DCFPyL, [^{18}F]PSMA-1007, [^{68}Ga][^{19}F]rhPSMA-7, -8 and -9 and somewhat higher for [^{68}Ga][^{19}F]rhPSMA-10. Non-target accumulation was low for all tracers with fast clearance *via* the renal pathway, except of [^{18}F]PSMA-1007, which showed higher uptake in a variety of

organs such as the gastrointestinal system, but also lung and pancreas, which is most probably a result of its low hydrophilicity (log $P_{O/PBS}$ = −1.6). Compared to all other tracers, [^{18}F]DCPFyL and [^{68}Ga][^{19}F]rhPSMA-9 were rapidly cleared from the blood, which correlates with the pronounced hydrophilicity of these two PSMA inhibitors.

In addition, the biodistribution of uncomplexed [^{18}F]rhPSMA-7 and ^{68}Ga-labeled [^{19}F]rhPSMA-7 were compared in order to examine the influence of the presence of the free chelator and a (radio-)metal chelate on the *in vivo* behavior in male LNCaP tumor-bearing SCID mice at 1 h p.i. (Figure 21).

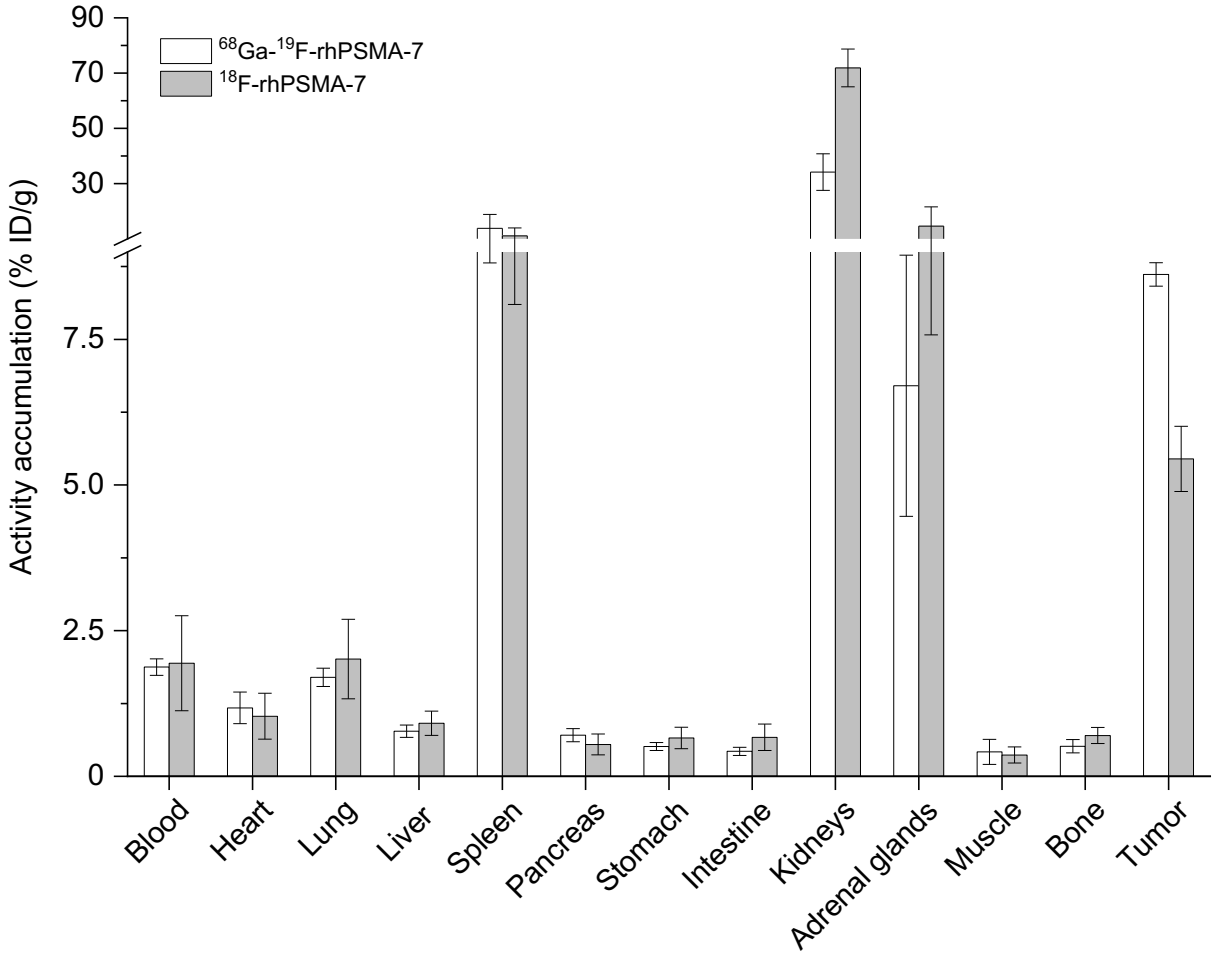

Figure 21: Comparative biodistribution of [^{68}Ga][^{19}F]rhPSMA-7 (white bars) and uncomplexed [^{18}F]rhPSMA-7 with free chelator (grey bars) at 1 h p.i. in LNCaP tumor-bearing SCID mice (n=3). Data expressed as a percentage of injected dose per gram (% ID/g), mean ± SD.

The uptake profiles of [^{68}Ga][^{19}F]rhPSMA-7 and non-metallated [^{18}F]rhPSMA-7 in mice were found to be quite identical with similar low uptake in most organs and pronounced uptake in spleen, kidneys, adrenal gland and tumor tissue. Marked differences were found in the

kidneys where the uncomplexed ^{18}F-labeled ligand showed stronger accumulation (72% ID/g vs. 34% ID/g). Despite its 1.3-fold higher internalization and comparable PSMA affinity, the tumor uptake of [^{18}F]rhPSMA-7 was unexpectedly low and only reached approx. 60% of the tumor uptake observed for [^{68}Ga][^{19}F]rhPSMA-7. The 2-fold increased kidney uptake of the uncomplexed ligand again demonstrates the negative influence of charges on kidney uptake[187-189]. Again, no elevated bone accumulation was found for [^{18}F]rhPSMA-7 indicating the absence of free [^{18}F]fluoride.

3.4 Isomer selection process of rhPSMA-7

Among the optimized third-generation ligands, [^{18}F][^{nat}Ga]rhPSMA-7 was selected for first proof-of-concept clinical studies (see chapter 5). In the course of the optimization of the chemical synthesis, it became apparent that [^{19}F][^{nat}Ga]rhPSMA-7 was present as a mixture of four different isomers. A new batch synthesis, which was monitored with high-resolution HPLC after each synthetic step revealed that diaminopropionic acid (dap) racemized during its conjugation at the chosen reaction conditions, resulting in the *D*-Dap and *L*-Dap containing peptides. Together with the *R*/*S*-configured glutamic acid pendant arm of DOTA-GA, four different stereoisomers were obtained. The aforedescribed preclinical studies and first evaluation in PCa patients have all been carried out employing this racemic rhPSMA-7.

In order to synthesize the enantiopure four isomers of rhPSMA-7, the synthetic procedure was modified (see Material and Methods for details). Briefly, the base DIPEA (*N,N*-diisopropylethylamine), which is used for pre-activation of Fmoc-*D*-Dap(Dde)-OH by means of active ester formation, was substituted by the sterically more demanding and weaker base collidine (2,3,4-trimethylpyridine). It has been described that collidine as base offers favorable properties to minimize racemization of cysteine, which is structurally related to dap, during solid-phase peptide synthesis[190, 191]. To the best of our knowledge, no publications have previously thematised racemization of dap during peptide synthesis. Employing this strategy, the desired products were obtained in 95% enantiomeric excess after the coupling of dap. Subsequent conjugation of the chelator was achieved by using enantiomeric pure *R*- or *S*-DOTA-GA. Remaining impurities including undesired isomers could be separated during RP-HPLC-based purification, yielding the different enantiomers in purities > 99% and chemical yields of 19-35%. The four isomers, differing in the stereoconfiguration of dap and DOTA-GA are henceforth referred to as rhPSMA-**7.1** (*D*-Dap – *R*-DOTA-GA), rhPSMA-**7.2** (*L*-Dap – *R*-DOTA-GA), rhPSMA-**7.3** (*D*-Dap – *S*-DOTA-GA) and rhPSMA-**7.4** (*L*-Dap – *S*-DOTA-GA).

3.4.1 Analytical characterization

In order to allocate each isomer to the four peaks found in the high-resolution HPLC profile of racemic [^{nat}Ga][^{19}F]rhPSMA-7, the enantiomeric pure compounds were successively co-injected with the mixture. Results of the characterization experiment with the identification of the isomers in an exemplary high-resolution HPLC chromatogram of typically produced

racemic [^{nat}Ga][^{19}F]rhPSMA-7 are shown in Figure 22. In order to quantify the respective amount of each isomer in different previously prepared batches of racemic [^{nat}Ga][^{19}F]rhPSMA-7, retained samples of [^{nat}Ga][^{19}F]rhPSMA-7 (n=6) were analyzed by means of the same optimized HPLC method.

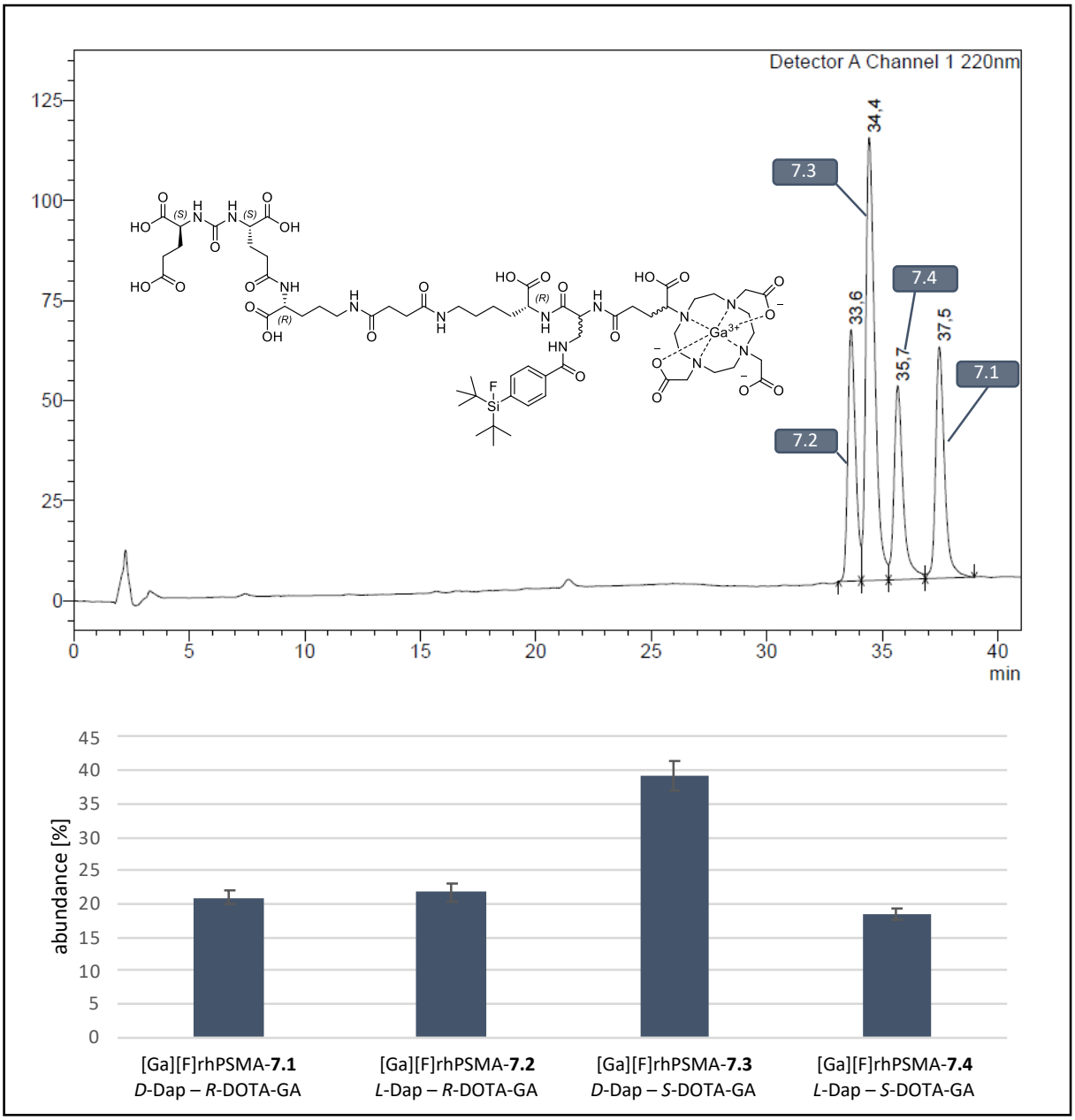

Figure 22: High-resolution HPLC chromatogram of racemic [^{nat}Ga][^{19}F]rhPSMA-7 (HPLC conditions: solvent A: H_2O + 0.1% TFA; solvent B: MeCN + 0.1% TFA. Gradient: 25-35% B 0-40 min, 95% B 40-45 min, flow: 1 mL/min, column: Nucleosil 100 C18 (125 × 4.6 mm, 5 µm)) and calculation of the mean abundance of [^{nat}Ga][^{19}F]rhPSMA-7.1 to -7.4, as determined by analyzing retained samples of previously produced batches of racemic [^{nat}Ga][^{19}F]rhPSMA-7 (n=6, mean ± SD).

High-resolution HPLC analysis of racemic [^{nat}Ga][^{19}F]rhPSMA-7 revealed that the *D*-Dap–*S*-DOTA-GA-configured isomer [^{nat}Ga][^{19}F]rhPSMA-7.3 was the dominant species in all previously produced batches with a mean abundance of 39.2 ± 2.2%, which is 1.9, 1.8 and 2.1 fold higher than the abundance of [^{nat}Ga][^{19}F]rhPSMA-7.1, -7.2 and -7.4, respectively. Noteworthy, no baseline separation of [^{nat}Ga][^{19}F]rhPSMA-7.2 and -7.3 was achieved but peak separation by means of the Systat software package Peakfit (see Material and Methods; Figure 10) allowed to accurately quantify the peaks of [^{nat}Ga][^{19}F]rhPSMA-7.1 to -7.4 and to determine the isomeric ratios.

3.4.2 *In vitro* characterization

Regarding regulatory guidelines, manufacturers are required to identify and characterize each individual isomer of a racemic compound if reasonably possible[192, 193]. Besides rare exceptions, the FDA (United States Food and Drug Admistration) and EMA (European Medicines Agency), both promote the development of new chiral drugs as single enantiomers[193]. Thus, and even though racemic [^{18}F][^{nat}Ga]rhPSMA-7 was applied in more than 1000 PCa patients and proved favorable PET imaging properties (see chapter 5), each of the four isomers was subsequently evaluated in a second series of preclinical studies. This selection process was initiated to identify the stereoisomer with the most promising characteristics for further clinical studies.
For all preclinical experiments, that required a radiolabeled rhPSMA compound, the respective [^{18}F][^{nat}Ga]rhPSMA ligand was used. Data of racemic rhPSMA-7 and results of fluorinated reference ligands DCFPyL and PSMA-1007, evaluated under identical experimental conditions, are included for comparison.

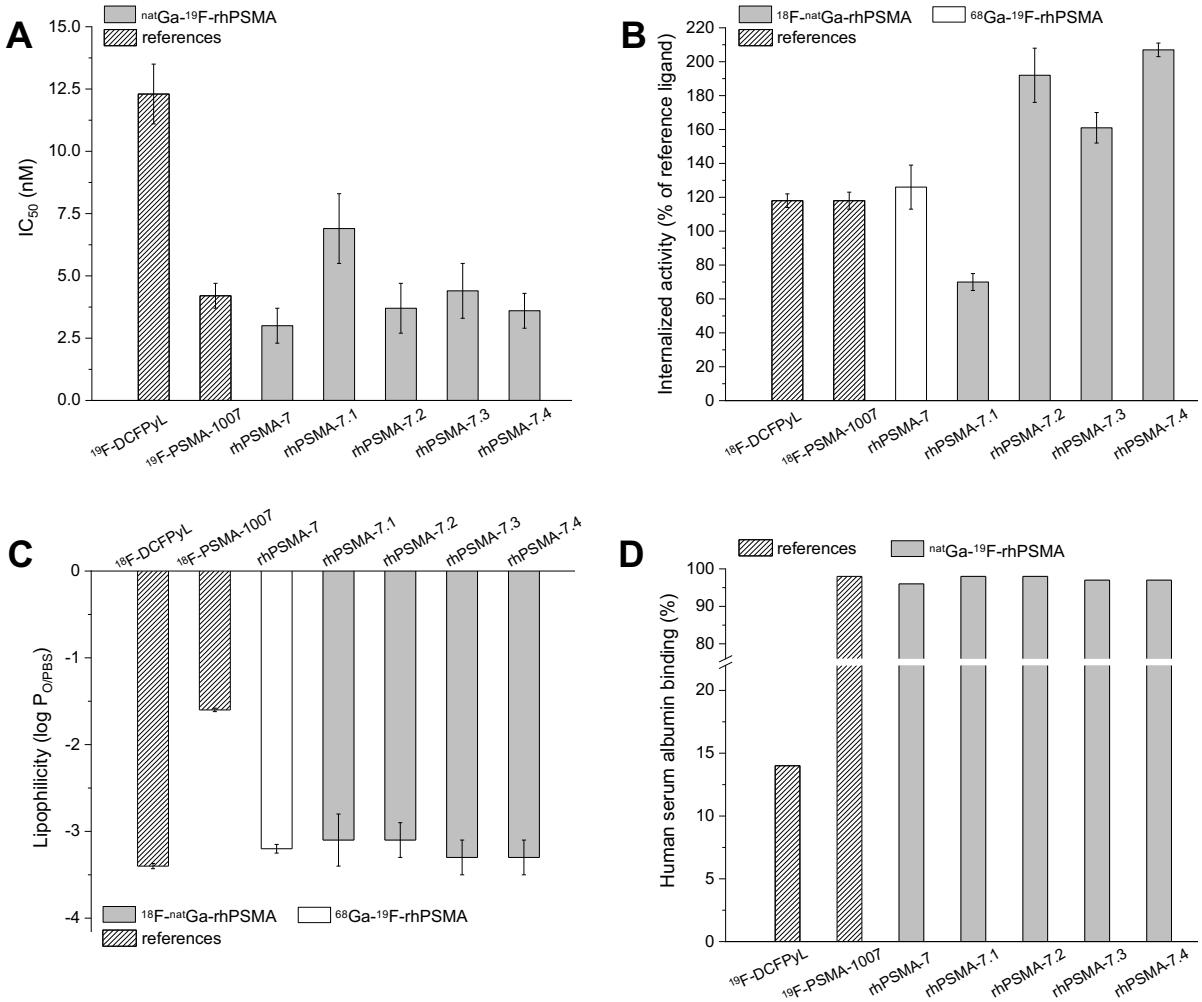

Figure 23: **A**) Binding affinities (IC_{50} [nM], 1 h, 4 °C; n=3) of [^{nat}Ga][^{19}F]rhPSMA-7 and [^{nat}Ga][^{19}F]rhPSMA-7.1 to -7.4, [^{19}F]DCFPyL and [^{19}F]PSMA-1007; **B**) internalized activity of [^{18}F]DCFPyL, [^{18}F]PSMA-1007, [^{68}Ga][^{19}F]rhPSMA-7 and [^{18}F][^{nat}Ga]rhPSMA-7.1 to -7.4 in LNCaP cells (1 h, 37 °C) as a percentage of the reference ligand ([^{125}I]I-BA)KuE; n=3); **C**) lipophilicity of [^{18}F]DCFPyL, [^{18}F]PSMA-1007, [^{68}Ga][^{19}F]rhPSMA-7 and [^{18}F][^{nat}Ga]rhPSMA-7.1 to -7.4, expressed as octanol/PBS (pH 7.4) partition coefficient (log $P_{O/PBS}$; n=6); **D**) human serum albumin binding of [^{19}F]DCFPyL, [^{19}F]PSMA-1007, [^{nat}Ga][^{19}F]rhPSMA-7 and [^{nat}Ga][^{19}F]rhPSMA-7.1 to -7.4, determined on a Chiralpak HSA column. Data of reference ligands [$^{18/19}$F]DCFPyL and [$^{18/19}$F]PSMA-1007 were taken from Robu *et al.*[86]. Values are expressed as mean ± SD

The affinity of racemic [^{nat}Ga][^{19}F]rhPSMA-7 was found to be similar to the affinity of [^{19}F]PSMA-1007 and significantly higher when compared to [^{19}F]DCFPyL (Figure 23 A). Noteworthy, the *D*-Dap – *R*-DOTA-GA-configured ligand [^{nat}Ga][^{19}F]rhPSMA-7.1 displayed slightly lower affinities compared to the isomers 7.2-7.4. The same applies for the measured internalization rates into LNCaP cells (Figure 23 B). While [^{18}F][^{nat}Ga]rhPSMA-7.1 showed the lowest internalization efficiency, internalization of [^{18}F][^{nat}Ga]rhPSMA-7.2 to -7.4 was 2.2- to

2.9-fold higher and even 1.3- to 1.7-fold higher when compared to the fluorinated non-radiohybrid reference ligands. As expected, the stereoinformation did not affect the measured log $P_{O/PBS}$ values and binding to human serum albumin, leading to nearly identical data sets as obtained for racemic [Ga][F]rhPSMA-7 (Figure 23 C and D).

3.4.3 Biodistribution studies

Biodistribution of [^{18}F][^{nat}Ga]rhPSMA-7.1 to -7.4 was determined in LNCaP tumor-bearing SCID mice 1 h p.i. and compared with the biodistribution of racemic [^{18}F][^{nat}Ga]rhPSMA-7 (Figure 24).

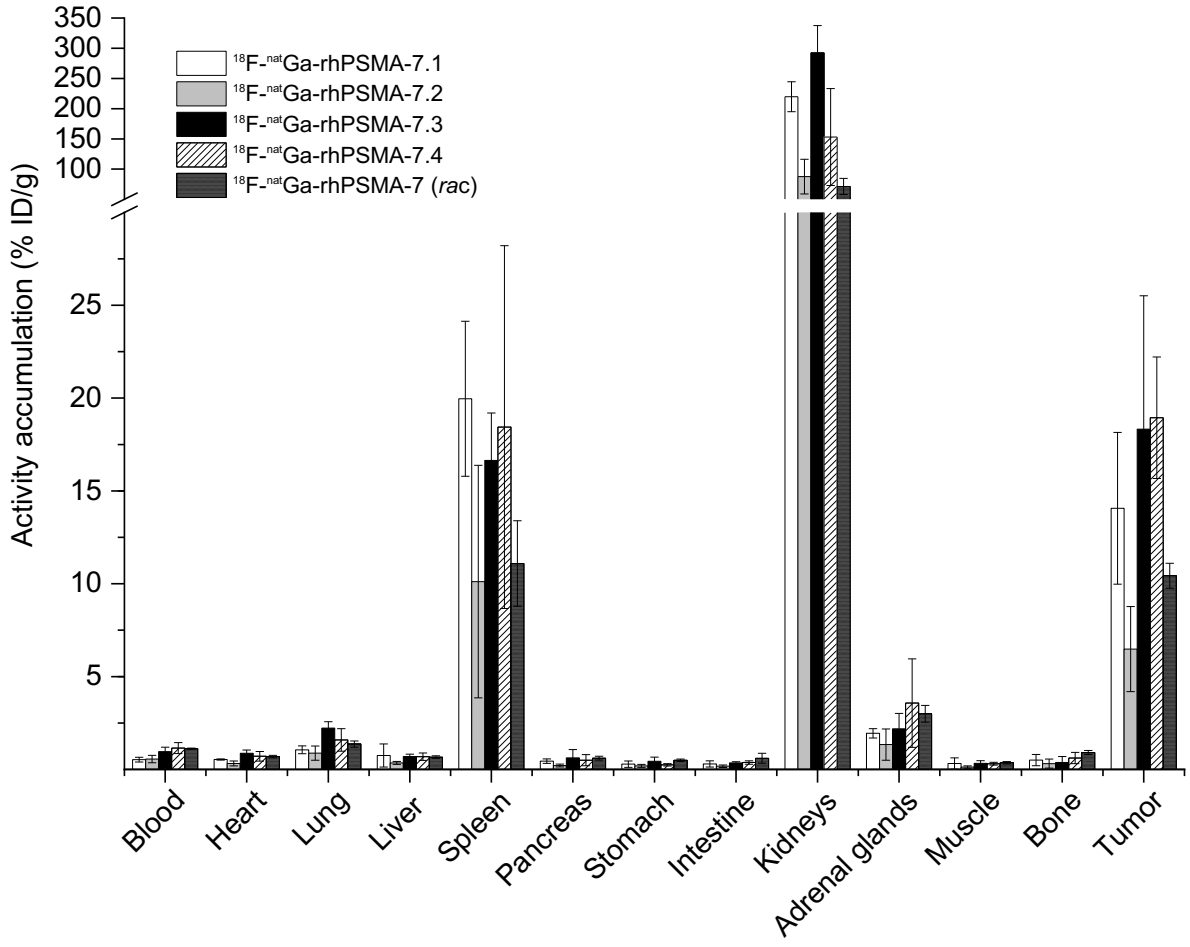

Figure 24: Biodistribution of [^{18}F][^{nat}Ga]rhPSMA-7 to -7.4 at 1 h p.i. in male LNCaP tumor-bearing SCID mice. Data expressed as a percentage of the injected dose per gram (% ID/g), mean ± standard deviation (n=4 for [^{18}F][^{nat}Ga]rhPSMA-7.1, n=5 for [^{18}F][^{nat}Ga]rhPSMA-7.2, n=4 for [^{18}F][^{nat}Ga]rhPSMA-7.3, n=5 for [^{18}F][^{nat}Ga]rhPSMA-7.4 and n=3 for [^{18}F][^{nat}Ga]rhPSMA-7).

Similar to racemic [^{18}F][^{nat}Ga]rhPSMA-7, [^{18}F][^{nat}Ga]rhPSMA-7.1 to -7.4 showed low and similar uptake profiles in most non-target tissues regardless of their stereoconfiguration. Slightly different individual blood clearance kinetics at 1 h p.i. are also reflected in the tissue distribution profiles. Highest tumor and kidney accumulation was found for the *S*-DOTA-GA-based [^{18}F][^{nat}Ga]rhPSMA-7.3 and -7.4, closely followed by -7.1. In contrast the *L*-Dap – *R*-DOTA-GA ligand [^{18}F][^{nat}Ga]rhPSMA-7.2 showed an approximately two-fold lower tumor and kidney uptake compared to the other isomers. Thus, a selection of the most promising compounds by assessment of the biodistribution profiles of [^{18}F][^{nat}Ga]rhPSMA-7.1, -7.3 and -7.4 at 1 h p.i. was found to be difficult or even impossible.

Most surprisingly, a clear correlation between *in vitro* parameters and *in vivo* behavior could not be identified: a) while PSMA affinity and internalization was approximately two-fold lower for [F][Ga]rhPSMA-7.1 (when compared to the other isomers), tumor uptake of [^{18}F][^{nat}Ga]rhPSMA-7.1 at 1 h p.i. was almost identical and b) the lower tumor uptake of [^{18}F][^{nat}Ga]rhPSMA-7.2 did not correlate with its high PSMA affinity and internalization rate.

Moreover, taking into account the abundance of the different isomers in the mixture and their individual accumulation in kidneys and the tumor, an approximately 1.5- and 3-fold higher uptake would have been theoretically expected for racemic [^{18}F][^{nat}Ga]rhPSMA-7 in tumor and kidneys.

Thus, metabolite analyses were carried out (see chapter 3.4.5) to overcome these differences presumably caused by differences in the biodistribution in individual mice within the small cohort of animals (n=3 for [^{18}F][^{nat}Ga]rhPSMA-7) and to investigate, whether *in vivo* degradation of *L*-Dap in rhPSMA-7.2 and -7.4 by peptidases might help to explain these contradictory results.

3.4.4 Biodistribution studies with competition

Specificity of binding was demonstrated in competition studies for ^{18}F-labeled [^{nat}Ga]rhPSMA-7.1 to -7.4 coinjected with the potent PSMA inhibitor 2-PMPA (8 mg/kg) in LNCaP tumor-bearing SCID mice. As expected, the competition experiments revealed significantly reduced accumulation of the respective isomers in kidneys, tumor, spleen and adrenal glands. The measured tumor uptakes (0.9-1.5% ID/g) were nearly identical to the background

accumulation in the blood pool (0.6-1.1% ID/g) for all of the isomers, thus confirming PSMA-specific uptake. Activity localized in kidneys (7-11% ID/g) was lowered but still high, reflecting the dynamics of renal excretion of the rhPSMA ligands (Figure 25).

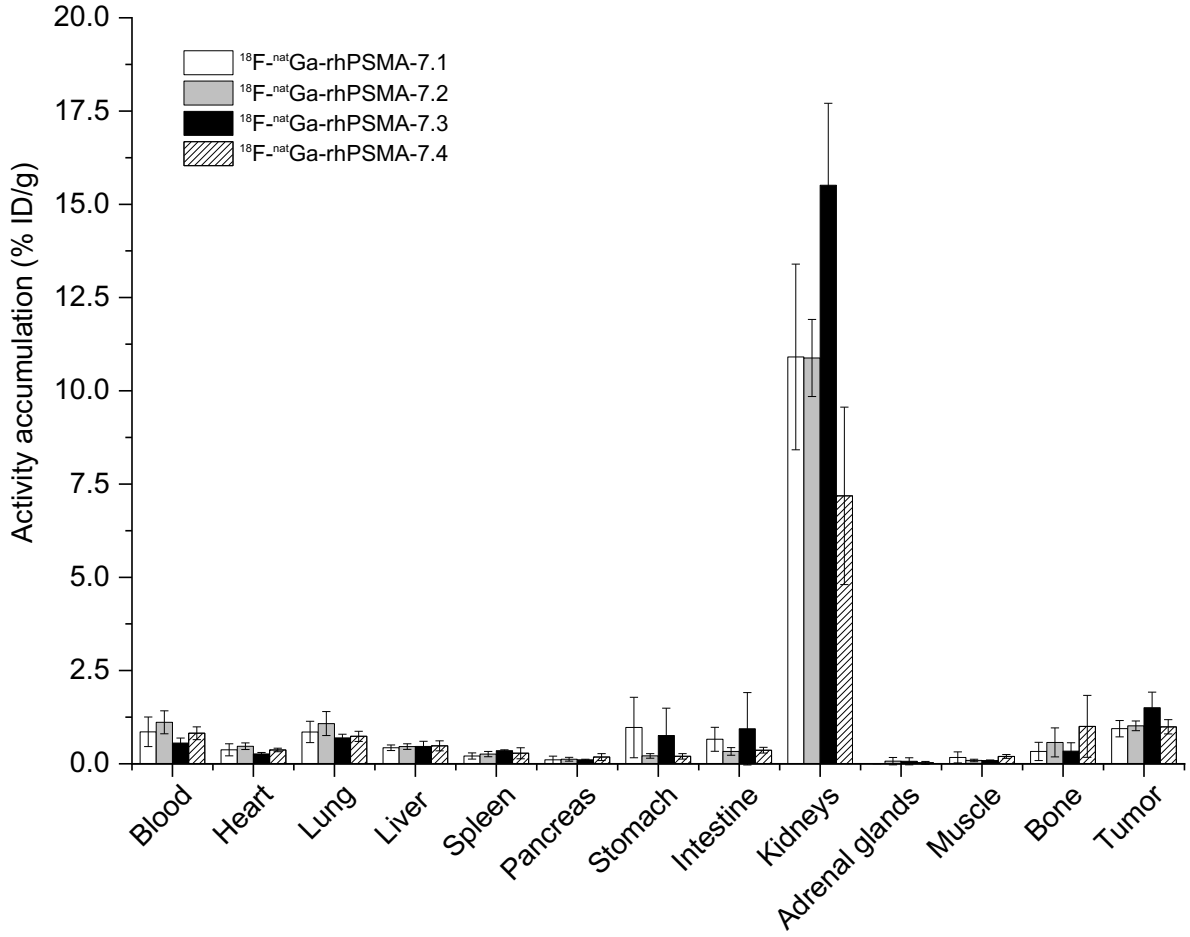

Figure 25: Biodistribution of [^{18}F][^{nat}Ga]rhPSMA-7.1 to -7.4, co-injected with 2-PMPA (8 mg/kg) at 1 h p.i. in male LNCaP tumor-bearing SCID mice. Data expressed as a percentage of the injected dose per gram (% ID/g), mean ± standard deviation (n=3).

3.4.5 Distribution and metabolite studies

To select the most promising isomer of the racemic rhPSMA-7 mixture for transfer into more detailed clinical studies, detailed distribution and metabolite studies were carried out. With the intention to identify even marginal differences in the *in vivo* behavior between each isomer and to minimize methodological errors, the differential *in vivo* uptake and excretion pattern of each isomer was quantified. For this purpose, a) racemic [^{18}F][^{nat}Ga]rhPSMA-7 was produced, b) the fraction of each isomer was determined by high-resolution HPLC, c) followed by injection of [^{18}F][^{nat}Ga]rhPSMA-7 into a LNCaP tumor-bearing mouse. D) 30 minutes p.i.,

urine and blood were collected and centrifuged, the organs of interest were homogenized and extracted. Thereafter, e) the prepared liquid samples were subjected to HPLC analysis, d) to quantify the fraction of each isomer in each sample f) to calculate the differential change of each isomer fraction in each tissue/body fluid in the relation to the fractions of each isomer as determined for the injected racemic mixture. Metabolic stability and tissue distribution were determined in four independent experiments.

Tissue extraction

In the following metabolite quantification experiments urine, blood, kidney, liver and tumor were analyzed (see Material and Methods section for detailed experimental procedures). The tracers were extracted from solid tissues by means of a Potter-Elvehjem tissue grinder or a ball mill and separated from the protein fraction by subsequent loading onto a solid-phase cartridge. The decay-corrected efficiencies for sample extraction, expressed as "extracted radioactivity", are summarized in Table 5.

Table 5: Determination of the decay corrected efficiencies of extraction (% extracted radioactivity) of [^{18}F][^{nat}Ga]rhPSMA-7 from blood, kidney, liver and tumor *via* the Potter-Elvehjem Tissue Grinder (n=1) and the MM-400 Ball Mill (n=3). Values are expressed as mean ± SD.

Potter-Elvehjem tissue grinder (n = 1)	**efficiency [% extracted radioactivity]**		
	sample extraction	loading SPE Cartridge	overall
blood	93	93	86
kidney	91	66	60
tumor	90	59	53
MM-400 ball mill (n = 3)	**efficiency [% extracted radioactivity]**		
	sample extraction	loading SPE cartridge	overall
blood	98 ± 2	94 ± 2	92 ± 3
liver	97	89 ± 2	86 ± 2
kidney	63 ± 5	68 ± 8	43 ± 8
tumor	64 ± 18	65 ± 3	42 ± 14

When compared with ball mill extraction, the extraction with the manual tissue grinder was slightly more efficient, especially for rather solid tissues like kidneys and tumor. Nevertheless, more than 60% of the radioactivity could be recovered. Due to their similar chemical

properties and *in vivo* behaviour, the extraction efficiencies of the isomers are expected to be nearly identical. Thus, a change of the isomeric composition during the analytical extraction process seems unlikely. The extraction by means of the ball mill could most probably be optimized if small-sized grinding balls that allow for more effective destruction of cell membranes would be applied.

For samples from blood and liver, most of the extracted activity could be trapped on the SPE cartridge. During processing of the samples from solid tissues, like kidney and tumor, a significant amount of the extracted activity could not be retained on the cartridge. Here again a more effective homogenization in the ball mill could be tested to improve cartridge-based purification. The elution-efficiency was > 99% in all experiments.

Metabolic stability

Radio-HPLC analyses of urine samples and the radioactivity extracted from the homogenized (kidney, liver, tumor) or diluted (blood) samples did not show any lipophilic or hydrophilic metabolic fragments of the four stereoisomers of [^{18}F][^{nat}Ga]rhPSMA-7.

Radioactive species formed by metabolic cleavage of amide bonds should exhibit an increased lipophilicity (Figure 26). In this context one could argue that some lipophilic metabolites which were not quantitatively extracted from the tissue samples by the aqueous extraction conditions did not appear in final radio-HPLC analysis and thus are ignored. However, this lipophilic species, formed *in vivo*, are excreted *via* the hepatobiliary pathway resulting in considerable accumulation in the liver and gastrointestinal system or would be bound to plasma proteins in the blood[194, 195]. However, due to the high extraction efficiencies (> 93%) of these tissues, such a worst-case scenario seems quite improbable. Moreover, no elevated uptake in these organs was observed in the biodistribution studies, indicating that [^{18}F][^{nat}Ga]rhPSMA-7.1 to -7.4 are stable *in vivo*.

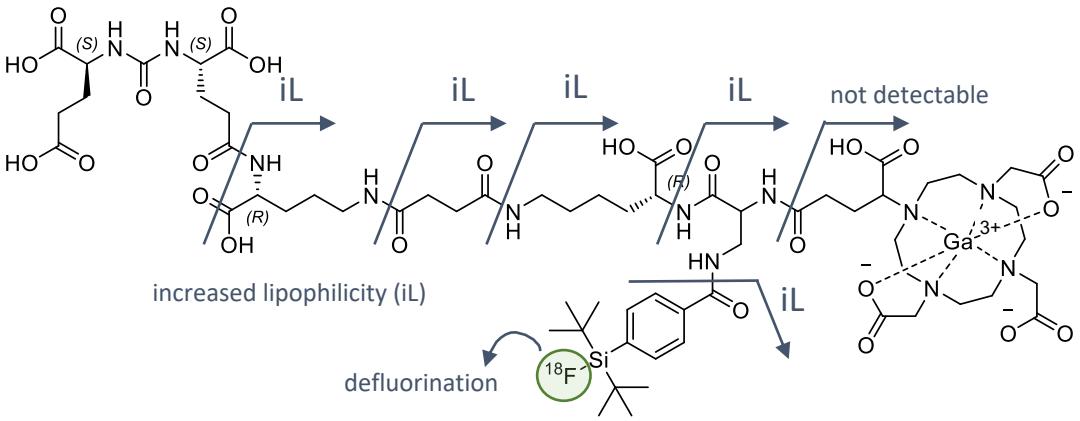

Figure 26: Selection of possibly generated radioactive fragments generated by either metabolic cleavage of amide bonds in [^{18}F][^{nat}Ga]rhPSMA-7 or defluorination *in vivo*. iL: Cleavage forms a species with increased lipophilicity.

Defluorinated species could occur by hydrolysis of the ^{18}F-SiFA moiety *in vivo*. In this case, free [^{18}F]fluoride with high affinity to the apatite matrix of the skeletal system would lead to an elevated activity accumulation in bone[196]. Elevated bone uptake, however, was not detected, neither in the biodistribution studies in mice, nor in clinical PET scans using racemic [^{18}F][^{nat}Ga]rhPSMA-7. *In vivo* degradation of the [^{18}F]organofluorosilane, followed by release of free [^{18}F]fluoride into the blood and unspecific uptake in organs or bones can therefore be excluded, too.

Further analytic studies about the defluorination of rhPSMA ligands are described in chapter 3.4.6 “Defluorination experiments”.

Determination of the organ distribution

The analysis of the differential *in vivo* uptake and excretion pattern of each isomer, expressed as relative percentage change of each isomer fraction in blood, liver, kidney, urine and tumor in relation to the fractions of each isomer as determined for the injected racemic mixture is depicted in Figure 27 and Figure 28, determined in four independent experiments. For quantification of each isomer in the racemic mixture, especially for the poorly separated first and second peak ([^{18}F][^{nat}Ga]rhPSMA-7.2 and -7.3), the HPLC chromatograms were processed using the Systat software package PeakFit (see Material and Methods), since PeakFit allows for nonlinear separation, analysis and quantification of HPLC elution profiles by deconvolution procedures that use a Gaussian response function with a Fourier deconvolution/filtering algorithm.

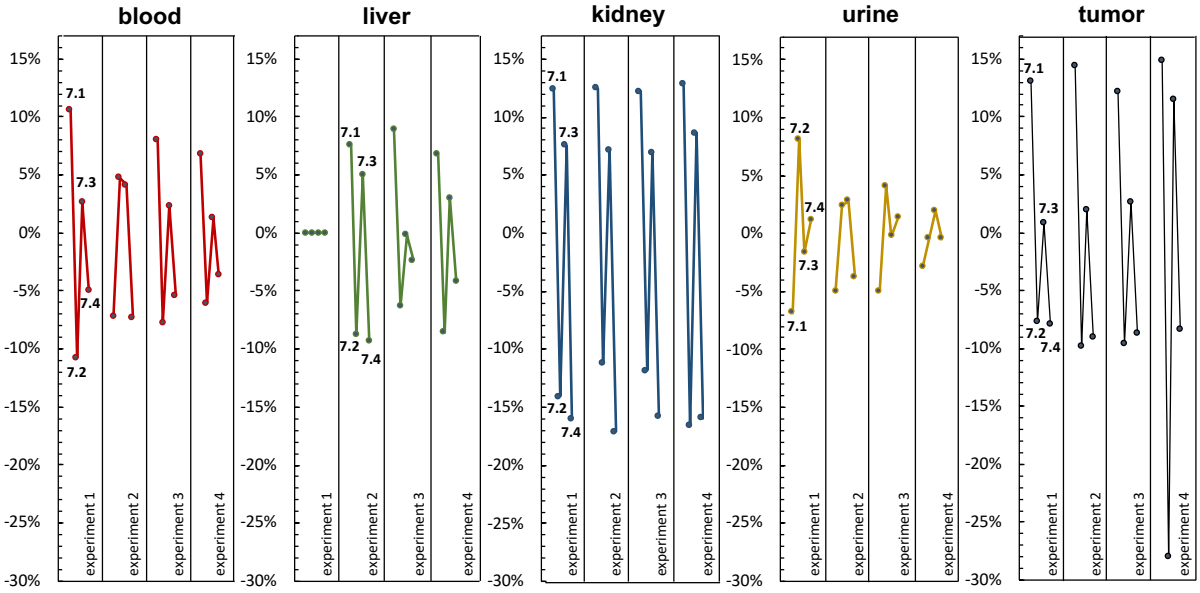

Figure 27: Relative percentage change of the uptake of [^{18}F][^{nat}Ga]rhPSMA-7.1 to -7.4 in blood, liver, kidney, urine and tumor of male LNCaP tumor-bearing SCID mice (30 min p.i.) compared to racemic [^{18}F][^{nat}Ga]rhPSMA-7, determined in four independent experiments (see also Figure 28).

In the radio-HPLC analysis of samples from blood, liver, kidney and tumor, the *D*-Dap-containing ligands [^{18}F][^{nat}Ga]rhPSMA-7.1 and -7.3 showed positive changes compared to the quality control and thus a higher uptake in these tissues when compared with the *L*-Dap-isomers [^{18}F][^{nat}Ga]rhPSMA-7.2 and -7.4. Due to slower blood clearance, [^{18}F][^{nat}Ga]rhPSMA-7.1 was not considered further as a promising candidate. [^{18}F][^{nat}Ga]rhPSMA-7.2 and -7.4 showed fastest excretion into the urine, and lowest uptake in the kidney, but also lowest uptake in the tumor. In contrast, [^{18}F][^{nat}Ga]rhPSMA-7.3 showed the best overall uptake pattern and the second best tumor uptake.

Interestingly, these data do not fully correlate with the expectations that arose from the *in vitro* studies.

The *L*-Dap-comprising compounds [^{18}F][^{nat}Ga]rhPSMA-7.2 and -7.4 showed lowest accumulation in all of the analyzed solid tissues and blood. Contradictory to their higher PSMA affinities and high internalization rates (e.g. when compared to [^{18}F][^{nat}Ga]rhPSMA-7.1), a significantly lower tumor uptake was found in this study. Due to the use of *L*-Dap as trifunctional linker, metabolic degradation could be considered as a potential reason for these results. However, since no metabolites were detected and no abnormalities were found in the

biodistribution experiments (e.g. high gastrointestinal or blood pool uptake), *in vivo* degradation of [^{18}F][^{nat}Ga]rhPSMA-7.2 and -7.4 seems unlikely.

In direct comparison to [F][Ga]rhPSMA-7.1, the *S*-DOTA-GA-based [F][Ga]rhPSMA-7.3 displayed superior *in vitro* properties with a 1.6-fold higher PSMA affinity and a 2.3-fold higher internalization rate. Moreover, it showed the highest tumor accumulation of all stereoisomers with a low background uptake in biodistribution studies at 1 h p.i.. Even though the HPLC-analysis revealed a lower relative percentage change of tumor uptake compared to [^{18}F][^{nat}Ga]rhPSMA-7.1, the overall distribution profile was similar with even lower percentage uptake in blood, liver and kidneys. Additionally, regarding the isomeric composition of the racemic compound, [F][Ga]rhPSMA-7.3 was determined as the most abundant species with 39 ± 2% (see Figure 22). Thus, significant problems (such as metabolism, unfavorable organ distribution or tumor uptake) would have been already detected during the clinical PET investigations with racemic [^{18}F][^{nat}Ga]rhPSMA-7.

One can speculate that homogenization of the tissue samples, did not result in a quantitative cell disruption. Thus, the [^{18}F][^{nat}Ga]rhPSMA tracers with the highest internalization rates (7.4 > 7.2 > 7.3 >> 7.1) might have been extracted in a less efficient manner, whereas [^{18}F][^{nat}Ga]rhPSMA-7.1 with its more than 2-fold lower internalization was efficiently extracted and is consequently over-estimated in the HPLC analysis. On the other hand, the analytical method described above summarizes all *in vivo* effects that determine tracer uptake *in vivo*, from the time point of injection up to the accumulation in a tumor cell. Thus, additional and perhaps unidentified parameters (not compared *in vitro*) are included.

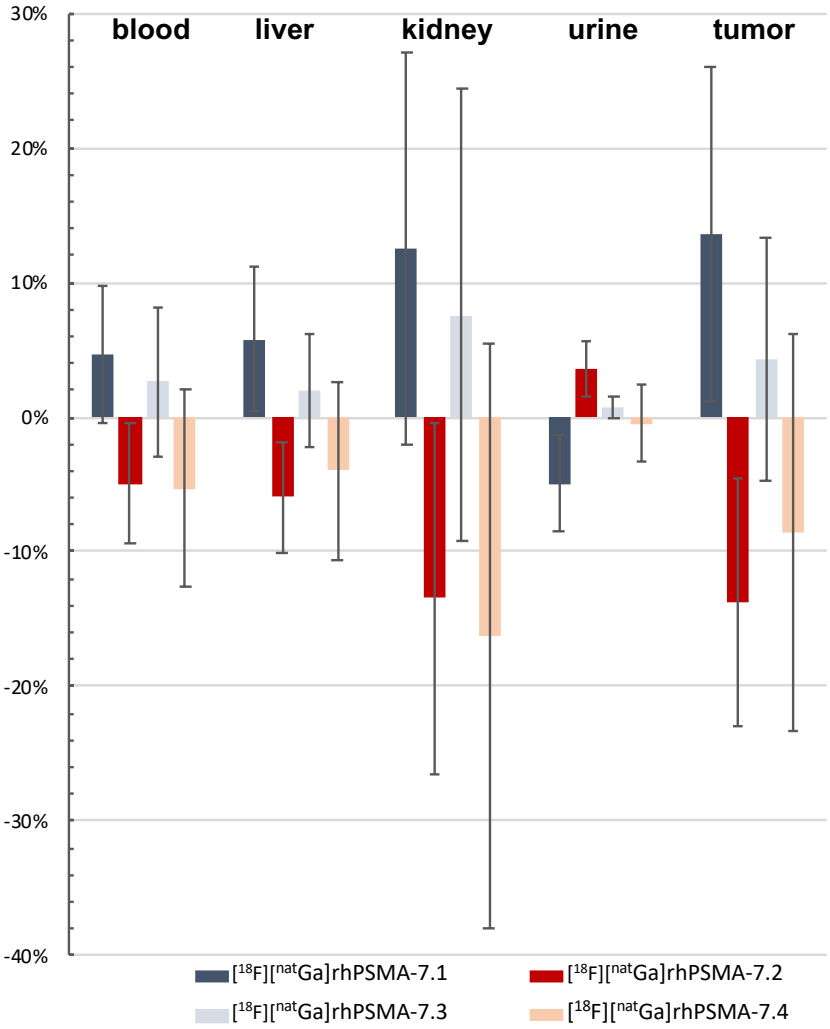

Figure 28: Relative percentage change of the uptake of [^{18}F][^{nat}Ga]rhPSMA-7.1 to -7.4 in blood, liver, kidney, urine and tumor of male LNCaP tumor-bearing SCID mice (30 min p.i.) compared to racemic [^{18}F][^{nat}Ga]rhPSMA-7. Values are expressed as mean ± SD, determined in the four independent experiments depicted in Figure 27.

Based on the results from all of the performed experiments, it was decided to prioritize the *D*-Dap – *S*-DOTA-GA-configured [F][Ga]rhPSMA-7.3 as the isomer of choice for further development.

3.4.6 Defluorination experiments

The aim of the following experiments was to detect [^{18}F]fluoride which could have been released by defluorination of ^{18}F-labeled rhPSMA ligands *in vivo*. Due to interactions of non-carrier added [^{18}F]fluoride with uncapped HPLC-column material, free [^{18}F]fluoride is difficult to detect by means of the aforedescribed HPLC method. Thus, further analysis was performed by using a novel RP-18 end-capped HPLC-column. Female healthy CB-17 SCID mice were injected with ^{18}F-labeled [^{nat}Ga]rhPSMA-7.1 to -7.4 (pooled, n=4 for each tracer). Urine samples were taken by means of a catheter 30 min p.i., pooled and analyzed by RP-HPLC. In a further test, fresh urine of mice was spiked with [^{18}F][^{nat}Ga]rhPSMA-7.1 to -7.4 and incubated over a period of up to 2 h (n=1).

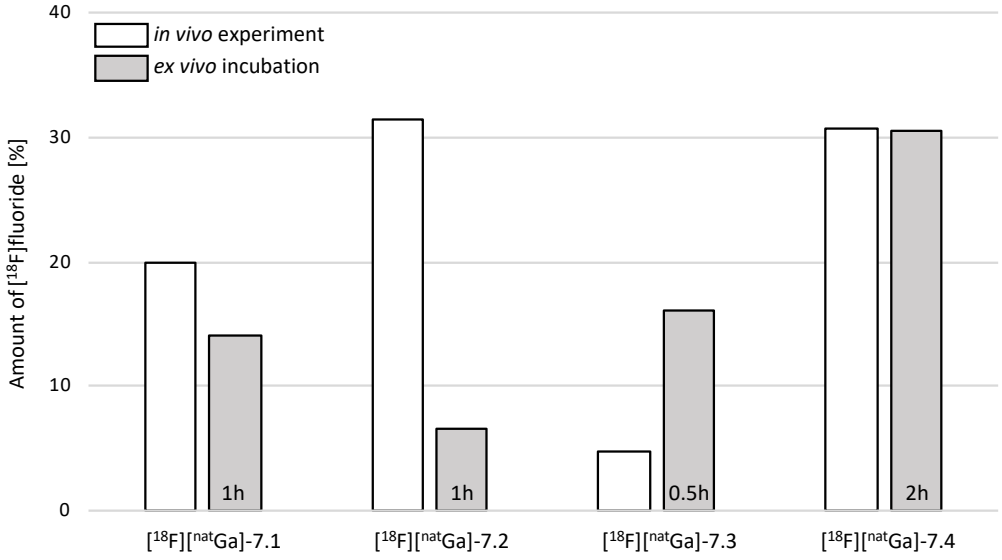

Figure 29: Quantification of a) free [^{18}F]fluoride in collected urine samples (*in vivo* experiment; white bars, n=4; pooled) 30 min p.i. of [^{18}F][^{nat}Ga]rhPSMA-7.1 to -7.4 into female healthy CB-17 SCID mice and b) free [^{18}F]fluoride in collected urine samples of female healthy CB-17 SCID mice, incubated *ex vivo* with [^{18}F][^{nat}Ga]rhPSMA-7.1 to -7.4 for certain time intervals (grey bars, n=1, incubation time depicted in bars). Analysis was performed by radio-RP-HPLC.

In all of the samples, free [^{18}F]fluoride was found to various degrees between 5 and 32% (Figure 29). Since no elevated bone activity accumulation or other abnormalities in biodistribution studies were found, it was concluded [^{18}F]fluoride might be released from the tracer downstream from glomerular filtration in kidneys. This would result in the experimentally observed formation and subsequent excretion of [^{18}F]fluoride in urine without detectable uptake of [^{18}F]fluoride in blood, organs or bones. This assumption is also supported

by the observed defluorination in *ex vivo* urine samples after incubation with the tracer, which occurred to a similar extent compared to samples from *in vivo* experiments. Reports on the toxicology of fluoride reveal that relevant amounts of fluoride are present in kidneys and urine of mice and rats. In mice, physiological urinary fluoride levels of 0.3 ppm were detected[197]. In a different publication, the average fluoride concentration in the urine of normal mice was determined to be 0.13-0.14 µg/mL[198] and Inkielewicz *et al.* found that the fluoride content in the serum of rats is about 5% of the concentration in the kidneys (serum: 0.051 µg/mL, kidneys: 0.942 µg/mL)[199]. Taken into account that most of the tracer is specifically taken up into and also physiologically cleared by the kidneys, an elevated fluoride level combined with a body temperature of 36.6 °C might result in a continuous elimination of ^{18}F-fluoride by ^{19}F-for-^{18}F isotopic exchange at the SiFA moiety even in aqueous media. The experimentally observed variability of released amounts of [^{18}F]fluoride could therefore be explained by animal-individual differences in physiological fluoride concentrations and/or excretion kinetics.

Further discussion of the isotopic exchange reaction in aqueous media and conclusions drawn for the development of a minimalistic ^{18}F-labeling approach for rhPSMA ligands is provided in chapter 7.4 “Isotopic exchange reaction in aqueous solutions”.

4. Therapeutic rhPSMA ligands

So far, the established radiohybrid platform was solely explored for diagnostic applications employing either the ^{68}Ga- or the ^{18}F-labeled twin compound. Since the cyclen-based chelators DOTA-GA and DOTA offer the advantage to form stable complexes with radiometals that are commonly used for endoradiotherapeutic approaches (such as ^{177}Lu, ^{90}Y, ^{213}Bi or ^{225}Ac), a transfer of the radiohybrid technology to theranostic applications seemed feasible. Due to the great potential of ^{177}Lu-labeled PSMA inhibitors in salvage therapy of late-stage PCa[120], the described rhPSMA ligands were evaluated by substituting gallium by lutetium.

In the context of radioligand therapy (RLT), the respective [^{18}F][^{nat}Lu]rhPSMA could be a valuable tool for PET imaging (patient stratification) and potentially pretherapeutic dosimetry, whereas the ^{177}Lu-labeled analogue would be applicable for therapeutic purposes. Furthermore, due to their identical chemical structures, the diagnostic agent [^{18}F][^{nat}Lu]rhPSMA and its therapeutic counterpart [^{19}F][^{177}Lu]rhPSMA would represent a true theranostic pair of identical probes with absolutely identical *in vivo* behavior and distribution.

4.1 *In vitro* characterization

For initial evaluation of the theranostic radiohybrid concept, Lu-complexed rhPSMA-7 and -7.3 as well as the DOTA-based structural analogue rhPSMA-10 were characterized in *in vitro* studies. Moreover, the inverse functionalized pendants (SiFA at the α-amine and chelator at the β-position of Dap) rhPSMA-8 and -11 were tested (Figure 30). The novel ligand rhPSMA-11 could be prepared in a similar procedure as described for rhPSMA-8, in an overall yield of 11%.

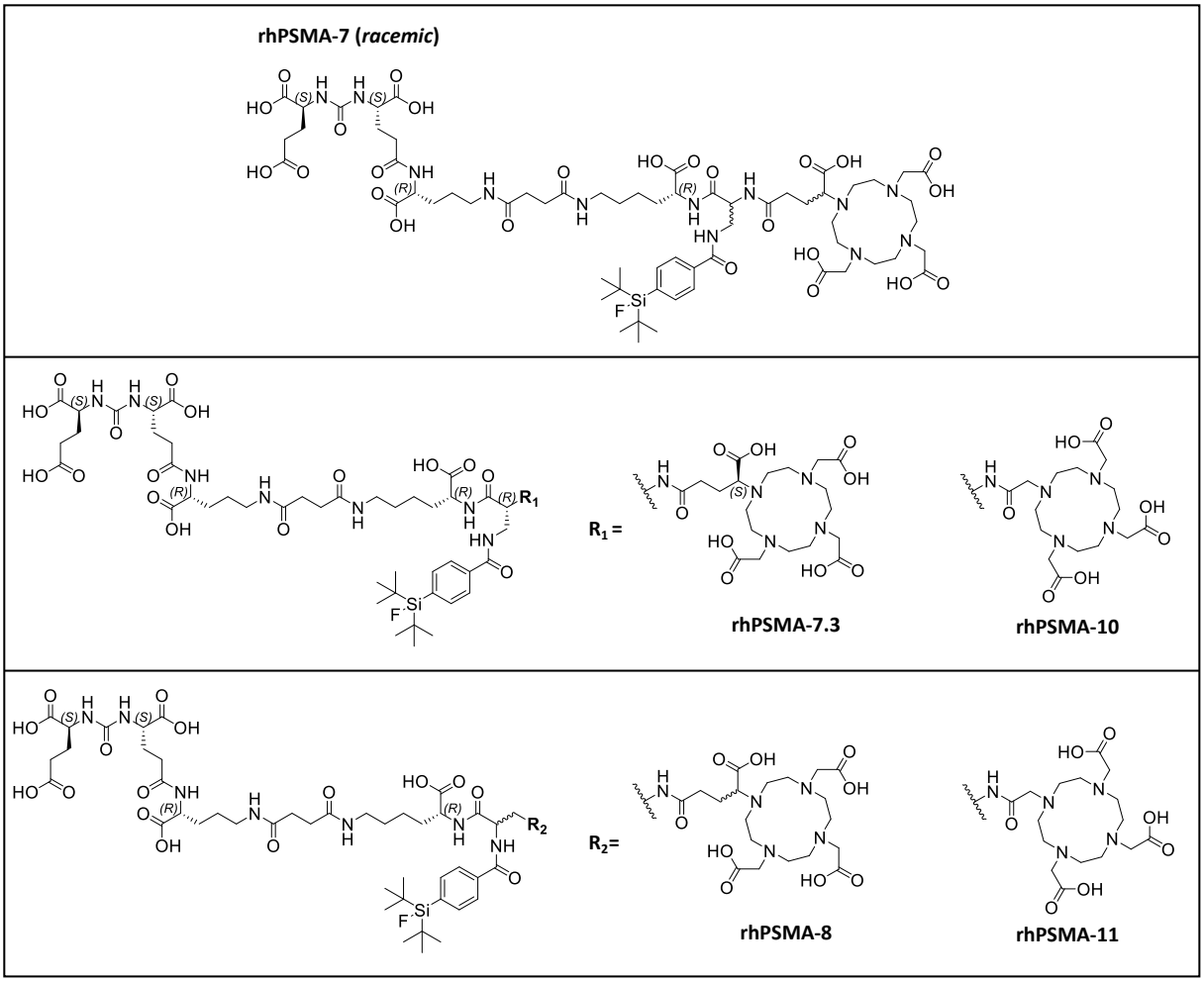

Figure 30: Structural formulas of rhPSMA precursor ligands used for complexation with radiometals, such as $^{177/nat}$Lu.

In experiments requiring the radioactively labeled compound, the respective [^{177}Lu][^{19}F]rhPSMA ligands were examined. The well-established therapeutic agents PSMA I&T and PSMA-617 as well as the respective Ga-chelated rhPSMAs are included for comparison.

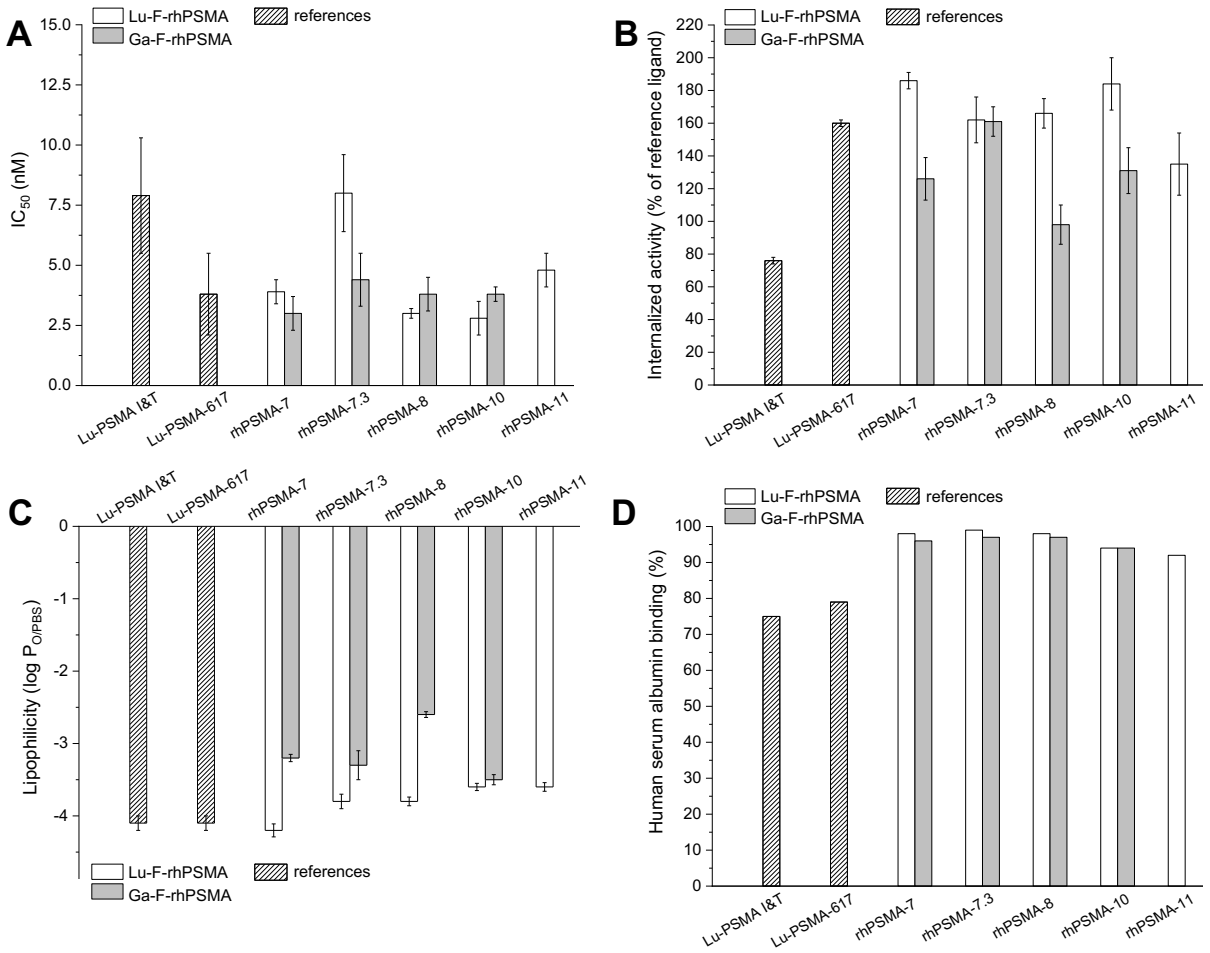

Figure 31: **A**) Binding affinities (IC_{50} [nM], 1 h, 4 °C; n=3) of [^{nat}Lu][^{19}F]rhPSMA-7 to -11 (white bars), [^{nat}Ga][^{19}F]rhPSMA-7 to -11 (grey bars), [^{nat}Lu]PSMA-617 and [^{nat}Lu]PSMA I&T; **B**) internalized activity of [^{177}Lu][^{19}F]rhPSMA-7 to -11 (white bars), [$^{68/nat}$Ga][$^{19/18}$F]rhPSMA-7 to -11 (grey bars), [^{177}Lu]PSMA-617 and [^{177}Lu]PSMA I&T in LNCaP cells (1 h, 37 °C) as a percentage of the reference ligand ([^{125}I]I-BA)KuE; n=3); **C**) lipophilicity of [^{177}Lu][^{19}F]rhPSMA-7 to -11 (white bars), [$^{68/nat}$Ga][$^{19/18}$F]rhPSMA-7 to -11 (grey bars), [^{177}Lu]PSMA-617 and [^{177}Lu]PSMA I&T, expressed as octanol/PBS (pH 7.4) partition coefficient (log $P_{O/PBS}$; n=6); **D**) human serum albumin binding of [^{nat}Lu][^{19}F]rhPSMA-7 to -11 (white bars), [^{nat}Ga][^{19}F]rhPSMA-7 to -11 (grey bars), [^{nat}Lu]PSMA-617 and [^{nat}Lu]PSMA I&T, determined on a Chiralpak HSA column. Data of the reference ligands were obtained from previous work of our group[96, 174]. Values are expressed as mean ± SD.

All ^{nat}Lu-complexed rhPSMA compounds and ^{nat}Lu-complexed reference ligands displayed high PSMA-affinities in the low nanomolar range (Figure 31 A). Interestingly, the enantiomeric pure [^{nat}Lu][^{19}F]rhPSMA-7.3 showed a 2-fold lower affinity compared to the racemic mixture. Since the different complex structures of Lu-DOTA-GA and Ga-DOTA-GA could have unpredictable effects on *in vitro* properties, it cannot be concluded that isomer rhPSMA-7.3 is also the best isomer for RLT. Therefore, further evaluation of [Lu][F]rhPSMA-7.1 to -7.4 is highly recommended.

The internalization rates (Figure 31 B) of [^{177}Lu][^{19}F]rhPSMA-7, -8 and -10 were significantly higher than those of [^{177}Lu]PSMA I&T (76%) and were similar to [^{177}Lu]PSMA-617 (160%). Surprisingly, the internalization rates of [^{177}Lu][^{19}F]rhPSMA-7, -8 and -10 were also significantly higher than those of the respective ^{68}Ga-chelated compounds; 1.5-fold for rhPSMA-7, 1.7-fold for rhPSMA-8 and 1.4-fold for rhPSMA-10. In the case of rhPSMA-7.3 an equally high internalization rate was found for both metal chelates. Regarding the log $P_{O/PBS}$ values, the ^{177}Lu-labeled rhPSMAs displayed overall higher hydrophilicities compared to their ^{68}Ga-labeled counterparts (Figure 31 C). The hexadentate complexation of gallium with DOTA and DOTA-GA results in an additional free carboxylate at the chelator, compared to the respective Lu-complexes[200]. Based on these results, it can be concluded that the absence of the uncoordinated negative charge in the Lu-DOTA and Lu-DOTA-GA chelate of rhPSMAs seemed to be favorable for the internalization rate and hydrophilicity in the examined set of SiFA-bearing PSMA ligands. Binding to HSA remained unaffected and similar values were measured as for the Ga-chelated rhPSMA inhibitors (Figure 31 D).

4.2 *In vivo* characterization

Biodistribution study (24 h)

The biodistribution of ^{177}Lu-labeled rhPSMA-7, -7.3, -8 and -10 was determined in LNCaP tumor-bearing SCID mice 24 h p.i.. The reference ligands [^{177}Lu]PSMA I&T and [^{177}Lu]PSMA-617 are included for comparison (Figure 32).

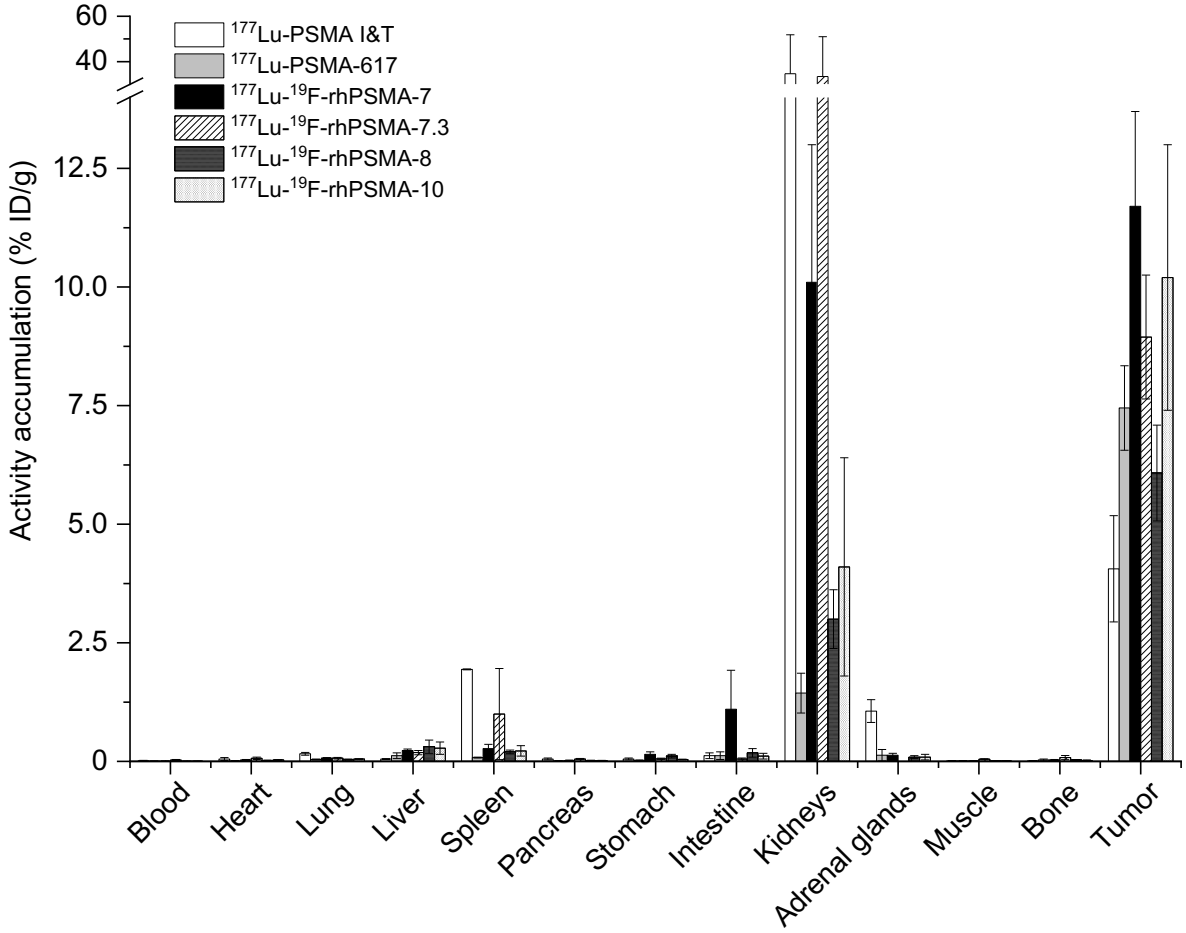

Figure 32: Biodistribution of [^{177}Lu][^{19}F]rhPSMA-7, -7.3, -8, -10, [^{177}Lu]PSMA I&T and [^{177}Lu]PSMA-617 at 24 h p.i. in male LNCaP tumor-bearing SCID mice. Data of the reference ligands were obtained from Schmidt et *al*.[174]. Evaluation of [^{177}Lu][^{19}F]rhPSMA-7.3 was carried out by N. Yusufi (Klinikum rechts der Isar). Values are expressed as a percentage of the injected dose per gram (% ID/g), mean ± standard deviation (n=4).

Not unexpectedly, the ^{177}Lu-labeled ligands showed high uptake in tumor and negligible accumulation in non-target tissues (< 0.3% ID/g), with varying degree of uptake in kidneys 24 h p.i.. Kidney uptake was highest for [^{177}Lu]PSMA I&T (35% ID/g) and [^{177}Lu][^{19}F]PSMA-7.3 (33% ID/g), whereas [^{177}Lu][^{19}F]rhPSMA-8 and -10, as well as the reference ligand [^{177}Lu]PSMA-617 displayed good clearance from the kidneys (< 5% ID/g). All ^{177}Lu-labeled rhPSMA ligands demonstrated at least 1.5-fold higher tumor uptakes compared to [^{177}Lu]PSMA I&T. Especially [^{177}Lu][^{19}F]PSMA-7 and -10 showed superior tumor accumulation which was even 1.6-fold and 1.4-fold higher than determined for [^{177}Lu]PSMA-617, respectively. Noteworthy, slightly elevated uptake of racemic [^{177}Lu][^{19}F]rhPSMA-7 was found in murine intestine (1% ID/g versus 0.1% ID/g of reference ligands). However, strong animal-individual differences were found for this organ which resulted in a high error bar of the corresponding uptake value and therefore further revalidation would be recommended.

Biodistribution study (1 h)

For further evaluation, the biodistribution of the most favorable therapeutic rhPSMA ligands was assessed in LNCaP tumor-bearing SCID mice also at 1 h p.i.. Despite the slightly lower tumor uptake but otherwise similar distribution profile at 24 h p.i., the enantiomeric pure compound [^{177}Lu][^{19}F]rhPSMA-7.3 was chosen over the racemic mixture. Results were compared to the reference ligands [^{177}Lu]PSMA-617 and [^{177}Lu]PSMA I&T (Figure 33).

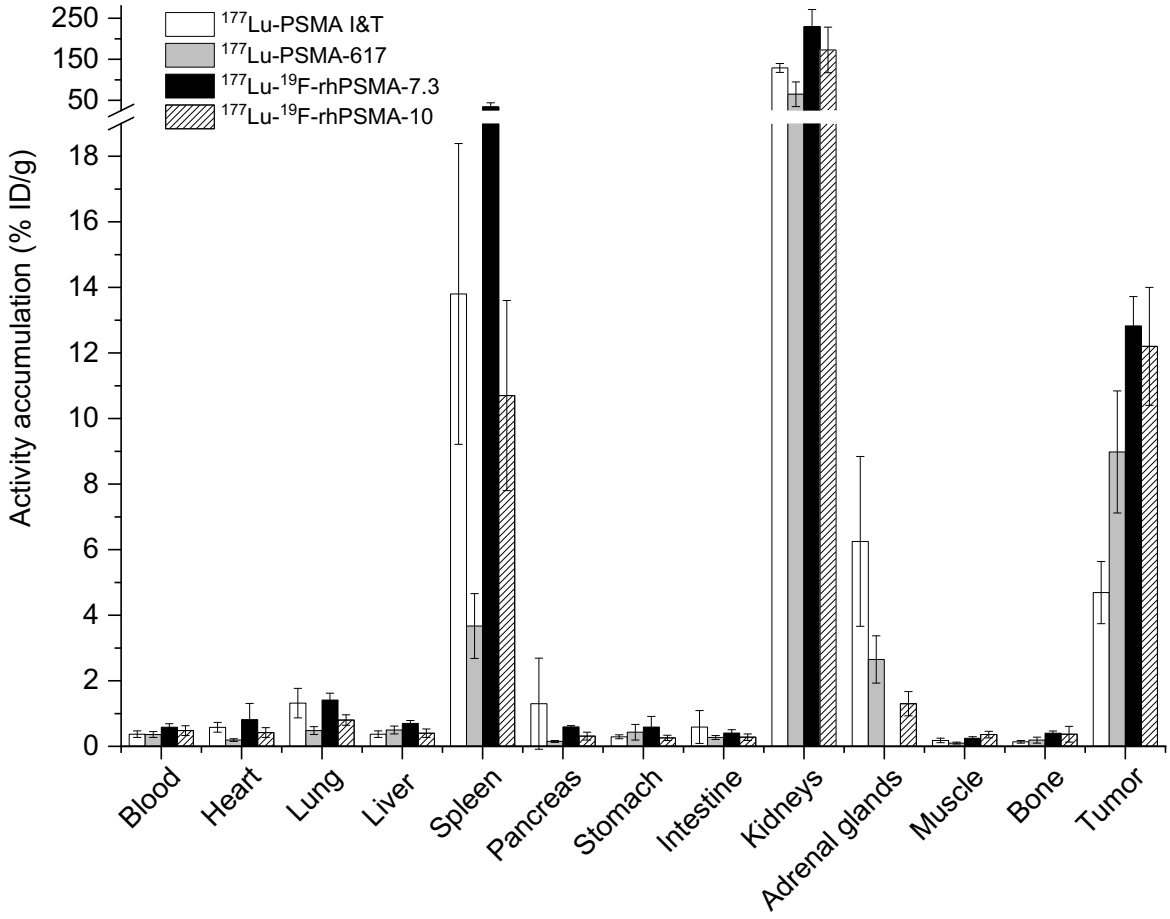

Figure 33: Biodistribution of [^{177}Lu][^{19}F]rhPSMA-7.3, -10, [^{177}Lu]PSMA I&T and [^{177}Lu]PSMA-617 at 1 h p.i. in male LNCaP tumor-bearing SCID mice. Data of the reference ligands were obtained from Schmidt et *al*.[174]. Evaluation of [^{177}Lu][^{19}F]rhPSMA-7.3 was carried out by N. Yusufi (Klinikum rechts der Isar). Data expressed as a percentage of the injected dose per gram (% ID/g), mean ± standard deviation (n=4).

After 1 h p.i. the ^{177}Lu-labeled rhPSMA ligands showed low accumulation in non-target tissues and fast renal excretion. Compared to [^{177}Lu][^{19}F]rhPSMA-7.3, [^{177}Lu][^{19}F]rhPSMA-10 displayed somewhat faster clearance kinetics. Otherwise, non-target accumulation was comparable and similar to the reference ligands. In accordance with the biodistribution data

after 24 h, tumor uptake was in the same range for both ^{177}Lu-labeled rhPSMA ligands and approximately 2.6- and 1.4-fold higher than those of the references [^{177}Lu]PSMA I&T and [^{177}Lu]PSMA-617, respectively.

Kidney uptake was higher for [^{177}Lu][^{19}F]rhPSMAs compared to the reference compounds at 1 h p.i.. Particularly [^{177}Lu]PSMA-617 demonstrated a very low uptake (65% ID/g), which was more than 2.7-fold lower as measured for the ^{177}Lu-rhPSMA ligands. Nevertheless, the low kidney uptakes after 24 h (33% ID/g for [^{177}Lu][^{19}F]rhPSMA-7.3 and 4% ID/g for [^{177}Lu][^{19}F]rhPSMA-10) indicate a suitable clearance profile for both radiohybrid ligands.

When compared with [^{177}Lu]PSMA I&T (129% ID/g at 1 h), the low kidney uptake of [^{177}Lu]PSMA-617 (65% ID/g at 1 h) has often been highlighted as the major selection criteria that promoted the rapid clinical development of [^{177}Lu]PSMA-617. However, contradictory to preclinical results in mice, head-to-head comparison of both ligands in patients has impressively demonstrated a nearly identical kidney uptake and clearance kinetic of both tracers in patients[117]. Thus, even though further investigations are necessary in order to fully understand the observed species and tracer differences and to draw conclusions for other PSMA-targeted ligands, different kidney uptakes of PSMA-targeted inhibitors (and thus [^{177}Lu]rhPSMA ligands) in mice at early time points should be treated with caution, should not be overrated and need final confirmation in humans.

In summary, the lead compounds [^{177}Lu][^{19}F]rhPSMA-7.3 and -10 demonstrated favorable PSMA-targeting characteristics *in vitro* and promising behavior *in vivo*. Moreover, the biodistribution experiments indicate that application of [^{177}Lu]rhPSMA ligands in patients could result in higher tumor uptake, both at early and late time points and thus higher absorbed tumor doses. Although the radiohybrid compounds showed improvable kidney uptake at 1 h p.i., they showed good clearance at 24 h p.i.. Further studies in preclinical models will be necessary to finally decide, whether [^{177}Lu][^{19}F]rhPSMA-10 or one of the [^{177}Lu][^{19}F]rhPSMA-7 isomers should be transferred into formal clinical studies.

5. Proof-of-Concept studies with ^{18}F-labeled rhPSMA inhibitors in patients

The radiosynthesis of ^{18}F-labeled rhPSMA ligands was performed in a fully automated GMP-compliant procedure, as described in Chapter 7.3 "Automated ^{18}F-labeling of rhPSMA ligands". Images were acquired after injection of 191-417 MBq of the radioligand at 50-220 min p.i. (further details are provided in the Material and Methods section).

5.1 Clinical PET imaging with [^{18}F][^{nat}Ga]rhPSMA-7

Taking into account the ease of synthesis, the excellent preclinical data, and the practical advantages that ^{18}F-labeled PSMA-targeted radiopharmaceuticals can provide in daily routine, racemic [^{18}F][^{nat}Ga]rhPSMA-7 was selected for a very early first proof-of-concept PET study in patients suffering from metastasized prostate cancer.

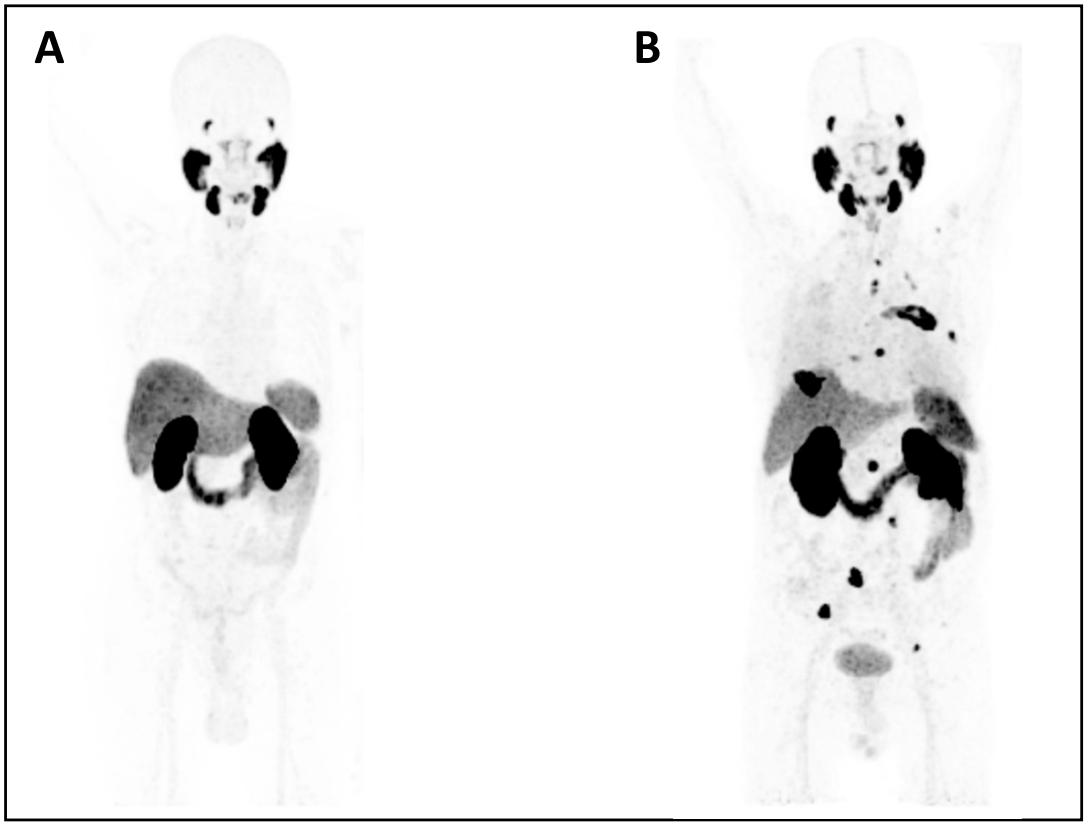

Figure 34: **A**) Maximum intensity projection (MIP) from PET of a subject with normal biodistribution with no detectable tumor lesions (76 min p.i., 272 MBq of [^{18}F][^{nat}Ga]rhPSMA-7). **B**) MIP of a patient with moderately advanced prostate cancer exhibiting multiple tumor lesions (111 min p.i., 312 MBq of [^{18}F][^{nat}Ga]rhPSMA-7). Studies were carried out at the Department of Nuclear Medicine at the Klinikum rechts der Isar, courtesy of M. Eiber.

The biodistribution of [^{18}F][^{nat}Ga]rhPSMA-7 in patients showed the typical distribution pattern of radiolabeled PSMA-inhibitors[105, 201], i.e. high uptake in kidneys, parotids, submandibular and sublingual glands, duodenum and small intestines; medium to low uptake in liver and spleen; and low to negligible uptake in other organs[202]. This overall distribution pattern is in accordance with the preclinical biodistribution in mice and the known PSMA expression profile in humans (Figure 34 A and B)[21, 203, 204]. Apart from this, and since a ^{18}F-SiFA-conjugated radiopharmaceutical has not been investigated in humans before, the first patient studies answered two important and crucial questions:

1) Is the ^{18}F-SiFA-moiety stable enough to resist *in vivo* defluorination in humans?
2) Is the blood clearance kinetics of [^{18}F][^{nat}Ga]rhPSMA-7 dominated by the hydrophilicity of the tracer and thus fast enough for an imaging agent, or is the clearance kinetics dominated by the high plasma protein binding and thus inappropriately slow?

Fortunately, as already observed in mice, [^{18}F][^{nat}Ga]rhPSMA-7 was found to be stable against defluorination *in vivo*. Although the ^{19}F-for-^{18}F-isotopic exchange at 37 °C would be fast enough to liberate ^{18}F-fluoride *in vivo*, the serum concentration of ^{19}F-fluoride in humans which is kept permanently low (0.017 ± 0.011 ppm)[205] by binding of fluoride to the hydroxyapatite matrix of bones, seems to be too small to create ^{19}F-fluoride in amounts sufficient to detect activity uptake in bones.

Regarding the blood clearance kinetics the first proof-of-concept studies demonstrated that although [^{18}F][^{nat}Ga]rhPSMA-7 almost quantitatively binds to human serum albumin, the binding is not strong enough to inappropriately delay the blood clearance kinetics of this SiFA conjugated tracer (log $P_{O/PBS}$ = −3.2). Consequently, high tumor-to-background ratios are rapidly reached and allow for PET imaging at early time points after application.

As demonstrated in Figure 34 B, high tumor uptake in combination with low accumulation in background tissues enabled visualization of multiple soft-tissue and bone lesions in high contrast. Most importantly, excretion of the tracer/radioactivity in the urine/bladder is low (although it shall be mentioned, that patients received an injection of 20 mg furosemide at the time of tracer application). The slow excretion *via* the urinary route is favorable for the detection of tumor lesions located in the pelvis in close distance to the ureters and bladder.

Since the first clinical application (July 2017) more than 1000 clinical PET scans were performed using [^{18}F][^{nat}Ga]rhPSMA-7 at two different sites, Klinikum rechts der Isar and Klinikum Großhadern (Munich, Germany). The following clinical cases (Figure 35 A-C) exemplarily illustrate the results obtained with [^{18}F][^{nat}Ga]rhPSMA-7-PET in patients at different disease stages. Mean and maximum standardized uptake values (SUV_{mean}, SUV_{max}) were determined for [^{18}F][^{nat}Ga]rhPSMA-7 in different tissues and organs of interest in 53 patients (Figure 35 D).

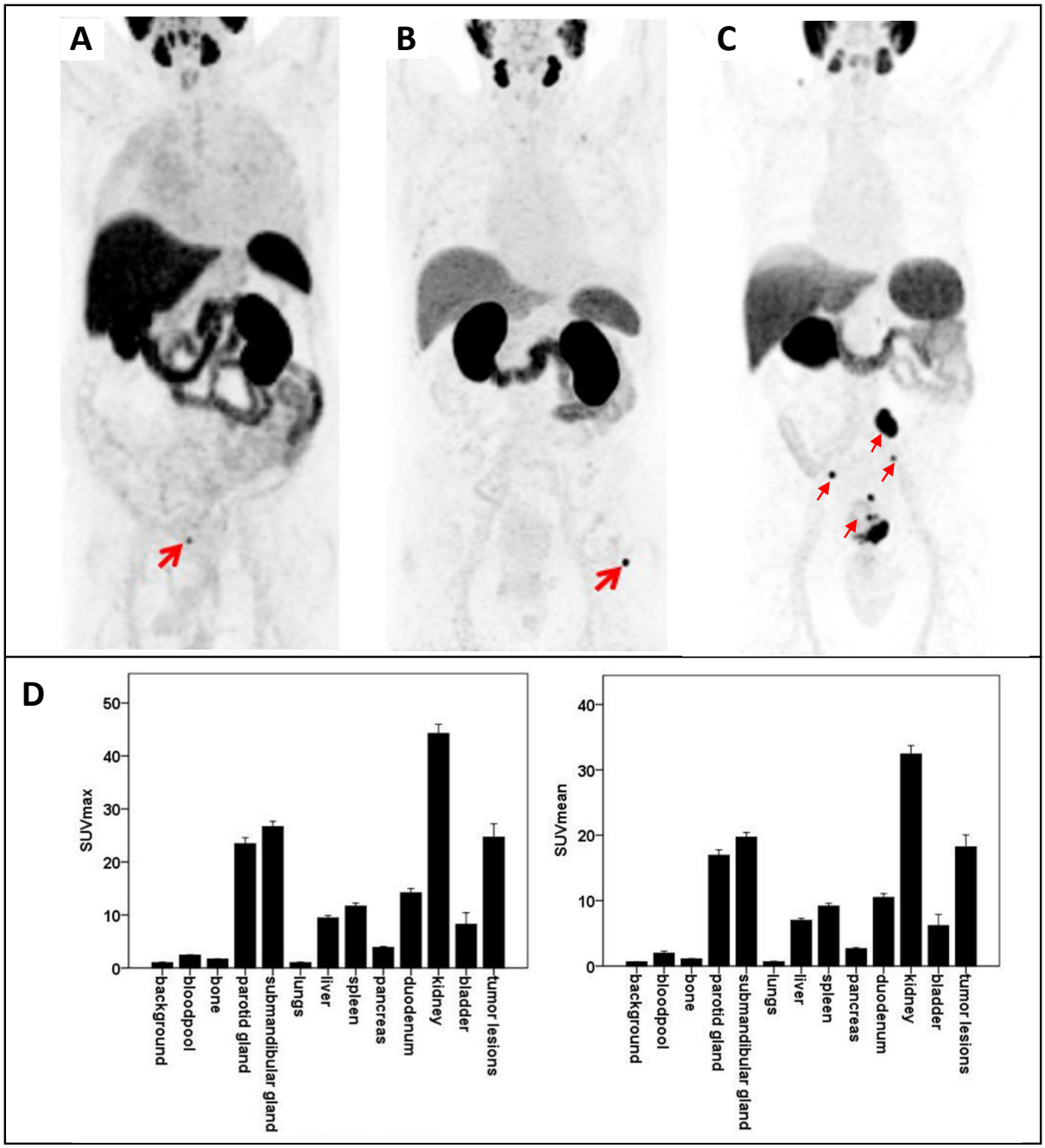

Figure 35: Maximum intensity projections from PET using [^{18}F][^{nat}Ga]rhPSMA-7: **A**) 78-year old patient after radical prostatectomy with rising PSA (0.35 ng/mL) and local recurrence (red arrow). **B**) 67-year old patient after radical prostatectomy and salvage radiation therapy with rising PSA (1.94 ng/mL) and a new bone metastasis (red arrow) on the left femur neck. **C**) primary staging of a patient displaying multiple lesions (red arrows); iPSA = 39 ng/mL. **D**) Maximum and mean standardized uptake values (SUV_{max}; left and SUV_{mean}; right) in different tissues of 53 subjects with PCa (tissues/organs: n=53, tumor lesions: n=72) with its standard error. Studies were carried out at the Department of Nuclear Medicine at the Klinikum rechts der Isar, courtesy of M. Eiber.

Similar to other PSMA-addressing ligands[105, 201], [^{18}F][^{nat}Ga]rhPSMA-7 exhibited considerable uptake in normal organs, such as the salivary glands (SUV_{mean}: 16.8-19.6), kidneys (SUV_{mean}: 32.1) and moderate uptake in liver (SUV_{mean}: 7.0), spleen (SUV_{mean}: 9.1) and duodenum (SUV_{mean}: 10.5)[21, 203, 204]. Low accumulation of the tracer in the blood pool and background tissues enabled localization of malignant lesions in high contrast (SUV_{mean}: 19.2). The data obtained so far indicate a trend to high detection rates even at low PSA values (< 1 ng/mL). Early detection of recurrent PCa is crucial in order to guide future salvage therapy. Recent studies demonstrated that there is an approximately 80% chance for progression-free survival at five years, if radioligand therapy is initiated before the PSA reaches 0.5 ng/mL in patients with recurrent disease[206-209].

The uptake pattern of [^{18}F][^{nat}Ga]rhPSMA-7 in liver, kidneys and the urinary bladder demonstrates that the tracer is in a mixed, but balanced hepatobiliary and renal excretion mode. Compared to the hydrophilic tracer [^{18}F]DCFPyL with predominantly renal excretion and fast excretion in urine and with the lipophilic tracer [^{18}F]PSMA-1007 with predominantly hepatobiliary excretion (liver uptake), the liver uptake of [^{18}F][^{nat}Ga]rhPSMA-7 is lower than that of [^{18}F]PSMA-1007, while renal excretion is still not as pronounced as that for [^{18}F]DCFPyL or [^{68}Ga]PSMA-11[105, 108, 210, 211].

Thus, the slow urinary excretion of [^{18}F][^{nat}Ga]rhPSMA-7 allows to overcome some of the limitations currently observed with other PSMA-targeted PET tracers, such as inappropriate detection of small metastases in close proximity to the ureters or induced halo-artefacts (that deteriorate image quality and thus impede diagnostic accuracy) and might increase detection efficacy[212-214]. This could be especially helpful for primary staging of patients with high-risk prostate cancer, due to good visualization of malignancies adjacent to the urinary bladder.

5.2 Clinical PET imaging with [^{18}F][^{nat}Ga]rhPSMA-7.3

In the course of the isomer selection process of racemic [^{18}F][^{nat}Ga]rhPSMA-7, the *D*-Dap – *S*-DOTA-GA-configured enantiomer [^{18}F][^{nat}Ga]rhPSMA-7.3 was found to have the most promising characteristics. With the intention to facilitate the clinical development according to the guidelines of the FDA and EMA which promote the investigation of enantiomeric pure compounds, [^{18}F][^{nat}Ga]rhPSMA-7.3 was chosen for further clinical evaluation (Figure 36)[193].

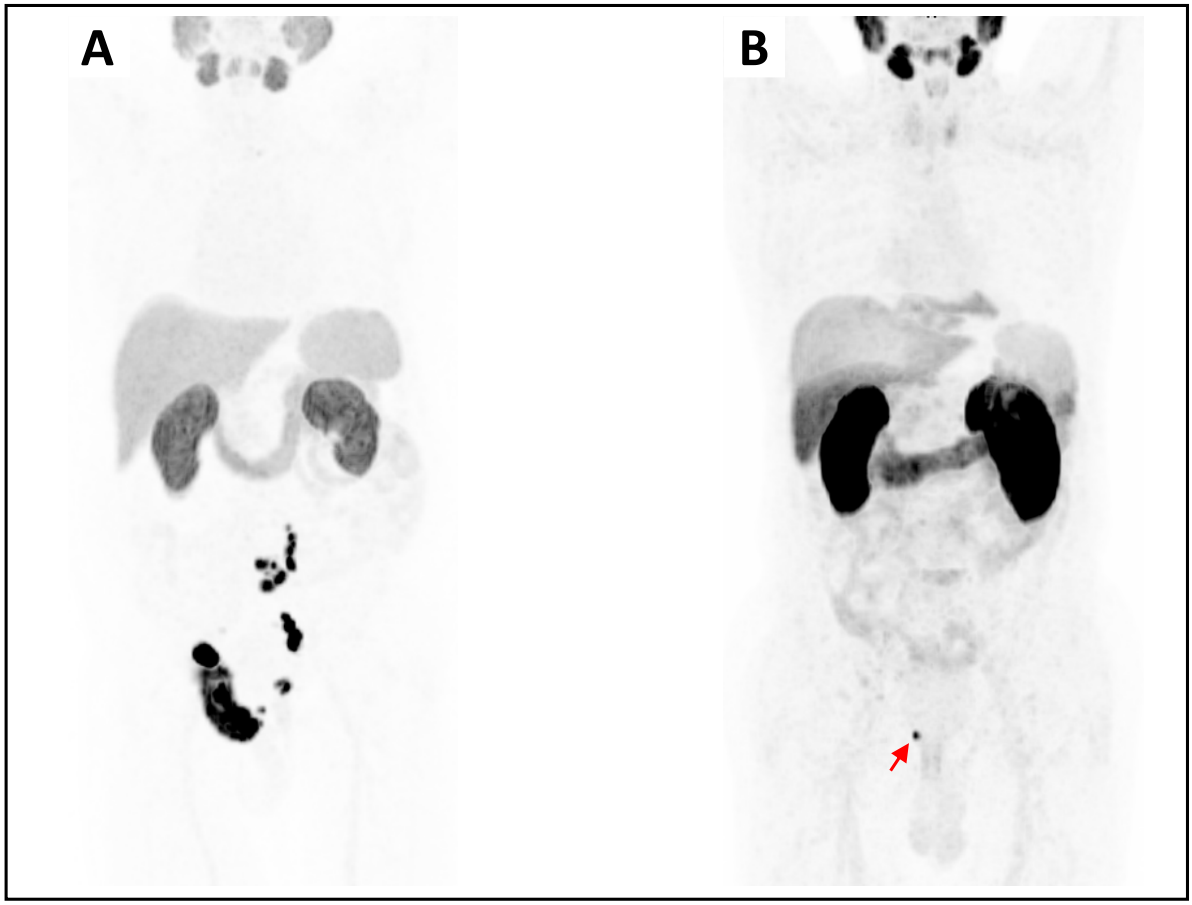

Figure 36: Maximum intensity projections (MIP) from PET using [^{18}F][^{nat}Ga]rhPSMA-7.3: **A**) subject after radical prostatectomy, chemotherapy and androgen deprivation therapy with a PSA of 22 ng/mL displaying multiple malignant lesions in the abdomen and pelvis. **B**) patient after radical prostatectomy with rising PSA (0.5 ng/mL) and small local recurrence (red arrow). Studies were carried out at the Department of Nuclear Medicine at the Klinikum rechts der Isar, courtesy of M. Eiber.

Compared with [^{18}F][^{nat}Ga]rhPSMA-7, [^{18}F][^{nat}Ga]rhPSMA-7.3 shows even lower liver uptake and more pronounced renal excretion, while maintaining the advantages of fast blood clearance and slow excretion into the urine.

Since December 2018 more than 1000 clinical [^{18}F][^{nat}Ga]rhPSMA-7.3-PET scans were performed in PCa patients. Recent analyses of these investigations revealed that, compared to [^{18}F][^{nat}Ga]rhPSMA-7, [^{18}F][^{nat}Ga]rhPSMA-7.3 shows an approximately 5-fold lower excretion of activity into the bladder and an approximately 1.5-fold higher tumor-accumulation. On one hand these impressive results demonstrate the superb imaging characteristics and outstanding clinical potential of [^{18}F][^{nat}Ga]rhPSMA-7.3, and on the other hand, fortunately clearly confirm the reliability and validity of the "differential tracer uptake analysis" that has been developed and applied for the first time in the context of the selection process of the best [^{18}F][^{nat}Ga]rhPSMA-7 isomer. In the meantime [^{18}F][^{nat}Ga]rhPSMA-7.3 has entered a formal clinical development process by Blue Earth Diagnostics (Oxford, United Kingdom).

6. Proof-of-Concept studies with ^{177}Lu-labeled rhPSMA inhibitors in patients

Due to the promising results of the ^{177}Lu-labeled rhPSMA ligands that were obtained in a comparative preclinical evaluation with the established reference ligands [^{177}Lu]PSMA I&T und [^{177}Lu]PSMA-617, the lead compound [^{177}Lu][^{19}F]rhPSMA-7.3 was subsequently evaluated in a first proof-of-concept RLT study in a patient with mCRPC.

To compare the dosimetry of [^{177}Lu]PSMA I&T and [^{177}Lu][^{19}F]rhPSMA-7.3, 1.03 GBq of [^{177}Lu]PSMA I&T was administered in a patient and the distribution kinetics quantified *via* scintigraphy at multiple time points between 1 and 168 h p.i. (approximately after 1, 3, 24, 48 and 168 h). After three weeks, the identical protocol was applied to determine the distribution kinetics of [^{177}Lu][^{19}F]rhPSMA-7.3 (0.91 GBq) in the same patient (Figure 37).

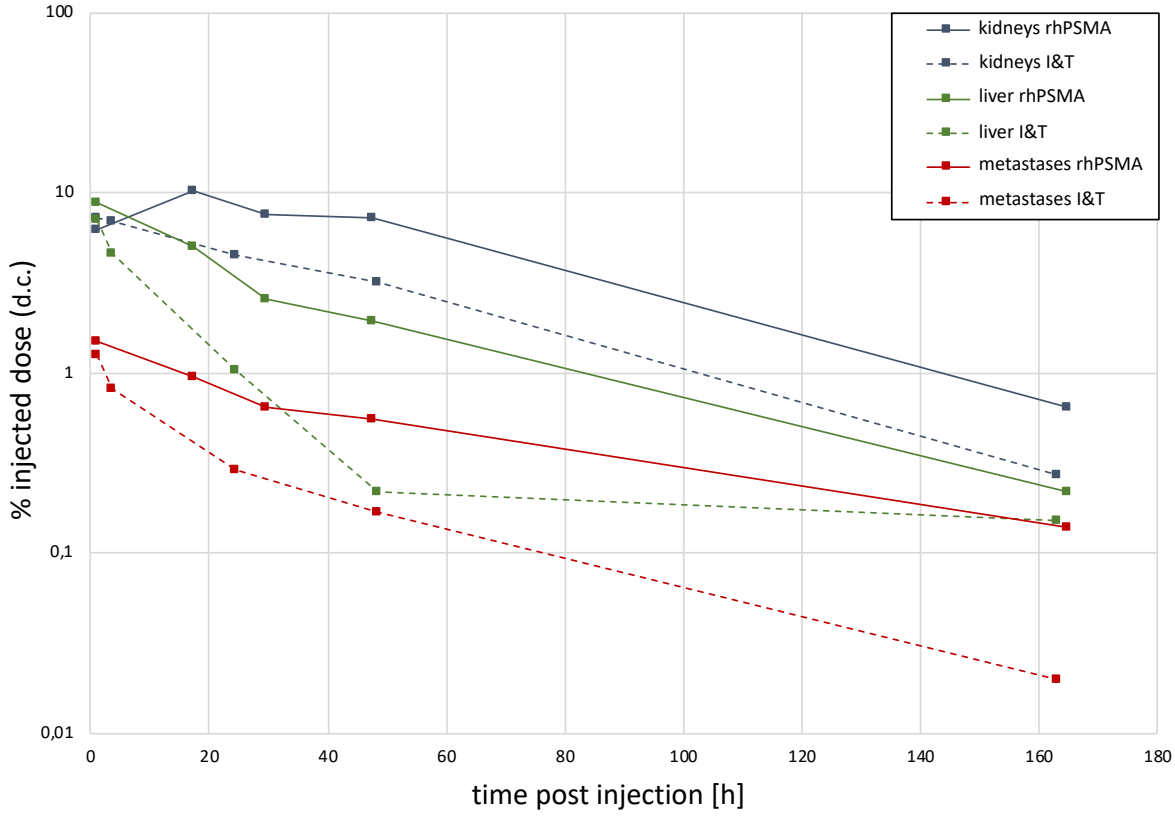

Figure 37: Uptake kinetics of [^{177}Lu][^{19}F]rhPSMA-7.3 (0.91 GBq) and [^{177}Lu]PSMA I&T (1.03 GBq, dashed lines) in kidneys (blue), liver (green) and metastases (red), determined in one single patient with mCRPC at various time points (approx. 1, 3, 24, 48 and 168 h p.i.) by scintigraphy. Values are expressed as a percentage of the injected activity and were decay corrected. Studies were carried out at the Department of Nuclear Medicine at the Klinikum rechts der Isar, courtesy of M. Eiber.

Compared to [^{177}Lu]PSMA I&T, this intrapatient comparison revealed an approximately 1.2-fold higher initial uptake of [^{177}Lu][^{19}F]rhPSMA-7.3 in liver and metastases. In kidneys a similar uptake was found for both tracers after 1 h, whereas after 24 h [^{177}Lu][^{19}F]rhPSMA-7.3 displayed a 1.5-fold higher accumulation. The time activity curves show a much slower washout of the radiohybrid ligand from all of the organs and tumor lesions.

Based on these uptake kinetics, the absorbed dose to metastases, kidneys and liver was determined for both tracers and extrapolated to a typically administered amount of 7.4 GBq of each tracer (Figure 38).

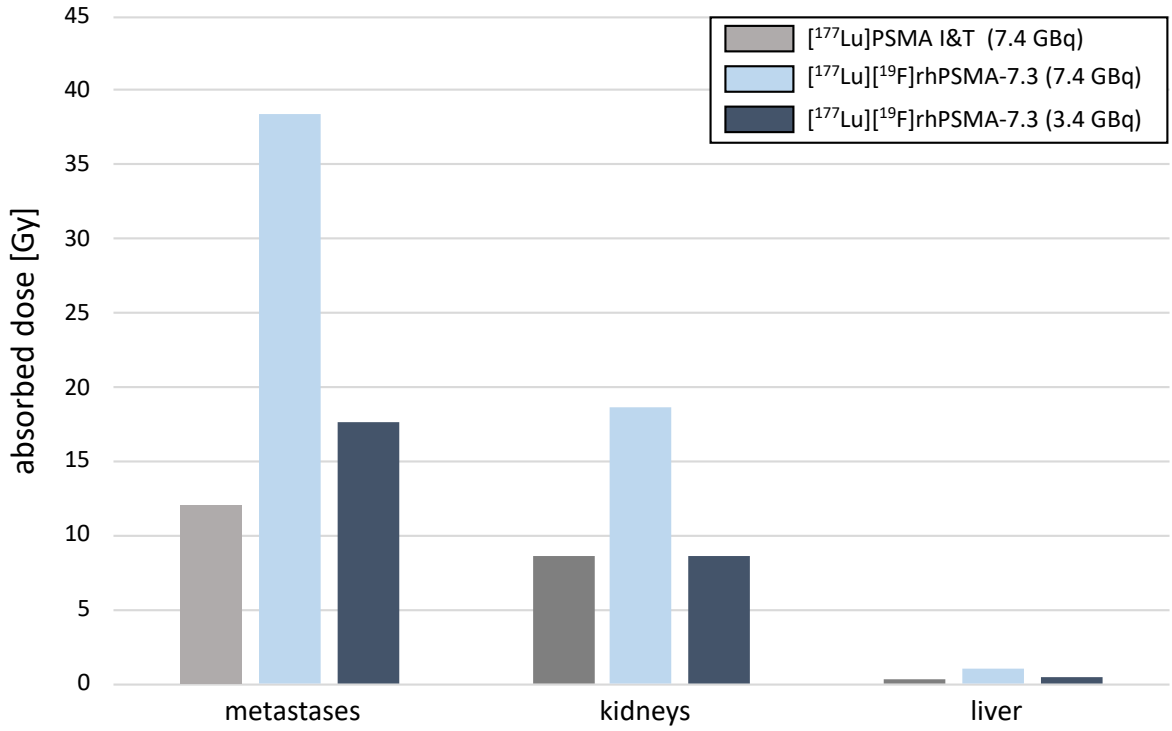

Figure 38: Absorbed dose (Gray) to metastases, kidneys and liver determined after extrapolation of the administered activity to 7.4 GBq [^{177}Lu]PSMA I&T (grey), 7.4 GBq [^{177}Lu][^{19}F]rhPSMA-7.3 (light blue) and 3.4 GBq [^{177}Lu][^{19}F]rhPSMA-7.3 (dark blue). Studies were carried out at the Department of Nuclear Medicine at the Klinikum rechts der Isar, courtesy of M. Eiber.

Interestingly, application of [^{177}Lu][^{19}F]rhPSMA-7.3 resulted in tumor-absorbed dose 3.2-fold higher than that of [^{177}Lu]PSMA I&T. Likewise, the absorbed dose to kidneys and liver was 2.2-fold and 2.6-fold higher, respectively, with [^{177}Lu][^{19}F]rhPSMA-7.3. In order to suitably adjust the overall activity of [^{177}Lu][^{19}F]rhPSMA-7.3 to be injected for RLT in this patient, the kidney uptake of both tracers was used for normalization. Consequently, when reducing the activity of [^{177}Lu][^{19}F]rhPSMA-7.3 from typically 7.4 GBq to 3.4 GBq, both tracers would lead to an identical absorbed dose to the kidneys, whereas the absorbed dose to metastases would be still 1.5-fold higher compared to [^{177}Lu]PSMA I&T. The superior pharmacokinetics of [^{177}Lu][^{19}F]rhPSMA-7.3 can most probably be attributed to its higher lipophilicity and higher HSA-binding that result in a slower clearance kinetic, and in combination with a favorable PSMA-affinity to increased uptake in tumor lesions. On the contrary, the hydrophilicity is still sufficient to ensure renal excretion.

Although the aforementioned analyses need to be confirmed, prolongation of the circulation half-life of PSMA-targeted inhibitors and therapeutic radiopharmaceuticals is considered a highly promising strategy to improve RLT. Lowering the dose per treatment cycle could lower costs per treatment cycle, shorten inpatient stays and reduce overall radiation burden for patients and staff, while still resulting in a higher absorbed dose to tumor lesions, compared to [^{177}Lu]PSMA I&T. On the other hand, so far no severe side effects and no acute radiation-induced impairment of renal function have been reported[117, 120, 215, 216], when using therapeutic doses of 7.4 GBq of the established ^{177}Lu-labeled PSMA-targeted ligands. Thus, even though further detailed examinations are required, i.e. on the effects of delayed blood clearance on bone marrow toxicity, patients could potentially benefit from higher radiation dose to metastases at activity levels that result in kidney doses higher than those currently established.

7. Radiolabeling

7.1 Radiometallation of rhPSMA ligands

^{68}Ga-labeling

For ^{68}Ga-labeling of uncomplexed rhPSMA ligands a fully automated GMP-compliant system (GallElut^{+} by Scintomics, Germany) was used[167]. The tracers were obtained applying a standardized protocol for ^{68}Ga-labeling of TRAP/DOTA(-GA) chelators, after a total synthesis time of 15 minutes in radiochemical yields (RCY) of 60 ± 7% and molar activities (A_M) of 59 ± 20 GBq/µmol. Radiochemical purities (RCP) were determined by radio-RP-HPLC and radio-TLC and were > 96% for all compounds.

^{177}Lu-labeling

The ^{177}Lu-labeled rhPSMA ligands were prepared according to a standard protocol for complexation of DOTA(-GA)-chelators[96, 168]. Radiochemical purities were determined by radio-TLC and radio-RP-HPLC and were ≥ 95% for all ligands. The tracers were obtained in A_M of 20-110 GBq/µmol.

As expected radiometallation of rhPSMA ligands with ^{68}Ga and ^{177}Lu was not negatively affected by the radiohybrid ligand design and well-known literature protocols could be applied for the labelling reactions.

7.2 Manual ^{18}F-Labeling of rhPSMA ligands

In first [^{18}F]fluorinations of SiFA-derivatives described by Schirrmacher and co-workers, aqueous [^{18}F]fluoride was dried azeotropically under reduced pressure[140]. In order to circumvent this time-consuming process, the so-called *Munich Drying Method*, developed in our group in 2012 by Wessmann *et al.*[157], was successfully applied for SiFA-bearing compounds[217]. For this purpose, aqueous $^{18}F^-$ is loaded onto a carbonate-based anion exchange cartridge and purged with air. Drying of the resin is subsequently carried out by purging the cartridge with 10 mL anhydrous MeCN. Thereafter, dried $^{18}F^-$ can be eluted using a solution of $[K^+ \subset 2.2.2]OH^-$ cryptate in dry MeCN. In order to partly neutralize the eluted alkaline solution, containing $[K^+ \subset 2.2.2]^{18}F^-$, $([K^+ \subset 2.2.2])_2CO_3^{2-}$, and excess $[K^+ \subset 2.2.2]OH^-$, a precise amount of oxalic acid is added, which was found to be mandatory for a successful IE at the SiFA moiety or SiFA-conjugated radiopharmaceuticals[217]. After IE at rt for 5 min, the mixture is diluted by the addition of a suitable buffer (e.g. HEPES or acetate) and subjected to cartridge-based purification (SPE)[156]. The described procedure was adapted and optimized for ^{18}F-labeling of rhPSMA ligands in this work (Figure 39).

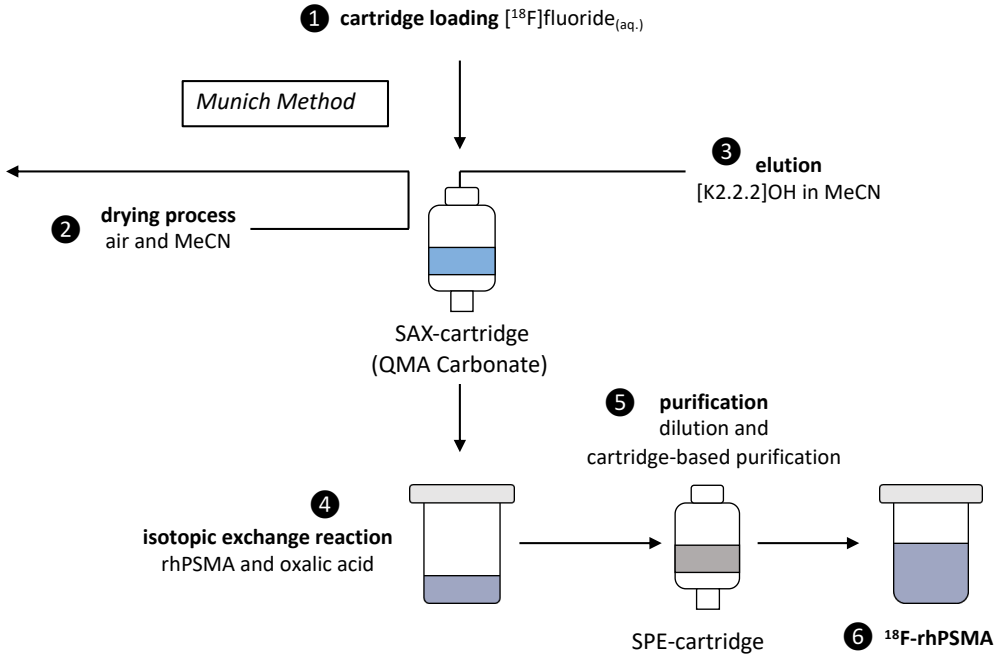

Figure 39: Schematic presentation of the ^{18}F-labeling procedure of [^{19}F]rhPSMA ligands by isotopic exchange via the *Munich Method*: Aqueous [^{18}F]fluoride is loaded on a strong anion exchange (SAX) cartridge preconditioned with carbonate (**1**) and dried with air and dry MeCN (**2**). After elution of [^{18}F]fluoride (**3**) by means of a solution of $[K^+ \subset 2.2.2]OH^-$ cryptate in dry MeCN and addition of oxalic acid, ^{18}F-for-^{19}F- IE on the [^{19}F]rhPSMA ligands is carried out for 5 min at rt (**4**). A cartridge-based purification (solid-phase extraction, SPE) yields the ^{18}F-labeled rhPSMA ligand (**5, 6**).

7.2.1 Drying of [^{18}F]fluoride

A carbonate-based anion exchange cartridge (Sep-Pak Accell Plus QMA Carbonate Plus Light) was used for fixation of [^{18}F]fluoride and following drying according to the *Munich Method*[156, 157]. Purging of the cartridge with anhydrous MeCN (10 mL, 2 mL/min) and a few mL of air allowed efficient and rapid on-column drying of [^{18}F]fluoride. Elution by means of [$K^+ \subset$ 2.2.2]OH^- (83 µmol KOH, 91 µmol Kryptofix 222) in 500 µL $MeCN_{dry}$ provided [^{18}F]fluoride in almost quantitative yield (96 ± 2%).

7.2.2 Optimization of the isotopic exchange reaction

The following optimizations were performed using [^{19}F][^{nat}Ga]rhPSMA-7/7.3 as precursor. Efficiency of the isotopic exchange reaction was measured by radio-TLC from the crude reaction mixture by determining the incorporation of [^{18}F]fluoride into the precursor. The eluate from the QMA was directly added to a mixture of the precursor (1 mM in $DMSO_{dry}$) and oxalic acid (1 M in $MeCN_{dry}$).

Optimization of the manual labeling procedure: Amount of oxalic acid

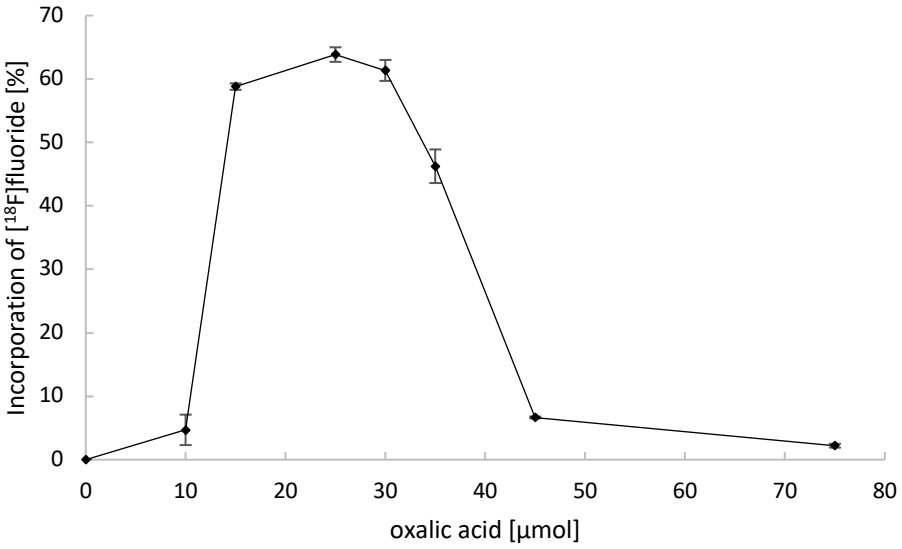

Figure 40: Incorporation of [^{18}F]fluoride into [^{19}F][^{nat}Ga]rhPSMA-7/7.3 as a function of the amount of oxalic acid (µmol). Reaction conditions: 50 nmol of [^{19}F][^{nat}Ga]rhPSMA-7/7.3, 50 MBq [^{18}F]fluoride, 5 min, rt. Incorporation of [^{18}F]fluoride (%) was determined by radio-TLC (n=2).

Investigations to determine the optimum oxalic acid concentration revealed that the addition of 17.5 to 30 µmol oxalic acid was required to reach an incorporation of [^{18}F]fluoride into 50 nmol of [^{19}F][^{nat}Ga]rhPSMA-7/7.3 of > 55% in 5 min at rt. This is approximately 21-36% of the amount of KOH, which is used as cryptate complex (83 µmol) for elution of dried [^{18}F]fluoride from the QMA cartridge. Lower and higher amounts of oxalic acid resulted in a decreased product formation (Figure 40). Similar findings were reported for ^{18}F-labeling of other SiFA ligands, employing the *Munich Method*. The optimum ^{18}F-incorporation yield in SiFA-functionalized octreotates was observed with 25 µmol of oxalic acid (using 10-25 nmol of precursor and otherwise very similar labeling conditions), corresponding to 25% of KOH, used in the cryptate complex (100 µmol)[143, 156]. It has been speculated that oxalic acid is necessary to partly neutralize the basic milieu resulting from the high hydroxide and carbonate concentration after cartridge elution which would otherwise decompose the precursor and/or the labeled product[154, 156, 217]. Moreover, the small quantities of water resulting from this neutralization could help to support the abstraction of [^{19}F]fluoride from the pentacoordinate transition state during the IE reaction. With further addition of oxalic acid, the increasing acidity significantly reduces the nucleophilicity of [^{18}F]fluoride.

Optimization of the manual labeling procedure: Amount of the precursor

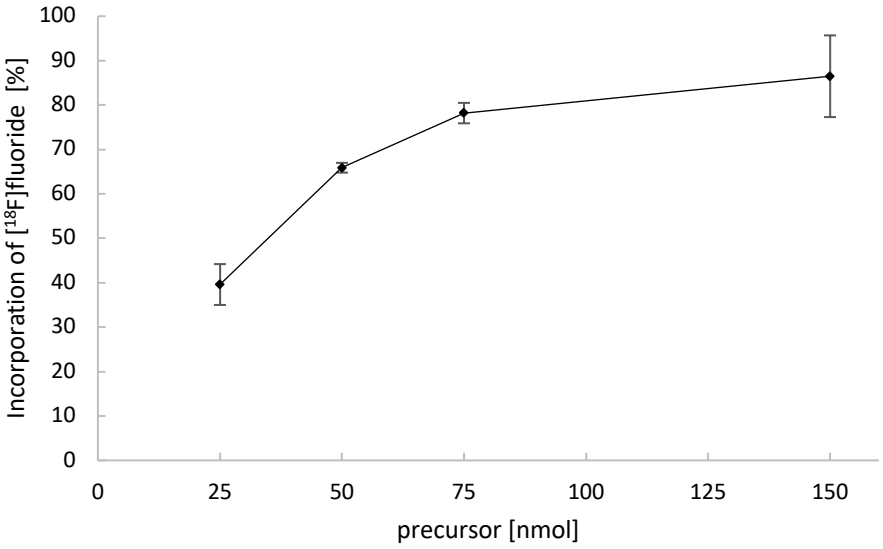

Figure 41: Incorporation of [^{18}F]fluoride into [^{19}F][^{nat}Ga]rhPSMA-7/7.3 as a function of the amount of precursor (nmol). Reaction conditions: 50 MBq [^{18}F]fluoride, 5 min, rt. Incorporation of [^{18}F]fluoride (%) was determined by radio-TLC (n=2).

In view of subsequent upscaling of the radiosynthesis to the multiple GBq range, the IE reaction was investigated at rt by using the highest value in the optimum range of oxalic acid (30 µmol) and increasing amounts of [^{19}F][^{nat}Ga]rhPSMA-7/7.3. As shown in Figure 41 incorporation of [^{18}F]fluoride continuously increased from 40 to 87% for 25 to 150 nmol of [^{19}F][^{nat}Ga]rhPSMA-7/7.3. In recent studies on the labeling of SiFA-conjugated peptides, yields of approximately 75 ± 10% (25 nmol of precursor) have been observed, which is almost 2-fold higher than that for rhPSMA ligands[143, 154-156]. Even though the ligands contain the same SiFA moiety, these observations might result from different ligand structures, especially the higher negative charge density around the organofluorosilane of rhPSMA ligands. In addition, it will be interesting to investigate the influence of trifluoroacetate versus acetate salts in precursor preparations in future studies on IE of SiFA conjugates.

Optimization of the manual labeling procedure: Reaction time

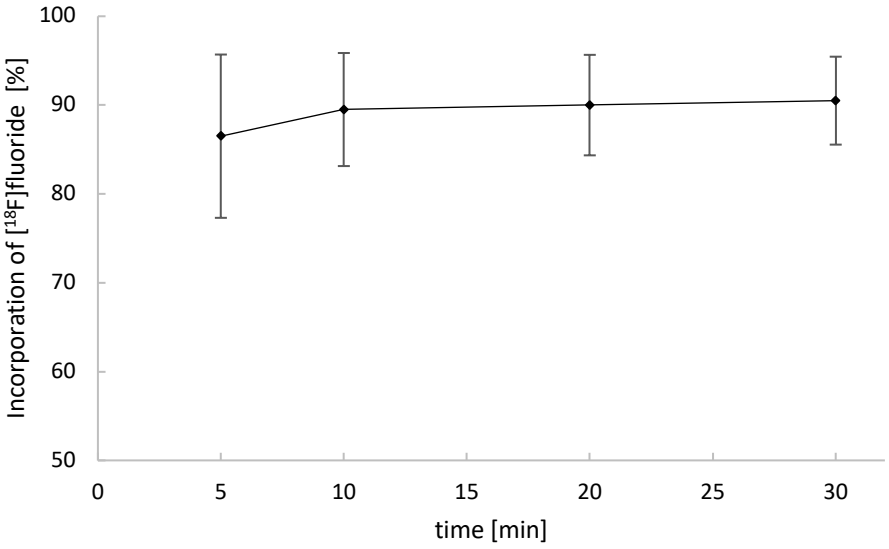

Figure 42: Incorporation of [^{18}F]fluoride into [^{19}F][^{nat}Ga]rhPSMA-7/7.3 as a function of time (min) on 150 nmol of [^{19}F][^{nat}Ga]rhPSMA-7/7.3. Reaction conditions: 50 MBq [^{18}F]fluoride, 5 min, rt. Incorporation of [^{18}F]fluoride (%) was determined by radio-TLC (n=2).

The kinetic of the isotopic exchange reaction was investigated using the optimum amounts of oxalic acid (30 µmol) and precursor (150 nmol). Maximum ^{18}F-incorporation could already be observed after 5 min, whereas prolonged reaction times did not result in significantly improved yields (Figure 42). This finding is consistent with previous reports of SiFA ligands, in which the maximum achievable ^{18}F-incorporation was already reached within 3-5 minutes[151]. Density functional theory calculations, as well as kinetic experiments revealed that the energy barrier for the isoenergetic replacement of [^{19}F]fluoride by [^{18}F]fluoride at SiFA groups is very low (E_A = 15.7 kcal/mol)[149, 151]. Moreover, the Arrhenius pre-exponential factor, which represents the frequency of collisions between reactant molecules, was determined to be extraordinary high – e.g. four orders of magnitudes larger compared to conventional nucleophilic [^{18}F]fluorination of the commonly applied labeling synthon ethyleneglycol-di-*p*-tosylate[151]. Both kinetic parameters account for the experimentally observed high rates of fluoride exchange at [^{19}F][^{nat}Ga]rhPSMA-7/7.3 after 5 min at rt.

Optimization of the manual labeling procedure: Substitution of oxalic acid by acetic acid

Due to the lower toxicity of acetate, the substitution of oxalic acid by acetic acid was also investigated (Figure 43)[218]. The experiment was carried out using 60 µmol of acetic acid with 150 nmol of [^{19}F][^{nat}Ga]rhPSMA-7/7.3 and compared to the respective value obtained for oxalic acid (30 µmol) after 5 min at rt.

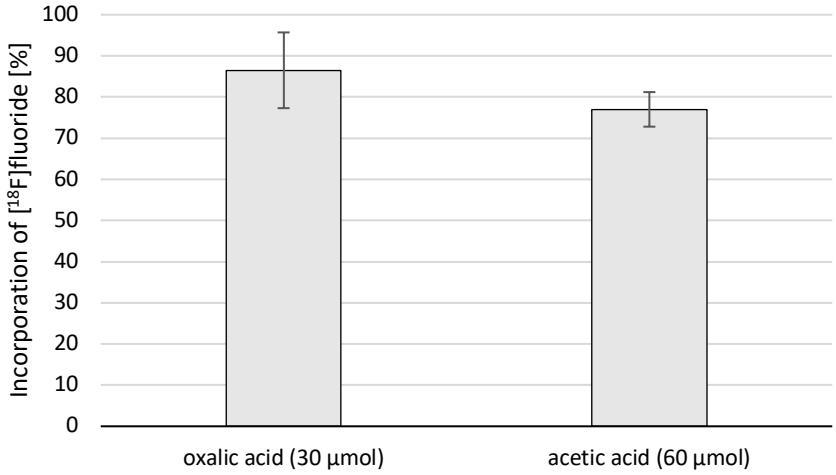

Figure 43: Incorporation of [^{18}F]fluoride into [^{19}F][^{nat}Ga]rhPSMA-7/7.3 with either oxalic acid (30 µmol) or acetic acid (60 µmol). Reaction conditions: 50 MBq [^{18}F]fluoride, 5 min, rt. Incorporation of [^{18}F]fluoride (%) was determined by radio-TLC (n=2).

Unexpectedly, substitution of 30 µmol oxalic acid by 60 µmol acetic acid resulted in a somewhat lower ^{18}F-incorporation yield (87 ± 9% versus 77 ± 4%, respectively). Nevertheless, with respect to the production of ^{18}F-labeled radiohybrids under Good Manufacturing Practice (GMP), acetate offers the advantage of being a well described ingredient in all pharmacopoeias and thus should be used in future automated productions under GMP.

7.2.3 Purification

In order to separate and purify the radiolabeled SiFA ligand from cryptate, acetonitrile or DMSO, and free ^{18}F- and ^{19}F-fluoride, a cartridge-based purification step is required. For solid-phase extraction, the organic reaction mixture has been diluted with a suitable slightly acidic aqueous buffer to prevent hydrolysis of the Si-F bond from aqueous basic conditions.

First purifications of ^{18}F-labeled rhPSMA ligands were carried out as described in literature by Wängler *et al.* for SiFA-bearing octreotates, using a HEPES buffer (pH 3) in combination with a C18 cartridge (Waters Sep-Pak C18 Plus Light, 130 mg sorbent)[156].

With respect to clinical applications, the HEPES buffer was substituted by phosphate buffered saline (PBS, pH 5) for dilution of the reaction mixture. Noteworthy, no differences in RCY and purity were observed by varying the buffer and increasing the pH to 5.

After purging the cartridge with the buffer, the ^{18}F-rhPSMA ligands were eluted in a 1:1 mixture (*v*/*v*) of ethanol and water (0.3-2.0 mL). Due to inefficient elution of the initially used C-18 cartridges (77 ± 11%), Oasis HLB cartridges (Oasis HLB Plus Light, 30 mg sorbent, 30 µm particle size) were employed, resulting in > 90% elution efficiency. Typically, the radiochemical purity of the ^{18}F-labeled rhPSMAs was > 97%, as determined by radio-HPLC and radio-TLC.

7.2.4 Summary of the optimized manual labeling results

Under optimized labeling conditions, [^{18}F]fluoride (< 10 GBq) is dried according to the *Munich Method* and eluted by means of a solution of $[K^+ \subset 2.2.2]OH^-$ cryptate (formed by 83 µmol KOH and 91 µmol Kryptofix 222) in dry MeCN (500 µL) directly onto a mixture of a rhPSMA precursor (50-150 nmol) solubilized in $DMSO_{dry}$ (1 mM) and oxalic acid (30 µL, 1 M, $MeCN_{dry}$). After 5 min at rt the reaction mixture is diluted (PBS, pH 5) and the solution passed through an Oasis HLB cartridge. After a washing step (10 mL PBS, pH 5), the ^{18}F-rhPSMA ligands are eluted in a 1:1 mixture (*v*/*v*) of ethanol and water (0.5 mL) and diluted with PBS (pH 5). On average, radiochemical yields of 58 ± 10% and molar activities of 11-60 GBq/µmol are obtained on activity levels < 10 GBq (50 nmol of precursor) in a total synthesis time of 20 min. For ^{18}F-fluorination of the lead compound [^{nat}Ga][^{19}F]rhPSMA-7/7.3 (150 nmol) on the manual scale a RCY of 74 ± 2% was achieved (n=3).

7.3 Automated ^{18}F-labeling of rhPSMA ligands

With respect to clinical evaluation, an automated production of [^{18}F][^{nat}Ga]rhPSMA-7/7.3 was developed that allows for large-scale synthesis of the described radiohybrid ligands in a GMP-compliant environment. Development and optimization of the process including suitable procedures for quality control were carried out in collaboration with the Radiopharmacy group at the Department of Nuclear Medicine at the Klinikum rechts der Isar (Technical University of Munich, Germany).

The key steps i.e. drying of [^{18}F]fluoride according to the *Munich Method*, the isotopic exchange reaction and the cartridge-based purification were transferred to an automated synthesis module, employing a double-cassette setup. Both automated valve units were equipped with a stopcock manifold with five 3-way valves and connected with fluidic transfer lines as shown in Figure 44.

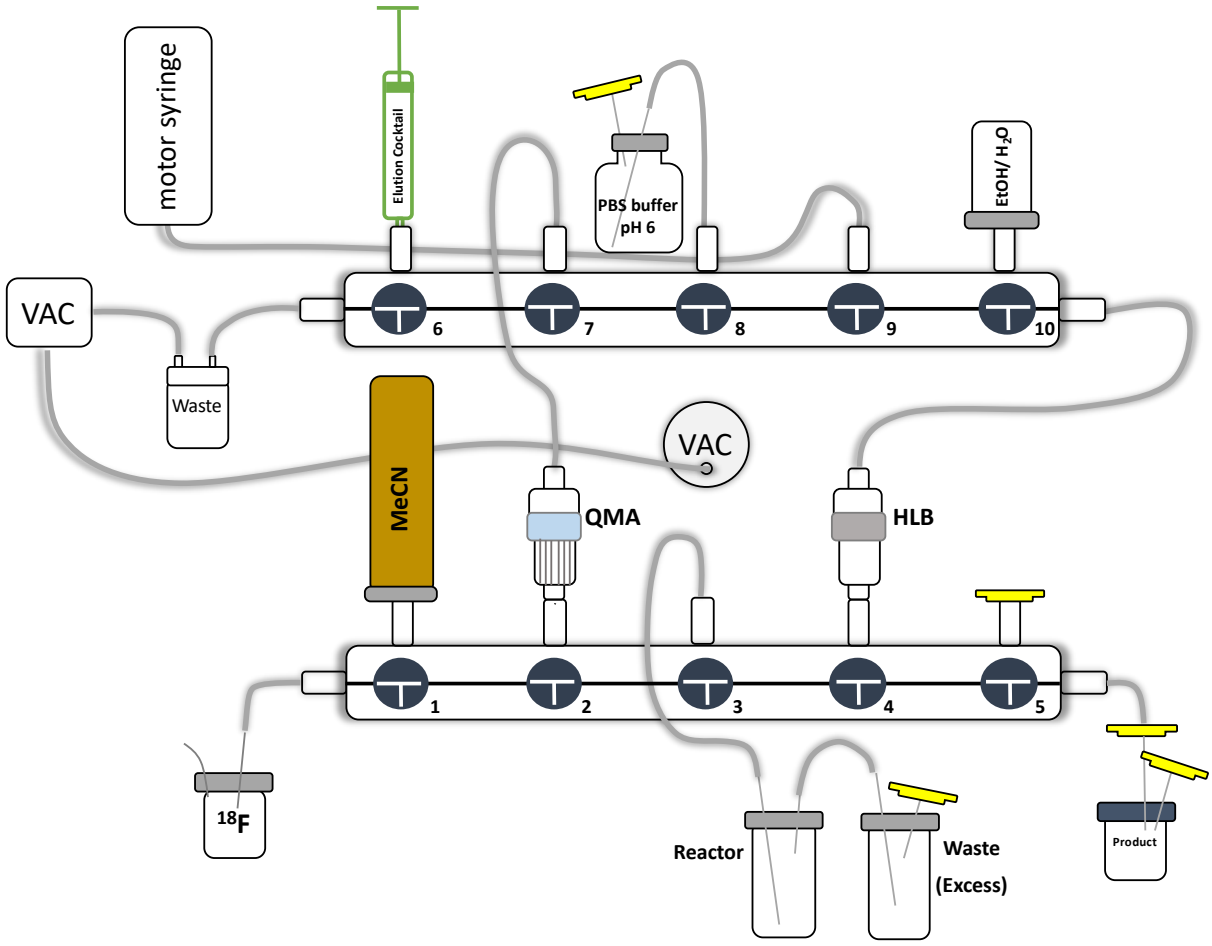

Figure 44: Setup of the automatized radiosynthesis of ^{18}F-labeled rhPSMA ligands on a "2-stop cock manifold module". VAC: pressure sensor and vacuum pump.

In a first step, aqueous [^{18}F]fluoride (up tp 100 GBq) in ^{18}O-enriched target water (2.5 mL) is drawn under vacuum on the QMA cartridge (Sep-Pak Accell Plus QMA Carbonate Plus Light cartridge, 46 mg, 40 µm, Waters), preconditioned with 10 mL water and attached to valve 2. Thereafter the QMA is flushed with air, followed by 10 mL of dry MeCN (valve 1) and air. The 2 mL syringe connected to valve 6 contains a solution of the cryptate complex [$K^+ \subset$ 2.2.2]OH^- in 750 µL of $MeCN_{dry}$ which is used for elution of dried [^{18}F]fluoride. Noteworthy, the amount of [$K^+ \subset$ 2.2.2]OH^- was increased by 1.5-fold (137.5 µmol Kryptofix 222 and 125 µmol KOH) compared to the manual synthesis (91 µmol Kryptofix 222 and 83 µmol KOH) in order to obtain a similar concentration of reagents due to loss of the elution cocktail in the syringe and the tubes during the automated production.

For the isotopic exchange reaction, the eluate is directly transferred into the reactor, attached to valve 3, which contains 150 nmol of the dissolved [^{nat}Ga][^{19}F]rhPSMA-7/7.3 precursor (150 µL, 1 mM in $DMSO_{dry}$) mixed with 30 µmol oxalic acid (30 µL, 1 M in $MeCN_{dry}$). After a reaction time of 5 min at rt, the mixture is diluted with 10 mL phosphate buffered saline (pH 6). For cartridge-based purification an Oasis HLB Plus Short (225 mg sorbent, 60 µm particle size, Waters) is used (valve 4).

After passing the diluted reaction mixture through the HLB cartridge, it is flushed with 10 mL of the PBS buffer and dried with air. The purified tracer is then eluted with 3 mL of a 1:1 mixture (*v*/*v*) of ethanol in water (valve 10), followed by 15 mL of PBS buffer and is sterile filtered into the product vial connected at position 5.

After installation of the automated production at the hospitals of the Technical University of Munich (TUM) in October 2017 and thereafter at the Ludwig Maximilian University of Munich (LMU) in February 2018, 390 productions have been made until April 2019. Overall, 95.9% of productions succeeded with a mean RCY of 49.6 ± 7.8% (TUM) and 54.1 ± 14.9% (LMU). [^{18}F][^{nat}Ga]rhPSMA-7/7.3 was obtained in molar activities of 300 GBq/µmol (TUM) and 100 GBq/µmol (LMU). The overall production was completed in 15.75 min. Regardless of the significantly different average starting activities (89.5 ± 17.7 GBq at TUM and 29.8 ± 9.7 GBq at LMU), [^{18}F][^{nat}Ga]rhPSMA-7/7.3 was obtained in a high radiochemical purity of > 99% (radio-RP-HPLC: 99.9 ± 0.4% at TUM and 99.7 ± 1.2% at LMU, radio-TLC: 97.8 ± 1.2% at TUM). In all cases the concentrations of residual solvents, Kryptofix and endotoxins were in accordance with the specifications.

7.4 Isotopic exchange reactions in aqueous solutions

The occurrence of ^{18}F-fluoride in urine of mice can be explained, as described above (see chapter 3.4.6), by a not insignificant concentration of [^{19}F]fluoride in the kidneys and urine of mice that result by ^{19}F-for-^{18}F isotopic exchange on intact ^{18}F-labeld radiohybrid PSMA ligands, such as [^{18}F][^{nat}Ga]PSMA-7.3. To further support the hypothesis that the IE can proceed in aqueous solutions, cold [^{19}F]fluoride (500 nmol, sodium fluoride) was added to fresh and nonradioactive urine of mice, followed by the addition of [^{18}F][^{nat}Ga]rhPSMA-7.3. The sample was incubated for 2 h at rt. Radio-RP-HPLC analysis revealed that under these conditions 99% of the silicon-bound [^{18}F]fluoride was exchanged by [^{19}F]fluoride (Figure 45).

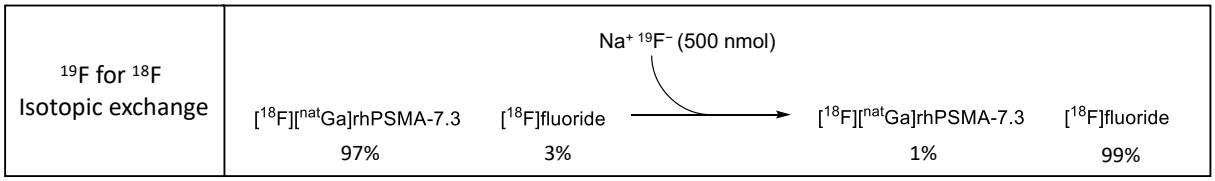

Figure 45: Experiment in a murine urine sample: Defluorination of [^{18}F][^{nat}Ga]PSMA-7.3 after the addition of 500 nmol of sodium fluoride ([^{19}F]fluoride) and incubation for 2 h at rt. The amount of the different species (%) was determined by radio-RP-HPLC analysis.

This experiment demonstrates that, despite reduced reactivity of solvated [^{19}F]fluoride anion in aqueous solutions, isotopic exchange at SiFA moieties occurs even in aqueous medium at ambient temperature. In order to potentially exploit the reverse exchange reaction for the production of [^{18}F][^{nat}Ga]rhPSMA, without prior drying, in aqueous solutions such as irradiated target water, a systematic evaluation of relevant reaction parameters was performed.

7.4.1 Selection of a buffer

Isotopic exchange reactions on [^{19}F]rhPSMA ligands in aqueous solutions (IE_{aq}) were carried out at elevated temperatures (95 °C) for up to 20 min. Since the SiFA-labeling chemistry was found to be strongly pH-dependent, the first aim was to select a suitable buffer and to identify the most favorable pH-value for the IE_{aq}. Therefore, 450 µL of an aqueous [^{18}F]fluoride solution (20-70 MBq) were added to 50 nmol of [^{nat}Ga][^{19}F]rhPSMA-7 (50 µL, 1 mM in DMSO) under variation of buffer, buffer concentration and pH. ^{18}F-incorporation was determined by radio-TLC (Figure 46).

A reaction conditions

total volume [µL]	500
aqueous volume [µL]	450
[^{19}F][^{nat}Ga]rhPSMA-7 [nmol]	50
DMSO [µL]	50
buffer	**B**
pH	**C**
amount of buffer [µmol]	**D**
temperature [°C]	95
reaction time [min]	20

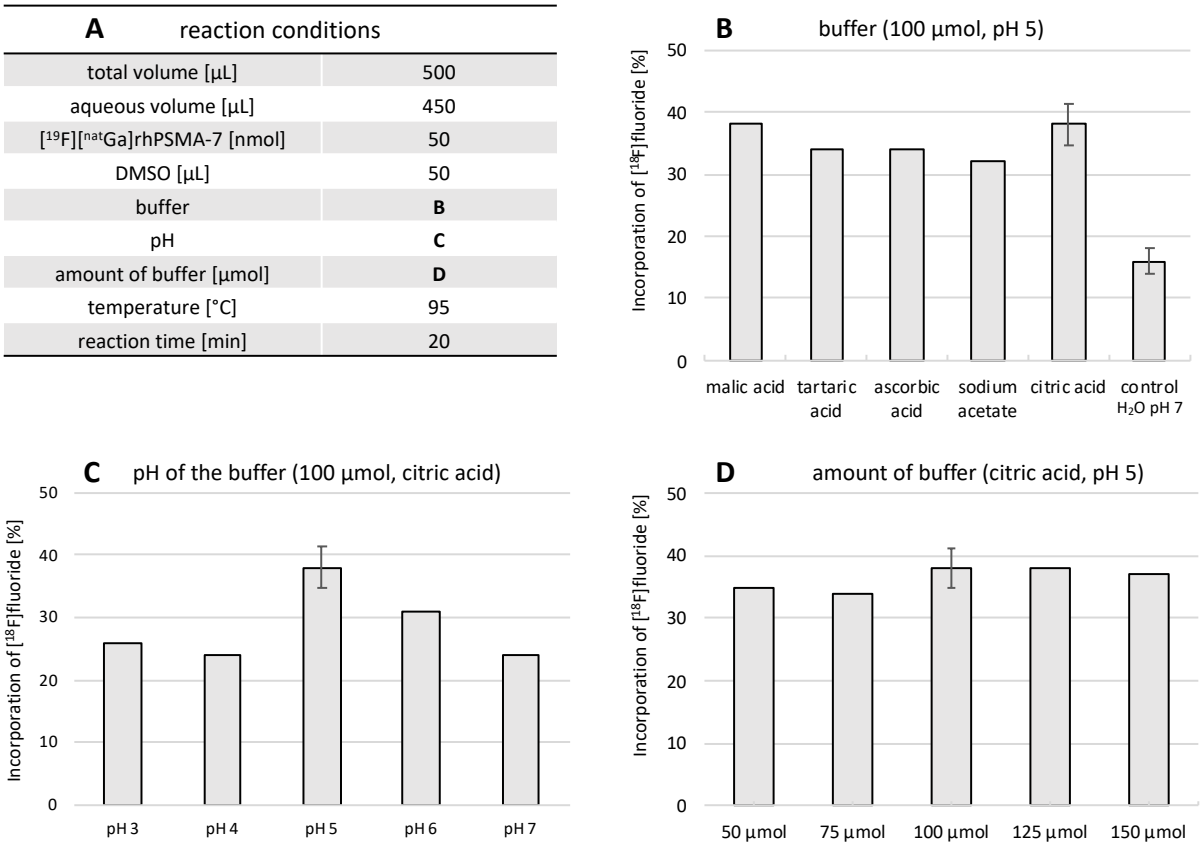

Figure 46: Reaction conditions for ^{18}F-labeling of [^{nat}Ga][^{19}F]rhPSMA-7 (50 nmol) by isotopic exchange in aqueous solutions (**A**) using various buffer salts (100 µmol, pH 5) (**B**), at various pH-values (100 µmol citric acid) (**C**) and increasing buffer concentrations (citric acid, 50-150 µmol) (**D**). Incorporation of [^{18}F]fluoride (%) was determined by radio-TLC after heating the test solutions for 20 min at 95 °C (n=1, n=3 if error bars are shown).

All five tested buffers, namely malic acid, tartaric acid, ascorbic acid, acetic acid and citric acid resulted in radiochemical yields between 32 and 38% at pH 5, whereas the control experiment (H_2O, pH 7) showed a more than 2-fold lower value of 16% (Figure 46 A). Especially ascorbic acid buffer provides the advantage to act as a radiolytic stabilizer, which could potentially improve stability of the precursor and product during the labeling reactions on the multi-GBq scale[219]. Due to the fact that ascorbic acid and all other buffers are separated from the product during the final cartridge purification step and so far no radiolytic instability, even for preparations of up to 40-60 GBq product has been observed, citrate buffer was selected for further optimization studies. As expected, the pH-value had a major effect on the isotopic exchange reaction in aqueous citrate solution (Figure 46 B). Optimum yields were reached at pH 5 with an ^{18}F-incorporation of 38%. Increasing the pH resulted in lower yields which might be explained by the increasing hydrolysis rate of the Si-F bond, especially at high temperatures[151], while decreased yields at lower pH-values could most probably be a result of reduced nucleophilicity of [^{18}F]fluoride (hydrofluoric acid pKa = 3.18)[220, 221]. Variation of the buffer concentration of citric acid (50-150 µmol at pH 5) did not significantly affect the labeling reaction (Figure 46 C).

Until now, only few aqueous ^{18}F-labeling reactions of SiFA moieties have been described. Glaser *et al.* successfully demonstrated aqueous labeling of a SiFA-bearing affibody with a RCY of 38% (95 °C, 15 min, 0.5 M NaOAc pH 4)[159]. Moreover, Schirrmacher and co-workers heated an aqueous solution of [^{18}F]fluoride and a first-generation SiFA-octreotate derivative to 95 °C for 15 min and observed an ^{18}F-incorporation of 70-90%[140]. Since both groups performed the labeling reactions in small aqueous volumes (200-300 µL) the effect of the precursor concentration was further analyzed in following labeling experiments of rhPSMA ligands.

7.4.2 Influence of reaction time and volume effects

In analogy to the aforedescribed experiments, an aqueous solution of [^{18}F]fluoride (citric acid, 100 µmol, pH 5) was incubated with different concentrations of [^{nat}Ga][^{19}F]rhPSMA-7 and heated to 95 °C (Figure 47 A).

A reaction conditions

total volume [µL]	**D**
aqueous volume	90%
[^{19}F][^{nat}Ga]rhPSMA-7 [nmol or µM]	**C**
DMSO	10%
buffer	citric acid
pH	5
amount of buffer [µmol]	100
temperature [°C]	95
reaction time [min]	**B**

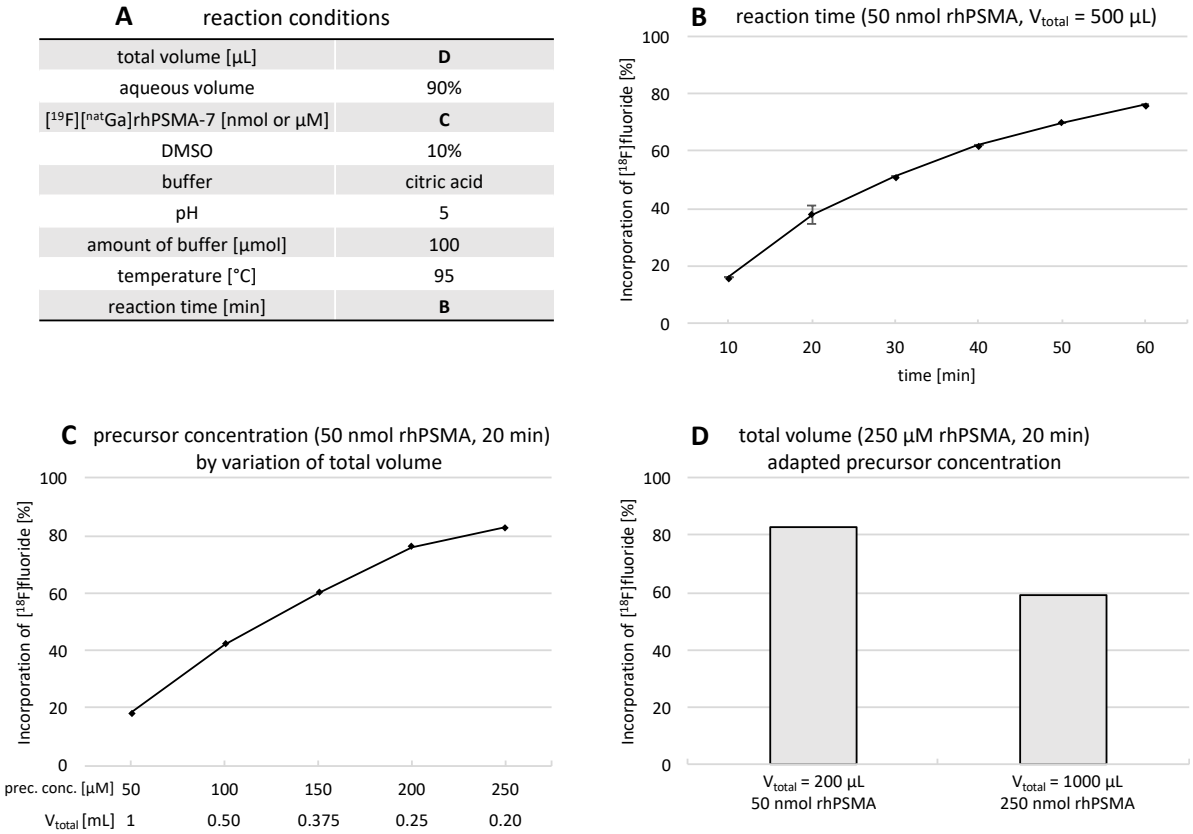

Figure 47: Reaction conditions (**A**) for ^{18}F-labeling of [^{nat}Ga][^{19}F]rhPSMA-7 by isotopic exchange in aqueous solutions at 95 °C in citric acid buffer (pH 5, 100 µmol), at different reaction times (50 nmol [^{nat}Ga][^{19}F]rhPSMA-7, V_{total} = 500 µL) (**B**), with different precursor concentrations by variation of the total aqueous volume (50 nmol [^{nat}Ga][^{19}F]rhPSMA-7, 20 min) (**C**) and a different total volume by adaption of the precursor concentration (250 µM rhPSMA, 20 min) (**D**). Incorporation of [^{18}F]fluoride (%) was determined by radio-TLC (n=1, n=3 if error bars are shown).

Between 10 and 60 min, ^{18}F-labeling yields increased from 16 to 76% for 50 nmol of [^{19}F][^{nat}Ga]rhPSMA-7 (Figure 47 B). To evaluate the influence of different precursor concentrations on IE_{aq} after 20 min at 95 °C, the total reaction volume was varied (1 to 0.20 mL) for 50 nmol of [^{19}F][^{nat}Ga]rhPSMA-7, resulting in precursor concentrations of 100 to 250 µM. As expected, the increasing precursor concentration shifted the equilibrium of the isotopic exchange reaction to the ^{18}F-labeled compound, resulting in ^{18}F-incorporation of up to 83% for 250 µM [^{19}F][^{nat}Ga]rhPSMA-7 (Figure 47 C).

Since the isotopic exchange rate is dependent from the concentration of both starting materials, i.e. the precursor and [^{18}F]fluoride, it was further investigated how a different reaction volume with unchanged precursor concentration affects labeling yields. For this purpose, a labeling reaction of 250 µM [^{19}F][^{nat}Ga]rhPSMA-7 (50 nmol) in a total volume of 200 µL was compared to 250 µM [^{19}F][^{nat}Ga]rhPSMA-7 (250 nmol) in 1000 µL with otherwise identical reaction conditions (95 °C, 20 min, citrate buffer pH 5, 20 MBq). The 5-fold larger reaction volume resulted in a 1.4-fold lower labeling yield and clearly demonstrates the influence of the decreased ^{18}F-fluoride concentration on the equilibrium of the isotopic exchange reaction (Figure 47 D). On the other side, this also means that higher starting activities and thus a higher concentration of ^{18}F-fluoride might result in improved labeling yields. Therefore, further experiments with starting activities in the multiple GBq range are highly desirable.

To ensure sufficient solubility of the precursor, all IE_{aq} investigated above were carried out in the presence of 10% DMSO. With the intention to omit DMSO and to further simplify the IE_{aq}, further optimizations were investigated (Figure 48). For this purpose, an aqueous solution of [^{18}F]fluoride (20-30 MBq) was mixed with 100 µL of citrate buffer (1 M, 100 µmol, pH 5) and diluted to a final volume of 450 µL. Thereafter the mixture was added to 50 nmol [^{19}F][^{nat}Ga]rhPSMA-7 and heated to 95 °C for 20 min.

Unexpectedly, incorporation of [^{18}F]fluoride was found to be even somewhat higher (45%) than the incorporation observed in the control experiment using 450 µL aqueous buffer (100 µmol, pH 5) plus 50 µl DMSO (38%). Using 500 µl citrate buffer and otherwise identical reactions conditions in the absence of DMSO, 39% ^{18}F-incorporation was observed.

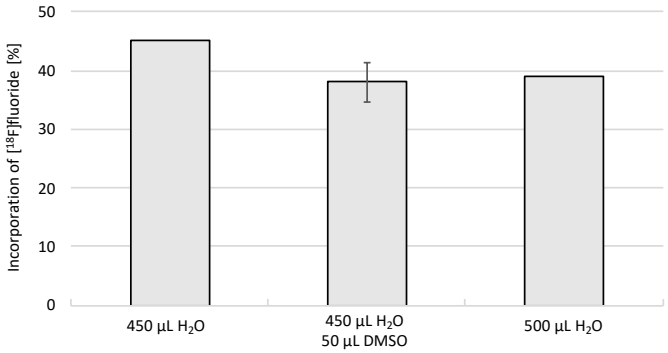

reaction conditions	
total volume [µL]	450 or 500
aqueous volume	90 or 100%
[^{19}F][^{nat}Ga]rhPSMA-7 [nmol]	50
DMSO	0 or 10%
buffer	citric acid
amount of buffer [µmol]	100
pH	5
temperature [°C]	95
reaction time [min]	20

Figure 48: ^{18}F-Labeling by isotopic exchange using 50 nmol of [^{19}F][^{nat}Ga]rhPSMA-7 in 450 µL (left column) and 500 µL (right column) citrate buffered solutions and a mixture of 450 µL citrate buffer and 50 µL DMSO (center column). Reaction conditions: 95 °C, 20 min, pH 5, 100 µmol citrate; n=1, n=3 if error bars are shown). Incorporation of [^{18}F]fluoride (%) as determined by radio-TLC.

These experiments demonstrate, that ^{18}F-for-^{19}F isotopic exchange in aqueous solution is feasible, even without DMSO, and could be a very promising new strategy towards a simplified strategy for large scale production of [^{18}F]rhPSMA inhibitors. In this context, potential obstacles arising from solubility problems of the corresponding precursors in aqueous media after dilution prior to cartridge purification can be overcome by using washing and formulation buffers with up to 7% (*v*/*v*) ethanol.

7.4.3 Comparison of isotopic exchange in aqueous and non-aqueous medium

Subsequently, the possibility to translate the results of the isotopic exchange reaction under aqueous conditions to a fast and simple process that directly uses cyclotron produced aqueous [^{18}F]fluoride solutions without further pre-processing was investigated. The bombardment of ^{18}O-enriched water (^{18}O(p,n)^{18}F) yields [^{18}F]fluoride in aqueous volumes typically ranging from 0.5 and 2.5 mL, dependent on the cyclotron and the target[222-226]. For comparison with the established anhydrous labeling method of [^{nat}Ga][^{19}F]rhPSMA-7 (150 nmol, 5 min, rt) *via* the *Munich Method*, the aqueous fluorination experiment was carried out exemplary in total volumes of 0.5 and 1.0 mL with 150 nmol of precursor (Figure 49).

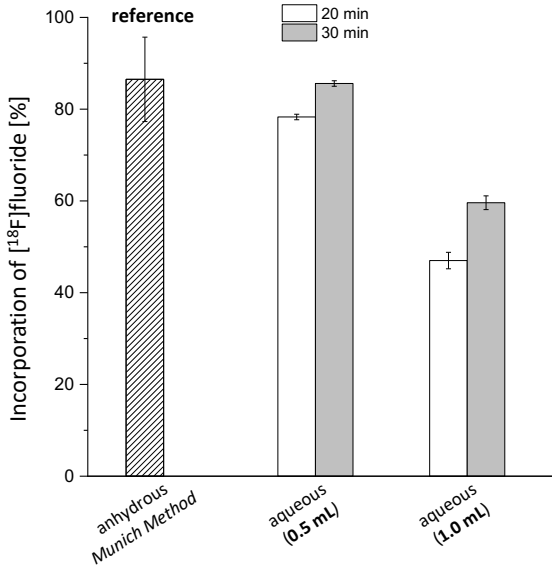

reaction conditions IE_{aq}	
aqueous volume [mL]	0.5 and 1.0
[^{19}F][^{nat}Ga]rhPSMA-7 [nmol]	150
buffer	citric acid
buffer concentration [mM]	200
pH	5
temperature [°C]	95
reaction time [min]	20 and 30

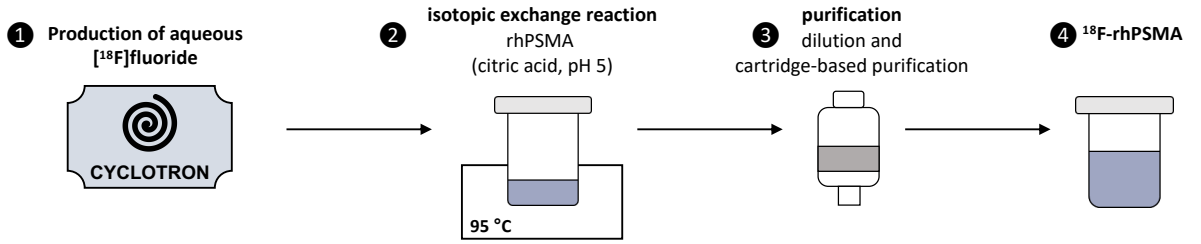

Figure 49: Comparison of the established anhydrous labeling procedure (150 nmol [^{nat}Ga][^{19}F]rhPSMA-7, 5 min, rt) to the aqueous labeling process for a total aqueous volume of 0.5 and 1.0 mL after heating for 20 min (white bars) and 30 min (grey bars) at 95 °C. Incorporation of [^{18}F]fluoride (%) was determined by radio-TLC (n=2). The exact reaction conditions are depicted in the table. Schematic representation of the labeling process: production of aqueous [^{18}F]fluoride (**1**), isotopic exchange reaction (**2**) and cartridge-based purification (**3**), yielding the [^{18}F]rhPSMA ligand (**4**).

Using an overall reaction volume of 0.5 mL, [^{18}F][^{nat}Ga]rhPSMA-7 was obtained in 86 ± 1% (30 min, 95 °C), which is similar as determined applying the established anhydrous labeling protocol (87 ± 9%). Dilution to 1.0 mL resulted in a significantly reduced yield of only 60 ± 2% (30 min, 95 °C). A shorter reaction time of 20 min further lowered the product formation. Radio-HPLC analysis of the aqueous labeling products (30 min, 95 °C) after cartridge-based purification revealed a radiochemical purity of > 97%.

In summary, the promising data above allow to envision the production of [^{18}F]rhPSMA radiopharmaceuticals by direct addition of target water to a lyophilized precursor/buffer mixture. Noteworthy, it needs to be further evaluated to which extent commonly obtained radionuclide impurities, released by the target, the target window or other co-irradiated technical components during the ^{18}O(p,n)^{18}F nuclear reaction, such as e.g. ^{52}Mn, ^{54}Mn, ^{55}Co, ^{56}Co, ^{57}Co, ^{58}Co, ^{57}Ni, ^{181}Re (in sum up to 10^3 Bq/mL), are actually present in an irradiated target water and whether these radioisotopes can be effectively separated from the product during the SPE-purification step[227, 228].

It is also important to mention that all experiments described above have been carried out with ^{18}F-activity on the laboratory scale using small fraction of the entire irradiated [^{18}O]H_2O target volume. Consequently, and due to the significant different molar activities (A_M) of [^{18}F]fluoride that are obtained with different cyclotrons, target material, different target loading and cleaning process, etc., the above described labeling results cannot be easily transferred or upscaled. Differences in the A_M of [^{18}F]fluoride of at least two orders of magnitude have been described in the literature[229]. Although such differences in the A_M can also affect the radiochemical yields of ^{18}F-labeled radiopharmaceuticals prepared by nucleophilic substitution, it is self-explanatory that an ^{18}F-for-^{19}F-isotopic exchange reaction is incomparably more sensitive towards changes of the A_M and ^{19}F-contaminations in irradiated or pre-processed target water.

In summary, the aqueous labeling process allows for the [^{18}F]fluorination of SiFA-bearing peptides in a simple and minimalistic manner. Despite the required heating step, the overall process time is only marginally longer (max. 5 min) when compared to the established anhydrous labeling method, and can be completed in approx. 20-30 min. In the case of small aqueous volumes (≤ 0.5 mL), high isotopic exchange rates are expected, which can be further optimized by adaption of the precursor amount. Regarding clinical productions, pure aqueous conditions significantly simplify quality control that otherwise needs additional gas chromatographic quantification of residual organic solvents (such as DMSO and MeCN).

IV. Summary and Conclusion

In this work a new class of PSMA-targeted radiopharmaceuticals, named radiohybrid ligands (rhPSMA), were developed, preclinically evaluated and finally assessed in first proof-of-concept studies in men. Such radiohybrid ligands feature a Silicon Fluoride Acceptor (SiFA) moiety and a chelator and therefore can be labeled in an independent manner. Depending on the radioisotope, the resulting series of radiopharmaceuticals ([^{18}F][free]rhPSMA-n, [^{18}F][M]rhPSMA-n (M=metal) and [^{19}F][R]rhPSMA-n (R=radiometal)) can be used for PET-imaging (e.g. ^{18}F, ^{44}Sc, ^{68}Ga), for SPECT-imaging (e.g. ^{111}In), and for radioligand therapy with either β^--emitters (e.g. ^{47}Sc, ^{90}Y, ^{177}Lu) or α-emitters (e.g. ^{212}Pb, $^{213/212}$Bi, ^{227}Th, ^{225}Ac). Accordingly, the concept represents a true theranostic bridge between ^{18}F- and radiometal-labeled tracers.

As representatives of diagnostic radiohybrids (e.g. [^{18}F][free]rhPSMA, [^{18}F][^{nat}Ga]rhPSMA and [^{19}F][^{68}Ga]rhPSMA), especially the third-generation EuE-based ligands rhPSMA-7 to -10 proofed to be powerful new inhibitors with equal or even better characteristics than established PSMA-addressing ligands [^{18}F]DCFPyL and [^{18}F]PSMA-1007. Noteworthy, the high lipophilicity of the SiFA moiety, which has been regarded as a key limitation of the SiFA technology in current literature, could be effectively outbalanced by the use of free chelators or metal-chelates in all rhPSMA inhibitors.

Detailed analysis of the binding affinities, internalization rates and biodistribution in mice of four different stereoisomers of rhPSMA-7, differing in the stereoconfiguration of the DOTA-GA chelator and the trifunctional amino acid linker diaminopropionic acid revealed optimum performance for the *D*-Dap – *S*-DOTA-GA isomer [F][Ga]rhPSMA-7.3.

Both [^{18}F][^{nat}Ga]rhPSMA-7 and -7.3 were selected for first proof-of-concept studies in PCa patients and demonstrated favorable biodistribution with high uptake in tumor lesions and low background accumulation even at early imaging time points. Moreover, occurrence of activity in the ureters and bladder at the time point of PET imaging (60-90 min p.i.) was low or even negligible, allowing for accurate visualization of adjacent lesions. In this first-ever human application of SiFA-bearing ligands, no elevated bone activity accumulation was found, indicating a sufficient stability of the Si-^{18}F towards *in vivo* hydrolysis and no release of [^{18}F]fluoride by isotopic exchange. In accordance with the preclinical results,

[^{18}F][^{nat}Ga]rhPSMA-7.3 showed an approximately 1.5-fold higher tumor uptake and 5-fold lower retention in the bladder, compared to racemic [^{18}F][^{nat}Ga]rhPSMA-7. [^{18}F][^{nat}Ga]rhPSMA-7.3 is currently used for clinical PET imaging of patients suffering from prostate cancer at two sites in Munich and is under clinical development by Blue Earth Diagnostics (Oxford, United Kingdom).

For the automated production of ^{18}F-labeled rhPSMA tracers, the manual radiosynthesis of [^{18}F][^{nat}Ga]rhPSMA-7/7.3 was optimized on the laboratory scale (< 10 GBq) and thereafter translated into a fully automatized GMP-compliant process. In almost 400 GMP productions with starting activities up to 100 GBq the automated production provided [^{18}F][^{nat}Ga]rhPSMA-7 and -7.3 in high RCYs of 50 ± 10% and molar activities of 100-300 GBq/µmol within an overall synthesis time of < 16 min.

It was also successfully investigated whether the ^{18}F-for-^{19}F-isotopic exchange can also be used for labeling of rhPSMAs in aqueous solutions by using [^{18}F]fluoride in ^{18}O-enriched target without pre-processing. When small reaction volumes (≤ 0.5 mL) were used, ^{18}F-labeling under aqueous conditions resulted in yields similar to those achieved under anhydrous conditions in MeCN ([^{18}F][^{nat}Ga]rhPSMA-7: 87% under anhydrous and 86% under aqueous conditions). Although more detailed studies are necessary to validate these results, this initial study confirms that the direct use of irradiated target water for the isotopic exchange reaction is feasible.

In another part of this work, ^{177}Lu-labeled rhPSMAs ([^{19}F][^{177}Lu]rhPSMA) were developed and preclinically evaluated. Compared to the radiopharmaceuticals [^{177}Lu]PSMA I&T and [^{177}Lu]PSMA-617, that represent the current state-of-the-art in radioligand therapy of prostate cancer, [^{177}Lu][^{19}F]rhPSMA-7, -7.3 and -10 demonstrated similar or even superior binding affinities and internalization rates in LNCaP cells, and promising *in vivo* characteristics in mice bearing LNCaP tumors. Compared to [^{177}Lu]PSMA I&T, a first proof-of-concept study with [^{177}Lu][^{19}F]rhPSMA-7.3 in a PCa patient revealed an improved tumor-to-kidney ratio.

Due to these promising results, further studies have been initiated to expand this concept to other established peptide and peptide-like compounds, such as SSTR agonists, GRPR-targeted tracers, CCK-2 antagonists, FAP inhibitors and others.

V. Supplemental Information

1. Figure and table index

2. Abbreviations

% ID	percentage of the injected dose
2-CTC	2-Chlorotrityl chloride
2-PMPA	2-(phosphonomethyl)pentanedioic acid
A	Arrhenius pre-exponential factor
AcOH	acetic acid
ahx	aminohexanoic acid
All	Allyl
A_M	molar activity
AP-2	adaptor protein-2
aq	aqueous
Boc	*tert*-butyloxycarbonyl
BA	benzoic acid
BSA	bovine serum albumin
Bzl	benzyl
CCK2	cholecystokinin 2 receptor
CDI	1,1'-carbonyldiimidazole
CT	computed tomography
Dap	2,3-Diaminopropionic acid
DCE	1,2-dichlorethane
DCM	dichlormethane
Dde	*N*-1-(4,4-dimethyl-2,6-dioxocyclohexylidene)ethyl
DFT	density functional theory
DIPEA	*N,N*-Diisopropylethylamine
DMAP	4-(dimethylamino)pyridine
DMF	dimethylformamide
DMSO	dimethyl sulfoxide
DOTA	1,4,7,10-tetraazacyclododecane-1,4,7,10-tetraacetic acid
DOTA-GA	1,4,7,10-tetraazacyclododecane,1-(glutaric acid)-4,7,10-triacetic acid
E_A	activation energy

EDTA	ethylenediaminetetraacetic acid
EMA	European Medicines Agency
eq	equivalent
EtOAc	ethyl acetate
EtOH	ethanol
FAP	fibroblast activation protein
FBS	fetal bovine serum
FDA	U.S. Food and Drug Administration
FDG	fluorodesoxyglucose
Fmoc	9-fluorenylmethyloxycarbonyl
GMP	good manufacturing practice
GP	general procedure
GRP	gastrin-releasing peptide
HATU	1-[Bis(dimethylamino)methylene]-1*H*-1,2,3-triazolo[4,5-b]pyridinium 3-oxid hexafluorophosphate
HBED-CC	*N,N*'-bis[2-hydroxy-5-(carboxyethyl)benzyl] ethylenediamine-*N,N*'-diacetic acid
HBSS	Hank's buffered salt solution
HEPES	2-(4-(2-hydroxyethyl)-1-piperazinyl)-ethanesulfonic acid
HOAt	1-Hydroxy-7-azabenzotriazole
HOBT	*N*-Hydroxybenzotriazole
HPLC	high-performance liquid chromatography
HSA	human serum albumin
IC_{50}	half maximal inhibitory concentration
IE	isotopic exchange
IE_{aq}	isotopic exchange in aqueous solutions
K'	capacity factor
Kryptofix	4,7,13,16,21,24-Hexaoxa-1,10-diazabicyclo[8.8.8]hexacosane
log $P_{O/PBS}$	partition coefficient in octanol and phosphate buffered saline
mCRPC	metastatic castration resistant prostate cancer
MeCN	acetonitrile

MeOH	methanol
MIP	maximum intensity projection
MRI	magnetic resonance imaging
NAAG	*N*-acetyl-aspartyl glutamate
NAALADase	*N*-acetylated-α-linked acidic dipeptidase
NMP	*N*-methyl-2-pyrrolidone
NMR	nuclear magnetic resonance
NOTA	1,4,7-triazacyclononane-triacetic acid
p.i.	post injection
PBS	phosphate-buffered saline
PCa	prostate cancer
PET	positron-emission tomography
PSA	prostate-specific antigen
PSMA	prostate-specific membrane antigen
RCP	radiochemical purity
RCY	radiochemical yield
rh	radiohybrid
RLT	radioligand therapy
ROI	region of interest
RP	reversed phase
rt	room temperature
sat	saturated
SAX	strong anion exchange
SD	standard deviation
SiFA	silicon fluoride acceptor
SiFA-A	4-(di-*tert*-butylfluorosilyl)benzaldehyde
SiFA-BA	4-(Di-tert-butylfluorosilyl)benzoic acid
SiFANBr	*N*-(4-(di-*tert*-butylfluorosilyl)benzyl)-2-hydroxy-*N*,*N*-dimethylethylammonium bromide
SPE	solid-phase extraction
SPECT	single-photon emission computed tomography

SPPS	solid-phase peptide synthesis
SSTR	somatostatin receptor
SUV	standardized uptake value
TBDMS	*tert*-butyldimethylsilyl
TBTU	*N,N,N',N'*-Tetramethyl-O-(benzotriazol-1-yl)uronium tetrafluoroborate
***t*Bu**	*tert*-Butyl
TEA	triethylamine
TFA	trifluoroacetic acid
THF	tetrahydrofuran
TIPS	triisopropylsilane
TLC	thin-layer chromatography
TRAP	1,4,7-triazacyclononane-triphosphinic acid
VOI	volume of interest

3. References

1. International Agency for Research on Cancer, Globocan 2018. https://gco.iarc.fr/.
2. Robert Koch Institut, Zentrum für Krebsregisterdaten. https://www.krebsdaten.de/Krebs/DE/Content/Krebsarten/Prostatakrebs/prostatakrebs_node.html.
3. Miller, K. D.; Siegel, R. L.; Lin, C. C.; Mariotto, A. B.; Kramer, J. L.; Rowland, J. H.; Stein, K. D.; Alteri, R.; Jemal, A., Cancer treatment and survivorship statistics, 2016. *CA Cancer J Clin* **2016,** *66* (4), 271-289.
4. Mottet, N.; Bellmunt, J.; Bolla, M.; Briers, E.; Cumberbatch, M. G.; De Santis, M.; Fossati, N.; Gross, T.; Henry, A. M.; Joniau, S.; Lam, T. B.; Mason, M. D.; Matveev, V. B.; Moldovan, P. C.; van den Bergh, R. C. N.; Van den Broeck, T.; van der Poel, H. G.; van der Kwast, T. H.; Rouviere, O.; Schoots, I. G.; Wiegel, T.; Cornford, P., EAU-ESTRO-SIOG Guidelines on Prostate Cancer. Part 1: Screening, Diagnosis, and Local Treatment with Curative Intent. *Eur Urol* **2017,** *71* (4), 618-629.
5. Fenton, J. J.; Weyrich, M. S.; Durbin, S.; Liu, Y.; Bang, H.; Melnikow, J., Prostate-specific antigen–based screening for prostate cancer: evidence report and systematic review for the US Preventive Services Task Force. *JAMA* **2018,** *319* (18), 1914-1931.
6. De Angelis, G.; Rittenhouse, H. G.; Mikolajczyk, S. D.; Blair Shamel, L.; Semjonow, A., Twenty Years of PSA: From Prostate Antigen to Tumor Marker. *Rev Urol* **2007,** *9* (3), 113-123.
7. Thompson, I. M.; Pauler, D. K.; Goodman, P. J.; Tangen, C. M.; Lucia, M. S.; Parnes, H. L.; Minasian, L. M.; Ford, L. G.; Lippman, S. M.; Crawford, E. D., Prevalence of prostate cancer among men with a prostate-specific antigen level ≤ 4.0 ng per milliliter. *N Engl J Med* **2004,** *350* (22), 2239-2246.
8. Nadler, R. B.; Humphrey, P. A.; Smith, D. S.; Catalona, W. J.; Timothy, L., Effect of inflammation and benign prostatic hyperplasia on elevated serum prostate specific antigen levels. *J Urol* **1995,** *154* (2), 407-413.
9. Benson, M. C.; Whang, I. S.; Pantuck, A.; Ring, K.; Kaplan, S. A.; Olsson, C. A.; Cooner, W. H., Prostate specific antigen density: a means of distinguishing benign prostatic hypertrophy and prostate cancer. *J Urol* **1992,** *147* (3), 815-816.
10. Potts, J. M., Prospective identification of National Institutes of Health category IV prostatitis in men with elevated prostate specific antigen. *J Urol* **2000,** *164* (5), 1550-1553.
11. Gleason, D. F.; Mellinger, G. T., Prediction of prognosis for prostatic adenocarcinoma by combined histological grading and clinical staging. *J Urol* **1974,** *111* (1), 58-64.
12. Humphrey, P. A., Gleason grading and prognostic factors in carcinoma of the prostate. *Mod Pathol* **2004,** *17* (3), 292-306.
13. Epstein, J. I.; Allsbrook, W. C., Jr.; Amin, M. B.; Egevad, L. L., The 2005 International Society of Urological Pathology (ISUP) Consensus Conference on Gleason Grading of Prostatic Carcinoma. *Am J Surg Pathol* **2005,** *29* (9), 1228-1242.
14. Egevad, L.; Granfors, T.; Karlberg, L.; Bergh, A.; Stattin, P., Prognostic value of the Gleason score in prostate cancer. *BJU Int* **2002,** *89* (6), 538-542.
15. Brierley, J. D.; Gospodarowicz, M. K.; Wittekind, C., TNM Classification of Malignant Tumours, 8th Edition. *Wiley-Blackwell* **2017**.
16. Cornford, P.; Bellmunt, J.; Bolla, M.; Briers, E.; De Santis, M.; Gross, T.; Henry, A. M.; Joniau, S.; Lam, T. B.; Mason, M. D.; van der Poel, H. G.; van der Kwast, T. H.; Rouviere, O.; Wiegel, T.; Mottet, N., EAU-ESTRO-SIOG Guidelines on Prostate Cancer. Part II: Treatment of

Relapsing, Metastatic, and Castration-Resistant Prostate Cancer. *Eur Urol* **2017,** *71* (4), 630-642.
17. National Comprehensive Cancer Network. Prostate Cancer **2018** https://www.nccn.org/patients/guidelines/prostate/files/assets/common/downloads/files/prostate.pdf.
18. Müller, J.; Ferraro, D. A.; Muehlematter, U. J.; Garcia Schuler, H. I.; Kedzia, S.; Eberli, D.; Guckenberger, M.; Kroeze, S. G. C.; Sulser, T.; Schmid, D. M.; Omlin, A.; Müller, A.; Zilli, T.; John, H.; Kranzbuehler, H.; Kaufmann, P. A.; von Schulthess, G. K.; Burger, I. A., Clinical impact of 68Ga-PSMA-11 PET on patient management and outcome, including all patients referred for an increase in PSA level during the first year after its clinical introduction. *Eur J Nucl Med Mol Imaging* **2019,** *46* (4), 889-900.
19. Fanti, S.; Minozzi, S.; Antoch, G.; Banks, I.; Briganti, A.; Carrio, I.; Chiti, A.; Clarke, N.; Eiber, M.; De Bono, J.; Fizazi, K.; Gillessen, S.; Gledhill, S.; Haberkorn, U.; Herrmann, K.; Hicks, R. J.; Lecouvet, F.; Montironi, R.; Ost, P.; O'Sullivan, J. M.; Padhani, A. R.; Schalken, J. A.; Scher, H. I.; Tombal, B.; van Moorselaar, R. J. A.; Van Poppel, H.; Vargas, H. A.; Walz, J.; Weber, W. A.; Wester, H. J.; Oyen, W. J. G., Consensus on molecular imaging and theranostics in prostate cancer. *Lancet Oncol* **2018,** *19* (12), e696-e708.
20. Leek, J.; Lench, N.; Maraj, B.; Bailey, A.; Carr, I.; Andersen, S.; Cross, J.; Whelan, P.; MacLennan, K.; Meredith, D., Prostate-specific membrane antigen: evidence for the existence of a second related human gene. *Br J Cancer* **1995,** *72* (3), 583-588.
21. Silver, D. A.; Pellicer, I.; Fair, W. R.; Heston, W. D.; Cordon-Cardo, C., Prostate-specific membrane antigen expression in normal and malignant human tissues. *Clin Cancer Res* **1997,** *3* (1), 81-85.
22. Sacha, P.; Zamecnik, J.; Barinka, C.; Hlouchova, K.; Vicha, A.; Mlcochova, P.; Hilgert, I.; Eckschlager, T.; Konvalinka, J., Expression of glutamate carboxypeptidase II in human brain. *Neuroscience* **2007,** *144* (4), 1361-1372.
23. Yao, V.; Berkman, C. E.; Choi, J. K.; O'Keefe, D. S.; Bacich, D. J., Expression of prostate-specific membrane antigen (PSMA), increases cell folate uptake and proliferation and suggests a novel role for PSMA in the uptake of the non-polyglutamated folate, folic acid. *Prostate* **2010,** *70* (3), 305-316.
24. Schülke, N.; Varlamova, O. A.; Donovan, G. P.; Ma, D.; Gardner, J. P.; Morrissey, D. M.; Arrigale, R. R.; Zhan, C.; Chodera, A. J.; Surowitz, K. G.; Maddon, P. J.; Heston, W. D.; Olson, W. C., The homodimer of prostate-specific membrane antigen is a functional target for cancer therapy. *Proc Natl Acad Sci U S A* **2003,** *100* (22), 12590-12595.
25. Mesters, J. R.; Barinka, C.; Li, W.; Tsukamoto, T.; Majer, P.; Slusher, B. S.; Konvalinka, J.; Hilgenfeld, R., Structure of glutamate carboxypeptidase II, a drug target in neuronal damage and prostate cancer. *EMBO J* **2006,** *25* (6), 1375-1384.
26. Robinson, M. B.; Blakely, R. D.; Couto, R.; Coyle, J. T., Hydrolysis of the brain dipeptide N-acetyl-L-aspartyl-L-glutamate. Identification and characterization of a novel N-acetylated alpha-linked acidic dipeptidase activity from rat brain. *J Biol Chem* **1987,** *262* (30), 14498-14506.
27. Tiffany, C. W.; Lapidus, R. G.; Merion, A.; Calvin, D. C.; Slusher, B. S., Characterization of the enzymatic activity of PSM: comparison with brain NAALADase. *Prostate* **1999,** *39* (1), 28-35.
28. Barinka, C.; Rojas, C.; Slusher, B.; Pomper, M., Glutamate carboxypeptidase II in diagnosis and treatment of neurologic disorders and prostate cancer. *Curr Med Chem* **2012,** *19* (6), 856-870.

29. Evans, J. C.; Malhotra, M.; Cryan, J. F.; O'Driscoll, C. M., The therapeutic and diagnostic potential of the prostate specific membrane antigen/glutamate carboxypeptidase II (PSMA/GCPII) in cancer and neurological disease. *Br J Pharmacol* **2016,** *173* (21), 3041-3079.
30. Rahn, K. A.; Watkins, C. C.; Alt, J.; Rais, R.; Stathis, M.; Grishkan, I.; Crainiceau, C. M.; Pomper, M. G.; Rojas, C.; Pletnikov, M. V.; Calabresi, P. A.; Brandt, J.; Barker, P. B.; Slusher, B. S.; Kaplin, A. I., Inhibition of glutamate carboxypeptidase II (GCPII) activity as a treatment for cognitive impairment in multiple sclerosis. *Proc Natl Acad Sci U S A* **2012,** *109* (49), 20101-20106.
31. Pinto, J. T.; Suffoletto, B. P.; Berzin, T. M.; Qiao, C. H.; Lin, S.; Tong, W. P.; May, F.; Mukherjee, B.; Heston, W. D., Prostate-specific membrane antigen: a novel folate hydrolase in human prostatic carcinoma cells. *Clin Cancer Res* **1996,** *2* (9), 1445-1451.
32. Heston, W. D., Characterization and glutamyl preferring carboxypeptidase function of prostate specific membrane antigen: a novel folate hydrolase. *Urology* **1997,** *49* (3A Suppl), 104-112.
33. Yao, V.; Parwani, A.; Maier, C.; Heston, W. D.; Bacich, D. J., Moderate expression of prostate-specific membrane antigen, a tissue differentiation antigen and folate hydrolase, facilitates prostate carcinogenesis. *Cancer Res* **2008,** *68* (21), 9070-9077.
34. Mhawech-Fauceglia, P.; Zhang, S.; Terracciano, L.; Sauter, G.; Chadhuri, A.; Herrmann, F. R.; Penetrante, R., Prostate-specific membrane antigen (PSMA) protein expression in normal and neoplastic tissues and its sensitivity and specificity in prostate adenocarcinoma: an immunohistochemical study using mutiple tumour tissue microarray technique. *Histopathology* **2007,** *50* (4), 472-483.
35. Kinoshita, Y.; Kuratsukuri, K.; Landas, S.; Imaida, K.; Rovito, P. M., Jr.; Wang, C. Y.; Haas, G. P., Expression of prostate-specific membrane antigen in normal and malignant human tissues. *World J Surg* **2006,** *30* (4), 628-636.
36. Ben Jemaa, A.; Bouraoui, Y.; Sallami, S.; Banasr, A.; Ben Rais, N.; Ouertani, L.; Nouira, Y.; Horchani, A.; Oueslati, R., Co-expression and impact of prostate specific membrane antigen and prostate specific antigen in prostatic pathologies. *J Exp Clin Cancer Res* **2010,** *29*, 171.
37. Bostwick, D. G.; Pacelli, A.; Blute, M.; Roche, P.; Murphy, G. P., Prostate specific membrane antigen expression in prostatic intraepithelial neoplasia and adenocarcinoma: a study of 184 cases. *Cancer* **1998,** *82* (11), 2256-2261.
38. Sweat, S. D.; Pacelli, A.; Murphy, G. P.; Bostwick, D. G., Prostate-specific membrane antigen expression is greatest in prostate adenocarcinoma and lymph node metastases. *Urology* **1998,** *52* (4), 637-640.
39. Ross, J. S.; Sheehan, C. E.; Fisher, H. A.; Kaufman, R. P., Jr.; Kaur, P.; Gray, K.; Webb, I.; Gray, G. S.; Mosher, R.; Kallakury, B. V., Correlation of primary tumor prostate-specific membrane antigen expression with disease recurrence in prostate cancer. *Clin Cancer Res* **2003,** *9* (17), 6357-6362.
40. Perner, S.; Hofer, M. D.; Kim, R.; Shah, R. B.; Li, H.; Moller, P.; Hautmann, R. E.; Gschwend, J. E.; Kuefer, R.; Rubin, M. A., Prostate-specific membrane antigen expression as a predictor of prostate cancer progression. *Hum Pathol* **2007,** *38* (5), 696-701.
41. Yao, V.; Bacich, D. J., Prostate specific membrane antigen (PSMA) expression gives prostate cancer cells a growth advantage in a physiologically relevant folate environment in vitro. *Prostate* **2006,** *66* (8), 867-875.
42. Conway, R. E.; Petrovic, N.; Li, Z.; Heston, W.; Wu, D.; Shapiro, L. H., Prostate-specific membrane antigen regulates angiogenesis by modulating integrin signal transduction. *Mol Cell Biol* **2006,** *26* (14), 5310-5324.

43. Chang, S. S.; O'Keefe, D. S.; Bacich, D. J.; Reuter, V. E.; Heston, W. D.; Gaudin, P. B., Prostate-specific membrane antigen is produced in tumor-associated neovasculature. *Clin Cancer Res* **1999,** *5* (10), 2674-2681.
44. Chang, S. S.; Reuter, V. E.; Heston, W. D.; Bander, N. H.; Grauer, L. S.; Gaudin, P. B., Five different anti-prostate-specific membrane antigen (PSMA) antibodies confirm PSMA expression in tumor-associated neovasculature. *Cancer Res* **1999,** *59* (13), 3192-3198.
45. Haffner, M. C.; Kronberger, I. E.; Ross, J. S.; Sheehan, C. E.; Zitt, M.; Muhlmann, G.; Ofner, D.; Zelger, B.; Ensinger, C.; Yang, X. J.; Geley, S.; Margreiter, R.; Bander, N. H., Prostate-specific membrane antigen expression in the neovasculature of gastric and colorectal cancers. *Hum Pathol* **2009,** *40* (12), 1754-1761.
46. Liu, H.; Rajasekaran, A. K.; Moy, P.; Xia, Y.; Kim, S.; Navarro, V.; Rahmati, R.; Bander, N. H., Constitutive and antibody-induced internalization of prostate-specific membrane antigen. *Cancer Res* **1998,** *58* (18), 4055-4060.
47. Goodman, O. B., Jr.; Barwe, S. P.; Ritter, B.; McPherson, P. S.; Vasko, A. J.; Keen, J. H.; Nanus, D. M.; Bander, N. H.; Rajasekaran, A. K., Interaction of prostate specific membrane antigen with clathrin and the adaptor protein complex-2. *Int J Oncol* **2007,** *31* (5), 1199-1203.
48. Anilkumar, G.; Rajasekaran, S. A.; Wang, S.; Hankinson, O.; Bander, N. H.; Rajasekaran, A. K., Prostate-specific membrane antigen association with filamin A modulates its internalization and NAALADase activity. *Cancer Res* **2003,** *63* (10), 2645-2648.
49. Davis, M. I.; Bennett, M. J.; Thomas, L. M.; Bjorkman, P. J., Crystal structure of prostate-specific membrane antigen, a tumor marker and peptidase. *Proc Natl Acad Sci U S A* **2005,** *102* (17), 5981-5986.
50. Barinka, C.; Sacha, P.; Sklenar, J.; Man, P.; Bezouska, K.; Slusher, B. S.; Konvalinka, J., Identification of the N-glycosylation sites on glutamate carboxypeptidase II necessary for proteolytic activity. *Protein Sci* **2004,** *13* (6), 1627-1635.
51. Ghosh, A.; Heston, W. D., Effect of carbohydrate moieties on the folate hydrolysis activity of the prostate specific membrane antigen. *Prostate* **2003,** *57* (2), 140-151.
52. Holmes, E. H.; Greene, T. G.; Tino, W. T.; Boynton, A. L.; Aldape, H. C.; Misrock, S. L.; Murphy, G. P., Analysis of glycosylation of prostate-specific membrane antigen derived from LNCaP cells, prostatic carcinoma tumors, and serum from prostate cancer patients. *Prostate Suppl* **1996,** *7*, 25-29.
53. Barinka, C.; Starkova, J.; Konvalinka, J.; Lubkowski, J., A high-resolution structure of ligand-free human glutamate carboxypeptidase II. *Acta Crystallogr Sect F Struct Biol Cryst Commun* **2007,** *63* (Pt 3), 150-153.
54. Barinka, C.; Rovenska, M.; Mlcochova, P.; Hlouchova, K.; Plechanovova, A.; Majer, P.; Tsukamoto, T.; Slusher, B. S.; Konvalinka, J.; Lubkowski, J., Structural insight into the pharmacophore pocket of human glutamate carboxypeptidase II. *J Med Chem* **2007,** *50* (14), 3267-3273.
55. Ferraris, D. V.; Shukla, K.; Tsukamoto, T., Structure-activity relationships of glutamate carboxypeptidase II (GCPII) inhibitors. *Curr Med Chem* **2012,** *19* (9), 1282-1294.
56. Mlcochova, P.; Plechanovova, A.; Barinka, C.; Mahadevan, D.; Saldanha, J. W.; Rulisek, L.; Konvalinka, J., Mapping of the active site of glutamate carboxypeptidase II by site-directed mutagenesis. *Febs j* **2007,** *274* (18), 4731-4741.
57. Barinka, C.; Hlouchova, K.; Rovenska, M.; Majer, P.; Dauter, M.; Hin, N.; Ko, Y. S.; Tsukamoto, T.; Slusher, B. S.; Konvalinka, J.; Lubkowski, J., Structural basis of interactions between human glutamate carboxypeptidase II and its substrate analogs. *J Mol Biol* **2008,** *376* (5), 1438-1450.

58. Chen, Y.; Foss, C. A.; Byun, Y.; Nimmagadda, S.; Pullambhatla, M.; Fox, J. J.; Castanares, M.; Lupold, S. E.; Babich, J. W.; Mease, R. C.; Pomper, M. G., Radiohalogenated prostate-specific membrane antigen (PSMA)-based ureas as imaging agents for prostate cancer. *J Med Chem* **2008,** *51* (24), 7933-7943.
59. Wüstemann, T.; Bauder-Wüst, U.; Schäfer, M.; Eder, M.; Benesova, M.; Leotta, K.; Kratochwil, C.; Haberkorn, U.; Kopka, K.; Mier, W., Design of Internalizing PSMA-specific Glu-ureido-based Radiotherapeuticals. *Theranostics* **2016,** *6* (8), 1085-1095.
60. Zhang, A. X.; Murelli, R. P.; Barinka, C.; Michel, J.; Cocleaza, A.; Jorgensen, W. L.; Lubkowski, J.; Spiegel, D. A., A remote arene-binding site on prostate specific membrane antigen revealed by antibody-recruiting small molecules. *J Am Chem Soc* **2010,** *132* (36), 12711-12716.
61. Kopka, K.; Benesova, M.; Barinka, C.; Haberkorn, U.; Babich, J., Glu-Ureido-Based Inhibitors of Prostate-Specific Membrane Antigen: Lessons Learned During the Development of a Novel Class of Low-Molecular-Weight Theranostic Radiotracers. *J Nucl Med* **2017,** *58* (Suppl 2), 17s-26s.
62. Jackson, P. F.; Cole, D. C.; Slusher, B. S.; Stetz, S. L.; Ross, L. E.; Donzanti, B. A.; Trainor, D. A., Design, synthesis, and biological activity of a potent inhibitor of the neuropeptidase N-acetylated alpha-linked acidic dipeptidase. *J Med Chem* **1996,** *39* (2), 619-622.
63. Mesters, J. R.; Henning, K.; Hilgenfeld, R., Human glutamate carboxypeptidase II inhibition: structures of GCPII in complex with two potent inhibitors, quisqualate and 2-PMPA. *Acta Crystallogr D Biol Crystallogr* **2007,** *63* (Pt 4), 508-513.
64. Kozikowski, A. P.; Nan, F.; Conti, P.; Zhang, J.; Ramadan, E.; Bzdega, T.; Wroblewska, B.; Neale, J. H.; Pshenichkin, S.; Wroblewski, J. T., Design of remarkably simple, yet potent urea-based inhibitors of glutamate carboxypeptidase II (NAALADase). *J Med Chem* **2001,** *44* (3), 298-301.
65. Stoermer, D.; Vitharana, D.; Hin, N.; Delahanty, G.; Duvall, B.; Ferraris, D. V.; Grella, B. S.; Hoover, R.; Rojas, C.; Shanholtz, M. K.; Smith, K. P.; Stathis, M.; Wu, Y.; Wozniak, K. M.; Slusher, B. S.; Tsukamoto, T., Design, synthesis, and pharmacological evaluation of glutamate carboxypeptidase II (GCPII) inhibitors based on thioalkylbenzoic acid scaffolds. *J Med Chem* **2012,** *55* (12), 5922-5932.
66. Majer, P.; Jackson, P. F.; Delahanty, G.; Grella, B. S.; Ko, Y. S.; Li, W.; Liu, Q.; Maclin, K. M.; Polakova, J.; Shaffer, K. A.; Stoermer, D.; Vitharana, D.; Wang, E. Y.; Zakrzewski, A.; Rojas, C.; Slusher, B. S.; Wozniak, K. M.; Burak, E.; Limsakun, T.; Tsukamoto, T., Synthesis and biological evaluation of thiol-based inhibitors of glutamate carboxypeptidase II: discovery of an orally active GCP II inhibitor. *J Med Chem* **2003,** *46* (10), 1989-1996.
67. Jackson, P. F.; Tays, K. L.; Maclin, K. M.; Ko, Y. S.; Li, W.; Vitharana, D.; Tsukamoto, T.; Stoermer, D.; Lu, X. C.; Wozniak, K.; Slusher, B. S., Design and pharmacological activity of phosphinic acid based NAALADase inhibitors. *J Med Chem* **2001,** *44* (24), 4170-4175.
68. Zhou, J.; Neale, J. H.; Pomper, M. G.; Kozikowski, A. P., NAAG peptidase inhibitors and their potential for diagnosis and therapy. *Nat Rev Drug Discov* **2005,** *4* (12), 1015-1026.
69. Hillier, S. M.; Maresca, K. P.; Femia, F. J.; Marquis, J. C.; Foss, C. A.; Nguyen, N.; Zimmerman, C. N.; Barrett, J. A.; Eckelman, W. C.; Pomper, M. G.; Joyal, J. L.; Babich, J. W., Preclinical evaluation of novel glutamate-urea-lysine analogues that target prostate-specific membrane antigen as molecular imaging pharmaceuticals for prostate cancer. *Cancer Res* **2009,** *69* (17), 6932-6940.
70. Tsukamoto, T.; Majer, P.; Vitharana, D.; Ni, C.; Hin, B.; Lu, X. C.; Thomas, A. G.; Wozniak, K. M.; Calvin, D. C.; Wu, Y.; Slusher, B. S.; Scarpetti, D.; Bonneville, G. W.,

Enantiospecificity of glutamate carboxypeptidase II inhibition. *J Med Chem* **2005,** *48* (7), 2319-2324.
71. Weineisen, M.; Simecek, J.; Schottelius, M.; Schwaiger, M.; Wester, H. J., Synthesis and preclinical evaluation of DOTAGA-conjugated PSMA ligands for functional imaging and endoradiotherapy of prostate cancer. *EJNMMI Res* **2014,** *4* (1), 63.
72. Benesova, M.; Bauder-Wüst, U.; Schäfer, M.; Klika, K. D.; Mier, W.; Haberkorn, U.; Kopka, K.; Eder, M., Linker Modification Strategies To Control the Prostate-Specific Membrane Antigen (PSMA)-Targeting and Pharmacokinetic Properties of DOTA-Conjugated PSMA Inhibitors. *J Med Chem* **2016,** *59* (5), 1761-1775.
73. Barinka, C.; Byun, Y.; Dusich, C. L.; Banerjee, S. R.; Chen, Y.; Castanares, M.; Kozikowski, A. P.; Mease, R. C.; Pomper, M. G.; Lubkowski, J., Interactions between human glutamate carboxypeptidase II and urea-based inhibitors: structural characterization. *J Med Chem* **2008,** *51* (24), 7737-7743.
74. Rong, S. B.; Zhang, J.; Neale, J. H.; Wroblewski, J. T.; Wang, S.; Kozikowski, A. P., Molecular modeling of the interactions of glutamate carboxypeptidase II with its potent NAAG-based inhibitors. *J Med Chem* **2002,** *45* (19), 4140-4152.
75. Kozikowski, A. P.; Zhang, J.; Nan, F.; Petukhov, P. A.; Grajkowska, E.; Wroblewski, J. T.; Yamamoto, T.; Bzdega, T.; Wroblewska, B.; Neale, J. H., Synthesis of urea-based inhibitors as active site probes of glutamate carboxypeptidase II: efficacy as analgesic agents. *J Med Chem* **2004,** *47* (7), 1729-1738.
76. Heesakkers, R. A.; Hövels, A. M.; Jager, G. J.; van den Bosch, H. C.; Witjes, J. A.; Raat, H. P.; Severens, J. L.; Adang, E. M.; van der Kaa, C. H.; Futterer, J. J.; Barentsz, J., MRI with a lymph-node-specific contrast agent as an alternative to CT scan and lymph-node dissection in patients with prostate cancer: a prospective multicohort study. *Lancet Oncol* **2008,** *9* (9), 850-856.
77. Hövels, A. M.; Heesakkers, R. A.; Adang, E. M.; Jager, G. J.; Strum, S.; Hoogeveen, Y. L.; Severens, J. L.; Barentsz, J. O., The diagnostic accuracy of CT and MRI in the staging of pelvic lymph nodes in patients with prostate cancer: a meta-analysis. *Clin Radiol* **2008,** *63* (4), 387-395.
78. Macheda, M. L.; Rogers, S.; Best, J. D., Molecular and cellular regulation of glucose transporter (GLUT) proteins in cancer. *J Cell Physiol* **2005,** *202* (3), 654-662.
79. Glunde, K.; Bhujwalla, Z. M.; Ronen, S. M., Choline metabolism in malignant transformation. *Nat Rev Cancer* **2011,** *11* (12), 835-848.
80. Jadvar, H., Prostate cancer: PET with 18F-FDG, 18F- or 11C-acetate, and 18F- or 11C-choline. *J Nucl Med* **2011,** *52* (1), 81-89.
81. Jadvar, H., Imaging evaluation of prostate cancer with 18F-fluorodeoxyglucose PET/CT: utility and limitations. *Eur J Nucl Med Mol Imaging* **2013,** *40 Suppl 1*, S5-10.
82. Brogsitter, C.; Zöphel, K.; Kotzerke, J., 18F-Choline, 11C-choline and 11C-acetate PET/CT: comparative analysis for imaging prostate cancer patients. *Eur J Nucl Med Mol Imaging* **2013,** *40 Suppl 1*, S18-27.
83. Lindenberg, L.; Choyke, P.; Dahut, W., Prostate Cancer Imaging with Novel PET Tracers. *Curr Urol Rep* **2016,** *17* (3), 18.
84. Krause, B. J.; Souvatzoglou, M.; Tuncel, M.; Herrmann, K.; Buck, A. K.; Praus, C.; Schuster, T.; Geinitz, H.; Treiber, U.; Schwaiger, M., The detection rate of [11C]choline-PET/CT depends on the serum PSA-value in patients with biochemical recurrence of prostate cancer. *Eur J Nucl Med Mol Imaging* **2008,** *35* (1), 18-23.

85. Evangelista, L.; Guttilla, A.; Zattoni, F.; Muzzio, P. C.; Zattoni, F., Utility of choline positron emission tomography/computed tomography for lymph node involvement identification in intermediate- to high-risk prostate cancer: a systematic literature review and meta-analysis. *Eur Urol* **2013,** *63* (6), 1040-1048.
86. Robu, S.; Schmidt, A.; Eiber, M.; Schottelius, M.; Günther, T.; Hooshyar Yousefi, B.; Schwaiger, M.; Wester, H. J., Synthesis and preclinical evaluation of novel 18F-labeled Glu-urea-Glu-based PSMA inhibitors for prostate cancer imaging: a comparison with 18F-DCFPyl and 18F-PSMA-1007. *EJNMMI Res* **2018,** *8* (1), 30.
87. Kesch, C.; Kratochwil, C.; Mier, W.; Kopka, K.; Giesel, F. L., 68Ga or 18F for Prostate Cancer Imaging? *J Nucl Med* **2017,** *58* (5), 687-688.
88. Donin, N. M.; Reiter, R. E., Why Targeting PSMA Is a Game Changer in the Management of Prostate Cancer. *J Nucl Med* **2018,** *59* (2), 177-182.
89. Eder, M.; Schäfer, M.; Bauder-Wüst, U.; Hull, W. E.; Wängler, C.; Mier, W.; Haberkorn, U.; Eisenhut, M., 68Ga-complex lipophilicity and the targeting property of a urea-based PSMA inhibitor for PET imaging. *Bioconjug Chem* **2012,** *23* (4), 688-697.
90. Afshar-Oromieh, A.; Holland-Letz, T.; Giesel, F. L.; Kratochwil, C.; Mier, W.; Haufe, S.; Debus, N.; Eder, M.; Eisenhut, M.; Schäfer, M.; Neels, O.; Hohenfellner, M.; Kopka, K.; Kauczor, H. U.; Debus, J.; Haberkorn, U., Diagnostic performance of 68Ga-PSMA-11 (HBED-CC) PET/CT in patients with recurrent prostate cancer: evaluation in 1007 patients. *Eur J Nucl Med Mol Imaging* **2017,** *44* (8), 1258-1268.
91. Eder, M.; Wängler, B.; Knackmuss, S.; LeGall, F.; Little, M.; Haberkorn, U.; Mier, W.; Eisenhut, M., Tetrafluorophenolate of HBED-CC: a versatile conjugation agent for 68Ga-labeled small recombinant antibodies. *Eur J Nucl Med Mol Imaging* **2008,** *35* (10), 1878-1886.
92. Maurer, T.; Gschwend, J. E.; Rauscher, I.; Souvatzoglou, M.; Haller, B.; Weirich, G.; Wester, H. J.; Heck, M.; Kübler, H.; Beer, A. J.; Schwaiger, M.; Eiber, M., Diagnostic Efficacy of 68Gallium-PSMA Positron Emission Tomography Compared to Conventional Imaging for Lymph Node Staging of 130 Consecutive Patients with Intermediate to High Risk Prostate Cancer. *J Urol* **2016,** *195* (5), 1436-1443.
93. Afshar-Oromieh, A.; Avtzi, E.; Giesel, F. L.; Holland-Letz, T.; Linhart, H. G.; Eder, M.; Eisenhut, M.; Boxler, S.; Hadaschik, B. A.; Kratochwil, C.; Weichert, W.; Kopka, K.; Debus, J.; Haberkorn, U., The diagnostic value of PET/CT imaging with the 68Ga-labelled PSMA ligand HBED-CC in the diagnosis of recurrent prostate cancer. *Eur J Nucl Med Mol Imaging* **2015,** *42* (2), 197-209.
94. Schwenck, J.; Rempp, H.; Reischl, G.; Kruck, S.; Stenzl, A.; Nikolaou, K.; Pfannenberg, C.; la Fougere, C., Comparison of 68Ga-labelled PSMA-11 and 11C-choline in the detection of prostate cancer metastases by PET/CT. *Eur J Nucl Med Mol Imaging* **2017,** *44* (1), 92-101.
95. Afshar-Oromieh, A.; Zechmann, C. M.; Malcher, A.; Eder, M.; Eisenhut, M.; Linhart, H. G.; Holland-Letz, T.; Hadaschik, B. A.; Giesel, F. L.; Debus, J.; Haberkorn, U., Comparison of PET imaging with a 68Ga-labelled PSMA ligand and 18F-choline-based PET/CT for the diagnosis of recurrent prostate cancer. *Eur J Nucl Med Mol Imaging* **2014,** *41* (1), 11-20.
96. Weineisen, M.; Schottelius, M.; Simecek, J.; Baum, R. P.; Yildiz, A.; Beykan, S.; Kulkarni, H. R.; Lassmann, M.; Klette, I.; Eiber, M.; Schwaiger, M.; Wester, H. J., 68Ga- and 177Lu-Labeled PSMA I&T: Optimization of a PSMA-Targeted Theranostic Concept and First Proof-of-Concept Human Studies. *J Nucl Med* **2015,** *56* (8), 1169-1176.
97. Schottelius, M.; Wirtz, M.; Eiber, M.; Maurer, T.; Wester, H. J., [111In]PSMA-I&T: expanding the spectrum of PSMA-I&T applications towards SPECT and radioguided surgery. *EJNMMI Res* **2015,** *5* (1), 68.

98. Benesova, M.; Schäfer, M.; Bauder-Wüst, U.; Afshar-Oromieh, A.; Kratochwil, C.; Mier, W.; Haberkorn, U.; Kopka, K.; Eder, M., Preclinical Evaluation of a Tailor-Made DOTA-Conjugated PSMA Inhibitor with Optimized Linker Moiety for Imaging and Endoradiotherapy of Prostate Cancer. *J Nucl Med* **2015,** *56* (6), 914-920.
99. Sanchez-Crespo, A., Comparison of Gallium-68 and Fluorine-18 imaging characteristics in positron emission tomography. *Appl Radiat Isot* **2013,** *76*, 55-62.
100. Mease, R. C.; Dusich, C. L.; Foss, C. A.; Ravert, H. T.; Dannals, R. F.; Seidel, J.; Prideaux, A.; Fox, J. J.; Sgouros, G.; Kozikowski, A. P.; Pomper, M. G., N-[N-[(S)-1,3-Dicarboxypropyl]carbamoyl]-4-[18F]fluorobenzyl-L-cysteine, [18F]DCFBC: a new imaging probe for prostate cancer. *Clin Cancer Res* **2008,** *14* (10), 3036-3043.
101. Cho, S. Y.; Gage, K. L.; Mease, R. C.; Senthamizhchelvan, S.; Holt, D. P.; Jeffrey-Kwanisai, A.; Endres, C. J.; Dannals, R. F.; Sgouros, G.; Lodge, M.; Eisenberger, M. A.; Rodriguez, R.; Carducci, M. A.; Rojas, C.; Slusher, B. S.; Kozikowski, A. P.; Pomper, M. G., Biodistribution, tumor detection, and radiation dosimetry of 18F-DCFBC, a low-molecular-weight inhibitor of prostate-specific membrane antigen, in patients with metastatic prostate cancer. *J Nucl Med* **2012,** *53* (12), 1883-1891.
102. Rowe, S. P.; Gage, K. L.; Faraj, S. F.; Macura, K. J.; Cornish, T. C.; Gonzalez-Roibon, N.; Guner, G.; Munari, E.; Partin, A. W.; Pavlovich, C. P.; Han, M.; Carter, H. B.; Bivalacqua, T. J.; Blackford, A.; Holt, D.; Dannals, R. F.; Netto, G. J.; Lodge, M. A.; Mease, R. C.; Pomper, M. G.; Cho, S. Y., 18F-DCFBC PET/CT for PSMA-Based Detection and Characterization of Primary Prostate Cancer. *J Nucl Med* **2015,** *56* (7), 1003-1010.
103. Plyku, D.; Mena, E.; Rowe, S. P.; Lodge, M. A.; Szabo, Z.; Cho, S. Y.; Pomper, M. G.; Sgouros, G.; Hobbs, R. F., Combined model-based and patient-specific dosimetry for 18F-DCFPyL, a PSMA-targeted PET agent. *Eur J Nucl Med Mol Imaging* **2018,** *45* (6), 989-998.
104. Chen, Y.; Pullambhatla, M.; Foss, C. A.; Byun, Y.; Nimmagadda, S.; Senthamizhchelvan, S.; Sgouros, G.; Mease, R. C.; Pomper, M. G., 2-(3-(1-Carboxy-5-((6-[18F]fluoro-pyridine-3-carbonyl)-amino)-pentyl)-ureido)-pen tanedioic acid, [18F]DCFPyL, a PSMA-based PET imaging agent for prostate cancer. *Clin Cancer Res* **2011,** *17* (24), 7645-7653.
105. Szabo, Z.; Mena, E.; Rowe, S. P.; Plyku, D.; Nidal, R.; Eisenberger, M. A.; Antonarakis, E. S.; Fan, H.; Dannals, R. F.; Chen, Y.; Mease, R. C.; Vranesic, M.; Bhatnagar, A.; Sgouros, G.; Cho, S. Y.; Pomper, M. G., Initial Evaluation of [18F]DCFPyL for Prostate-Specific Membrane Antigen (PSMA)-Targeted PET Imaging of Prostate Cancer. *Mol Imaging Biol* **2015,** *17* (4), 565-574.
106. Dietlein, M.; Kobe, C.; Kuhnert, G.; Stockter, S.; Fischer, T.; Schomacker, K.; Schmidt, M.; Dietlein, F.; Zlatopolskiy, B. D.; Krapf, P.; Richarz, R.; Neubauer, S.; Drzezga, A.; Neumaier, B., Comparison of [18F]DCFPyL and [68Ga]Ga-PSMA-HBED-CC for PSMA-PET Imaging in Patients with Relapsed Prostate Cancer. *Mol Imaging Biol* **2015,** *17* (4), 575-584.
107. Cardinale, J.; Schäfer, M.; Benesova, M.; Bauder-Wüst, U.; Leotta, K.; Eder, M.; Neels, O. C.; Haberkorn, U.; Giesel, F. L.; Kopka, K., Preclinical Evaluation of 18F-PSMA-1007, a New Prostate-Specific Membrane Antigen Ligand for Prostate Cancer Imaging. *J Nucl Med* **2017,** *58* (3), 425-431.
108. Giesel, F. L.; Hadaschik, B.; Cardinale, J.; Radtke, J.; Vinsensia, M.; Lehnert, W.; Kesch, C.; Tolstov, Y.; Singer, S.; Grabe, N.; Duensing, S.; Schäfer, M.; Neels, O. C.; Mier, W.; Haberkorn, U.; Kopka, K.; Kratochwil, C., F-18 labelled PSMA-1007: biodistribution, radiation dosimetry and histopathological validation of tumor lesions in prostate cancer patients. *Eur J Nucl Med Mol Imaging* **2017,** *44* (4), 678-688.

109. Rahbar, K.; Afshar-Oromieh, A.; Bögemann, M.; Wagner, S.; Schäfers, M.; Stegger, L.; Weckesser, M., 18F-PSMA-1007 PET/CT at 60 and 120 minutes in patients with prostate cancer: biodistribution, tumour detection and activity kinetics. *Eur J Nucl Med Mol Imaging* **2018,** *45* (8), 1329-1334.
110. Rahbar, K.; Afshar-Oromieh, A.; Seifert, R.; Wagner, S.; Schäfers, M.; Bögemann, M.; Weckesser, M., Diagnostic performance of 18F-PSMA-1007 PET/CT in patients with biochemical recurrent prostate cancer. *Eur J Nucl Med Mol Imaging* **2018,** *45* (12), 2055-2061.
111. Kirby, M.; Hirst, C.; Crawford, E. D., Characterising the castration-resistant prostate cancer population: a systematic review. *Int J Clin Pract* **2011,** *65* (11), 1180-1192.
112. Fendler, W. P.; Rahbar, K.; Herrmann, K.; Kratochwil, C.; Eiber, M., 177Lu-PSMA Radioligand Therapy for Prostate Cancer. *J Nucl Med* **2017,** *58* (8), 1196-1200.
113. Moreira, D. M.; Howard, L. E.; Sourbeer, K. N.; Amarasekara, H. S.; Chow, L. C.; Cockrell, D. C.; Pratson, C. L.; Hanyok, B. T.; Aronson, W. J.; Kane, C. J.; Terris, M. K.; Amling, C. L.; Cooperberg, M. R.; Freedland, S. J., Predicting Time From Metastasis to Overall Survival in Castration-Resistant Prostate Cancer: Results From SEARCH. *Clin Genitourin Cancer* **2017,** *15* (1), 60-66.e2.
114. Jadvar, H., Targeted Radionuclide Therapy: An Evolution Toward Precision Cancer Treatment. *AJR Am J Roentgenol* **2017,** *209* (2), 277-288.
115. Barrett, J. A.; Coleman, R. E.; Goldsmith, S. J.; Vallabhajosula, S.; Petry, N. A.; Cho, S.; Armor, T.; Stubbs, J. B.; Maresca, K. P.; Stabin, M. G.; Joyal, J. L.; Eckelman, W. C.; Babich, J. W., First-in-man evaluation of 2 high-affinity PSMA-avid small molecules for imaging prostate cancer. *J Nucl Med* **2013,** *54* (3), 380-387.
116. Zechmann, C. M.; Afshar-Oromieh, A.; Armor, T.; Stubbs, J. B.; Mier, W.; Hadaschik, B.; Joyal, J.; Kopka, K.; Debus, J.; Babich, J. W.; Haberkorn, U., Radiation dosimetry and first therapy results with a 124I/ 131I-labeled small molecule (MIP-1095) targeting PSMA for prostate cancer therapy. *Eur J Nucl Med Mol Imaging* **2014,** *41* (7), 1280-1292.
117. Kulkarni, H. R.; Singh, A.; Schuchardt, C.; Niepsch, K.; Sayeg, M.; Leshch, Y.; Wester, H. J.; Baum, R. P., PSMA-Based Radioligand Therapy for Metastatic Castration-Resistant Prostate Cancer: The Bad Berka Experience Since 2013. *J Nucl Med* **2016,** *57* (Suppl 3), 97s-104s.
118. Heck, M. M.; Retz, M.; D'Alessandria, C.; Rauscher, I.; Scheidhauer, K.; Maurer, T.; Storz, E.; Janssen, F.; Schottelius, M.; Wester, H. J.; Gschwend, J. E.; Schwaiger, M.; Tauber, R.; Eiber, M., Systemic Radioligand Therapy with 177Lu Labeled Prostate Specific Membrane Antigen Ligand for Imaging and Therapy in Patients with Metastatic Castration Resistant Prostate Cancer. *J Urol* **2016,** *196* (2), 382-391.
119. Ahmadzadehfar, H.; Eppard, E.; Kürpig, S.; Fimmers, R.; Yordanova, A.; Schlenkhoff, C. D.; Gartner, F.; Rogenhofer, S.; Essler, M., Therapeutic response and side effects of repeated radioligand therapy with 177Lu-PSMA-DKFZ-617 of castrate-resistant metastatic prostate cancer. *Oncotarget* **2016,** *7* (11), 12477-12488.
120. Rahbar, K.; Ahmadzadehfar, H.; Kratochwil, C.; Haberkorn, U.; Schäfers, M.; Essler, M.; Baum, R. P.; Kulkarni, H. R.; Schmidt, M.; Drzezga, A.; Bartenstein, P.; Pfestroff, A.; Luster, M.; Lützen, U.; Marx, M.; Prasad, V.; Brenner, W.; Heinzel, A.; Mottaghy, F. M.; Ruf, J.; Meyer, P. T.; Heuschkel, M.; Eveslage, M.; Bögemann, M.; Fendler, W. P.; Krause, B. J., German Multicenter Study Investigating 177Lu-PSMA-617 Radioligand Therapy in Advanced Prostate Cancer Patients. *J Nucl Med* **2017,** *58* (1), 85-90.
121. Cai, L.; Lu, S.; Pike, V. W., Chemistry with [18F]Fluoride Ion. *Eur J Org Chem* **2008,** *2008* (17), 2853-2873.

122. Wester, H. J., *Pharmaceutical Radiochemistry (I)*. Scintomics Print Media and Publishing: Fürstenfeldbruck, Germany, 2010.
123. Jacobson, O.; Kiesewetter, D. O.; Chen, X., Fluorine-18 radiochemistry, labeling strategies and synthetic routes. *Bioconjug Chem* **2015,** *26* (1), 1-18.
124. Kilbourn, M. R.; Welch, M. J.; Dence, C. S.; Tewson, T. J.; Saji, H.; Maeda, M., Carrier-added and no-carrier-added syntheses of [18F]spiroperidol and [18F]haloperidol. *Int J Appl Radiat Isot* **1984,** *35* (7), 591-598.
125. Cacace, F.; Speranza, M.; Wolf, A. P.; Fowler, J. S., Labelling of fluorinated aromatics by isotopic exchange with [18F]fluoride. *J Label Compd Radiopharm* **1981,** *18* (12), 1721-1730.
126. Farrokhzad, S.; Diksic, M., The syntheses of no-carrier-added and carrier-added 18F-labelled haloperidol. *J Label Compd Radiopharm* **1985,** *22* (7), 721-733.
127. Bernard-Gauthier, V.; Bailey, J. J.; Liu, Z.; Wängler, B.; Wängler, C.; Jurkschat, K.; Perrin, D. M.; Schirrmacher, R., From Unorthodox to Established: The Current Status of 18F-Trifluoroborate- and 18F-SiFA-Based Radiopharmaceuticals in PET Nuclear Imaging. *Bioconjug Chem* **2016,** *27* (2), 267-279.
128. Askenasy, H. M.; Anbar, M.; Laor, Y.; Lewitus, Z.; Kosary, I. Z.; Guttmann, S., The localization of intracranial space-occupying lesions by fluoroborate ions labelled with fluorine 18. *Am J Roentgenol Radium Ther Nucl Med* **1962,** *88*, 350-354.
129. Entzian, W.; Aronow, S.; Soloway, A. H.; Sweet, W. H., A preliminary evaluation of F-18-labelled Tetrafluoroborate as a scanning agent for intracranial tumors. *J Nucl Med* **1964,** *5*, 542-550.
130. Ting, R.; Adam, M. J.; Ruth, T. J.; Perrin, D. M., Arylfluoroborates and alkylfluorosilicates as potential PET imaging agents: high-yielding aqueous biomolecular 18F-labeling. *J Am Chem Soc* **2005,** *127* (38), 13094-13095.
131. Liu, Z.; Pourghiasian, M.; Benard, F.; Pan, J.; Lin, K. S.; Perrin, D. M., Preclinical evaluation of a high-affinity 18F-trifluoroborate octreotate derivative for somatostatin receptor imaging. *J Nucl Med* **2014,** *55* (9), 1499-1505.
132. Pourghiasian, M.; Liu, Z.; Pan, J.; Zhang, Z.; Colpo, N.; Lin, K. S.; Perrin, D. M.; Benard, F., 18F-AmBF3-MJ9: a novel radiofluorinated bombesin derivative for prostate cancer imaging. *Bioorg Med Chem* **2015,** *23* (7), 1500-1506.
133. Li, Y.; Guo, J.; Tang, S.; Lang, L.; Chen, X.; Perrin, D. M., One-step and one-pot-two-step radiosynthesis of cyclo-RGD-18F-aryltrifluoroborate conjugates for functional imaging. *Am J Nucl Med Mol Imaging* **2013,** *3* (1), 44-56.
134. Kuo, H. T.; Lepage, M.; Lin, K. S.; Pan, J.; Zhang, Z.; Liu, Z.; Pryyma, A.; Zhang, C.; Merkens, H.; Roxin, A.; Perrin, D.; Benard, F., One-step 18F-labeling and preclinical evaluation of prostate specific membrane antigen trifluoroborate probes for cancer imaging. *J Nucl Med* **2019,** *60* (8), 1160-1166.
135. Gens, T. A.; Wethington, J. A.; Brosi, A. R., The Exchange of F18 between Metallic Fluorides and Silicon Tetrafluoride. *J Phys Chem* **1958,** *62* (12), 1593-1593.
136. Poole, R. T.; Winfield, J. M., Radiotracers in fluorine chemistry. Part IV. Fluorine-18 exchange between labelled alkylfluorosilanesand fluorides, or fluoride methoxides, of tungsten(VI), molybdenum(VI), tellurium(VI), and iodine(V). *Dalton Trans* **1976,** (16), 1557-1560.
137. Winfield, J. M., Preparation and use of 18-fluorine labelled inorganic compounds. *J Fluor Chem* **1980,** *16* (1), 1-17.

138. Rosenthal, M. S.; Bosch, A. L.; Nickles, R. J.; Gatley, S. J., Synthesis and some characteristics of no-carrier added [18F]fluorotrimethylsilane. *Int J Appl Radiat Isot* **1985,** *36* (4), 318-319.
139. Walsh, J.; Fleming, L.; Satyamurthy, N.; Barrio, J.; Phelps, M.; Gambhir, S.; Toyokuni, T., Application of silicon-fluoride chemistry for the development of amine-reactive F-18-labeling agents for biomolecules. *J Nucl Med* **2000,** *41* (5), 249P-249P.
140. Schirrmacher, R.; Bradtmöller, G.; Schirrmacher, E.; Thews, O.; Tillmanns, J.; Siessmeier, T.; Buchholz, H. G.; Bartenstein, P.; Wängler, B.; Niemeyer, C. M.; Jurkschat, K., 18F-labeling of peptides by means of an organosilicon-based fluoride acceptor. *Angew Chem Int Ed Engl* **2006,** *45* (36), 6047-6050.
141. Choudhry, U.; Martin, K. E.; Biagini, S.; Blower, P. J., A49 Alkoxysilane groups for instant labelling of biomolecules with 18F. *Nucl Med Commun* **2006,** *27* (3), 293.
142. Höhne, A.; Yu, L.; Mu, L.; Reiher, M.; Voigtmann, U.; Klar, U.; Graham, K.; Schubiger, P. A.; Ametamey, S. M., Organofluorosilanes as model compounds for 18F-labeled silicon-based PET tracers and their hydrolytic stability: experimental data and theoretical calculations (PET = positron emission tomography). *Chemistry* **2009,** *15* (15), 3736-3743.
143. Niedermoser, S.; Chin, J.; Wängler, C.; Kostikov, A.; Bernard-Gauthier, V.; Vogler, N.; Soucy, J. P.; McEwan, A. J.; Schirrmacher, R.; Wängler, B., In Vivo Evaluation of 18F-SiFAlin-Modified TATE: A Potential Challenge for 68Ga-DOTATATE, the Clinical Gold Standard for Somatostatin Receptor Imaging with PET. *J Nucl Med* **2015,** *56* (7), 1100-1105.
144. King, R. B.; Crabtree, R. H.; Lukehart, C. M.; Atwood, D. A.; Scott, R. A., *Bond Energies*. Wiley: Chichester, United Kingdom, 2006.
145. Murphy, L. R.; Meek, T. L.; Allred, A. L.; Allen, L. C., Evaluation and Test of Pauling's Electronegativity Scale. *J Phys Chem* **2000,** *104* (24), 5867-5871.
146. Bernard-Gauthier, V.; Wängler, C.; Schirrmacher, E.; Kostikov, A.; Jurkschat, K.; Wängler, B.; Schirrmacher, R., 18F-labeled silicon-based fluoride acceptors: potential opportunities for novel positron emitting radiopharmaceuticals. *Biomed Res Int* **2014,** *2014*, 454503.
147. Brook, M. A., *Silicon in Organic, Organometallic and Polymer Chemistry*. Wiley: New York, United States, 2000.
148. Corriu, R., Hypervalent species of silicon: structure and reactivity. *J Organomet Chem* **1990,** *400* (1-2), 81-106.
149. Schirrmacher, E.; Wängler, B.; Cypryk, M.; Bradtmöller, G.; Schäfer, M.; Eisenhut, M.; Jurkschat, K.; Schirrmacher, R., Synthesis of p-(di-tert-butyl[18F]fluorosilyl)benzaldehyde ([18F]SiFA-A) with high specific activity by isotopic exchange: a convenient labeling synthon for the 18F-labeling of N-amino-oxy derivatized peptides. *Bioconjug Chem* **2007,** *18* (6), 2085-2089.
150. Bassindale, A. R.; Taylor, P. G., Reaction Mechanisms of Nucleophilic Attack at Silicon. In *PATAI'S Chemistry of Functional Groups*, Wiley: New York, United States, 1998.
151. Kostikov, A. P.; Iovkova, L.; Chin, J.; Schirrmacher, E.; Wängler, B.; Wängler, C.; Jurkschat, K.; Cosa, G.; Schirrmacher, R., N-(4-(di-tert-butyl[18F]fluorosilyl)benzyl)-2-hydroxy-N,N-dimethylethylammonium bromide ([18F]SiFAN+Br−): A novel lead compound for the development of hydrophilic SiFA-based prosthetic groups for 18F-labeling. *J Fluor Chem* **2011,** *132* (1), 27-34.
152. Block, D.; Coenen, H. H.; Stöcklin, G., N.C.A. 18F-fluoroalkylation of H-acidic compounds. *J Label Compd Rad* **1988,** *25* (2), 201-216.

153. Iovkova, L.; Wängler, B.; Schirrmacher, E.; Schirrmacher, R.; Quandt, G.; Boening, G.; Schürmann, M.; Jurkschat, K., para-Functionalized Aryl-di-tert-butylfluorosilanes as Potential Labeling Synthons for 18F Radiopharmaceuticals. *Chem Eur J* **2009,** *15* (9), 2140-2147.
154. Lindner, S.; Michler, C.; Leidner, S.; Rensch, C.; Wängler, C.; Schirrmacher, R.; Bartenstein, P.; Wängler, B., Synthesis and in vitro and in vivo evaluation of SiFA-tagged bombesin and RGD peptides as tumor imaging probes for positron emission tomography. *Bioconjug Chem* **2014,** *25* (4), 738-749.
155. Wängler, C.; Waser, B.; Alke, A.; Iovkova, L.; Buchholz, H.-G.; Niedermoser, S.; Jurkschat, K.; Fottner, C.; Bartenstein, P.; Schirrmacher, R.; Reubi, J.-C.; Wester, H.-J.; Wängler, B., One-Step 18F-Labeling of Carbohydrate-Conjugated Octreotate-Derivatives Containing a Silicon-Fluoride-Acceptor (SiFA): In Vitro and in Vivo Evaluation as Tumor Imaging Agents for Positron Emission Tomography (PET). *Bioconjugate Chem* **2010,** *21* (12), 2289-2296.
156. Wängler, C.; Niedermoser, S.; Chin, J.; Orchowski, K.; Schirrmacher, E.; Jurkschat, K.; Iovkova-Berends, L.; Kostikov, A. P.; Schirrmacher, R.; Wängler, B., One-step 18F-labeling of peptides for positron emission tomography imaging using the SiFA methodology. *Nat Protoc* **2012,** *7*, 1946-1955.
157. Wessmann, S. H.; Henriksen, G.; Wester, H. J., Cryptate mediated nucleophilic 18F-fluorination without azeotropic drying. *Nuklearmedizin* **2012,** *51* (1), 1-8.
158. Zhan, C.-G.; Dixon, D. A., Hydration of the Fluoride Anion: Structures and Absolute Hydration Free Energy from First-Principles Electronic Structure Calculations. *J Phys Chem* **2004,** *108* (11), 2020-2029.
159. Glaser, M.; Iveson, P.; Hoppmann, S.; Indrevoll, B.; Wilson, A.; Arukwe, J.; Danikas, A.; Bhalla, R.; Hiscock, D., Three methods for 18F labeling of the HER2-binding affibody molecule Z(HER2:2891) including preclinical assessment. *J Nucl Med* **2013,** *54* (11), 1981-1988.
160. Wängler, C.; Chowdhury, S.; Hofner, G.; Djurova, P.; Purisima, E. O.; Bartenstein, P.; Wängler, B.; Fricker, G.; Wanner, K. T.; Schirrmacher, R., Shuttle-cargo fusion molecules of transport peptides and the hD2/3 receptor antagonist fallypride: a feasible approach to preserve ligand-receptor binding? *J Med Chem* **2014,** *57* (10), 4368-4381.
161. Litau, S.; Niedermoser, S.; Vogler, N.; Roscher, M.; Schirrmacher, R.; Fricker, G.; Wängler, B.; Wängler, C., Next Generation of SiFAlin-Based TATE Derivatives for PET Imaging of SSTR-Positive Tumors: Influence of Molecular Design on In Vitro SSTR Binding and In Vivo Pharmacokinetics. *Bioconjug Chem* **2015,** *26* (12), 2350-2359.
162. Notni, J.; Steiger, K.; Hoffmann, F.; Reich, D.; Kapp, T. G.; Rechenmacher, F.; Neubauer, S.; Kessler, H.; Wester, H. J., Complementary, Selective PET Imaging of Integrin Subtypes alpha5beta1 and alphavbeta3 Using 68Ga-Aquibeprin and 68Ga-Avebetrin. *J Nucl Med* **2016,** *57* (3), 460-466.
163. Pohle, K.; Notni, J.; Bussemer, J.; Kessler, H.; Schwaiger, M.; Beer, A. J., 68Ga-NODAGA-RGD is a suitable substitute for 18F-Galacto-RGD and can be produced with high specific activity in a cGMP/GRP compliant automated process. *Nucl Med Biol* **2012,** *39* (6), 777-784.
164. Maresca, K. P.; Hillier, S. M.; Femia, F. J.; Keith, D.; Barone, C.; Joyal, J. L.; Zimmerman, C. N.; Kozikowski, A. P.; Barrett, J. A.; Eckelman, W. C.; Babich, J. W., A series of halogenated heterodimeric inhibitors of prostate specific membrane antigen (PSMA) as radiolabeled probes for targeting prostate cancer. *J Med Chem* **2009,** *52* (2), 347-357.
165. Notni, J.; Hermann, P.; Havlickova, J.; Kotek, J.; Kubicek, V.; Plutnar, J.; Loktionova, N.; Riss, P. J.; Rosch, F.; Lukes, I., A triazacyclononane-based bifunctional phosphinate ligand

for the preparation of multimeric 68Ga tracers for positron emission tomography. *Chemistry* **2010,** *16* (24), 7174-7185.
166. Reich, D.; Wurzer, A.; Wirtz, M.; Stiegler, V.; Spatz, P.; Pollmann, J.; Wester, H.-J.; Notni, J., Dendritic poly-chelator frameworks for multimeric bioconjugation. *Chem Commun* **2017,** *53* (17), 2586-2589.
167. Notni, J.; Pohle, K.; Wester, H. J., Comparative gallium-68 labeling of TRAP-, NOTA-, and DOTA-peptides: practical consequences for the future of gallium-68-PET. *EJNMMI Res* **2012,** *2* (1), 28.
168. Sosabowski, J. K.; Mather, S. J., Conjugation of DOTA-like chelating agents to peptides and radiolabeling with trivalent metallic isotopes. *Nat Protoc* **2006,** *1* (2), 972-976.
169. Vaidyanathan, G.; Zalutsky, M. R., Preparation of N-succinimidyl 3-[*I]iodobenzoate: an agent for the indirect radioiodination of proteins. *Nat Protoc* **2006,** *1* (2), 707-713.
170. Valko, K.; Nunhuck, S.; Bevan, C.; Abraham, M. H.; Reynolds, D. P., Fast gradient HPLC method to determine compounds binding to human serum albumin. Relationships with octanol/water and immobilized artificial membrane lipophilicity. *J Pharm Sci* **2003,** *92* (11), 2236-2248.
171. Yamazaki, K.; Kanaoka, M., Computational prediction of the plasma protein-binding percent of diverse pharmaceutical compounds. *J Pharm Sci* **2004,** *93* (6), 1480-1494.
172. Heck, M. M.; Tauber, R.; Schwaiger, S.; Retz, M.; D'Alessandria, C.; Maurer, T.; Gafita, A.; Wester, H. J.; Gschwend, J. E.; Weber, W. A.; Schwaiger, M.; Knorr, K.; Eiber, M., Treatment Outcome, Toxicity, and Predictive Factors for Radioligand Therapy with 177Lu-PSMA-I&T in Metastatic Castration-resistant Prostate Cancer. *Eur Urol* **2018,** *75* (6), 920-926.
173. Baranyai, Z.; Reich, D.; Vagner, A.; Weineisen, M.; Toth, I.; Wester, H. J.; Notni, J., A shortcut to high-affinity Ga-68 and Cu-64 radiopharmaceuticals: one-pot click chemistry trimerisation on the TRAP platform. *Dalton Trans* **2015,** *44* (24), 11137-11146.
174. Schmidt, A. Structural modifications of PSMA ligands to optimize their pharmacokinetics. Dissertation, Technical University Munich, 2017.
175. Kelly, J. M.; Amor-Coarasa, A.; Ponnala, S.; Nikolopoulou, A.; Williams, C., Jr.; DiMagno, S. G.; Babich, J., Albumin-Binding PSMA Ligands: Implications for Expanding the Therapeutic Window. *J Nucl Med* **2018,** *60* (5), 656-663.
176. Benesova, M.; Umbricht, C. A.; Schibli, R.; Müller, C., Albumin-Binding PSMA Ligands: Optimization of the Tissue Distribution Profile. *Mol Pharm* **2018,** *15* (3), 934-946.
177. Baranski, A. C.; Schäfer, M.; Bauder-Wüst, U.; Roscher, M.; Schmidt, J.; Stenau, E.; Simpfendorfer, T.; Teber, D.; Maier-Hein, L.; Hadaschik, B.; Haberkorn, U.; Eder, M.; Kopka, K., PSMA-11-Derived Dual-Labeled PSMA Inhibitors for Preoperative PET Imaging and Precise Fluorescence-Guided Surgery of Prostate Cancer. *J Nucl Med* **2018,** *59* (4), 639-645.
178. Liu, T.; Nedrow-Byers, J. R.; Hopkins, M. R.; Berkman, C. E., Spacer length effects on in vitro imaging and surface accessibility of fluorescent inhibitors of prostate specific membrane antigen. *Bioorg Med Chem Lett* **2011,** *21* (23), 7013-7016.
179. Wirtz, M.; Schmidt, A.; Schottelius, M.; Robu, S.; Günther, T.; Schwaiger, M.; Wester, H. J., Synthesis and in vitro and in vivo evaluation of urea-based PSMA inhibitors with increased lipophilicity. *EJNMMI Res* **2018,** *8* (1), 84.
180. Schottelius, M.; Wurzer, A.; Wissmiller, K.; Beck, R.; Koch, M.; Gorpas, D.; Notni, J.; Buckle, T.; van Oosterom, M. N.; Steiger, K.; Ntziachristos, V.; Schwaiger, M.; van Leeuwen, F. W. B.; Wester, H. J., Synthesis and Preclinical Characterization of the PSMA-Targeted Hybrid Tracer PSMA-I&F for Nuclear and Fluorescence Imaging of Prostate Cancer. *J Nucl Med* **2019,** *60* (1), 71-78.

181. Banerjee, S. R.; Pullambhatla, M.; Byun, Y.; Nimmagadda, S.; Green, G.; Fox, J. J.; Horti, A.; Mease, R. C.; Pomper, M. G., 68Ga-labeled inhibitors of prostate-specific membrane antigen (PSMA) for imaging prostate cancer. *J Med Chem* **2010,** *53* (14), 5333-5341.
182. Robu, S.; Schottelius, M.; Eiber, M.; Maurer, T.; Gschwend, J.; Schwaiger, M.; Wester, H. J., Preclinical Evaluation and First Patient Application of 99mTc-PSMA-I&S for SPECT Imaging and Radioguided Surgery in Prostate Cancer. *J Nucl Med* **2017,** *58* (2), 235-242.
183. Simecek, J.; Hermann, P.; Havlickova, J.; Herdtweck, E.; Kapp, T. G.; Engelbogen, N.; Kessler, H.; Wester, H. J.; Notni, J., A cyclen-based tetraphosphinate chelator for the preparation of radiolabeled tetrameric bioconjugates. *Chemistry* **2013,** *19* (24), 7748-7757.
184. Kularatne, S. A.; Zhou, Z.; Yang, J.; Post, C. B.; Low, P. S., Design, synthesis, and preclinical evaluation of prostate-specific membrane antigen targeted 99mTc-radioimaging agents. *Mol Pharm* **2009,** *6* (3), 790-800.
185. Hillier, S. M.; Maresca, K. P.; Lu, G.; Merkin, R. D.; Marquis, J. C.; Zimmerman, C. N.; Eckelman, W. C.; Joyal, J. L.; Babich, J. W., 99mTc-labeled small-molecule inhibitors of prostate-specific membrane antigen for molecular imaging of prostate cancer. *J Nucl Med* **2013,** *54* (8), 1369-1376.
186. Lu, G.; Maresca, K. P.; Hillier, S. M.; Zimmerman, C. N.; Eckelman, W. C.; Joyal, J. L.; Babich, J. W., Synthesis and SAR of 99mTc/Re-labeled small molecule prostate specific membrane antigen inhibitors with novel polar chelates. *Bioorg Med Chem Lett* **2013,** *23* (5), 1557-1563.
187. Eder, M.; Lohr, T.; Bauder-Wüst, U.; Reber, M.; Mier, W.; Schäfer, M.; Haberkorn, U.; Eisenhut, M., Pharmacokinetic properties of peptidic radiopharmaceuticals: reduced uptake of (EH)3-conjugates in important organs. *J Nucl Med* **2013,** *54* (8), 1327-1330.
188. Behe, M.; Kluge, G.; Becker, W.; Gotthardt, M.; Behr, T. M., Use of polyglutamic acids to reduce uptake of radiometal-labeled minigastrin in the kidneys. *J Nucl Med* **2005,** *46* (6), 1012-1015.
189. Gotthardt, M.; van Eerd-Vismale, J.; Oyen, W. J.; de Jong, M.; Zhang, H.; Rolleman, E.; Maecke, H. R.; Behe, M.; Boerman, O., Indication for different mechanisms of kidney uptake of radiolabeled peptides. *J Nucl Med* **2007,** *48* (4), 596-601.
190. Han, Y.; Albericio, F.; Barany, G., Occurrence and Minimization of Cysteine Racemization during Stepwise Solid-Phase Peptide Synthesis. *J Org Chem* **1997,** *62* (13), 4307-4312.
191. Carpino, L. A.; El-Faham, A., Effect of Tertiary Bases on O-Benzotriazolyluronium Salt-Induced Peptide Segment Coupling. *J Org Chem* **1994,** *59* (4), 695-698.
192. Nguyen, L. A.; He, H.; Pham-Huy, C., Chiral drugs: an overview. *Int J Biomed Sci* **2006,** *2* (2), 85-100.
193. Brooks, W. H.; Guida, W. C.; Daniel, K. G., The significance of chirality in drug design and development. *Curr Top Med Chem* **2011,** *11* (7), 760-770.
194. Ghibellini, G.; Leslie, E. M.; Brouwer, K. L., Methods to evaluate biliary excretion of drugs in humans: an updated review. *Mol Pharm* **2006,** *3* (3), 198-211.
195. Kratochwil, N. A.; Huber, W.; Müller, F.; Kansy, M.; Gerber, P. R., Predicting plasma protein binding of drugs: a new approach. *Biochem Pharmacol* **2002,** *64* (9), 1355-1374.
196. Even-Sapir, E.; Metser, U.; Flusser, G.; Zuriel, L.; Kollender, Y.; Lerman, H.; Lievshitz, G.; Ron, I.; Mishani, E., Assessment of malignant skeletal disease: initial experience with 18F-fluoride PET/CT and comparison between 18F-fluoride PET and 18F-fluoride PET/CT. *J Nucl Med* **2004,** *45* (2), 272-278.

197. Bouaziz, H.; Ghorbel, H.; Ketata, S.; Guermazi, F.; Zeghal, N., Toxic effects of fluoride by maternal ingestion on kidney function of adult mice and their suckling pups. *Fluoride* **2005,** *38* (1), 23-31.
198. Dimcevici Poesina, N.; Balalau, C.; Nimigean, V. R.; Nimigean, V.; Ion, I.; Baconi, D.; Barca, M.; Baran Poesina, V., Histopathological changes of renal tissue following sodium fluoride administration in two consecutive generations of mice. Correlation with the urinary elimination of fluoride. *Rom J Morphol Embryol* **2014,** *55* (2), 343-349.
199. Inkielewicz, I.; Krechniak, J., Fluoride content in soft tissues and urine of rats exposed to sodium fluoride in drinking water. *Fluoride* **2003,** *36* (4), 263-266.
200. Wadas, T. J.; Wong, E. H.; Weisman, G. R.; Anderson, C. J., Coordinating radiometals of copper, gallium, indium, yttrium, and zirconium for PET and SPECT imaging of disease. *Chem Rev* **2010,** *110* (5), 2858-2902.
201. Prasad, V.; Steffen, I. G.; Diederichs, G.; Makowski, M. R.; Wust, P.; Brenner, W., Biodistribution of [68Ga]PSMA-HBED-CC in Patients with Prostate Cancer: Characterization of Uptake in Normal Organs and Tumour Lesions. *Mol Imaging Biol* **2016,** *18* (3), 428-436.
202. Demirci, E.; Sahin, O. E.; Ocak, M.; Akovali, B.; Nematyazar, J.; Kabasakal, L., Normal distribution pattern and physiological variants of 68Ga-PSMA-11 PET/CT imaging. *Nucl Med Commun* **2016,** *37* (11), 1169-1179.
203. Israeli, R. S.; Powell, C. T.; Corr, J. G.; Fair, W. R.; Heston, W. D., Expression of the prostate-specific membrane antigen. *Cancer Res* **1994,** *54* (7), 1807-1811.
204. Chang, S. S., Overview of prostate-specific membrane antigen. *Rev Urol* **2004,** *6 Suppl 10*, S13-18.
205. Sener, Y.; Tosun, G.; Kahvecioglu, F.; Gokalp, A.; Koc, H., Fluoride levels of human plasma and breast milk. *Eur J Dent* **2007,** *1* (1), 21-24.
206. Stish, B. J.; Pisansky, T. M.; Harmsen, W. S.; Davis, B. J.; Tzou, K. S.; Choo, R.; Buskirk, S. J., Improved Metastasis-Free and Survival Outcomes With Early Salvage Radiotherapy in Men With Detectable Prostate-Specific Antigen After Prostatectomy for Prostate Cancer. *J Clin Oncol* **2016,** *34* (32), 3864-3871.
207. Pfister, D.; Bolla, M.; Briganti, A.; Carroll, P.; Cozzarini, C.; Joniau, S.; van Poppel, H.; Roach, M.; Stephenson, A.; Wiegel, T.; Zelefsky, M. J., Early salvage radiotherapy following radical prostatectomy. *Eur Urol* **2014,** *65* (6), 1034-1043.
208. Siegmann, A.; Bottke, D.; Faehndrich, J.; Brachert, M.; Lohm, G.; Miller, K.; Bartkowiak, D.; Hinkelbein, W.; Wiegel, T., Salvage radiotherapy after prostatectomy - what is the best time to treat? *Radiother Oncol* **2012,** *103* (2), 239-243.
209. Ohri, N.; Dicker, A. P.; Trabulsi, E. J.; Showalter, T. N., Can early implementation of salvage radiotherapy for prostate cancer improve the therapeutic ratio? A systematic review and regression meta-analysis with radiobiological modelling. *Eur J Cancer* **2012,** *48* (6), 837-844.
210. Afshar-Oromieh, A.; Malcher, A.; Eder, M.; Eisenhut, M.; Linhart, H. G.; Hadaschik, B. A.; Holland-Letz, T.; Giesel, F. L.; Kratochwil, C.; Haufe, S.; Haberkorn, U.; Zechmann, C. M., PET imaging with a [68Ga]gallium-labelled PSMA ligand for the diagnosis of prostate cancer: biodistribution in humans and first evaluation of tumour lesions. *Eur J Nucl Med Mol Imaging* **2013,** *40* (4), 486-495.
211. Giesel, F. L.; Will, L.; Lawal, I.; Lengana, T.; Kratochwil, C.; Vorster, M.; Neels, O.; Reyneke, F.; Haberkon, U.; Kopka, K.; Sathekge, M., Intraindividual Comparison of 18F-PSMA-1007 and 18F-DCFPyL PET/CT in the Prospective Evaluation of Patients with Newly Diagnosed Prostate Carcinoma: A Pilot Study. *J Nucl Med* **2018,** *59* (7), 1076-1080.

212. Freitag, M. T.; Radtke, J. P.; Afshar-Oromieh, A.; Roethke, M. C.; Hadaschik, B. A.; Gleave, M.; Bonekamp, D.; Kopka, K.; Eder, M.; Heusser, T.; Kachelriess, M.; Wieczorek, K.; Sachpekidis, C.; Flechsig, P.; Giesel, F.; Hohenfellner, M.; Haberkorn, U.; Schlemmer, H. P.; Dimitrakopoulou-Strauss, A., Local recurrence of prostate cancer after radical prostatectomy is at risk to be missed in (68)Ga-PSMA-11-PET of PET/CT and PET/MRI: comparison with mpMRI integrated in simultaneous PET/MRI. *Eur J Nucl Med Mol Imaging* **2017,** *44* (5), 776-787.
213. Heusser, T.; Mann, P.; Rank, C. M.; Schäfer, M.; Dimitrakopoulou-Strauss, A.; Schlemmer, H. P.; Hadaschik, B. A.; Kopka, K.; Bachert, P.; Kachelriess, M.; Freitag, M. T., Investigation of the halo-artifact in 68Ga-PSMA-11-PET/MRI. *PLoS One* **2017,** *12* (8), e0183329.
214. Afshar-Oromieh, A.; Wolf, M.; Haberkorn, U.; Kachelriess, M.; Gnirs, R.; Kopka, K.; Schlemmer, H. P.; Freitag, M. T., Effects of arm truncation on the appearance of the halo artifact in 68Ga-PSMA-11 (HBED-CC) PET/MRI. *Eur J Nucl Med Mol Imaging* **2017,** *44* (10), 1636-1646.
215. Yordanova, A.; Becker, A.; Eppard, E.; Kürpig, S.; Fisang, C.; Feldmann, G.; Essler, M.; Ahmadzadehfar, H., The impact of repeated cycles of radioligand therapy using [177Lu]Lu-PSMA-617 on renal function in patients with hormone refractory metastatic prostate cancer. *Eur J Nucl Med Mol Imaging* **2017,** *44* (9), 1473-1479.
216. Baum, R. P.; Kulkarni, H. R.; Schuchardt, C.; Singh, A.; Wirtz, M.; Wiessalla, S.; Schottelius, M.; Mueller, D.; Klette, I.; Wester, H. J., 177Lu-Labeled Prostate-Specific Membrane Antigen Radioligand Therapy of Metastatic Castration-Resistant Prostate Cancer: Safety and Efficacy. *J Nucl Med* **2016,** *57* (7), 1006-1013.
217. Kostikov, A. P.; Chin, J.; Orchowski, K.; Niedermoser, S.; Kovacevic, M. M.; Aliaga, A.; Jurkschat, K.; Wängler, B.; Wängler, C.; Wester, H.-J.; Schirrmacher, R., Oxalic Acid Supported Si–18F-Radiofluorination: One-Step Radiosynthesis of N-Succinimidyl 3-(Di-tert-butyl[18F]fluorosilyl)benzoate ([18F]SiFB) for Protein Labeling. *Bioconjugate Chem* **2012,** *23* (1), 106-114.
218. GESTIS-Stoffdatenbank, Gefahrstoffinformationssystem der Deutschen Gesetzlichen Unfallversicherung. https://www.dguv.de/ifa/gestis/gestis-stoffdatenbank/index.jsp.
219. Liu, S.; Ellars, C. E.; Edwards, D. S., Ascorbic acid: useful as a buffer agent and radiolytic stabilizer for metalloradiopharmaceuticals. *Bioconjug Chem* **2003,** *14* (5), 1052-1056.
220. Liang, S.; Hammond, G. B.; Xu, B., Hydrogen Bonding: Regulator for Nucleophilic Fluorination. *Chemistry* **2017,** *23* (71), 17850-17861.
221. Hefter, G., Acidity constant of hydrofluoric acid. *J Solution Chem* **1984,** *13* (7), 457-470.
222. Solin, O.; Bergman, J.; Haaparanta, M.; Reissell, A., Production of 18F from water targets. Specific radioactivity and anionic contaminants. *Int J Rad Appl Instrum A* **1988,** *39* (10), 1065-1071.
223. Gonzalez Lepera, C. E.; Dembowski, B., Production of [18F]fluoride with a high-pressure disposable [18O]water target. *Appl Radiat Isot* **1997,** *48* (5), 613-617.
224. Pellicioli, M.; Schuler, J.; Marchand, P.; Brasse, D., Small volume target for F-18 production. *AIP Conf Proc* **2017,** *1845* (1), 020018.
225. Nye, J. A.; Dick, D. W.; Nickles, R. J., Pushing the Limits of an O-18 Water Target. *AIP Conf Proc* **2003,** *680* (1), 1098-1101.
226. Guillaume, M.; Luxen, A.; Nebeling, B.; Argentini, M.; Clark, J. C.; Pike, V. W., Recommendations for fluorine-18 production. *Int J Rad Appl Instrum A* **1991,** *42* (8), 749-762.

227. Ishiwata, K.; Hayashi, K.; Sakai, M.; Kawauchi, S.; Hasegawa, H.; Toyohara, J., Determination of radionuclides and radiochemical impurities produced by in-house cyclotron irradiation and subsequent radiosynthesis of PET tracers. *Ann Nucl Med* **2017,** *31* (1), 84-92.
228. Köhler, M.; Degering, D.; Zessin, J.; Füchtner, F.; Konheiser, J., Radionuclide impurities in [18F]F− and [18F]FDG for positron emission tomography. *Appl Radiat Isot* **2013,** *81*, 268-271.
229. Sergeev, M.; Lazari, M.; Morgia, F.; Collins, J.; Javed, M. R.; Sergeeva, O.; Jones, J.; Phelps, M. E.; Lee, J. T.; Keng, P. Y.; van Dam, R. M., Performing radiosynthesis in microvolumes to maximize molar activity of tracers for positron emission tomography. *Commun Chem* **2018,** *1* (1), 10.

4. Publications

Peer-reviewed journal articles

- **Wurzer, A.**; Di Carlo, D.; Schmidt, A.; Beck, R.; Eiber, M.; Schwaiger, M.; Wester, H. J., Radiohybrid ligands: a novel tracer concept exemplified by ^{18}F- or ^{68}Ga-labeled rhPSMA-inhibitors. J Nucl Med 2019, accepted.

- Eiber, M.; Kroenke, M.; **Wurzer, A.**; Ulbrich, L.; Jooß, L.; Maurer T.; Horn, T.; Schiller, K.; Buschner, K.; Wester, H. J.; Weber, W. A., ^{18}F-rhPSMA-7 positron emission tomography for the detection of biochemical recurrence of prostate cancer following radical prostatectomy. J Nucl Med 2019, submitted.

- Kroenke, K.; **Wurzer, A.**; Schwamborn, K.; Ulbrich, L.; Jooß, L.; Maurer, M.; Horn, T.; Haller, B.; Herz, M.; Wester, H. J.; Weber, W. A.; Eiber, M., Histologically-confirmed diagnostic efficacy of ^{18}F-rhPSMA-7 positron emission tomography for N-staging of patients with primary high risk prostate cancer. J Nucl Med 2019, submitted.

- Oh, S. O.; **Wurzer, A.**; Teoh, E.; Oh, S.; Langbein, T.; Kroenke, M.; Herz, M.; Kropf, S.; Wester, H. J.; Weber, A. W.; Eiber, M., Quantitative and Qualitative Analyses of Biodistribution and PET Image Quality of Novel Radiohybrid PSMA, ^{18}F- rhPSMA-7, in Patients with Prostate Cancer. J Nucl Med 2019, submitted.

- Schottelius, M.; **Wurzer, A**.; Wissmiller, K.; Beck, R.; Koch, M.; Gorpas, D.; Notni, J.; Buckle, T.; van Oosterom, M. N.; Steiger, K.; Ntziachristos, V.; Schwaiger, M.; van Leeuwen, F. W. B.; Wester, H. J., Synthesis and Preclinical Characterization of the PSMA-Targeted Hybrid Tracer PSMA-I&F for Nuclear and Fluorescence Imaging of Prostate Cancer. J Nucl Med 2019, 60 (1), 71-78.

- Reichart, F.; Maltsev, O. V.; Kapp, T. G.; Rader, A. F. B.; Weinmuller, M.; Marelli, U. K.; Notni, J.; **Wurzer, A.**; Beck, R.; Wester, H. J.; Steiger, K.; Di Maro, S.; Di Leva, F. S.; Marinelli, L.; Nieberler, M.; Reuning, U.; Schwaiger, M.; Kessler, H., Selective Targeting of Integrin alphavbeta8 by a Highly Active Cyclic Peptide. J Med Chem 2019, 62 (4), 2024-2037.

- **Wurzer, A.**; Seidl, C.; Morgenstern, A.; Bruchertseifer, F.; Schwaiger, M.; Wester, H. J.; Notni, J., Dual-Nuclide Radiopharmaceuticals for Positron Emission Tomography Based Dosimetry in Radiotherapy. Chemistry 2018, 24 (3), 547-550.

- Kapp, T. G.; Di Leva, F. S.; Notni, J.; Rader, A. F. B.; Fottner, M.; Reichart, F.; Reich, D.; **Wurzer, A.**; Steiger, K.; Novellino, E.; Marelli, U. K.; Wester, H. J.; Marinelli, L.; Kessler, H., N-Methylation of isoDGR Peptides: Discovery of a Selective alpha5beta1-Integrin Ligand as a Potent Tumor Imaging Agent. J Med Chem 2018, 61 (6), 2490-2499.

- **Wurzer, A.**; Vagner, A.; Horvath, D.; Fellegi, F.; Wester, H. J.; Kalman, F. K.; Notni, J., Synthesis of Symmetrical Tetrameric Conjugates of the Radiolanthanide Chelator DOTPI for Application in Endoradiotherapy by Means of Click Chemistry. Front Chem 2018, 6, 107.

- Vagner, A.; Forgacs, A.; Brucher, E.; Toth, I.; Maiocchi, A.; **Wurzer, A.**; Wester, H. J.; Notni, J.; Baranyai, Z., Equilibrium Thermodynamics, Formation, and Dissociation Kinetics of Trivalent Iron and Gallium Complexes of Triazacyclononane-Triphosphinate (TRAP) Chelators: Unraveling the Foundations of Highly Selective Ga-68 Labeling. Front Chem 2018, 6, 170.
- **Wurzer, A.**; Pollmann, J.; Schmidt, A.; Reich, D.; Wester, H. J.; Notni, J., Molar Activity of Ga-68 Labeled PSMA Inhibitor Conjugates Determines PET Imaging Results. Mol Pharm 2018, 15 (9), 4296-4302.
- Färber, S. F.; **Wurzer, A.**; Reichart, F.; Beck, R.; Kessler, H.; Wester, H. J.; Notni, J., Therapeutic Radiopharmaceuticals Targeting Integrin alphavbeta6. ACS Omega 2018, 3 (2), 2428-2436.
- Reich, D.; **Wurzer, A.**; Wirtz, M.; Stiegler, V.; Spatz, P.; Pollmann, J.; Wester, H. J.; Notni, J., Dendritic poly-chelator frameworks for multimeric bioconjugation. Chem Commun (Camb) 2017, 53 (17), 2586-2589.

Patents

- Dual mode radiotracer and -therapeutics: WO 2019/020831 A1, **Wurzer, A.**; Wester, H. J.; Eiber M., 2019.

Selected conference abstracts

- **Wurzer, A.**; Di Carlo, D.; Schmidt, A.; Beck, R.; Schwaiger, M.; Herz, M.; Eiber, M.; Wester, H., PSMA-targeted 18F-labeled Radiohybrid Inhibitors: Labeling chemistry and automated GMP production of ^{18}F-rhPSMA-7. Journal of Nuclear Medicine 2019, 60 (supplement 1), 342.
- **Wurzer, A.**; Di Carlo, D.; Schmidt, A.; Beck, R.; Eiber, M.; Schwaiger, M.; Wester, H., PSMA-targeted ^{18}F-labeled Radiohybrid Inhibitors: Concept, preclinical evaluation and first proof of concept study in men. Journal of Nuclear Medicine 2019, 60 (supplement 1), 344.
- Eiber, M.; Kroenke, M.; **Wurzer, A.**; Ulbrich, L.; Jooß, L.; Maurer, T.; Kropf, S.; Horn, T.; Wester, H.; Weber, W., ^{18}F-rhPSMA-7 positron emission tomography (PET) for the detection of biochemical recurrence of prostate cancer following radical prostatectomy. Journal of Nuclear Medicine 2019, 60 (supplement 1), 649.
- Ilhan, H.; Kroenke, M.; **Wurzer, A.**; Ulbrich, L.; Jooß, L.; Unterrainer, M.; Bartenstein, P.; Kropf, S.; Wester, H.; Weber, W.; Eiber, M., ^{18}F-rhPSMA-7 positron emission tomography (PET) for the detection of biochemical recurrence of prostate cancer following curative-intent radiation therapy. Journal of Nuclear Medicine 2019, 60 (supplement 1), 592.

- Kroenke, M.; **Wurzer, A.**; Schwamborn, K.; Ulbrich, L.; Jooß, L.; Maurer, T.; Horn, T.; Kropf, S.; Haller, B.; Wester, H.; Weber, W.; Eiber, M., Histologically-confirmed diagnostic efficacy of ^{18}F-rhPSMA-7 positron emission tomography for N-staging of patients with high risk primary prostate cancer. Journal of Nuclear Medicine 2019, 60 (supplement 1), 1567.

- Oh, S. W.; **Wurzer, A.**; Yusufi, N.; Nekolla, S.; Herz, M.; Kropf, S.; Weber, W.; Wester, H.; Eiber, M., Preclinical dosimetry and human biodistribution of ^{18}F-rhPSMA-7 and 18F-rhPSMA-7.3. Journal of Nuclear Medicine 2019, 60 (supplement 1), 1635.

- Oh, S. W.; **Wurzer, A.**; Teoh, E.; Oh, S.; Buschner, G.; Herz, M.; Kropf, S.; Wester, H.; Weber, W.; Eiber, M., Quantitative and qualitative analysis of biodistribution and PET image quality of novel radiohybrid PSMA ligand, ^{18}F-rhPSMA-7, in patients with prostate cancer. Journal of Nuclear Medicine 2019, 60 (supplement 1), 1557.

- **Wurzer, A.**; Seidl, C.; Morgenstern, A.; Bruchertseifer, F.; Schwaiger, M.; Wester, H. J.; Notni, J., Binuklid-Radiopharmaka für PET-basierte therapeutische Dosimetrie, Jahrestagung der Deutschen Gesellschaft für Nuklearmedizin 2017.

- **Wurzer, A.**; Vágner, A.; Baranyai, Z.; Wirtz, M.; Tóth, I.; Wester, H. J.; Notni, J., Synthese tetramerer DOTPI-Biokonjugate für radiotherapeutische Anwendungen mittels Click-Chemie, Jahrestagung der Deutschen Gesellschaft für Nuklearmedizin 2016.

5. Acknowledgments

Mein besonderer Dank gilt Herrn **Prof. Dr. Hans-Jürgen Wester**, der mir diese Arbeit an seinem Lehrstuhl ermöglichte und mich dieses äußerst interessante Thema bearbeiten ließ. Des Weiteren bedanke ich mich für die exzellente Förderung, das entgegengebrachte Vertrauen und insbesondere seinen unermüdlichen Einsatz, der es erst ermöglichte, dass die Arbeit in dieser Form zustande kam.

Ferner danke ich Frau **Prof. Dr. Margret Schottelius** und Herrn **PD Dr. Johannes Notni** für die aufschlussreichen Diskussionen zu kleineren und größeren wissenschaftlichen Fragestellungen.

Mein weiterer Dank gilt den Mitarbeitern der Nuklearmedizin am Klinikum rechts der Isar, insbesondere Herrn **Prof. Dr. Matthias Eiber** für die gute Zusammenarbeit und sein Engagement bei der Translation der entwickelten Verbindungen in die Klinik. Außerdem bedanke ich mich bei Herrn **Michael Herz** für die exzellente Versorgung mit [^{18}F]Fluorid und seine Mitarbeit bei der Fertigstellung der automatisierten Synthese.

Ein spezieller Dank gilt meinen Laborkollegen **Dr. Martina Wirtz**, **Dr. Alexander Schmidt**, **Dr. Stephanie Robu**, **Dr. Theresa Osl**, **Dr. Andreas Poschenrieder**, **PD Dr. Behrooz Yousefi**, **Dr. Frauke Richter**, **Monika Beschorner** und **Sven Hintze**, die mir mit Ihrem Wissen und ihrer Hilfsbereitschaft den Einstieg in die Arbeitsgruppe erleichterten. Ein großes Dankeschön möchte ich auch an **Dr. Roswitha Beck** für die kompetente Betreuung bei den gesamten *in vivo* Studien richten, vor allem für die fundierten Kenntnisse im Umgang mit Labortieren. Weiterhin danke ich den derzeitigen Doktoranden **Thomas Günther**, **Daniel Di Carlo**, **Veronika Felber**, **Matthias Konrad**, **Mara Parzinger**, **Markus Fahnauer**, **Sebastian Fischer** und **Jan-Philip Kunert**, sowie **Stefanie Färber** und **Jana Herbst**, für die großartige Unterstützung während meiner Promotion (insbesondere während den rhPSMA-Marathon-Evaluierungen) und natürlich auch für die vielen schönen Momente im und außerhalb des Labors.

Außerdem ein recht herzliches Vergelt`s Gott an meine Studentinnen und Studenten, **Mirjam Wenig**, **Stefanie Ludwig**, **Jonas Demlehner**, **Philip Spatz**, **Aleksander Jaglicic**, **David Nippa**, **Silva Kronawitter** und **Sebastian Schleser**, die mich mit ihrem großartigen Einsatz bei meiner Promotion begleitet haben.

Bei Frau **Sybille Reder** und Herrn **Markus Mittelhäuser** möchte ich ebenfalls für Ihre Unterstützung bei den *in vivo* Studien am Klinikum rechts der Isar bedanken.

Frau **Christine Winkler** und Frau **Irmgard Kaul** möchte ich für das exzellente Management rund um die Promotion und die großartige Hilfsbereitschaft bei organisatorischen Fragen danken.

Ein herzliches Dankeschön möchte ich an meine Freundin **Alexandra Kraus** richten, die mich mit ihrer liebevollen und humorvollen Art durch die Promotion manövrierte und mich mit offenem Ohr und zahlreichen Ratschlägen unentwegt unterstützt und motiviert hat.

Ein besonderer Dank gilt außerdem **meiner Familie**, insbesondere meinem Bruder **Sebastian** und meinen Eltern, **Dagmar und Josef Wurzer**, die mir während meines ganzen Studiums und während der Promotion, stets zur Seite standen.